Institut für Biochemie
Universität Freiburg (Schweiz)

# Nuclear Translocation of Components of the Neuronal Plasma Membrane Oxidoreductase after Oxidative Stress and its Effects on Induction of Apoptosis

## INAUGURAL – DISSERTATION

zur Erlangung der Würde eines Doctor rerum naturalium der Mathematisch-Naturwissenschaftlichen Fakultät der Universität Freiburg (Schweiz)

vorgelegt von

## Zubin Dastoor

aus  Riehen (BS)

These No 1293

Mécanographie
Freiburg
2000

Accepté par la Faculté des Sciences de l'Université de Fribourg (Suisse) sur la proposition de:

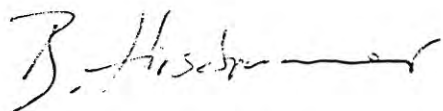Prof. Dr. Albert Gossauer, président du jury
Prof. Dr. Jean-Luc Dreyer, directeur de thèse
Prof. Dr. Andreas Conzelmann, coréférent
M. Dr. Peter G.H. Clarke, coréférent

Fribourg, le 2 mars 2000

Le Doyen:

Prof. Dr. Beat Hirsbrunner

Le directeur de thèse:

Prof. Dr. Jean-Luc Dreyer

# __Acknowledgements__

First of all, I would like to thank Professor Jean-Luc Dreyer for giving me the opportunity to work in his laboratory and for his permanent readiness to help. He spent much of his valuable time in giving me guidance, help and advice during my thesis.

My next very big "thank you" goes to all the people which worked in the Dreyer Lab in these years: To Maria Brenz Verca, with whom I shared excitement, breakthroughs as well as set-backs throughout the thesis and with whom I started to discover Fribourg, to Rinaldo Zurbriggen who supplied help at the beginning of my thesis, to Christine Déforel who was a marvellous help in technical and practical work, to Mahamadou Faty, with whom I had many very interesting discussions and who made me fond of African food, to Joëlle Tornare who helped me with my S1-mapping assays, to David Widmer and Bernhard Sonderegger, who made my night sessions of working, in which I shared joy, frustrations and Pizzas with them, much more enjoyable and with whom I did not only spend a good time in the lab, but also otherwise, to Guido Miescher who was an invaluable help in answering questions of any type and who inspired me with his enthusiasm for sports and science, to Antoinette Hayoz who was an excellent help with my Two-hybrid system assays and with whom it was a pleasure to work together, to Gaël Hedou, Michel Maret and Jean-Claude Jenny who all of them helped creating a really pleasant and motivating working spirit.

I would like to express my special gratitude to Prof. Sandro Rusconi and Stefano Brenz Verca for providing invaluable help in molecular biology, to Dr. Christoph Borner and his group, especially Thierry Rosset, for their help and advice for my apoptosis experiments, to Prof. Andreas Conzelmann, Dr. Beat Schwaller, Mahamadou Faty, Isabella Imhof and Urs Meyer for providing material and help to perform my Two-hybrid-System assays, to Prof. Marco Celio, Stefan Halter and Dr. Merdol Ibrahim, who all were an invaluable help with my confocal studies.

Furthermore I would like to thank all other permanent and temporary members of the Institute of Biochemistry for all scientific and non-scientific help and for a friendly and stimulating working environment.

I also wish to thank Prof. Andreas Conzelmann and Dr. Peter G.H. Clarke for having accepted to be my referees and for taking some of their precious time to look at my thesis.

A special thank goes to Roland Pach with whom I did not only exchange scientific discussions and excitement, but also the latest news of our beloved Basel. I also would like to thank all my other friends in Fribourg and Basel, especially Eva Schabel for her loving support and for standing my impossible working timetables caused by my interest in science.

My last and greatest thanks I would like to express to my parents and to my sister. I thank them with all my heart for their constant love, help and support they provided. Without them I would never have been able to write this thesis.

# **<u>Abbreviations</u>**

| | |
|---|---|
| Ab | antibody |
| Aldolase-GFP | aldolase C coupled to a GFP tag |
| AP1 | adapter primer 1 |
| Apaf | apoptosis associated factor |
| Bag-1 | Bcl-2-associated  athanogene 1 |
| Bcl-2 | B-cell lymphoma/leukemia-2 |
| BFP | blue fluorescent protein |
| CNS | central nervous system |
| Enolase-GFP | enolase γ coupled to a GFP tag |
| FITC | fluorescein isothiocyanate |
| GAPDH | glyceraldehyde-3-phosphate dehydrogenase |
| GAPDH-GFP | GAPDH coupled to a GFP tag |
| GFP | enhanced green fluorescent protein |
| HIV-1 | human immunodeficiency virus type 1 |
| Hsc70 | heat shock cognate protein 70 |
| Hsc70-GFP | Hsc70 coupled to a GFP tag |
| HSP | heat shock proteins |
| Ig | immunoglobulin |
| Mab | monoclonal antibody |
| MG132 | carbobenzoxyl-leucinyl-leucinyl-leucinal-H |
| NB41A3 | mouse neuroblatoma cell line |
| NB41A3$^{aldolase}$ | mouse neuroblatoma cell line overexpressing aldolase |
| NB41A3$^{enolase}$ | mouse neuroblatoma cell line overexpressing enolase |
| NB41A3$^{GAPDH}$ | mouse neuroblatoma cell line overexpressing GAPDH |
| NF-κ B | nuclear factor kappa B |
| PMO | transplasma membrane oxidoreductase |
| R6 | rat 6 embryo fibroblast cell line |

| | |
|---|---|
| R6$^{Bcl-2}$ | rat 6 embryo fibroblast cell line overexpressing Bcl-2 |
| RACE | rapid amplification of cDNA ends |
| ROS | reactive oxygen species |
| TNF$\alpha$ | tumour necrosis factor $\alpha$ |
| TR | Texas Red |
| Ulip | Unc33 like protein |
| Ulip-GFP | Ulip-3   coupled to a GFP tag |

*To my parents*

# CONTENTS

**Curriculum Vitae**

**Statement of academic integrity**

**Publications**

# 1.1 <u>Abstract</u>

The plasma membrane oxidoreductase (PMO) complex may exert important functions in cellular defence mechanism against oxidative stress and in apoptosis. Thus, we aimed to investigate the function of the five proteins GAPDH, Hsc70, enolase γ, aldolase C and Ulip, all of them tightly bound members of a neuronal PMO multi-protein complex, previously isolated and purified from synaptic vesicles and synaptic plasma membranes by our group. Earlier reports have shown an altered subcellular distribution of some these members in both apoptosis and in the cellular response to oxidative stress. We have now extended these studies using confocal laser scanning microscopy in the hope of uncovering clues to the elusive role of these five proteins by immunocytochemistry. Furthermore, CNS-derived cells, the mouse neuroblastoma NB41A3, and non-CNS derived cells, R6 fibroblast and an apoptosis-resistant Bcl-2 expressing transfectant (R6$^{\text{Bcl-2}}$), were transiently and stably transfected with GFP- and BFP-fusion constructs containing either GAPDH, Hsc70, enolase γ, aldolase C or Ulip.

Expression of endogenous GAPDH, the major protein associated with the PMO complex, was predominantly nuclear in NB41A3 cells and cytoplasmic in R6 and R6-Bcl-2 cells. Induction of apoptosis and oxidative stress by $H_2O_2$ or FeCN enhanced the nuclear translocation of endogenous GAPDH in all cell types. In apoptotic cells, GAPDH expression was 3 times higher as compared to non-apoptotic cells. Consistent with a role of GAPDH in apoptosis, cells transfected by a vector coding for a GAPDH-GFP hybrid increased nuclear import of GAPDH-GFP and conferred a higher sensitivity to induction of apoptosis caused by exposure to staurosporine or MG132. *Per se* 10% of cells overexpressing GAPDH-GFP are apoptotic. Bcl-2 overexpression prevents nuclear translocation of GAPDH and apoptosis in untransfected cells, but not in transfected cells overexpressing GAPDH-GFP fusion protein.

Hsc70 is localised in the cytoplasm of neuroblastomas and fibroblasts. Partial translocation of endogenous Hsc70 into the nucleus is induced by oxidative stress, but not by apoptosis. The predominantly cytoplasmic localisation of overexpressed Hsc70-GFP in unstressed cells and its subsequent translocation into the nucleus after oxidative stress is similar to what is observed with endogenous Hsc70. Overexpression of Hsc70 makes cells more resistant to oxidative stress. However, in cells exposed to MG132 or staurosporine, no nuclear translocation of Hsc70-GFP is observed and no indications of a protective function of Hsc70 against apoptosis are found.

Aldolase and overexpressed aldolase-GFP, which are present both in a soluble and in a cytoskeleton bound form, are expressed predominantly in the cytoplasm of unstressed cells. The expression is highest at the perinuclear area and in the somal area at the bases of axons. Induction of oxidative stress leads to enhanced nuclear expression of endogenous aldolase in NB41A3 cells. The cellular response to apoptosis induced by MG132 or staurosporine is not influenced by overexpression of aldolase-GFP, suggesting that aldolase C does not have a crucial function during apoptosis.

Translocation of endogenous Ulip from the cytoplasm to the nucleus in response to oxidative stress is observed in NB41A3 and in R6 cells. In transfected cells overexpressed Ulip-GFP is also imported into the nucleus during oxidative stress, but it is still expressed predominantly in the cytoplasm and often concentrated in Ulip-GFP-positive speckles.

Enolase shows the least oxidative stress-induced changes among the five proteins of the PMO complex. The typical cytoplasmic expression of enolase is not significantly altered, except for a slight rise in nuclear enolase-GFP in transfected NB41A3 cells.

Finally we were able to show that many combinations between two of the five PMO proteins in double-transfection experiments, enhance differential translocation into the nucleus or into speckles in response to oxidative stress.

From this study we conclude, that the translocation of these PMO associated proteins, especially of GAPDH and Hsc70, may be an important event in apoptosis and oxidative stress. Our results also indicate that the effect of these proteins, when they are overexpressed, cannot be counteracted by Bcl-2.

# 1.2 <u>Zusammenfassung</u>

Mittels Immunocytochemie untersuchten wir die Rolle der fünf Komponenten des Plasmamembran-Oxidoreduktase (PMO) Komplexes, GAPDH, Hsc70, Enolase γ, Aldolase C und Ulip, während des Oxidativen Stresses und in der Apoptose. Um die Rolle dieser fünf Proteine, welche von unserer Forschungsgruppe isoliert worden waren, zu erforschen, machten wir uns die Konfokal Laser Scanning Microscopie zu nutze. Darüberhinaus wurden Zellen aus dem Zentral-Nervensystem (ZNS), Maus NB41A3 Neuroblastomen, und Nicht-ZNS Zellen, namentlich R6 Fibroblasten und eine Apoptose-resistente Bcl-2 exprimierende Transfektanten (R6$^{Bcl-2}$), sowohl transient als auch stabil mit GFP- und BFP-Fusions Konstrukten, die entweder GAPDH, Hsc70, Enolase γ, Aldolase C oder Ulip enthalten, transfektiert.

Expression von GAPDH, dem wichtigsten Protein des PMO Komplexes, war vorwiegend im Zellkern in NB41A3 und cytoplasmisch in R6 and R6-Bcl-2 Zellen. Induktion von Apoptose und Oxidativem Stress erhöhte den Import von zelleigenem GAPDH in den Kern. In apoptotischen Zellen war die GAPDH-Expression 3 mal höher als in nicht-apoptotischen. Zellen, in denen GAPDH gekoppelt an GFP überexprimiert wurde, waren *per se* zu 10% apoptotisch und erhöhten den Zellkern-Import von GAPDH-GFP und und die Sensibilität auf durch Staurosporine oder MG132 induzierte Apoptose. Bcl-2 Ueberexpression vermindert den Kern-Import von GAPDH als auch Apoptose in nicht transfektierten, nicht aber in GAPDH-GFP transfektierten Zellen.

Kern-Import von zelleigenem Hsc70 oder überexprimiertem Hsc70-GFP wird nur während des Oxidativen Stresses, nicht aber während der Apoptose beobachtet. Ausserdem zeigen Hsc70-GFP überexprimierende Zellen verminderte Anfälligkeit gegenüber Effekten des Oxidativen Stresses, aber nicht gegenüber der Apoptose.

Aldolase und überexprimiertes Aldolase-GFP werden vorwiegend in Kernnähe und am Ansatz von Axonen im Cytoplasma exprimiert. Währendem sich die Aldolase-Expression nach Induktion von Oxidativem Stress im Kern erhöhte, wurde sie durch Apoptose weder in Zellen mit noch ohne Aldolase-GFP Ueberexpression beeinflusst.

Bei Oxidativem Stress translosziert Ulip vom Cytoplasma in den Kern, währenddem Ulip-GFP auch häufig in intrazellulären Aggregaten zu finden ist.

Von den fünf Proteinen des PMO Komplexes, zeigt die cytoplasmische Exxpression von Enolase die geringsten stress-induzierten Veränderungen.

Die gleichzeitige Ueberexpression verschiedener dieser PMO Komponenten steigerte den Kern-Import während des Oxidativen Stresses zusätzlich.

Wir schliessen aus dieser Studie, dass die Translokation der PMO assoziierten Proteine, speziell von GAPDH und Hsc70, eine bedeutende Rolle während der Apoptose und des Oxidativen Stresses spielen. Zudem können die Effekte dieser Proteine bei Ueberexpression scheinbar nicht durch Bcl-2 verhindert werden

# 2 <u>Introduction</u>

## 2.1 <u>Oxidative stress</u>

During the course of evolution, aerobic organisms adapted to oxygen, partially by using oxygen as an electron acceptor in the process of generating energy. However, reactive oxygen species (ROS) are formed as by-products in this process. These ROS include the superoxide anion, the hydroxyl radical, the oxygen singlet and hydrogen peroxide. Superoxide anions originate from a single electron transfer to molecular oxygen. They have a relatively short diffusion radius inside the cell but may be converted by superoxide dismutase to hydrogen peroxide, the most stable and diffusible ROS. Aerobic organisms are therefore equipped with a large enzymatic and non-enzymatic anti-oxidant system, in order to protect other cellular components against the harmful effects of these reactive oxygen metabolites. Under some conditions however, ROS are generated in such quantities that the anti-oxidants capacities are insufficient, leading to situations described as oxidative stress. All aerobic cells are subject to endogenous oxidative stress. This process implicates reactions with $O_2$ or ROS. In several biological processes ROS are produced in a controlled fashion. These species are able to control gene regulation through the activation of transcription factors that are dependent on the cellular redox state (Abate et al., 1990, Demple and Amabile-Cuevas, 1991, Schreck et al., 1992). However, uncontrolled production of ROS leads to oxidative stress, resulting in cellular damage, because ROS can react with and damage cellular macromolecules including DNA, proteins and lipids (Ames et al., 1993, Ames et al., 1995, Cerutti, 1985, Shigenaga et al., 1994, Stadtman, 1992).

Oxygen intermediates act as signal transducers and represent a versatile cellular control mechanism for gene regulation. Earlier evidence has shown that the redox environment of the cell plays a regulatory role in controlling the activation and DNA binding of several transcription factors (Abate et al., 1990, Schreck et al., 1992, Schulze-Osthoff et al., 1992). The first inducible transcription factors identified in this context were the proto-oncogenes c-fos and c-jun which function co-operatively in signal transduction processes (Abate et al., 1990). Their protein products, Fos and Jun, form a heterodimeric complex that interacts with the DNA regulatory element known as the activator protein-1 (AP-1) binding site. Dimerisation occurs via interaction between leucine zipper domains and serves to bring into proper juxtaposition a region in each protein that is rich in basic amino acids and that forms a DNA-binding domain. DNA binding of the Fos-Jun heterodimer was modulated by reduction of a single conserved cysteine residue in the DNA-binding domains of the two proteins. Furthermore, a nuclear protein was identified that reduced Fos and Jun and stimulated DNA-binding activity *in vitro*. This raises the possibility that transcriptional activity mediated by AP-1 binding factors is regulated by a redox mechanism.

Evidence for redox regulation was provided by studies on the tumour necrosis factor $\alpha$ (TNF$\alpha$)-mediated cytotoxicity. Inhibitors with different sites of action modulated TNF$\alpha$ cytotoxicity, however, with contrasting effects on final cell viability (Schulze-Osthoff et al., 1992). Inhibition of mitochondrial electron transport at complex III (cytochrome c reductase) by antimycin A resulted in a marked potentiation of TNF$\alpha$-mediated injury. In contrast, when the electron flow to ubiquinone was blocked, either at complex I (NADH- ubiquinone oxidoreductase) with amytal or at complex II (succinate-ubiquinone reductase) with thenoyltrifluoroacetone, cells were markedly protected against TNF$\alpha$ cytotoxicity. Neither uncouplers nor inhibitors of oxidative phosphorylation nor inhibitors of complex IV (cytochrome c oxidase) interfered significantly with TNF$\alpha$-mediated effects, ruling out the involvement of energy-coupled phenomena. In addition, the toxic effects of TNF$\alpha$ were counteracted by the addition of antioxidants and iron chelators. Treatment of cells with TNF$\alpha$ led to an early degeneration of the mitochondrial ultrastructure without any pronounced damage of other cellular organelles. Analysis of the mitochondrial electron flow revealed that TNF$\alpha$ treatment led to a rapid inhibition of the mitochondria to oxidise succinate and NADH-linked substrates. Different effects observed with the mitochondrial respiratory chain inhibitors provided evidence that mitochondrial production of oxygen radicals is a causal mechanism of TNF$\alpha$ cytotoxicity.

Oxygen radicals also play an important role in the activation of NF-$\kappa$ B and HIV-1 (Schreck et al., 1992). Dithiocarbamates which are considered for the treatment of AIDS and neurodegenerative diseases can potently block the activation of nuclear factor kappa B (NF-$\kappa$ B), a transcription factor involved in human immunodeficiency virus type 1 (HIV-1) expression, signalling, and activation of immediate early genes during inflammatory processes. Micromolar amounts of the pyrrolidine derivative of dithiocarbamate (PDTC reversibly suppressed the release of the inhibitory subunit I$\kappa$B from the latent cytoplasmic form of NF-$\kappa$ B in cells treated with phorbol ester, interleukin 1, and tumour necrosis factor $\alpha$, whereas other DNA binding activities and the induction of AP-1 by phorbol ester were not affected. The antioxidant PDTC also blocked the activation of NF-$\kappa$ B by bacterial lipopolysaccharide (LPS), also suggesting a role of oxygen radicals in the intracellular signalling of LPS. Further, treatment of pre-B and B cells with LPS induced the production of $O^{2-}$ and $H_2O_2$. PDTC prevented specifically the $\kappa$ B-dependent transactivation of reporter genes under the control of the HIV-1 long terminal repeat and simian virus 40 enhancer.

Another report also showed that mitochondria-derived ROS intermediates are not only cytotoxic but, in addition, are required in their function as signal transducers of TNF$\alpha$-induced gene expression (Schulze-Osthoff et al., 1993). The activation of NF$\kappa$B could be blocked by interference with the mitochondrial electron transport system. Furthermore, antimycin A, a mitochondrial inhibitor that increases the generation of ROS, potentiated TNF$\alpha$-triggered NF$\kappa$B activation. Further subclones which lacked a functional respiratory chain and were therefore depleted of the mitochondrial oxidative metabolism, resulted in resistance towards TNF$\alpha$ cytotoxicity, as well as in inhibition of NF$\kappa$B activation and interleukin-6 gene induction by TNF$\alpha$. This demonstrates that mitochondria serve as common mediators of the TNF$\alpha$-cytotoxic and gene-regulatory signalling pathways.

On the other hand, the involvement of ROS as causal effectors in apoptosis has been established (Shimizu et al., 1996, Slater et al., 1995b, Slater et al., 1995a)**.** It was shown that one of the most reproducible inducers is mild oxidative stress (e.g. via exposure to hydrogen peroxide, redox-cycling quinones or thiol-alkylating agents) (Slater et al., 1995b, Slater et al., 1995a). It had also been observed that oxidative stress more readily modifies proteins and lipids in cells undergoing apoptosis in response to non-oxidative stimuli such as glucocorticoids or topoisomerase II inhibitors than in normal cells. Further, apoptosis was typically accompanied in its initial steps by a depletion of intracellular reduced glutathione (GSH). Pre-treatment of cells with antioxidants was shown to protect cells against programmed cell death.

Further, cell death due to reoxygenation after hypoxia was characterised in primary cultured hepatocytes (Shimizu et al., 1996). Reoxygenated hepatocytes revealed morphological characteristics of apoptosis, including chromatin condensation, nuclear fragmentation, and formation of apoptotic bodies. However, also few necrosis, defined by loss of plasma membrane integrity, mitochondrial swelling, and formation of large vacuoles, was observed. Production of oxygen radicals was enhanced by reoxygenation of hypoxic cells, and reoxygenation-induced apoptosis was inhibited by oxygen radical scavengers.

Concerning neurodegenerative disorders, such as Parkinson's and Alzheimer's disease, it is possible that a gradual impairment of cellular defence mechanisms leads to cell damage by apoptosis.

# 2.2 <u>Apoptosis</u>

Apoptosis is the most common form of physiological cell death (for recent reviews see (Adams and Cory, 1998, Ashkenazi and Dixit, 1998, Green, 1998, Green and Reed, 1998, Hofmann, 1999, Raff, 1998, Salvesen and Dixit, 1997, Thornberry and Lazebnik, 1998, Vaux, 1997, Vaux and Korsmeyer, 1999, Wolf and Green, 1999)) and plays an important role in animal development and homeostasis, controlling cell numbers in both vertebrate and invertebrate tissues (Oppenheim, 1991, Raff et al., 1993) Recently, several families of molecules that regulate apoptosis in different settings have been identified (for review, see (Hengartner and Horvitz, 1994)). The Ced-9$^{Bcl-2}$ family of apoptosis regulators is composed of a large number of intracellular proteins with opposing effects in regulating cell death. Some family members, including Bcl-2 (Bakhshi et al., 1985, Hengartner and Horvitz, 1994) and Bcl-xL (Boise et al., 1993), function to inhibit apoptosis, whereas other members such as Bax (Oltvai et al., 1993), Bcl-xS (Boise et al., 1993), Bad (Yang et al., 1995), and Bak (Chittenden et al., 1995, Farrow et al., 1995, Kiefer et al., 1995) function to promote apoptosis. It appears that homodimerization and heterodimerization between the various death-promoting and death-inhibiting family members regulates the activation of caspases, which execute the cell death program (Reed, 1997, Yang et al., 1995). Although most of the analysis of these molecules has been done in extraneural tissues, there is now compelling evidence that their actions are quite general including in neurones.

The time course of transcription factor expression in tissues undergoing apoptosis, as well as the effect of transcription and translation inhibitors on neuronal injury, suggest that some transcription factors may participate in the regulation of the destructive process (Hughes et al., 1997, Pittman et al., 1994). One such transcription factor is NF-κB. NF-κB is expressed in neurones and glia throughout the mammalian CNS (Kaltschmidt et al., 1993, Kaltschmidt et al., 1994) and can be activated by glutamate receptor agonists (Guerrini et al., 1995, Kaltschmidt et al., 1995). Increased NF-κB levels have recently been observed in areas of neuronal degeneration in animal models of ischemia, as well as in patients with Alzheimer's disease and Parkinson's disease (Kaltschmidt et al., 1997). Although recently it was shown that inhibition of NF-κB potentiates amyloid β-mediated neuronal apoptosis (Kaltschmidt et al., 1999), its role in the regulation of apoptosis is still rather controversial (Baeuerle and Baltimore, 1996, Baichwal and Baeuerle, 1997, Lin et al., 1995). Evidence suggesting that NF-κB protects dividing cells against apoptosis derives mainly from studies of tumour necrosis factor-induced cell death (Beg et al., 1993, Van

Antwerp et al., 1996) but has been observed in certain other situations, including an NF-κB p65 subunit knock-out animal model (Beg et al., 1993, Wu and Lozano, 1994).

The activation of cell death program is also responsible for pathological cell death in neurodegenerative disorders, including Alzheimer's disease (Thompson, 1995). Known elements of this program include members of the Bcl-2 gene family, Apaf-1, and proteases of the caspase family (Cohen, 1997, Reed, 1997, Reed, 1997, Salvesen and Dixit, 1997). Once thought to be merely the centre of cellular ATP production, mitochondria are increasingly implicated as sensors and executioners in the cell's decision to live or die  and may even influence the mode of cell death, necrosis or apoptosis, depending on their functional state (Reed, 1998, Reed et al., 1998). Mitochondria are capable of releasing pro-apoptotic factors into the cytosol, including apoptosis-inducing factor (AIF), which induces chromatin condensation and oligonucleosomal DNA fragmentation in isolated nuclei (Susin et al., 1999, Susin et al., 1998, Zamzami et al., 1998), and cytochrome c, which activates procaspase-9 and the caspase cascade with the help of Apaf-1 and (d)ATP (Li et al., 1998). What remains as yet unresolved is the mechanism by which pro-apoptotic factors are released into the cytosol. One candidate, the so-called mitochondrial permeability transition pore (PTP) (Marzo et al., 1998), is triggered by an increase in matrix $Ca^{2+}$, pro-oxidants, and mitochondrial depolarisation and is responsible for unspecific transport of low molecular weight products (<1.5 kDa) across the inner mitochondrial membrane (Zoratti and Szabo, 1995). Because this results in inner membrane permeability to protons, PTP is associated with a decrease in mitochondrial transmembrane potential (Zoratti and Szabo, 1995). The opening of PTP is probably not sufficient to release cytochrome c directly but could trigger cytochrome c release by causing mitochondrial swelling and/or rupture of the outer mitochondrial membrane (Vander Heiden et al., 1997).

A reduction in mitochondrial transmembrane potential has been observed in a number of models of apoptosis (Ankarcrona et al., 1996, Heiskanen et al., 1999, Wadia et al., 1998, Zamzami et al., 1998). On the other hand, however, studies in non-neuronal cells have suggested that this is not a primary event in apoptosis (Vander Heiden et al., 1997). Thus, although the importance of mitochondria in programmed cell death seems fairly clear with respect to the release of pro-apoptotic factors, the events preceding this release remain unresolved.

Reactive oxygen species (ROS) also act as mediators of cell death that occurs in mitotic cells during their normal turnover, in neurones during development of the nervous system, and in neurodegenerative

disorders (Benzi and Moretti, 1995, Mattson, 1996). Examples include the killing of lymphocytes by tumour necrosis factor and chemotherapeutic drugs (Schreck et al., 1991), trophic factor withdrawal-induced apoptosis of sympathetic neurones (Greenlund et al., 1995), and neuronal apoptosis induced by amyloid-β-peptide (Loo et al., 1993). Although these studies have documented increased signs of oxidative stress in cells undergoing apoptosis, the specific ROS involved, their subcellular sources, and their mode of action in inducing apoptosis are poorly known. Mitochondria, a major subcellular source of ROS (Dugan et al., 1995, Piantadosi and Zhang, 1996), may play pivotal roles in apoptosis (Kroemer et al., 1997). Alterations occur in mitochondria before nuclear manifestations of apoptosis, including impairment of energy charge and redox state, disruption of mitochondrial transmembrane potential, permeability transition, and release of cytochrome C (Zamzami et al., 1996a). Radical scavengers, thiol reducing agents, and cyclosporin A block both mitochondrial permeability transition and apoptosis in several paradigms (Marchetti et al., 1996, Zamzami et al., 1996b), suggesting essential roles for mitochondrial ROS generation and permeability transition in apoptosis. Superoxide anion radical is the major ROS generated in mitochondria and can interact with nitric oxide (NO) to form peroxynitrite, which may damage cells by promoting membrane lipid peroxidation and nitration of proteins on tyrosine residues (Beckman and Crow, 1993). NO donors and peroxynitrite can induce, and NO synthase inhibitors can prevent, apoptosis in many types of cultured cells including neurones (Estevez et al., 1995, Szabo, 1996). Superoxide accumulation is prevented by its conversion to hydrogen peroxide, a process catalysed by the superoxide dismutases Cu/ZnSOD and MnSOD (Weisiger and Fridovich, 1973). Correlation between expression of mitochondrial MnSOD and increased resistance to cell injury and death have been established in several paradigms, including resistance of tumour cells to killing by TNFα (Wong and Goeddel, 1988) and resistance of cardiac myocytes treated with TNFα to ischemic injury (Nelson et al., 1995). Despite such correlation, it is not known whether and how mitochondrial MnSOD exerts its anti-apoptotic function.

Recent evidence implicates the mitochondrion as a critical site at which different apoptotic signals converge. Findings in some non-neuronal models of cell death suggest that a death signal induces translocation of a BH3 (homology domain)-containing, pro-apoptotic Bcl-2 family member to the mitochondria, followed by the release of mitochondrial proteins, such as cytochrome c, via an unknown mechanism that may involve the permeability transition pore (PTP) and/or a channel formed by pro-apoptotic Bcl-2 family proteins (Gross et al., 1999, Li et al., 1998, Luo et al., 1998, Shimizu et al., 1999). Once released, cytochrome c forms a complex with Apaf-1 and procaspase-9, which in the presence of

ATP or dATP, becomes activated, resulting in further caspase activation, cleavage of cellular substrates, and cell death.

Bcl-2 is a widely expressed cytoplasmic protein that plays a key role in regulating cell survival in the immune system and nervous system. Mice with targeted null mutations in the Bcl-2 gene have markedly reduced numbers of B and T cells attributable to increased apoptosis (Nakayama et al., 1994, Nakayama et al., 1993, Veis et al., 1993), whereas mice carrying a transgene causing high levels of Bcl-2 expression in the immune system show extended survival of B and T cells (McDonnell et al., 1989, McDonnell et al., 1990). Overexpression of Bcl-2 in cultured neurones prevents their death after neurotrophin deprivation (Allsopp et al., 1993, Garcia et al., 1992), and mice expressing a Bcl-2 transgene under the control of neurone-specific enolase promoter have increased numbers of neurones in several regions (Martinou et al., 1994). The survival response of cultured cranial sensory neurones to neurotrophins during the phase of naturally occurring neuronal death is markedly reduced by antisense Bcl-2 RNA (Allsopp et al., 1995). Likewise, cranial sensory neurones from Bcl-2(-/-) embryos do not survive *in vitro* with neurotrophins as well as wild-type embryos during the peak period of naturally occurring neuronal death and are lost to a greater extent than wild-type neurones during this period of development *in vivo* (Pinon et al., 1997). Sympathetic neurones from postnatal Bcl–2(-/-) mice die more rapidly after nerve growth factor (NGF) deprivation *in vitro* than wild-type neurones (Greenlund et al., 1995), and postnatal Bcl-2(-/-) mice have significantly fewer sensory, autonomic, and motor neurones than wild-type mice (Michaelidis et al., 1996). Furthermore, Bcl-2 is structurally and functionally similar to the ced-9 gene product of *Caenorhabditis elegans* that also prevents programmed cell death (Hengartner and Horvitz, 1994). Recently, Bcl-2 has been shown to prevent both apoptotic and necrotic cell death induced by a variety of stimuli in several systems (e.g. (Rosse et al., 1998, Shimizu et al., 1999, Zhivotovsky et al., 1998); for review, see (Allen et al., 1998, Chao and Korsmeyer, 1998))

In addition Bcl-2 also influences neuronal differentiation. Its overexpression in a neural crest-derived line enhances neurite outgrowth and increases the expression of neurone-specific enolase (Zhang et al., 1996). Midbrain-derived dopaminergic lines stably expressing Bcl-2 extended longer neurites than control-transfected cells (Oh et al., 1996), and Bcl-2 enhances the differentiation of the PC12 cells grown in serum-free conditions (Batistatou et al., 1993).

# 2.3 <u>PMO</u>

It is known that transplasma membrane electron transport, which exists in both plant and animal cells (reviewed in Barr et al., 1991, Barr et al., 1988, Brightman et al., 1992, Crane, 1989b, Crane et al., 1989a, Crane et al., 1991, Dreyer, 1990), may play an important role in the response mechanisms to oxidative stress and in apoptosis. The nature and components of the electron transport system and the mechanism by which proton release is activated is only poorly understood to date. Reduced pyridine nucleotides are substrates for the plasma membrane dehydrogenases. Oxidants such as ferricyanide (FeCN) are used to probe the activity. Stimulation of electron transport with impermeable oxidants and hormones activates proton release from cells. Inhibitors of electron transport, such as certain anti-tumour drugs, inhibit proton release. In some cells transmembrane electron transport has been shown to cause cytoplasmic pH changes or to stimulate protein kinases which may be the basis for activation of proton channels in the membrane. The redox-induced proton release causes internal and external pH changes which can be related to stimulation of animal and plant cell growth by external, impermeable oxidants or by oxygen.

More evidence that the transmembrane electron transport is associated with proton release involved in internal pH control was given by studies in Tetrahymena (Barr et al., 1991). Transmembrane ferricyanide reduction by Tetrahymena was not inhibited by mitochondrial inhibitors such as antimycin A, 2-n-heptyl-4- hydroxyquinoline N-oxide, or potassium cyanide, but it responded to inhibitors of glycolysis. Thus, transmembrane ferricyanide reduction by Tetrahymena appears to involve a plasma membrane electron transport chain similar to those of other animal cells.

NADH/acceptor oxidoreductase activities using oxygen as electron acceptor have been demonstrated most unambigously with isolated plasma membranes. NADH oxidase activity of plasma membranes was stimulated by growth factors and hormones 2- to 3-fold. In contrast, NADH oxidase was inhibited up to 80% by several agents known to inhibit growth or induce differentiation, like retinoic acid, calcitriol, and the monosialoganglioside, GM3. The growth factor-responsive NADH oxidase of isolated plasma membranes was not inhibited by common inhibitors of oxidoreductases of endoplasmic reticulum or mitochondria. As well, NADH oxidase of the plasma membrane was stimulated by concentrations of detergents which strongly inhibited mitochondrial NADH oxidases and by lysophospholipids or fatty acids. Growth factor-responsive NADH oxidase, however, was inhibited greater than 90% by chloroquine and quinone analogues. Addition of coenzyme Q10 stimulated the activity and partially reversed the

14

analogue inhibition. Coenzyme Q is an important electron and proton carrier within the lipid phase of membranes (Crane and Navas, 1997, Crane et al., 1994). The first function of coenzyme Q was defined in the energy transduction process in mitochondria. Later it was shown that the presence of coenzyme Q in other cellular membranes has dynamic rather than passive significance. Coenzyme Q functions in the plasma membrane electron transport involved in the activation of signalling protein kinases related to gene activation for cellular proliferation. Furthermore, the antioxidant potential of the reduced coenzyme Q is significant in the evidence that the reduced quinone can act to maintain tocopherol in the reduced state in membranes and ascorbate reduced both inside and outside the cell.

Very recent findings suggest the potential participation of the plasma membrane NADH oxidase as a terminal oxidase of plasma membrane electron transport from cytosolic NAD(P)H via naturally occurring hydroquinones to acceptors at the cell surface (Kishi et al., 1999).

Although electron transport across biological membranes is a well-known feature of bacteria, mitochondria and chloroplasts, where it provides motive forces for vectorial transport processes, electron transport is generally not found in the plasma membrane of eukaryotic cells, because it would possibly interfere with electric processes at the plasma membrane. An exception is provided by the phagocyte NADPH oxidase, which generates superoxide through electron transfer from cytosolic NADPH to extracellular oxygen (Brightman et al., 1992). The enzyme is essential for host defence, and patients with chronic granulomatous disease, who lack the functional enzyme, suffer from severe infections.

Neutrophils possess a unique membrane-associated NADPH oxidase system, which only becomes activated upon exposure to the appropriate stimuli and catalyses the one-electron reduction of molecular oxygen to superoxide, $O_2^-$ (Umeki, 1994). Oxidase activation involves the assembly of membrane-bound and cytosolic constituents of the oxidase system, which are disassembled in the resting state. The oxidase system consists of two plasma membrane-bound components: a low-potential cytochrome b558 and a flavoprotein related to the electron transport between NADPH and heme-binding domains of the oxidase. Recent reports have indicated that FAD-binding sites of the oxidase are contained in cytochrome b558 (flavocytochrome b558). Cytosolic components are known to translocate to the plasma membrane, ensuring assembly of an active $O_2(-)$-generating NADPH oxidase system. Further, the membrane (Raps) and cytosolic (Racs) GTP-binding proteins have been established as essential to oxidase assembly. In

summary this oxidase is controlled by hormones, growth factors and other ligands which bind to receptors in the plasma membrane, as well as by oncogenes.

The electrogenic nature of electron transfer by the NADPH oxidase was demonstrate by using the whole-cell patch-clamp technique (Schrenzel et al., 1998). It was the first study to demonstrate electron currents across the plasma membrane of a eukaryotic cell. This generation of electron currents by the NADPH oxidase was shown in human eosinophil granulocytes. The currents were absent in granulocytes of sufferers of chronic granulomatous disease and under conditions of low oxygen. Generation of electron currents across the plasma membrane of eukaryotic cells had not been observed previously and might be, independently of the generation of superoxide, a physiologically relevant function of the phagocyte NADPH oxidase. The precise functions of the NADPH oxidase in host defence remain to be defined, however. Interestingly NADPH oxidase can generate large currents, even against major electrical gradients.

Several studies investigated the role of PMOs in the antioxidant defence of the brain to oxidative stress (reviewed in (May, 1999, Wilson, 1997)). Oxidative injury has been implicated in degenerative diseases, epilepsy, trauma, and stroke. It is a threshold phenomenon that occurs after antioxidant mechanisms are overwhelmed. Oxidative stress is initiated by numerous factors: acidosis; transition metals; amyloid β-peptide; the neurotransmitters dopamine, glutamate, and nitric oxide; and uncouplers of mitochondrial electron transport. Antioxidant defences include the enzymes superoxide dismutase, glutathione peroxidase, and catalase, as well as the low molecular weight reductants α- tocopherol (vitamin E), glutathione, and ascorbate (reduced vitamin C). Cells like astrocytes maintain high intracellular concentrations of certain antioxidants, making these cells resistant to oxidative stress relative to oligodendrocytes and neurones. Following reactive gliosis, the neuroprotective role of astrocytes may be accentuated because of increases in a number of activities: expression of antioxidant enzymes; transport and metabolism of glucose that yields reducing equivalents for antioxidant regeneration and lactate for neuronal metabolism; synthesis of glutathione; and recycling of vitamin C. In the latter process, astrocytes take up oxidised vitamin C (dehydroascorbic acid, DHAA) through plasma membrane transporters, reduce it to ascorbate, and then release ascorbate to the extracellular fluid, where it may contribute to antioxidant defence of neurones. Vitamin C can also interact with the plasma membrane by donating electrons to the α-tocopheroxyl radical and a trans-plasma membrane oxidoreductase activity. Ascorbate-derived reducing capacity is thus transmitted both into and across the plasma membrane.

Recycling of α-tocopherol by ascorbate helps to protect membrane lipids from peroxidation. The oxidoreductase activity has typically been studied using extracellular ferricyanide as an electron acceptor. Whereas an NADH-ferricyanide reductase activity is evident in open membranes, ascorbate is the preferred electron donor within cells. The oxidoreductase may be a single membrane-spanning protein or may only partially span the membrane as part of a trans-membrane electron transport chain composed of a cytochrome or even hydrophobic antioxidants such as α-tocopherol or ubiquinol-10. Proposed functions for the oxidoreductase include stimulation of cell growth, reduction of the ascorbate free radical outside cells, recycling of α-tocopherol, reduction of lipid hydroperoxides, and reduction of ferric iron prior to iron uptake by a transferrin-independent pathway. Diferric transferrin and ceruloplasmin which stimulate proliferation also stimulate membrane oxidase activity measured by the reduction of ferricyanide. The oxidants activate growth-related signals such as cytosolic alkalinisation and calcium mobilisation. Antiproliferative agents such as adriamycin and retinoic acid inhibit the plasma membrane electron transport (for reviews see Crane et al., 1994, Medina et al., 1997, Rauchova et al., 1995).

Our group recently identified and characterised a new trans-plasma-membrane NADH-dichlorophenol-indophenol oxidoreductase (PMO) in neuronal synaptic plasma membranes, in synaptic vesicles and in the murine neuroblastoma cell line NB41A3 (Yong and Dreyer, 1995, Yong and Dreyer, 1995, Zurbriggen and Dreyer, 1994, Zurbriggen and Dreyer, 1996). We were able to purify this PMO from bovine brain, rat brain and from NB41A3 cells (Bulliard et al., 1997). Several purification steps were performed to isolate the PMO activity: protein extraction with detergents, (NH4)2SO4 precipitation, stringent chromatography and native PAGE. Finally enzyme activity could be attributed to a very tight complex of several proteins that could not be separated except by SDS/PAGE. By SDS/PAGE we were able to isolate and identify five components: Hsc70, Ulip (TOAD-64), glyceraldehyde-3-phosphate dehydrogenase (GAPDH), brain specific enolase γ and brain specific aldolase c (zebrin II). The association of PMO in a tight complex was confirmed by its immunoprecipitation from extracts of NB41A3 using antibodies directed against any of the five proteins of the complex followed by immunodetection with antibodies directed against the other members.

Little is known about the molecular mechanism and about the proteins involved in the response to elevated ROS concentrations during the oxidative stress. Therefore we wanted to characterise in more detail the function of each of the 5 proteins that are aggregated in the neuronal PMO complex.

# 2.3.1 <u>GAPDH</u>

The major component of the PMO complex, glyceraldehyde-3-phosphate dehydrogenase (GAPDH), is a tetramer composed of four identical 37 kDa subunits. It is a central glycolytic protein with pivotal role in energy production. It was used as a paradigm not only for analysis of protein structure and function but also for model studies on gene structure and expression. Recent studies demonstrated that GAPDH or some of its isoforms (>200) display a number of activities unrelated to its glycolytic function as a dehydrogenase.

Initial studies identified the structural association of GAPDH with cell membranes (Allen et al., 1987, Kliman and Steck, 1980, Lin and Allen, 1986, Tsai et al., 1982). Two-dimensional gel electrophoresis were used in theses investigations to detect a series of GAPDH variants. It was shown that GAPDH colocalised with the band 3 anion exchanger protein in erythrocytes (Ercolani et al., 1992). Its glycolytic activity was diminished by its protein-protein interaction. Competition was observed with $NAD^+$. Later studies revealed a functional role for GAPDH in membrane fusion (Glaser and Gross, 1995). Facilitated membrane fusion by plasmenylethanolamine was catalysed by GAPDH in a highly plasmenylethanolamine- and cholesterol-specific manner. Intriguingly, these investigations suggested that an isoform of GAPDH, lacking its glycolytic dehydrogenase activity, was the active species. GAPDH fusogenic activity was inhibited by glyceraldehyde-3-phosphate but not by koningic acid, an effective inhibitor of the dehydrogenase activity. Further, the composition of synthetic phospholipid membranes influenced both the binding and fusogenic capacity of rabbit GAPDH (Kaneda et al., 1997). This results were substantiated by the finding that under physiological conditions the GAPDH isoform bound to naturally occurring membranes and was able to fuse them (Han et al., 1998). Furthermore, another group identified GAPDH as a $Ca^{2+}$ -dependent fusogen in human neutrophil cytosol (Hessler et al., 1998). In neutrophil degeneration membrane fusion is required for invagination of the plasma membrane to engulf foreign particles. Robbins provided the first mutational evidence to demonstrate the role of GAPDH in membrane fusion (Robbins et al., 1995).

GAPDH was identified as a tubulin binding protein, catalysing tubulin bundling into microtubule bundles (Durrieu et al., 1987, Durrieu et al., 1987, Kumagai and Sakai, 1983, Muronetz et al., 1994). Tubulin bundling by GAPDH, which was able to modulate the cytoskeletal structure, was inhibited by ATP (Huitorel and Pantaloni, 1985). The functional role of tubulin-bound GAPDH was demonstrated by

analysis of mutant CHO cells deficient in endocytosis (Robbins et al., 1995). It was shown that a mutation in microtubule-associated GAPDH was causing the deficiency.

GAPDH was identified as a specific mRNA binding protein in experimental protocols used to identify specific proteins that interact with either cellular or viral 5'-UTR or 3'-UTR mRNA sequences (De et al., 1996, Nagy and Rigby, 1995, Schultz et al., 1996). These sequences seem to be important for the translational regulation of gene expression and are necessary for viral infection of eukaryotic cells. Competition experiments indicated that GAPDH-RNA binding was inhibited by poly(U) or $NAD^+$. These results suggest the involvement of the $NAD^+$ binding site within GAPDH. Furthermore GAPDH increases the activity of TNF$\alpha$ *in vitro* and *in vivo*. Its binding to GAPDH was inhibited by $NAD^+$ and ATP (Sioud and Jespersen, 1996).

Initial investigations identified GAPDH as a DNA binding protein (Tsai and Green, 1973) and as a non-histone nuclear protein important in enhancement of gene expression (Morgenegg et al., 1986). Recent studies have indicated more nuclear functions of GAPDH in mammalian cells. Singh and Green identified GAPDH as a nuclear tRNA export protein (Singh and Green, 1993). Normal and export-defective tRNA were used in mobility shift assays to purify GAPDH as the export protein. Human erythrocyte GAPDH exhibited tRNA binding that was competitively inhibited by $NAD^+$.

Investigating the role of $A_{P4}A$ in DNA replication and DNA repair with the help of photoaffinity probes, GAPDH was identified as $A_{P4}A$ binding protein (Baxi and Vishwanatha, 1995). The physiological significance of this $Mg^{2+}$ dependent interaction is indicated by previous studies demonstrating the physical association of mammalian GAPDH with replicating DNA (Lee and Sirover, 1989). Radiolabeling with ($^{35}S$)methionine demonstrated that the biosynthesis of nuclear GAPDH paralleled its DNA association. Different studies indicate a role of GAPDH in DNA repair. Initially, nuclear GAPDH was identified as a uracil DNA glycosylase (UDG) based on its ability to release uracil from a poly(dA)-poly(dU) substrate (Meyer-Siegler et al., 1991). This report was confirmed by findings that the purified $A_{P4}A$ binding protein exhibited UDG activity (Baxi and Vishwanatha, 1995). Physiological significance was demonstrated *in vivo* showing that human cells, treated with 2,3,7,8-tetrachlorodibenzo-p-dioxin (TCDD), increased GAPDH gene transcription and translation.

Several independent studies provide evidence that mammalian GAPDH exhibits phosphotransferase/kinase activity and described autophosphorylation of GAPDH (Duclos-Vallee et al.,

1998, Kawamoto and Caswell, 1986, Wu et al., 1997). One of these studies demonstrate that GAPDH may also phosphorylate other proteins. It was suggested that GAPDH is a cellular kinase which might interfere in the life-cycle of hepatitis B virus (HBV). Other roles for GAPDH in phosphate group transfer recently discovered, related to its phosphorylation by a number of cellular protein kinases, including protein kinase C, epidermal-growth-factor kinase and $Ca^{2+}$/calmodulin-dependent protein kinase II (Ashmarina et al., 1988, Engel et al., 1998, Reiss et al., 1996, Reiss et al., 1986, Reiss et al., 1996, Reiss and Schwartz, 1987, Sergienko et al., 1992).

Furthermore, GAPDH is known to be a specific target of nitric oxide (NO), which catalyses the non-enzymatic covalent modification of GAPDH by $NAD^+$ (Brune and Lapetina, 1995, Brune and Lapetina, 1996, McDonald and Moss, 1993, McDonald and Moss, 1994).

Initial indications for the role of GAPDH in apoptosis were demonstrated first in cerebellar granular cells (Ishitani and Chuang, 1996a, Ishitani et al., 1996c, Ishitani et al., 1996b, Ishitani et al., 1997, Sunaga et al., 1995). Mature cerebellar granular cells underwent an age-induced apoptotic death in culture between day 15 and day 17 *in vitro*. This apoptosis was closely associated with an enhanced level of 38-kDa protein in the particulate fraction, which was identified as GAPDH. Moreover, GAPDH antisense, but not sense, oligodeoxyribonucleotides specifically suppress the age-induced accumulation of GAPDH mRNA and protein before apoptotic neuronal cell death. GAPDH overexpression in the particulate fraction has also been implicated in ara-C and low potassium chloride-induced apoptosis. Analysis of the subcellular regulation of GAPDH during apoptosis showed that overexpressed GAPDH in cells undergoing apoptosis is localised in the nuclear compartment (Ishitani et al., 1998, Saunders et al., 1999, Sawa et al., 1997). This was established using cell fractionation coupled with immunoblot analysis or immunocytochemistry to detect the presence of nuclear GAPDH. Antisense GAPDH studies demonstrated that its inhibition of apoptosis precluded the appearance of nuclear GAPDH. Furthermore the absence of GAPDH glycolytic activity subsequent to its translocation into the nucleus was demonstrated by enzymatic analysis.

Recently it was shown that GAPDH exerts a very interesting role in neurodegenerative disease. Studies have identified interrelated characteristics of a series of age-related, autosomal dominant, neurodegenerative disorders (Albin and Tagle, 1995, Gusella and MacDonald, 1996, Nasir et al., 1996). They are characterised by the expansion of CAG repeats in the coding region of the primary gene defective in the respective disorder. The resulting mutant protein containing polyglutamine tracts in its N-

20

terminal region are detected in a wide variety of cells. Since disruption of the respective gene does not result in the abnormal phenotype (Ambrose et al., 1994, Mangiarini et al., 1996), it was hypothesised that the molecular mechanisms that underlie each disease are based on a gain of function involving protein-protein interaction. Studies have identified GAPDH binding as a specific protein-protein interaction in each disorder. These include its binding to huntingtin, the gene product deficient in Huntington's disease (HD) (Burke et al., 1996); atrophin, the gene product deficient in dentatorubral-pallidoluysian atrophy (DRPLA) (Burke et al., 1996); ataxin, the molecular defect in spinocerebellar ataxia type-1 (Koshy et al., 1996); and the androgen receptor, the gene product which underlies spinobulbar muscular atrophy (Koshy et al., 1996). In each case, high affinity binding of GAPDH was demonstrated by yeast two-hybrid studies and by *in vitro* analysis.

The pathology of HD is marked by a preferential loss of neurones in the striatum and cortex (Cudkowicz and Kowall, 1990, de la Monte et al., 1988, Graveland et al., 1985, Myers et al., 1991). The genetic mutation in HD is an unstable and expanded CAG repeat in the gene that encodes huntingtin (Group, 1993). The CAG triplet repeat produces a poly-glutamine domain in the expressed proteins. Larger poly-glutamine expansions in huntingtin are associated with earlier onset and increased severity of the disease (Duyao et al., 1993, Stine et al., 1993). A pathogenic process involving interaction of mutant huntingtin with other proteins to produce a change of function has been suggested as the basis for neurodegeneration in HD. GAPDH has been identified as one of the proteins that interact more avidly with NH2-terminal products of mutant huntingtin than with wild-type (Burke et al., 1996). Analysis of the HD brain with an antiserum that recognises an internal region of huntingtin in wild-type and mutant proteins showed that the subcellular distribution of huntingtin in the cytoplasm of neurones was abnormal, but the contribution of mutant huntingtin to these changes was unclear. Finally in a recent study of HD transgenic mice expressing an NH2-terminal mutant huntingtin fragment with 115 to 156 glutamine repeats, it was found that intraneuronal nuclear inclusions reactive to NH2-terminal antiserum to huntingtin developed in the brain (Davies et al., 1997).

Studies showing interactions between β-amyloid precursor protein (βAPP) and GAPDH (Schulze et al., 1993) indicate another role of GAPDH, namely in apoptosis. βAPP has been intensively described in studies with Alzheimer's Disease (Checler, 1995, Selkoe, 1994). βAPP is a membrane bound protein containing a cytoplasmic tail. Its improper cytoplasmic processing results in the formation of a β-amyloid

protein (βAP) which is deprived of the carboxyterminal end of βAPP. There is ample evidence that βAP is a major factor in the formation of senile plaques in Alzheimer's Disease.

Recent work by Kratgen et al. indicates that GAPDH may also be involved in Parkinson's disease. They showed that GAPDH is the putative target of the anti-apoptotic compounds CGP 3466 and R-(-)-deprenyl. R-(-)-Deprenyl (Selegiline) represents one of the drugs currently used for the treatment of Parkinson's disease. The compound was shown to protect neurones or glia cells from programmed cell death in a variety of models. CGP 3466 is a structurally related analogue of R-(-)-deprenyl that exhibits virtually no monoamine oxidase type B inhibiting activity but is neuro-protective in the picomolar concentration range. Specific binding of CGP 3466 to GAPDH was shown by means of affinity binding, affinity labelling, and BIAcore(R) technology. The importance of this interaction for mediating drug-induced inhibition of programmed cell death was established by apoptosis assays in the human neuroblastoma cell line PAJU.

In contrast to the definitive studies described above, the specific role of GAPDH in the phenotype of these disorders is unknown at the present time. A proposed scenario is that GAPDH binding to each protein diminishes glycolytic activity. As neuronal cells depend on glycolysis for ATP production, such inhibition would have severe consequences *in vivo*. Recent studies suggest that GAPDH glycolytic activity was unaltered in brain samples from patients with CAG triplet repeat disorders (Kish et al., 1998). In contrast, studies in fibroblasts from Huntington's disease patients indicated a difference in their regulation of GAPDH dehydrogenase activity (Cooper et al., 1998). GAPDH glycolytic catalysis increased 8-fold in control cells but only 3-fold in Huntington's disease cell strains. Other studies indicate normal GAPDH activity in Huntington's disease brain (Tabrizi et al., 1999). Another possibility examined was the effect of transglutaminase on GAPDH. This analysis demonstrates inhibition of GAPDH dehydrogenase activity (Cooper et al., 1997).

In summary, these recent studies demonstrate selective interactions of GAPDH with proteins intimately involved in neurodegenerative disease. However, at this time the functional consequences of these interactions are unknown.

Finally a function of GAPDH in cellular phenotype of prostate cancer has been proposed by studies that quantified GAPDH mRNA levels in rat prostatic adenocarcinoma cell lines in comparison with normal rat ventral tissue, showing high GAPDH mRNA levels in highly metastatic cells (Epner et al., 1993). Investigations using patient samples also demonstrated that GAPDH mRNA levels were greater in neoplastic tissue than in benign prostate tissue (Sharief et al., 1994). Recent studies have described further changes in GAPDH gene expression in prostatic cancer cells and showed that androgen responsive human prostate cancer cells regulate both GAPDH mRNA and GAPDH glycolytic activity as a function of hormone exposure (Epner and Coffey, 1996, Ripple and Wilding, 1995).

## 2.3.2 <u>Ulip</u>

The second protein of the neuronal PMO complex that we have described (Bulliard et al., 1997) was a member of the Ulip (Unc-33-LIke Phosphoprotein) family. Investigations by several independent groups identified unknown proteins which all belong to this common phosphoprotein family. The encoding genes of their members show homology to liver dihydropyrimidinase (DHPase) (Wang and Strittmatter, 1997) and to the unc-33 gene from *Caenorhabditis elegans*, a gene associated with neuritic outgrowth and axonal guidance (Desai et al., 1988, Li et al., 1992, McIntire et al., 1992). The Ulip family is highly conserved throughout evolution. The various members of the family within a single species display about 75% similarity. There exist highly similar domains and subdomains, including a 32-aminoacid region highly conserved from bacterial hydantoinase to human Ulips. The first identification of a member of this family resulted from a search for proteins whose expression was regulated as an early marker of differentiated neurones in the rat cortex and in the rat spinal cord (Geschwind et al., 1996, Minturn et al., 1995b, Minturn et al., 1995a). Using two-dimensional gel electrophoresis, membrane-associated proteins that were up-regulated over the course of neurogenesis were identified. One of these, TOAD-64 (Turned On After Division, 64 kDa), was expressed early in neuronal differentiation and was dramatically down-regulated in the adult. In later studies it was shown, that TOAD-64 corresponds to Ulip2 (Byk et al., 1998). Northern blot and *in situ* hybridisation showed that TOAD-64 mRNA was enriched in the nervous system and is developmentally regulated in parallel with the protein. TOAD-64 is transiently expressed in postmitotic spinal cord neurones early in their development and sharply down-regulated after the second postnatal week. In the adult spinal cord, TOAD-64 expression is remarkably restricted to a subset of

primary afferents to the spinal cord. It was suggested that TOAD-64 may have a fundamental role in axon pathfinding.

This hypothesis was substantiated by the results of Goshima et al. with another protein corresponding to Ulip2 (Goshima et al., 1995). They used a Xenopus laevis oocyte expression system to identify molecules involved in collapsin signalling. Collapsin, a member of the semaphorin family, contributes to axonal pathfinding during neural development by inhibiting growth cone extension. They isolated a collapsin response mediator protein (CRMP-62) required for collapsin-induced inward currents. CRMP-62 (=Ulip2) was localised exclusively in the developing chick nervous system. Introduction of anti-CRMP-62 antibodies into dorsal root ganglion neurones blocked collapsin-induced growth cone collapse. CRMP-62 appeared to be an intracellular component of a signalling cascade initiated by an unidentified transmembrane collapsin-binding protein.

A major work in the field of the Ulip-family was performed by the group of Sobel (Byk et al., 1996, Byk et al., 1998). The search for intracellular phosphoproteins implicated in the regulation of neuronal differentiation led to the identification of four complete coding sequences for members of the Ulip family in the mouse, Ulips 1-4, all preferentially expressed in the nervous system. The expression level and phosphorylation pattern of Ulip1 were shown to be strongly regulated during development and neuronal differentiation. Furthermore, two Ulip sequences, Ulips A and Ulips B, could be identified in *C. elegans*. The Ulip family is highly conserved throughout evolution (more than 96% for Ulips 1-3 and 92.5% for Ulip4 between mouse and human) and the various members of the family within a single species display about 75% similarity. Two-dimensional immunoblot analysis of *in vitro* translated Ulips 1-4 demonstrated the existence, for each Ulip protein, of several, most probably differentially phosphorylated forms, in agreement with the presence of conserved phosphorylation consensus sites within their sequences. The expression of Ulips 1-4 mRNAs was differentially regulated during development and NGF-induced neuronal differentiation of PC12 cells.

Recently, several cDNA sequences corresponding to members of the Ulip family were isolated and their biological function has been characterised in more detail in various species (Gaetano et al., 1997, Hamajima et al., 1996, Kamata et al., 1998, Kamata et al., 1998, Quach et al., 1997, Torres and Polymeropoulos, 1998, Wang and Strittmatter, 1996, Wang and Strittmatter, 1997). It was shown that

brain collapsin response mediator protein (CRMP/Ulip) forms heterotetramers similar to liver dihydropyrimidinase, an enzyme that corresponds to Ulip5.

In relation with their likely biological roles in the nervous system, Ulip proteins are also implicated in pathological disorders since Ulips were identified as the antigens against which autoantibodies from patients with paraneoplasic neurological syndromes were directed (Antoine et al., 1999).
The presently available data suggest that the proteins of the Ulip family may be involved in the differentiation and the functional integrity of the nervous system, through the control of neurite elongation and axonal furdance, their potential stability or the transduction of extracellular collapse signals. Taken together, these studies suggest a differential, possibly complementary, multi-functional role of phosphoproteins of the highly conserved Ulip family in the control of neuronal differentiation, in relation with the development and plasticity of the nervous system.

## 2.3.3 <u>Hsc70</u>

The third protein identified in the neuronal PMO complex was the 70kD heat shock cognate protein (Hsc70) (Bulliard et al., 1997). Hsc70 and the heat shock protein 70 (Hsp70) are molecular chaperones that participate in many important cellular processes. Molecular chaperones were originally defined as a group of proteins that mediate the correct assembly of other proteins, but are not themselves components of the final functional structures (Ellis, 1987, Gething and Sambrook, 1992, Hendrick and Hartl, 1993, Rothman, 1989). They occur ubiquitously and are classified as stress proteins, although they have essential functions under normal growth conditions. Later chaperones have been defined as proteins that bind to and stabilise an otherwise unstable conformation of another protein. They catalyse the correct fate of the protein they bind to *in vivo,* like folding, oligomeric assembly, transport to a particular subcellular compartment, or disposal by degradation (Hendrick and Hartl, 1993). Molecular chaperones (Laskey et al., 1978) prevent incorrect interactions within and between non-native polypetides, thus increasing the yield but not the rate of folding reactions.

Based on their striking heat inducibility, it was proposed that the Hsp70s aid the repair or degradation of polypeptides that denature under stress (Hightower, 1980, Pelham, 1986). Later studies indicated that Hsc70 has an equally important role under non-stress conditions in stabilising the folding and assembly intermediates of newly synthesised polypeptides in the ER (Gething and Sambrook, 1992, Haas and

Wabl, 1983). Similarly in yeast, cytosolic Hsc70 associates with newly synthesised precursor polypeptides, stabilising them for uptake into the mitochondrion and the ER (Chirico et al., 1988, Deshaies et al., 1988, Zimmermann et al., 1988). Mammalian Hsc70 was shown to interact with nascent polypeptide chains in the cytosol (Beckmann et al., 1990) by binding hydrophobic peptide segments in an ATP-dependent manner (Flynn et al., 1991).

The most compelling evidence that protein folding *in vivo* requires molecular chaperones was provided by *Escherichia coli* cells with mutations in the gene coding for the chaperonin, GroEL (Coppo et al., 1973, Georgopoulos et al., 1973). They were shown to be defective in assembling bacteriophage particles. The significance of this finding was demonstrated by showing that before assembly in chloroplasts, the ribulose biphosphate carboxylase oxygenase (Rubisco) subunits form a complex with a homlogue of GroEL and of Hsp60 from which they dissociate in an ATP-dependent reaction (Barraclough and Ellis, 1980, Cannon et al., 1986, Davidoff and Mendelow, 1993, Hemmingsen et al., 1988, McMullin and Hallberg, 1988). Purified GroEL allowed the reconstitution of correctly assembled bacterial Rubisco *in vitro* (Goloubinoff et al., 1989). Finally, evidence was provided that the chaperonins mediate the folding of monomeric proteins, rather than actively promoting assembly (Ostermann et al., 1989).

It was demonstrated that the Hsp70 and chaperonin families can cooperate functionally *in vitro* (Langer et al., 1992). The Hsp70 homologue of E.coli, DnaK, and its partner chaperone DnaJ maintain an unfolded polypeptide in a soluble, folding competent confirmation, in which it can be transferred to GroEL for folding the native state. Cycling of DnaK between different nucleotide states is regulated by the chaperone cofactors DnaJ and GrpE in a ATp-dependent manner (Hartl, 1996, McCarty et al., 1995).

Later, Hip was identified as another chaperone cofactor of the cytosolic and nuclear Hsc70 (Hohfeld et al., 1995). The mechanism for the regulation of Hsp70 family members in the eukaryotic cell by Hip was distinct from the GrpE-mediated dissociation of chaperone-substrate complexes observed in prokaryotes (Frydman and Hohfeld, 1997). Hip appeared to stabilise the ADP-bound form of Hsc70 by interacting with its ATPase domain (Hohfeld et al., 1995).

Moreover, evidence involving Hsc70 in the response to oxidative stress was provided by a study that determined whether anti-oxidants prevented the stress gene expression in the focal brain injury regions (Turner et al., 1999). Another report showed protection against nitric oxide mediated by hsp70 even in the absence of heat stress in the rat insulinoma cell line RINm5F into which the human hsp70 gene was

stably transfected (Bellmann et al., 1996). Constitutive expression of hsp70 caused protection from NO-induced cell lysis which was of the same extent as seen after heat stressing cells. These results identify hsp70 as a defence molecule against nitric oxide. NO and TNF$\alpha$ play important roles in the pathogenesis of liver disease during acute inflammation. Pre-treatment of primary cultures of rat hepatocytes with the NO donor S-nitroso-N- acetylpenicillamine (SNAP) induces the expression of HSP70 mRNA and protein (Kim et al., 1997), which was associated with thermal tolerance and cytoprotection from TNF$\alpha$ and actinomycin D-induced hepatotoxicity and apoptosis. SNAP transiently changed the intracellular redox state by inducing glutathione (GSH) oxidation associated with the formation of S-nitrosoglutathione (GSNO). HSP70 mRNA was also induced by the GSH- oxidising agent diamide and the GSH-conjugating agent N-ethylmaleimide, suggesting that NO induces HSP70 expression through GSH oxidation. The protective effect of SNAP pre-treatment on TNF$\alpha$-induced apoptosis correlated with the level of HSP70 expression. SNAP pre-treatment inhibited reactive oxygen intermediate generation and lipid peroxidation effects that were reversed by blocking HSP70 expression using an antisense oligonucleotide to HSP70. Finally, endogenous NO formation, induced in hepatocytes stimulated with interferon-$\gamma$ and interleukin-1$\beta$, led to the formation of GSNO and GSSG, induced HSP70, and attenuated TNF$\alpha$-mediated cytotoxicity. These findings indicated that NO can also induce resistance to TNF$\alpha$-induced hepatotoxicity, possibly through the stimulation of HSP70 expression.

Further, a study shows the relationship between oxygen radicals and posthypoxic injury of cellular proteins which leads to the synthesis of HSPs (Gebhardt et al., 1999). It was shown that various periods of hypoxia and 30 min of reoxygenation resulted in an increased generation of superoxide. The inhibitor of superoxide dismutase (SOD), diethyldithiocarbamate (DDC) increased and addition of SOD decreased intracellular superoxide levels. HSP70 synthesis was detectable after 2 h of hypoxia. Similar to superoxide production, DDC increased and SOD reduced the HSP70 synthesis. The production of superoxide correlates with HSP70 induction. Thus, hypoxia/reoxygenation seems to induce heat shock protein production by increased superoxide generation.

Besides their function as inducible proteins by the physical stress to protect cells, recent evidence suggests that HSPs are likely involved in cell cycle control under normal conditions without stress. Hsc70 seems to directly interact with P27Kip1, an inhibitor of cyclin-dependent kinases, during G1/S transition (Nakamura et al., 1999).

Other recent studies describe how regulation of Hsc70 may be modulated at the molecular level. Therefore the role of Hsc70 in regulating the activity of the heme-regulated eIF-2α kinase (HRI) in hemin- supplemented rabbit reticulocyte lysate (RRL) in response to heat and oxidative stress was examined and compared with the effect of Hsc70 on HRI activation in response to heme deficiency (Thulasiraman et al., 1998). Hsc70 suppressed eIF- 2α phosphorylation and maintained the guanine nucleotide exchange activity of eIF-2B in heme-deficient RRL and in hemin-supplemented RRL exposed to elevated temperatures (42 degrees C), denatured protein (reduced carboxymethylated bovine serum albumin, RCM-BSA), oxidised glutathione or $Hg^{2+}$. The ability of Hsc70 to inhibit HRI activation was mediated through its ability to inhibit the hyper-autophosphorylation of transformed HRI, which causes the hyperactivation of HRI. Further observations indicate that heat shock induced the accumulation of a sufficient quantity of Hsc70 binding substrates (e.g., denatured protein) to sequester Hsc70 and inhibit the ability of Hsc70 to suppress HRI activation. Hsc70 interacts with nascent HRI and with transformed HRI (Uma et al., 1999). Interaction of HRI with Hsc70 is required for the transformation of HRI. Clofibric acid disrupted the interaction of Hsc70 with transformed HRI that had been matured and transformed in the absence of the drug. Disruption of Hsc70 interaction with transformed HRI in heme-deficient RRL results in its hyperactivation. Furthermore, activation of HRI in response to heat shock or denatured proteins also results in a similar blockage of Hsc70 interaction with transformed HRI. Thus, Hsc70 may be required for the folding and transformation of HRI into an active kinase but is subsequently required to attenuate the activation of transformed HRI. Furthermore, Hsc70 may modulate the activation of HRI not only in heme-deficient RRL, but also in hemin-supplemented RRL in response to oxidative stress.

Recently another, new role of Hsc70 was revealed in development of chicken embryo (de la Rosa et al., 1998). Insights have emerged concerning insulin function during development, from the finding that apoptosis during chicken embryo neurulation is prevented by prepancreatic (pro)insulin. An insulin-dependent regulation of Hsc70 was discovered. mRNA and protein levels of this chaperone were regulated in unstressed embryos during early development. More important, Hsc70 levels were found to depend on endogenous (pro)insulin, as shown by using antisense oligodeoxynucleotides against (pro)insulin mRNA in cultured neurulating embryos. Further, in the cultured embryos, apoptosis affected mainly cells with the lowest level of Hsc70. These results argue in favour of Hsc70 involvement in the prevention of apoptosis during early development and suggest a role for a molecular chaperone in normal embryogenesis.

The most spectacular recent findings on the HSP70 family concern their binding ability to the anti-apoptotic protein BAG-1 (Bimston et al., 1998, Hohfeld, 1998, Hohfeld and Jentsch, 1997, Stuart et al., 1998, Takayama et al., 1997, Takayama et al., 1998, Takayama et al., 1999). Evidence was shown that the protein BAG-1 is a potential modulator of the molecular chaperones, Hsp70 and Hsc70 (Takayama et al., 1997). BAG-1 binds to the ATPase domain of Hsp70 and Hsc70, without requirement for their carboxy-terminal peptide-binding domain. Purified BAG-1 and Hsp/Hsc70 efficiently form heteromeric complexes *in vitro*. BAG-1 inhibits Hsp/Hsc70-mediated *in vitro* refolding of an unfolded protein substrate, whereas BAG-1 mutants that fail to bind Hsp/Hsc70 do not affect chaperone activity. Further, the binding of BAG-1 to Bcl-2 depends on ATP. Overexpression of BAG-1 also protected certain cell lines from heat shock-induced cell death. The identification of Hsp/Hsc70 as a partner protein for BAG-1 may explain the diverse interactions observed between BAG-1 and several other proteins, including Raf-1, steroid hormone receptors and certain tyrosine kinase growth factor receptors. The inhibitory effects of BAG-1 on Hsp/Hsc70 chaperone activity suggest that BAG-1 represents a novel type of chaperone regulatory proteins and thus suggest a link between cell signalling, cell death and the stress response. Functional characterisation of BAG-1 revealed an unexpected versatility in the regulation of Hsc70 and appeared to provide a link between apoptosis and the cellular chaperone machinery (Hohfeld, 1998). Mechanistic basis for BAG-1 as a negative regulator of the Hsp70 chaperone was given by Bimston et al. (Bimston et al., 1998). Further sudies demonstrated that there exist three isoforms of human BAG-1 (BAG-1, BAG-1M, and BAG-1L) which all retained the ability to bind Hsc70 (Takayama et al., 1998). Furthermore, experiments using a green fluorescence protein (GFP)-BAG-1 fusion protein demonstrated that overexpression of Bcl-2 cause intracellular redistribution of GFP-BAG-1, producing a membranous pattern typical of Bcl-2.

BAG-1 also interacts with several steroid hormone receptors which require the molecular chaperones Hsc70 and Hsp90 for activation. It was shown that BAG-1 is a regulator of the Hsc70 chaperone (Hohfeld and Jentsch, 1997). BAG-1 bound to the ATPase domain of Hsc70 and, in co-operation with Hsp40, stimulated Hsc70's steady-state ATPase activity. BAG-1 accelerated the release of ADP from Hsc70. These results reveal an unexpected diversity in the regulation of Hsc70 and raise the possibility that the observed anti-apoptotic function of BAG-1 may be exerted through a modulation of the chaperone activity of Hsc70 on specific protein folding and maturation pathways.

## 2.3.4 <u>Aldolase C</u>

Aldolase C (=Zebrin II) is the fourth protein associated with the neuronal PMO complex. Three isozymes of the phylogenetically ancient enzyme aldolase (fructose-1,6-bisphosphate aldolase) exist: aldolases A, B, and C, each of which is encoded by a separate gene. The kinetics of aldolase A favour the cleavage of fructose-1,6-bisphosphate to glyceraldehyde-3-phosphate and dihydroxyacetone phosphate, and its gene was found on human chromosome 16 (Tolan et al., 1987). Generally considered to be a muscle enzyme, the transcriptional regulation of this gene is unusually complex with three alternative promoters (Izzo et al., 1988, Joh et al., 1986, Maire et al., 1987, Mukai et al., 1986) that result in three different mRNA species. Curiously, the three transcripts differ only in their 5'-untranslated regions; each mRNA encodes the same structural enzyme. Of the three promoters, the 5'-most and 3'-most are expressed broadly in foetal tissues as well as in adult muscle and red blood cells. The central promoter (M-type or Hsc70-type) is highly active in skeletal muscle, particularly in fast-twitch fibres (Salminen et al., 1996, Salminen et al., 1994). The 5'-most promoter is active, albeit at lower levels, in a range of other tissues, including brain (Mukai et al., 1986). In the nervous system, the exact cellular location of the aldolase A isozyme is uncertain; Northern analysis of cultured cells suggests that it is present in both neurones and glia (Popovici et al., 1990).

Aldolase B, found on human chromosome 9 (Lebo et al., 1985), is generally considered to be a liver enzyme, although it is also found in kidney proximal tubule cells and enterocytes. This form of aldolase favours gluconeogenesis, befitting its higher concentration in the liver. During hepatic development, aldolase A and C are expressed earlier, but aldolase B soon takes over. Unlike the other isozymes, aldolase B is transcriptionally activated by signals from hormones and dietary factors (Weber et al., 1984). A proximal promoter region, approximately 200 bp in length, has been identified that contains many of the elements (including overlapping hepatic nuclear factor binding sites) necessary for properly regulated expression if it is paired with sequences in the first intron (Gregori et al., 1991, Sabourin et al., 1996, Tsutsumi et al., 1989).

Aldolase C, found on human chromosome 17 (Tolan et al., 1987), has kinetic properties that are intermediate between those of the A and B isoforms. In the adult, aldolase C is considered to be the brain-specific isozyme, with low but detectable activity in foetal tissues and hepatocarcinomas (Mukai et al., 1991, Popovici et al., 1990, Royds et al., 1987, Schapira et al., 1970, Thompson et al., 1982). The exact

cellular location of aldolase C is controversial. Studies of mRNA by Northern blot analysis, *in situ* hybridisation, or transgene expression studies indicated that the gene is transcribed mostly in neurones (Arai et al., 1994, Mukai et al., 1991, Popovici et al., 1990). On the other hand, earlier studies using isozyme-specific antibodies reported its location in grey matter astrocytes and cells of the pia mater (Thompson et al., 1982, Wachsmuth et al., 1975). All reports agree that Purkinje cells of the cerebellum contain by far the highest levels of the enzyme. By sequence analysis, the aldolase C promoter region is typical of a "housekeeping" type of promoter. A normal TATA box is missing; instead a GC-rich region was found just upstream of the transcription start site (Vibert et al., 1989). A CAAT box was present, but it was located far upstream from its expected position (Buono et al., 1993). Northern analysis using a probe specific for aldolase C mRNA demonstrated a 1.6-kb band. There was no evidence of alternative splicing. Two DNase I-sensitive sites flank the transcription unit: one immediately 5' and the other about 1.5 kb 3' to the nine exons of the gene. Several tissue-specific methylation sites have been identified in the immediate vicinity of the transcription unit (Makeh et al., 1994). In transgenic mice (Arai et al., 1994, Makeh et al., 1994) large rat genomic fragments (or fragments with short marker tags inserted) have been shown to direct central nervous system (CNS)-specific expression. Expression outside of the CNS was suppressed. Even a short, 115-bp promoter element contained sufficient cis-active sequences to drive marker gene expression solely in the CNS (Thomas et al., 1995).

The interest in the aldolase isozymes grew with the discovery that aldolase C was identical to Zebrin II (Ahn et al., 1994). Zebrin II had long been recognised as a Purkinje cell biochemical marker of the sagittal compartments of the adult cerebellar cortex (reviewed in (Hawkes et al., 1993, Hawkes and Gravel, 1991, Hawkes and Herrup, 1995, Herrup and Kuemerle, 1997)).

Already very early studies report about aldolase binding to F-actin (Arnold and Pette, 1970, Morton et al., 1977). First evidence of interaction of aldolase with the regulatory proteins of skeletal muscle was provided by investigations of interactions of aldolase with regulatory proteins of rabbit skeletal muscle (Stewart et al., 1980, Walsh et al., 1980). A salt-dependent interaction of troponin, tropomyosin and the tropomyosin-troponin complex with aldolase was detected, the tropomyosin-troponin complex displaying a greater affinity for the enzyme than did either regulatory protein alone. The results indicate that aldolase possesses multiple binding sites for these cytoskeletal proteins. Quantitative studies of the binding of aldolase to actin-containing filaments showed the interaction to be influenced markedly by the presence of these regulatory proteins on the filaments. Later studies first located binding sites for aldolase and

GAPDH on the actin monomer in microfilaments (Mejean et al., 1989). That led to the identification of an actin binding region in aldolase (O'Reilly and Clarke, 1993). The sequence of this region is highly homologous to a region of sequence near the C-terminus of actin itself and which is also found in the actin binding domains of a number of other actin binding proteins. The molecular nature of the F-actin binding activity of aldolase was confirmed by site-directed mutants (Wang et al., 1996). Most recent studies show that aldolase mediates the association of F-actin with the insulin-responsive glucose transporter GLUT4 (Kao et al., 1999).

Finally, some studies show that under conditions of oxidative stress the induction of aldolase is markedly reduced (Hamm-Kunzelmann et al., 1997, Schafer et al., 1997, Schafer et al., 1996). Furthermore, reactive oxygen intermediates dramatically decrease the transcriptional activities of the Sp1-dependent aldolase A promoters. This indicates that cellular redox changes can regulate gene expression by reversible oxidative inactivation of Sp1 binding. Another study reported that ROS cause self-inactivation of aldolase (Gupta et al., 1993). Aldolase was paracatalytically modified in the presence of fructose 1,6-bisphosphate and hexacyanoferrate(III).

## 2.3.5 <u>Neurone-specific enolase γ (NSE)</u>

The last identified component of the neuronal PMO multi-protein complex is neurone-specific enolase γ (NSE). As one of the classical enzymes in the glycolytic pathway, enolase is usually considered to be a soluble cytoplasmic protein. The enzyme is dimeric with three types of isozymes: αα, ββ and γγ, each encoded by different genes (Marangos and Schmechel, 1987, Schmechel et al., 1980). Only the γγ enolase form is present at high levels in brain and at intermediate levels in peripheral nervous tissue and various neuroendocrine glands, such that it is considered to be a specific marker for neurones or endocrine cells and their derived tumours (Hayashi et al., 1987, Marangos and Schmechel, 1987). It can account for up to 1.5% of total protein in some neurones and thus may have functions other than enzymatic (Kivela, 1986, Molnar et al., 1984, Schmechel et al., 1980). cDNA analysis indicates that NSE does not contain the usual leader sequence thought to facilitate the extracellular secretion of proteins (Sakimura et al., 1985). However, other studies reported the extracellular presence of NSE in some tumour (Hayashi et al., 1987) and its localisation in at least one extracellular matrix, the retinal interphotoreceptor matrix of the neural retina (Li et al., 1995).

Another interesting observation is the close relationship of α-enolase with tau-Crystallin (Wistow et al., 1988). Tau-Crystallin possesses enolase activity, but the activity is greatly reduced with age, probably because of age-related posttranslational modification. Tau-Crystallin is up-regulated in differentiation (Deloulme et al., 1996).

Along with its enzymatic role in glycolysis, evidence indicates that NSE can act as a neuronal survival factor in the central nervous system (Takei et al., 1991). Neuronal survival factors in the central nervous system were investigated by using a primary culture of embryonic rat neocortical neurones. One factor found to significantly promote survival of these cells over a 4-6 day period was identified as NSE. This was confirmed by showing that commercially available NSE itself also possessed neuronal survival activity for the cultured neocortical neurones and that the effects of NSE were inhibited completely by anti-NSE polyclonal antibody. Furthermore, highly purified NSE supported the survival of cultured neurones in a dose-dependent manner, and the neurotrophic effect was inhibited by anti-NSE monoclonal antibody.

Recent studies use NSE as a sensitive marker for various brain damage or disease. Levels of NSE were increased in patients after seizures (Buttner et al., 1999, Correale et al., 1998, DeGiorgio et al., 1999). Furthermore expression of NSE was raised in patients with neuroendocrine tumors (Bajetta et al., 1999), with benign lung diseases (Szturmowicz et al., 1998), with Creutzfeldt-Jakob disease (Evers et al., 1998, Kropp et al., 1999) and with hyperglycemic cortical ischemic stroke (Sulter et al., 1998)

# 2.4 <u>Aims of this thesis</u>

As listed above, numerous studies have been performed to investigate the structure, regulation and function of each of the 5 proteins (GAPDH, Ulip, Hsc70, aldolase c and enolase γ) which we isolated in a tight complex as a neuronal PMO. Recent studies have revealed new, intriguing observations concerning specific functions of the proteins. GAPDH and Hsc70 seem to be directly involved in cell death or in cell survival decisions, and may have key roles in different neurodegenerative diseases. Neurone specific enolase γ is already being used as sensitive marker in various brain damage and diseases. Furthermore, the phospoprotein Ulip is involved in neuronal differentiation and axon guidance.

There is growing evidence that these proteins have a high impact on major cellular processes and they are essential factors in various neurodegenerative diseases. However, although a considerable number of reports exist that underline their importance at physiological level, much less is known about the molecular mechanisms and the cellular dynamics of these proteins in the cell. Furthermore, up to date nothing is known about the interaction of the members of the multi-protein-complex, its function and its relevance in biological processes.

Thus, we aimed at obtaining knowledge about these five proteins by characterising the expression and the subcellular localisation of the five proteins. We hoped to receive additional information by overexpression of the proteins and comparison with endogenous expression. We therefore amplified cDNA of the five proteins by means of PCR from total RNA that was isolated from NB41A3 cells. We then constructed chimeric green fluorescent protein (GFP) and blue fluorescent protein (BFP) fusion proteins for each member of the multi-protein-complex. The protein-GFP hybrids were transfected into neuronal and non-neuronal cell lines and detected together with endogenous protein expression by direct or indirect immunofluorescence with a confocal laser scanning microscope. The chimerical BFP constructs were used in double transfections.

Since PMOs are known to be involved in the response to oxidative stress, we first compared cellular distribution of the endogenous proteins and of the overexpressed proteins coupled to GFP (or BFP) before and after induction of oxidative stress.

Our observations, together with the latest findings published on apoptosis, convinced us to expand our studies by observing changes in expression and subcellular localisation in cells exposed to apoptotic agents.

By using this approach based on immunofluorescence and confocal microscopy, we wanted to increase our understanding on the response of each protein to both oxidative stress and induction of apoptosis. In order to investigate whether the effects observed with endogenous proteins in untransfected cells changed when the appropriate protein was overexpressed, each of these proteins was overexpressed in control cells and in cells exposed to apoptotic drugs or to stress agents. We used two different cell lines, NB41A3 and R6, to compare, which of the observed effects are neuroblastoma specific and which were also reproducible in embryonal fibroblasts. We also were interested to detect observations that indicate interactions between members of the protein-complex, especially by co-transfection experiments. Finally,

to extend our knowledge of the molecular processes during apoptosis, a cell line that stably expresses Bcl-2 ($R6^{Bcl-2)}$) was used for investigations together with members of the complex.

# 3 <u>Methods</u>

(For details see Appendix)

## 3.1 <u>Cell culture growth</u>

Cells of the clonal mouse neuroblastoma line NB41A3 were obtained from the American Type Culture Collection (Bethesda, MD) and maintained according to Augusti-Tocco and Sato (Augusti-Tocco and Sato, 1969) as monolayers on tissue culture plastic flasks at 37° C in 5% $CO_2$. The growth medium was Dulbecco's modification of Eagle's medium (DMEM) at pH 7.4 containing 3.7 g/l $NaHCO_3$, 4.5 g/l D-glucose, 0.11 g/l sodium pyruvate and 0.58 g/l glutamine, 10% foetal calf serum, 50 units/l of penicillin and 50 µg/l of streptomycin.

The rat embryo fibroblast cell line 6 (R6) and the rat embryo fibroblast cell line 6 stably overexpressing Bcl-2 ($R6^{Bcl-2}$) were obtained through the courtesy of Dr Christoph Borner, Institute of Biochemistry, Fribourg, Switzerland, who has described the construction of $R6^{Bcl-2}$ earlier (Borner, 1996). Both cultures were grown at 37° C in Dulbecco's modification of Eagle's medium (DMEM) at pH 7.4 containing 3.7 g/l $NaHCO_3$, 4.5 g/l D-glucose, 0.11 g/l sodium pyruvate and 0.58 g/l glutamine , 5% foetal calf serum, 50 units/l of penicillin and 50 µg/l of streptomycin in a humidified atmosphere of 5% $CO_2$ / 95% air.

For all cell lines the medium was changed every 3 days; starving of the cultures and growth to post confluence were strictly avoided. The cells were trypsinised in the presence of 0.25% trypsin and 0.1% EDTA for splitting or harvested for RNA or protein extracts when they were subconfluent.

## 3.2 <u>S1 nuclease protection assay</u>

Total RNA from cells was purified by the "IsoHi" method described in the appendix. For S1 nuclease protection assay, 1 pmol of linearised and dephosphorylated DNA, was radioactively labelled with (γ-$^{32}$P)-ATP. We used four different probes of 114, 203, 250 and 395 nt of length. The mixture was incubated for 40 min at RT together with T4 polinucleotide kinase. After heat-inactivation of the enzyme and subsequent digestion of the fragment, the resulting probe was purified by electrophoresis on preparative agarose gel. Approximately 100000 cpm of single-stranded probe was mixed with 40 µg of

total RNA isolated from NB41A3 cells that were synchronised as described by Zurbriggen and Dreyer (Zurbriggen and Dreyer, 1996) and stressed for 1 h in the presence of DCIP (0-400 μM). After overnight hybridisation, S1 nuclease buffer and 150 units of S1 nuclease (Sigma) were added, and the mixture was incubated at RT for 1 h. The protected fragments were electrophoresed on an 8.3 M urea/6% polyacrylamide gel. The results were quantified by densitometric scanning of different film exposures. Evaluation of relative transcripzion was performed against the internal control β-actin (122 nt).

# 3.3 Construct of plasmids

The coding regions of enolase, Hsc70 II, aldolase, Ulip2 and Ulip3 were amplified by PCR with the Advantage Klentaq polymerase mixture (CLONTECH) from mouse cDNA (mouse brain Marathon cDNA, CLONTECH) with the following downstream (dp) and upstream primer (up) pairs:

| Primer | Oligo sequence in 5' --> 3' direction |
|---|---|
| Hsc70 (dp) | AAAA**CCCGGG**GGT<u>ACCACCTCC</u>ATCGACCTCTTCAATAGTGGGGCCTG |
| Hsc70 (up) | TCGTCGTCAGCGCAGCTGGGCCTACA |
| Enolase (dp) | AAAA**CCCGGG**GGT<u>ACCACCTCC</u>AAGCACACTAGGATTTCGGAAATTAT |
| Enolase (up) | GCCGCCGCCGTCACCACCGCCACTGC |
| Aldolase (dp) | AAAA**CCCGGG**GGT<u>ACCACCACC</u>GTAGGCATGGTTGGCGATGTAGAGGG |
| Aldolase (dp) | CCGCGGCTGACTGGCTGAGTGACTGG |
| Ulip2 (dp) | AAAA**CCCGGG**GGT<u>ACCACCTCC</u>TCCTAGGCTGGTGATGTTGGCACGGC |
| Ulip2 (up) | TTTGCTTTAAAGCTGTCCTCTTGAAA |
| Ulip3 (dp) | AAAA**CCCGGG**GGT<u>ACCACCTCC</u>ACCGAGGCTGGTGATGTTGGAGCGGC |
| Ulip3 (up) | CTTTCATCCCTCCCTGGCCTTTGTCG |

All downstream primers were designed in such a way, that the stop codon was replaced by nucleotides (red letters) coding for three gly in a row. Additionally, two artificial restriction sites were added: KpnI/Asp718I (GGTACC, underlined letters) (Tomassini et al., 1978) to perform frameshift if necessary and XmaI (GGGCCC, **bold letters**) to facilitate ligation. Frameshifted clones were produced either by using KpnI which produces a 4-base 3' extension which was subsequently digested in a T4 DNA polymerase reaction or by using Asp718I (=Acc65I) which produces a 4-base 5' extension which was used as template to add the missing nucleotides by Klenow fragment. Blunt end re-ligation with the KpnI

cut fragment(s) produces a -1 nucleotide frameshift, whereas the Asp718I cut fragment(s) produce a +1 nucleotide frameshift.

The complete coding region of GAPDH was amplified as two overlapping pieces by RACE from mouse brain Marathon cDNA (CLONTECH) according to the manufactures instruction. The 3'-end and the overlapping 5' end were created with Adapter primer 1 (AP1) and the GAPDH specific downstream (GAPDH sdp), or upstream primer (GAPDH sup), respectively.

| Primer | Oligo sequence in 5' --> 3' direction |
|--------|----------------------------------------|
| GAPDH sup | CTCACGGCAAATTCAACGGACCAG |
| GAPDH sdp | TTGGCAGGTTTCTCCAGGCGGCAC |
| AP1 | CCATCCTAATACGACTCACTATAGGGC |

The amplified products were subcloned into the pKS+ Bluescript cloning vector (Stratagene, La Jolla, CA, USA) and the correct sequence confirmed by sequencing (Microsynth). Subsequently, the amplified DNA sequence was cut out of pKS+ Bluescript and subcloned in-frame with the GFP-coding sequence in pEGFP-N1 (Clontech) or pEBFP-N1 (Clontech), respectively.

In the case of GAPDH, the obtained 5'-RACE fragment and the 3'-RACE fragment were joined at their common NsiI restriction site found in the overlapping sequence. To remove the stop codon of the 3'-RACE fragment, both fragments were cloned together with the help of an adapter (see *figure 1* below), which was ligated to the SfiI restriction site located 15 bp in front of the stop codon, in-frame into the appropriate expression vector.

```
                          Adapter for GAPDH


        5'-    TGGCCTCCAAGGAGGGGGGTGGTAC     -3'
        3'-TGTACCGGAGGTTCCTCCCCCCACCATGGGCC-5'


   Red letters:  Nucleotides coding for three gly which replace the stop codon
   Underlined:  Complement sequence to SfiI restricted 3'-RACE fragment
   Bold letters:        Complement sequence to XmaI restricted expression vector
```

**Figure 1: Sequence of the oligonucleotide adapters for GAPDH.** The adapter was used to clone GAPDH fragments in-frame into the pEGFP vector.

To construct negative controls not expressing the GFP protein, but only the inserted gene, either the complete GFP sequence was cut out with restriction enzymes or otherwise disrupted by a frame-shift mutation at the artificial KpnI/Asp718 restriction site between the 3'-end of the subcloned gene and the start codon of GFP. All plasmids were purified on QIAGEN Midi columns according to the manual of the Qiagen Plasmid purification kit.

# 3.4 <u>Transfection</u>

Unless explicitly mentioned, cells grown on glass coverslips of 1.2 cm diameter in 6 well plates were transfected at 80 - 90% confluence using SuperFect transfection reagent (Quiagen) according to the manufactures instruction. 1 µg of plasmid DNA suspended in 60 µl fresh DMEM without serum and 5 µl SuperFect transfection reagent were mixed together, briefly vortexed and then incubated for 10 min to allow complex formation. 600 µl of complete growth medium was then added to the complex mixture and all together immediately transferred to the PBS washed cells. After 3-4 hours of incubation at 37° C / 5% $CO_2$, cells were washed once with PBS.

To produce stable NB41A3 cell lines overexpressing enolase-GFP, aldolase-GFP or GAPDH-GFP, NB41A3 cells plated on tissue culture plastic were transfected. Cells were splitted 2 days later in medium containing 0.75 mg/ml G418 (Life Technologies). Selection medium was changed every 3 d for a period of 3 weeks, after which G418-resistant colonies were selected and analysed under the microscope for GFP expression. For each transfection, all G418 resistant clones expressing GFP were pooled together to obtain mixed bulk populations of cells stably overexpressing either enolase-GFP (NB41$^{enolase-GFP}$), aldolase-GFP (NB41$^{aldolase-GFP}$) or GAPDH-GFP (NB41$^{GAPDH-GFP}$).

# 3.5 <u>Induction of oxidative stress and apoptosis</u>

Immediately after transient transfection, cells were trypsinised, splitted 1:3 and plated on glass coverslips of 1.2 cm diameter in 6 well plates. After 24 h the growth medium was replaced by either a) new growth medium (control) or b) new growth medium containing either 300 µM FeCN, 100 µM $H_2O_2$, 1.5 µM proteasome inhibitor MG132 (carbobenzoxyl-leucinyl-leucinyl-leucinal-H) or 200 nM staurosporine.

Staurosporine, is a potent inhibitor of protein kinases (Bertrand et al., 1994) and is widely used to activate apoptosis in neuronal and non-neuronal cells.

Unless specified otherwise, cells were exposed for 3 h to 300 $\mu$M FeCN or 100 $\mu$M $H_2O_2$ and for 6 h and 24 h to 200 nM staurosporine or 1.5 $\mu$M MG132. Growth medium without phenolred was used in experiments where cells were directly analysed after incubation under the microscope without prior fixation.

# 3.6 <u>Antibodies</u>

For immunocytochemistry the following primary antibodies were used: mouse anti-Hsc70 monoclonal antibody (Mab) (IgG) (Affinity BioReagents), mouse anti-GAPDH Mab (IgG), mouse anti-neurone specific enolase $\gamma$ Mab (Chemicon International Inc.), rabbit anti-NSE $\gamma$ polyclonal antibody (Chemicon International Inc.), mouse anti-zebrin II Mab (IgG) (obtained through the courtesy of Dr R. Hawkes, University of Calgary, Calgary, Alberta, Canada), rabbit anti-Ulip3 polyclonal antibody (IgG) (generation of antibody as described by Bulliard et al., 1997) and rabbit anti-GFP polyclonal antibody (IgG) (Clontech Laboratories, Inc., Palo Alto, CA, USA).

As secondary antibodies Texas Red dye-conjugated goat anti-mouse IgG, Texas Red dye-conjugated goat anti-rabbit IgG, fluorescein isothiocyanate (FITC)-conjugated goat anti-mouse IgG or Fluorescein isothiocyanate (FITC)-conjugated goat anti-rabbit IgG (all from Jackson ImmunoResearch Laboratories, Inc., Bar Harbor, ME, USA) were used for immunocytochemistry. For Western blotting horseradish peroxidase conjugated goat anti-rabbit IgG or horseradish peroxidase conjugated goat anti-mouse IgG (both from SIGMA) was used.

# 3.7 <u>Immunocytochemistry</u>

When native GFP fluorescence was used to localise the GFP fusion proteins, the coverslip containing the adherent cells was directly placed on top of a drop of growth medium without phenolred on a microscope slide and immediately analysed.

Otherwise cells were rinsed twice in PBS and fixed for 15 min in 4% p-formaldehyde in 0.1 M PIPES (pH 6.8) containing 0.1% Hoechst 33342. Cells were rinsed in PBS twice, permeabilised for 5 min with 0.05% saponin in PIPES, again rinsed twice in PBS and then incubated for 10 min at -20° C in acetone. After 2 washes with PBS cells were incubated in 1% BSA (in PBS) for 2 h on the coverslip with the first antibody. Subsequently cells were rinsed twice in PBS and then incubated for 2 h with the fluorescent secondary anti-IgG before two further washes in PBS. Fluorescence was extended by using SlowFade (Molecular Probes, Leiden, Netherlands) according to the manufacture's instruction. All incubations were performed in a light protected environment and, except for acetone, at room temperature.

# 3.8 <u>Fluorescence microscopy</u>

Cells were examined with a Nikon Eclipse E800 microscope under a 100x oil immersion objective (Nikon Inc.) using a MRC-1024 Bio-Rad laser confocal microscope system equipped with an Krypton/Argon laser (Bio-Rad Labs, Hercules, CA, USA) and the LaserSharp acquisition software (Bio-Rad). Serial sections (at 0.5 - 1.5 um intervals) in the z-axis of cells were collected in the slow scanning mode (~160 Hz) with 1.5 - 4.5 mm-diam iris aperture by averaging pictures by Kalman (3 scan). Green fluorescence (GFP or FITC) and Texas Red were detected in parallel at 512 x 512 pixels. The pictures were processed with the LaserSharp processing software (Bio-Rad) or alternatively with ConfocalAssistant before picture files were transferred to Adobe Photoshop 4.0 and printed on a Kodak printer.

Additionally a 100x oil immersion Plan-Neofluar objective (Zeiss) with a inverted Zeiss Axiovert 135 TV microscope equipped with a HBO 100-XBO 75 lamp was used to visualise DNA staining with Hoechst 33342.

# 3.9 <u>Quantification</u>

The serial sections through the z-axis of the cell were collected within a linear range of fluorescence intensity, superimposed to a 3D stack and analysed as a 2D projection. To compare GFP expression in different subcellular structures, the mean pixel intensity in a selected area was determined (for details see

instruction manual for LaserSharp processing software from Bio-Rad) and normalised by subtracting the background.

In short the procedure was as follows: To compare the expressed amount of proteins between different cells or between different subcellular compartments within one cell, all sections collected in the z-axis of the appropriate picture by LSCM are stacked to a two-dimensional projection in which the intensities of the various sections are accumulated. A histogram is then prepared by defining the area to be analysed in the 2D-projection. The histogram is evaluated by looking at the mean pixel intensity and at the distribution of different pixel intensities by looking at the standard deviation. A high mean pixel intensity correlates to high amount of expressed protein, whereas a high standard deviation indicates a patchy, irregular expression in the specific area.

# 4 <u>RESULTS</u>

## 4.1 <u>Construction of plasmids and stable cell lines</u>

### 4.1.1 <u>Construction of Hsc70-, enolase-, aldolase- and Ulip-GFP hybrids in expression vectors</u>

The construction of the different vectors used for transfection is described in detail in the methods section. In short, cDNAs of Hsc70, enolase, aldolase-C (zebrin II) and different Ulip (MMUNC33) isoforms were isolated from NB41A3 mouse neuroblastoma mRNA and from mouse brain Marathon cDNA (CLONTECH) by means of PCR. All lower (downstream) primers were designed in such a way, that the stop codon of the gene is removed and replaced by a sequence coding for 3 glycine in a row. A suitable upper primer was selected with the help of the software program OLIGO (see methods section). We looked for primers with preferentially high melting temperatures to enable touch down PCR and modified primers to avoid hairpin, duplex and dimer formation. Ulip-3 (1857 bp), Hsc70 (1997 bp), and aldolase C (1159 bp) were amplified very specifically as one fragment by touchdown PCR at an annealing and elongation temperature of 72° C.  The 1412 bp fragment of enolase was produced together with a much less abundant fragment of 1050 bp by touchdown PCR at a less restrictive temperature of 68° C. At the same conditions the Ulip-2 fragment (1789 bp) was specifically amplified.

The ends of all amplified fragments were made blunt by T4 DNA polymerase treatment and subsequently cloned into pKS+ Bluescript vector. Their correct sequence was confirmed by sequencing the cloned fragment from the 5'- as well as from the 3'-end. The cDNAs of the different proteins were then cut out of pKS+ Bluescript vector and cloned individually in-frame into the expression vector pEGFP-N1 and pEBFP-N1 (Clontech, *figure 2a, figure 2b*). Each of this vectors was tested for expression after transfection in cultured cell lines.
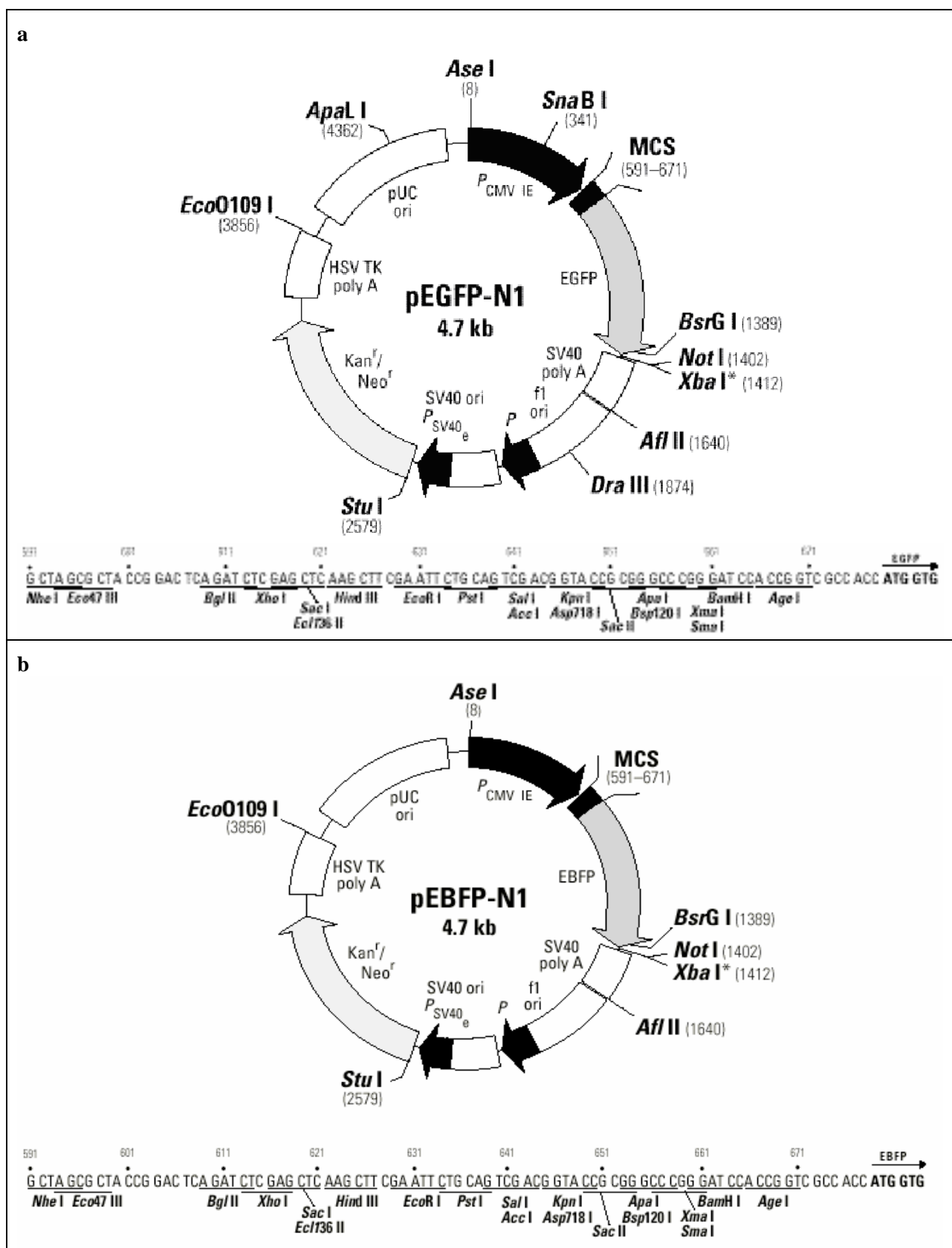
**Figure 2: Maps of (a) pEGFP-N1 and (b) pEBFP-N1.** All sites shown are unique. The Xba I site (*) is methylated. The Not I site follows the EGFP stop codon. All proteins were ligated in frame with either EGFP or EBFP with help of the multiple cloning site (MCS). Reference: Living Colors[TM] application notes of Clontech.

Control vectors for each protein were constructed by inhibiting the expression of GFP by either a frameshift mutation (aldolase, Ulip and enolase) or by deletion (Hsc70) of the complete coding region for GFP. Correct expression of these vectors was confirmed by immunofluorescence assays in transfected cells.

# **Construction of GAPDH-GFP hybrids in expression vectors**

Since its known that several isoforms of GAPDH do exist, we tried to obtain various isoforms of GAPDH by rapid amplification of 5'- and 3'-cDNA ends (5'-RACE and 3'-RACE) with the Marathon-Ready mouse brain cDNA of Clontech. Therefore, four different specific upstream (up) and four different downstream primers (dp) were used together with AP1 (see method section):

| Primer | Oligo sequence in 5' --> 3' direction |
|---|---|
| GAPDH 1 (up) | GCCGGTGCTGAGTATGTCGTGGAG |
| GAPDH 1 (dp) | GCATCGAAGGTGGAAGAGTGGGAG |
| GAPDH 2 (up) | GTGAAGGTCGGTGTGAACCCATTT |
| GAPDH 2 (dp) | CATTGGGGGTAGGAACACGGAAGG |
| GAPDH 3 (up) | CTCACGGCAAATTCAACGGACCAG |
| GAPDH 3 (dp) | TTGGCAGGTTTCTCCAGGCGGCAC |
| GAPDH 4 (up) | GACCACAGTCCATGCCATCACT |
| GAPDH 4 (dp) | TCCACCACCCTGTTGCTGTAG |

All reactions produced fragments of the size expected from the known GAPDH sequence available in the gene bank *(figure 3)*. We did not observe any RACE reactions producing additional fragments. I.e. if different isoforms were present, they seemed to be of the same length. After subcloning the fragments into pKS+ Bluescript vector, 10 clones of each 5'- and 3'-RACE reaction were investigated by means of restriction analysis. All clones showing different restriction patterns were sequenced. Quite surprisingly, besides their different orientation in the vector, no different isoforms were found. All fragments corresponded to mouse GAPDH sequence found in the gene bank.
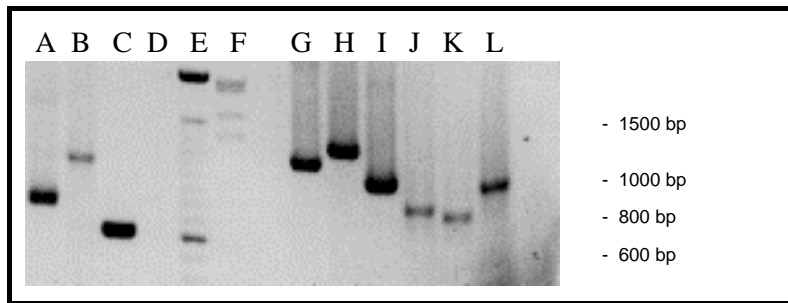
**Figure 3: 0.8% agarose gel showing results of RACE experiment.** 3 ul of PCR product from reaction A-L were loaded per lane. The 3'-RACE fragments were produced in reaction A by adding primer GAPDH 4 (up), in G with GAPDH 3 (up) , in H with GAPDH 2 (up) and in I with GAPDH 1 (up), whereas the 5'-RACE fragments were produced in B with GAPDH 4 (dp), in J with GAPDH 3 (dp) , in K with GAPDH 2 (dp) and in L with GAPDH 1 (dp). C is the positive control where the GAPDH fragment was amplified with the primer pair GAPDH 3 (up) and GAPDH 3 (dp), and D is the negative RACE control containing AP1 alone. E: 100 bp Marker, F: lambda Marker. All fragments are of the expected size.

Finally,  the 5'-Race and the appropriate 3'-Race fragment were cut out of the cloning vector and ligated together with a special oligo adapter (figure 1), which replaces the stop codon by a sequence coding for 3 gly, in-frame into pEGFP or pEBFP expression vector. Control vectors for GAPDH were constructed by inhibiting the expression of GFP by deletion of the complete coding region for GFP. Correct expression of these constructs was confirmed by immunofluorescence  assays in transfected cells.

Therefore the sequence of all fusion-proteins are organised similarly: At the $NH_2$-terminus is the appropriate protein to be investigated, followed by three glycines replacing the stop codon and than, in-frame with the protein, the GFP- or BFP-tag at the COOH-terminus of the fusion protein. These constructs ensure that GFP- or BFP-expression is coupled to the expression of the protein to be analysed.

# 4.1.2 Establishing stable NB41A3 cell lines expressing GFP-fusion proteins

To obtain stable cell lines overexpressing the proteins of the neuronal PMO complex, we selected for neomycin+ cells, since the transfection vector contains a neomycin resistance gene. Survival tests at different concentrations of G418 have been performed (see *figure 4a)*.
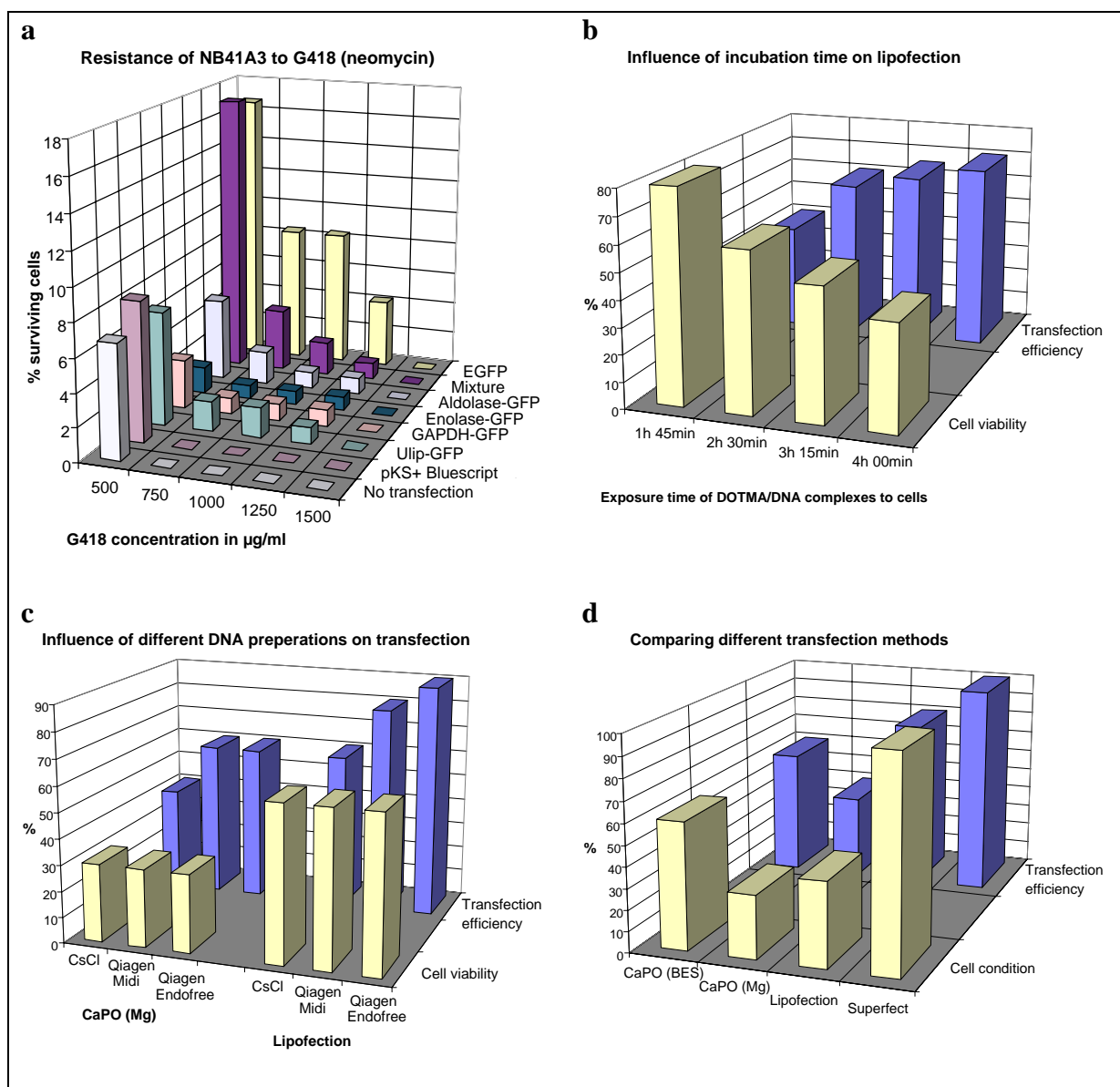
**Figure 4: Analysis of (a) resistance to G418 (neomycin) and (b-d) transfection efficiency and cell viability in NB41A3 cells. (a)** Cells were transfected by SuperFect with either pEGFP (which contains a neo[+] gene) alone or with pEGFP containing Ulip, GAPDH, aldolase or enolase gene. Additionally one set of cells was transfected with a mixture of Ulip-GFP, GAPDH-GFP, aldolase-GFP and enolase-GFP plasmids. As negative controls cells transfected with pBluescript or untransfected cells were used. NB41A3 cells were grown in normal growth medium containing different amounts of G418. Dead cells were counted by trypan blue method. **(b)** Influence of exposure time on lipofection. NB41A3 cells were transfected according to the lipofection method described in the appendix. Incubation time of pEGFP/DOTMA complex on cell plates was between 1 h 45 min up to 4 h. Efficiency increased, whereas cell condition decreased with time. **(c)** Influence of DNA purification on transfection. pEGFP plasmids were purified either by CsCl-method, Midi columns (Qiagen) or Midi columns using Endofree buffers and solutions (see protocols), and subsequently tested by CaPO - or DOTMA-transfection method. **(d)** Comparing different transfection methods. pEGFP purified on Midi columns was transfected by different, optimised methods. For figures**(b-d)** transfection efficiency and the condition of cells was analysed 36 h after start of transfection in various experiments. The efficiency was defined as percentage of cells expressing GFP. Transfection efficiency is compared with SuperFect transfection with pEGFP purified on a Midi-column of Qiagen which corresponds to 100 %, since maximal transfection efficiency (up to 20%) was observed under these conditions. Cell condition was quantified by comparing the percentage of cell death and with the one of untransfected control cells (100%).

47

After one week exposure to 500 μg/ml of G418, 7% untransfected NB41A3 cells survived. The survival rate was very similar (8%) in cells transfected with control pKS$^+$ Bluescript vector devoid of neomycin resistance gene. Cells expressing GFP alone or transfected with 1 μg of each hybrid-GFP vector had a two fold higher survival rate under the same conditions, but other cells transfected with pEGFP vector containing either GAPDH, Hsc70, aldolase or Ulip had survival rates between only 2-7%.

Whereas 750 μg/ml G418, untransfected cells were no more alive after one week, at least 1% transfected cells were still alive after one week exposure to 1250 μl/ml G418. Thereby cells transfected with pEGFP vector alone showed highest resistance, 2-4 fold higher than the other cells. We therefore chose 750 μg/ml G418 as an appropriate concentration to select for stably transfected cells.

After transfection the selection medium containing 750 μg G418/ml was changed every 3 days. After seven passages G418-resistant colonies were selected and analysed under the microscope for GFP expression. By handling the cell clones as described in the method section, we obtained stable NB41A3 cell lines overexpressing GAPDH (NB41$^{\text{GAPDH-GFP}}$), aldolase (NB41$^{\text{aldolase-GFP}}$) and enolase (NB41$^{\text{enolase-GFP}}$).

# 4.2 Optimisation of transfection and incubation conditions

## 4.2.1.1 Optimisation of transfection

Different transfection methods were tested in respect to their transfection efficiency and their influence on cell viability. We tested four different transfection procedures (see methods section and appendix): two CaPO$_4$- methods, a lipofection method with Dotma and SuperFect (Quiagen). Incubation time and DNA purification method was optimised separately for each method (see e.g. *figure 4b* and *figure 4c*). Transfection efficiency was higher with Qiagen-column-purified than with CsCl-purified DNA in all tested transfection methods, whereas the cell viability is unchanged. SuperFect transfection from Qiagen purified cDNA produced the best results regarding high transfection efficiency as well as in terms of low cytotoxicity (*figure 4d*) and was therefore used routinely in all our experiments.

The SuperFect procedure was optimised in a series of investigations. Varring the amount of totally transfected plasmid DNA, the ratio of DNA to SuperFect reagent and the incubation times of DNA/SuperFect complexes with the. With the optimised conditions for suspected transfection of 1 μg plasmid DNA, 5 μl SuperFect, 3-4 h incubation time on cells, we obtained 15-20% transfection efficiency, what is extraordinary high for neuroblastoma cell lines.

## 4.2.1.2 <u>Influence of SuperFect transfection on protein-GFP expression</u>

Whether the interval between transfection and start of exposure to oxidative stress was 24 h, 36 h, 48 h or 72 h did not influence the results of the experiments. The cell confluency does not affect the effects of oxidative stress. Nevertheless we standardised the growth of cells to 60 % confluency before incubation with FeCN or $H_2O_2$.

The efficiency of transfection was about 5-15 % for all GFP constructs, so over 85 % of the cells did not express heterologous GAPDH. Comparing the endogenous GAPDH pattern in these cells with the GAPDH pattern of cells which never had been used for transfection showed that GAPDH distribution is not influenced by the transfection procedure. This was also confirmed for the four other proteins of the PMO complex.

## 4.2.1.3 <u>Optimisation of induction of apoptosis and oxidative stress</u>

Cells were oxidatively stressed with different concentrations of $H_2O_2$ and of FeCN. The stressing agent was directly added to fresh medium (containing 10 % FCS) in which NB41A3 cells at 80% confluency were incubated for 3 h. Cell death was then evaluated by trypan blue in a Neubauer cell chamber. The percentage of dead cells correlated logarithmically with increasing concentrations of $H_2O_2$ and FeCN. 50 % of cells were dead with 300 μM $H_2O_2$ or 1 mM FeCN. Thus, for standard experiments 100 μM $H_2O_2$ and 300 μM FeCN were used, i.e. concentrations where less than 20 % dead cells was observed. Hoechst staining, that at these concentrations there was no significant nuclear fragmentation and therefore that the death cells had not died from apoptosis. For R6 cells, although these cells were more sensitive to oxidative stress, they also did not show nuclear fragmentation in cells stressed by100 μM $H_2O_2$ or 300 μM FeCN.

For investigating apoptosis we tested three potent inducers of apoptosis at different concentrations: FAS APO(100 ng/ml and 400 ng/ml), MG132 (1 μM, 2uM and 3 μM) and staurosporine (100 nM, 200 nM and 500 nM). The number of dead NB41A3 and R6 cells was estimated after 6, 12, 18, 24 and 48 h. We found that FAS APO did not efficiently induce cell death. After 24 h 200 nM staurosporine yielded apoptosis in about 25% NB41A3 cells and in over 50 % R6 cells. With 1 μM MG132 the rate of dead cells at different time points was always smaller, while at 2 μM MG132 they were too high. We therefore used 1.5 μM MG132, yielding 20 % cell death for NB41A3 cells and 70 % cell death for R6 cells after 24h exposure.

# 4.3 Controls for transfection experiments

## 4.3.1 GFP

Using the transfection conditions described above, we observed GFP expression in about 15 % of the cells. In NB41A3 cells *(picture 1a)*, as well as in R6 cells *(picture 1b)* GFP was uniformly expressed all over the cell, except in the nucleolus. No binding of GFP to cytoskeletal structures was found. In none of the cells was the nucleus fragmented. Independent of the level of GFP expression, no differences in morphology or cell viability were observed compared to untransfected neuroblastomas.

It was shown in control experiments by immunocytochemistry, that polyclonal anti-GFP Ab specifically detected only GFP.

Induction of oxidative stress did not change the cell morphology nor the expression of GFP. It was still distributed all over the cell. After exposure to pro-apoptotic reagents, the percentage of GFP-transfected apoptotic NB41A3 and R6 cells were comparable to untransfected cells *(see table 1)*. These cells were shrivelled up, and showed slightly increased levels of GFP compared to non-apoptotic cells, but no increased molecular translocation of GFP.

## 4.3.2 Influence of the GFP- or BFP-tag on protein-expression

### 4.3.2.1 GAPDH

To establish that the GFP-tag or BFP-tag did not influence the expression of GAPDH, cells were transfected with either the GAPDH-GFP (or GAPDH-BFP) expression vector or with an analogous vector without an immunofluorescent tag.

The distribution of GAPDH as detected by the Texas-Red fluorescence was identical in cells transfected with GAPDH alone or in GAPDH-GFP transfected cells, independently of whether cells were unstressed *(picture 1c)* or stressed with either FeCN *(picture 1d)* or $H_2O_2$ *(picture 1e)*. Also the number of cells

showing an effect to exposure to apoptotic agents was comparable in both cases. These observations suggest that the coupled GFP does not influence the expression and localisation of GAPDH.

In the cells transfected with GAPDH-GFP, the green fluorescence from GFP and the red fluorescence from Texas-Red co-localised. This observation was confirmed in cells stressed by $H_2O_2$, suggesting that the endogenous GAPDH co-localises with GAPDH-GFP in transfected cells. Cells that did not contain any GAPDH-GFP were also stained by Texas-Red, indicating that endogenous GAPDH is detected by these antibodies.

### 4.3.2.2 Hsc70

The distribution of Hsc70-GFP and Hsc70 (without GFP tag) was identical, indicating that the GFP-tag did not influence the localisation of the tagged protein. Also after apoptosis, both, the tagged and the untagged Hsc70 behaved in the same manner. However, after oxidative stress it seemed that transfected untagged Hsc70 translocated more into the nucleus than the tagged protein.

### 4.3.2.3 Aldolase

Again, to test whether the GFP tag could influence the pattern of expression after aldolase-GFP transfection, cells were plated and transiently transfected either with the aldolase-GFP expressing vector or with a plasmid expressing untagged aldolase only. The immunofluorescence pattern of cells transfected by aldolase only was identical to the one of aldolase-GFP transfected cells. The effects to oxidative stress or apoptosis were identical in both cell types. Finally cells were co-transfected with both of these vectors, one carrying aldolase-GFP and the other one carrying untagged aldolase, yielding a complete colocalisation between GFP and antibodies against aldolase. These data further substantiated that the GFP-tag does not influence the expression and localisation of aldolase.

### 4.3.2.4 Ulip

First, we examined whether Ulip coupled to GFP gives the same results like Ulip coupled to BFP. Distribution of both of them, Ulip-GFP and Ulip-BFP, was detected by confocal microscopy and by fluorescence microscopy. Although the fluorescence of BFP was much weaker than the one of GFP, the distribution was comparable. Further, immunofluorescence studies showed identical distribution of anti-ULIP antibodies after transfection with either ULIP alone or ULIP tagged with GFP or BFP.

We also checked whether the polyclonal Ab against Ulip specifically recognised Ulip-GFP by comparing the distribution of Ulip-GFP with the distribution of Texas-Red-coupled antibody, which bound with high affinity to a anti-ULIP polyclonal antibody. 90% co-localisation between GFP and Texas-Red was observed in oxidatively stressed cells as well as in unstressed cells transiently transfected with Ulip-GFP. All cell areas where GFP was expressed were also stained by Texas-Red. However additional Texas-Red staining near the cell plasma membrane was also observed, where no GFP was expressed. This means either that some endogenous Ulip is expressed in the cell plasma membrane and weakly also in the nucleus where transfected Ulip-GFP is not expressed, or that the Texas-Red staining was due to another isoform of Ulip detected by the polyclonal antibody, or that GFP-tag changed Ulip-GFP expression in those specific regions. The last hypothesis could be ruled out however, since immunostaining in cells transfected either by ULIP-GFP or by an Ulip-vector devoid of GFP, was identical, displaying a strong patchy staining in the cytoplasm with some Texas-Red at the cell membrane.

## 4.3.2.5 <u>Enolase</u>

The immunofluorescence pattern in cells transfected by enolase alone was identical to the one in enolase-GFP transfected cells. Also the small changes observed after oxidative stress treatment were identical.

# 4.4 <u>GAPDH</u>

## 4.4.1 <u>NB41A3</u>

### 4.4.1.1 <u>Untransfected cells</u>

The intensity of endogenous GAPDH expression in most unstressed NB41A3 cells was about the same in the cytoplasm and in the nucleus *(picture 1f, figure 5a)*. None of the cells were apoptotic *(table 1)*.

After oxidative stress with $H_2O_2$, 70% of GAPDH was expressed in the nucleus of untransfected cells *(picture 1i, figure 5a)*. Treatment with 300 μM FeCN had the same effects as 100 μM $H_2O_2$ and did not promote translocation to the cytoplasm: 75% of GAPDH expression was nuclear. The "speckled" GAPDH pattern associated with cell surface blebbing was only seen very infrequently.

Staurosporine caused nuclear translocation of GAPDH. 6 h after exposure to 200 nM staurosporine, nuclear GAPDH expression was twice as high as the cytoplasmic expression *(figure 6a)*. Whereas in the vast majority of non-apoptotic cells, the GAPDH levels increased only by about 50%, in apoptotic cells (about 5%) GAPDH expression increased up to 300%, but is excluded from the fragmented DNA *(picture 1g, 1h)*. After 24 h of staurosporine exposure, the number of apoptotic cells is about 20% *(figure 6b)*. Interestingly, later on some apoptotic cells become depleted of GAPDH *(picture 1j, 1k)*.

MG132 had effects very similar to staurosporine *(figure 6c)*. 6 h after exposure, 90% of GAPDH was expressed in the nucleus *(picture 1m, 1n)*. Some of these cells also had changed to a hedgehog like morphology, other cells *(picture 1l)* were round and formed blebs containing GAPDH but did not have nuclear fragmentation. The percentage of apoptotic cells was slightly higher than in untreated cells. After 24 h, however, 20% of the cells were apoptotic and had very high GAPDH expression, which later on disappeared sometimes, similar to the effects induced by staurosporine.
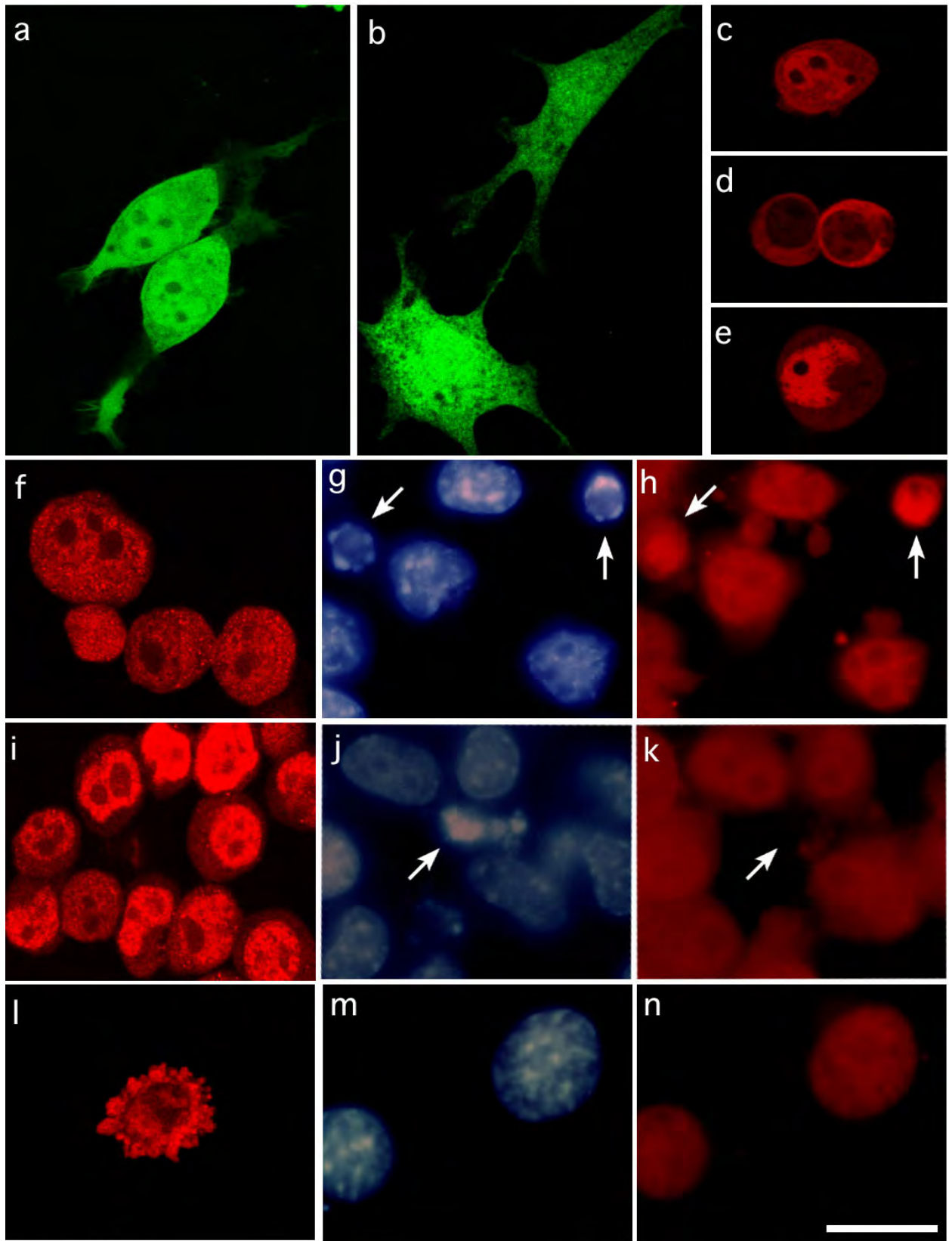
**Picture 1**

| | Control | MG132 6h | MG132 24h | Staurosporine 6h | Staurosporine 24h |
|---|---|---|---|---|---|
| NB41A3 untransfected | 0 | 2 | 20 | 5 | 20 |
| NB41A3 transiently transfected | 10 | 15 | 35 | 20 | 40 |
| NB41A3$^{GAPDH-GFP}$ | 5 | 15 | 35 | 15 | 35 |
| R6 untransfected | 0 | 10 | 70 | 10 | 50 |
| R6 transfected | 10 | 50 | 90 | 70 | 85 |
| R6$^{Bcl-2}$ untransfected | 0 | 2 | 20 | 5 | 15 |
| R6$^{Bcl-2}$ transfected | 10 | 50 | 85 | 60 | 90 |

**Table 1: Apoptosis in untansfected and GAPDH-GFP transfected cells.** The percentage of apoptotic cells after 6 h and 24 h of incubation with either MG132 (1.5 μM) or staurosporine (200 nM) is indicated. Cells showing chromatin condensation or nuclear fragmentation, which was visualised by Hoechst blue staining, were considered as apoptotic cells. Standard deviation is smaller than 5 % in all tested conditions.

←

**Picture 1: Subcellular localisation of endogenous GAPDH after oxidative stress or apoptosis in NB41A3 neuroblastoma cells.**
**(a-e) Controls: effects of transfection on cellular localisation of GFP or GAPDH. (a-b)**: controls of transfection with pEGFP**: (a)** NB41A3 neuroblastoma cells cells or **(b)** R6 retinoblastoma cells were transfected with pEGFP (a control vector devoid of GADPH gene) to test viability and distribution of the GFP. **(c-e)** : NB41A3 cells were transfected with pGAPDH (a vector devoid of GFP-tag) and the expression of GAPDH was tested, as detected by TR immunohistochemistry, in **(c)** unstressed cells and in cells stressed with**(d)** 300 μM FeCN or with **(e)** 100 μM H$_2$O$_2$, respectively.
(**f-n)** Subcellular localisation of GAPDH in untransfected NB41A3 cells.
 **(f, i)** Distribution of endogeneous GAPDH in untransfected NB41A3, either **(f)** unstressed or **(i)** stressed with 100 μM H$_2$O$_2$ detected by TR-immunohistochemistry. **(g, h)** Apoptosis induced in NB41A3 after exposure to 200 nM staurosporine for 6 h. **(j, k)** Apoptotic cells devoid of GAPDH observed at later stages of apoptosis (200 nM staurosporine for 24 h). **(m, n)** Nuclear translocation and **(l)** bleb-forming cell after induction of apoptosis for 6h with 1.5 μM MG132.
DNA is detected by Hoechst staining **(g, j, m)**. See methods for details. Scale bar is 50 μm
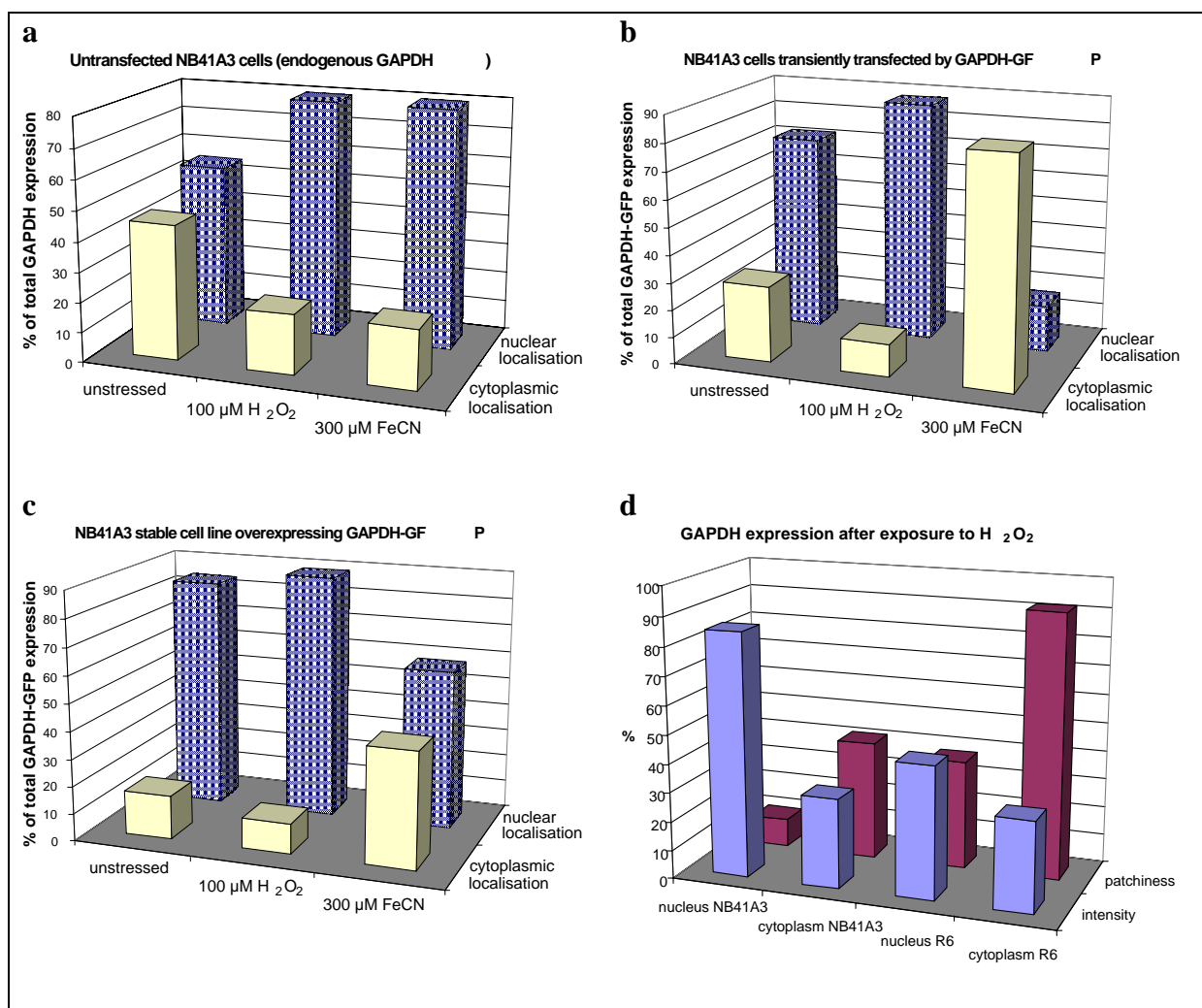
**Figure 5: Subcellular localisation of GAPDH in NB41A3 cells.** (**a**) Untransfected, (**b**) transiently transfected and (**c**) stably transfected cells were analysed under unstressed conditions or after 3 h of oxidative stress with either 100 μM $H_2O_2$ or 300 μM FeCN. The percentage of total GAPDH (or of GAPDH-GFP for transfected cells) in the nucleus and in the cytoplasm is indicated. Standard deviation is smaller than 5 % in all tested conditions. (**d**) GAPDH-GFP expression was analysed after oxidative stress with regard to its intensity and to its uniformity/patchiness in NB41A3 and R6 cells. Histograms of GAPDH expression in cells exposed to 100 μM $H_2O_2$ for 3 h were evaluated regarding the mean intensity and the variation (= standard deviation squared) of expression. Intensity (=expression level) and variation (=patchiness) are presented for nucleus and cytoplasm. Both cell lines show higher and less patchy GAPDH expression in the nucleus. Expression in R6 cells is more patchy than in NB41A3 cells.
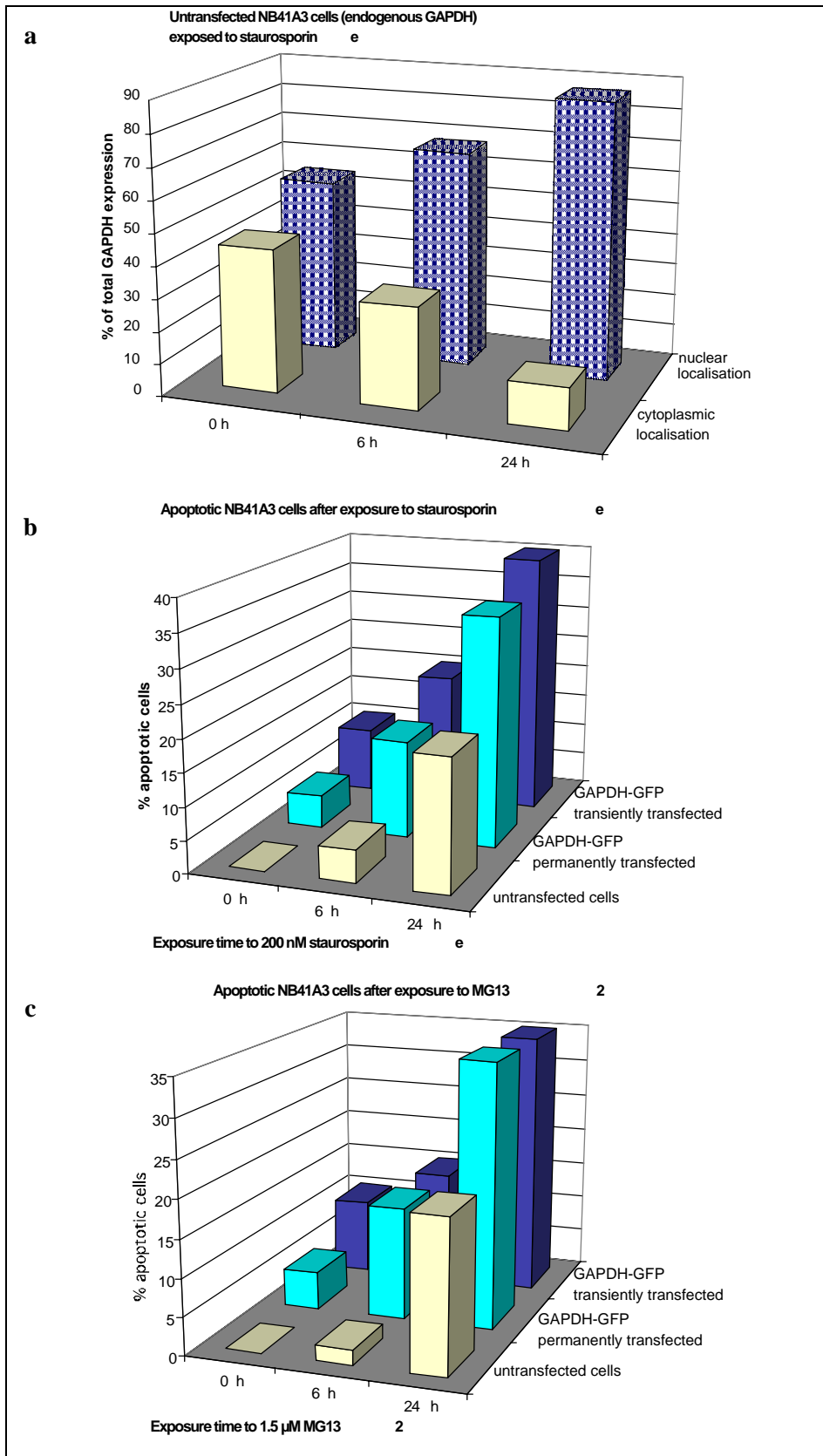
**Figure 6: Induction of apoptosis by staurosporine and MG132.** Induction of apoptosis by staurosporine (200 nM) and MG132 (1.5 μM) in NB41A3 cells was performed as described for 0, 6 or 24 h.**(a)** Untransfected cells exposed to staurosporine: the percentage of total endogenous GAPDH in the nucleus and in the cytoplasm is indicated.  **(b, c)** The percentage of cells showing nuclear fragmentation or chromatin condensation after exposure to **(b)** staurosporine and  **(c)** MG132 is indicated in NB41A3 cells expressing endogenous GAPDH or transfected GAPDH-GFP.

**a**

**GAPDH-GFP expression in stressed NB41A3 cells**
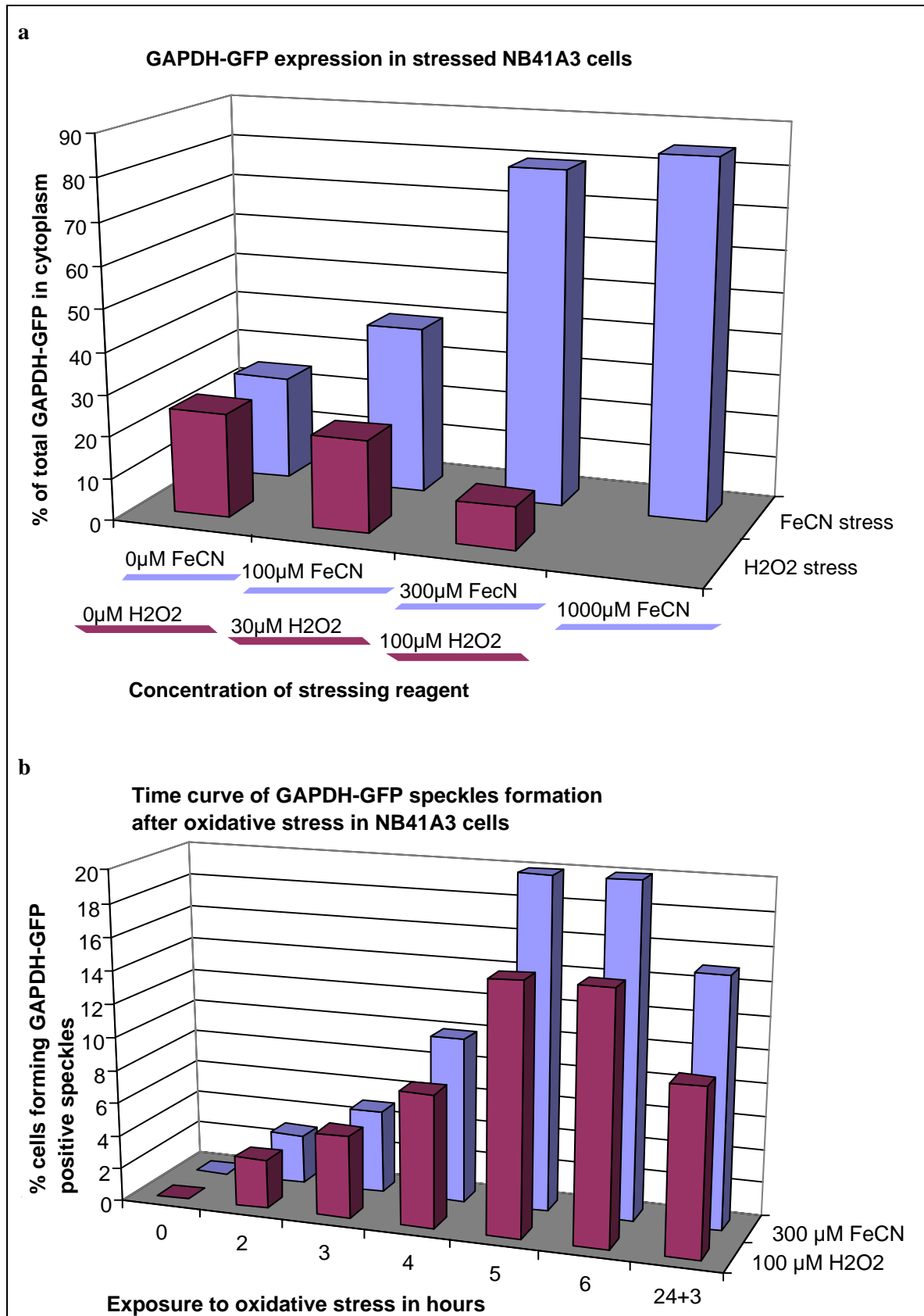
**Figure 7: Effects of oxidative stress to GAPDH-GFP transfected NB41A3 cells. (a)** Percentage of total GAPDH-GFP expressed in the cytoplasm of transiently transfected NB41A3 cells exposed to either to either $H_2O_2$ (0-300 μM) or FeCN (0-1000 μM) for 3 h. **(b)** Percentage of cells exposed for different time (from 0-6 h) to 100 μM $H_2O_2$ or to 300 μM FeCN forming GAPDH-GFP positive speckles. Additionally, a set of cells (24+3) was first stressed for 6 h, incubated further for 18 h in normal growth medium and then stressed again for 3 h.

## 4.4.1.2 **Transiently GAPDH-GFP transfected cells**

Controls

The distribution of GAPDH in transfected neuroblastoma cells was different to the one in untransfected cells *(figure 5b)*. Most of the transfected GAPDH-GFP (65%) was concentrated in the nucleus under basal conditions *(picture 2a)*. No GAPDH-GFP fluorescence could be detected in the nucleolus of any cells examined under various experimental conditions. Further, no formation of GAPDH-GFP speckles was observed in the cells. The cellular distribution of GAPDH-GFP did not depend on the shape of the neuroblastoma cells.

Nuclear fragmentation was seen in 10% of GAPDH-GFP transfected neuroblastoma cells in the absence of apoptotic reagents *(table 1)*. These apoptotic cells expressed 3 times more GAPDH-GFP than other cells *(picture 2b, 2c)*.

Induction of Oxidative Stress

After treatment with 300 μM FeCN, the majority of GAPDH-GFP fluorescence (80%) was found in the cytoplasm *(picture 2e, figure 5b)*. Compared with unstressed cells, a 0.4 fold increase of GAPDH-GFP in the cytoplasm was observed.

The ratio between cytoplasmic and nuclear GAPDH-GFP expression varied from 1.5:1 up to 4:1. This variation may be due to the phenotypic heterogeneity of NB41A3 cells, which may in particular involve their response to oxidative stress, and the cell to cell variability of transfection.

This translocation was dose-dependent *(figure 7a)*: Cells stressed with only 100 μM FeCN showed qualitatively similar changes but, the percentage of cells displaying a change of pattern was only about 40% and the effect was less pronounced (ratio cytoplasm : nucleus from 1:1 to 3:1). Incubation with 1000 μM of FeCN killed about 50% of the cells, but in the surviving cells 90% GAPDH-GFP was expressed predominantly in the cytoplasm. The majority of these cells were rounded up; additionally, in few cells GAPDH-GFP was associated with cell surface blebs *(picture 2f)*.

In contrast, exposure to $H_2O_2$ enhanced nuclear expression of GAPDH-GFP *(picture 2g)*. Most cells treated with 30 μM of $H_2O_2$ for 3 h, like control cells, expressed 1-3 fold more GAPDH-GFP in the

nucleus than in the cytoplasm. 100 μM $H_2O_2$ raised the nuclear GAPDH-GFP fluorescence from 65% to 80%. For both concentrations no expression was observed in the nucleolus. A minority of cells (5%) accumulated GAPDH-GFP in small intracellular speckles *(picture 2h)*.

The relationship between this "speckled" phenotype and oxidative stress was explored by incubating cells with either 300 μM FeCN or 100 μM $H_2O_2$ for 2 h to 6 h. On one plate cells were stressed for 4 hours, re-incubated with standard medium for another 20 hours and again exposed for 4 hours with the stressing agent, before examination under the microscope. The percentage of cells forming GAPDH-GFP "speckles" increased with the duration of the stress from less than 4% after 2h up to 20% after 5 h with $H_2O_2$ or 15% with FeCN *(figure 7b)*. These results indicate that the accumulation of GAPDH-GFP "speckles" correlates with oxidative stress. Some cells were in an intermediate stage, changing from nuclear or cytoplasmic GFP-pattern to a speckled pattern *(picture 2i)*.

Oxidative stress by both 100 μM $H_2O_2$ or 300 μM FeCN did not increase the percentage of nuclear fragmentation in GAPDH-GFP overexpressing cells. Nevertheless, a phenomenon that was exclusively observed in stressed cells overexpressing GAPDH-GFP (mostly at very high amounts) was that in few cells GAPDH-GFP fluorescence was associated with pronounced blebbing of the cell surface membrane.

➡

**Picture 2: Subcellular localisation of GAPDH-GFP in transiently or stably transfected NB41A3 neuroblastoma cells.**
**(a-j) GAPDH-GFP expression in transiently transfected cells.**
**(a)** Expression of GAPDH-GFP in transiently transfected NB41A3 neuroblastoma cell under unstressed conditions. **(b, c)** Apoptotic cell under unstressed condition, detected by **(b)** Hoechst staining or **(c)** as GFP fluorescence. **(e)** Cytoplasmic translocation and **(f)** formation of GAPDH-GFP blebs after oxidative stress induced **(e)** by 300 μM and **(f)** 1 mM FeCN. **(g)** Nuclear translocation in the majority and **(h)** speckle formation accumulating GAPDH-GFP in a minority of cells, observed after oxidative stress with 100 $H_2O_2$. **(i)** Stressed cell in an intermediate stage changing from nuclear to speckled expression pattern. **(d, j)** Induction of apoptosis for 6 h with 200 nM staurosporine, displaying **(d)** apoptotic cells or **(j)** network-like structures. **(k-o)** Hedgehog like cell after apoptosis induced with 1.5 μM MG132 for 6 h. While **(k-n)** are confocal images of single planes at different z-axis values, **(o)** is a x-y projection of all sections trough the z-axis. **(p-r)** Permanent expression of GAPDH-GFP in NB41A3[GAPDH-GFP] cell line, under **(p)** unstressed conditions, or after oxidative stress with **(q)** 100 μM $H_2O_2$ or **(r)** 300 μM FeCN, respectively. The green fluorescence displays GADPH-GFP expression. In **(q)** and **(r)**, the cytoplasm was made visible by immunostaining with anti-enolase-γ.
The scale is the same for all figures, except for **(j)**. Scale bars are 50 μm.
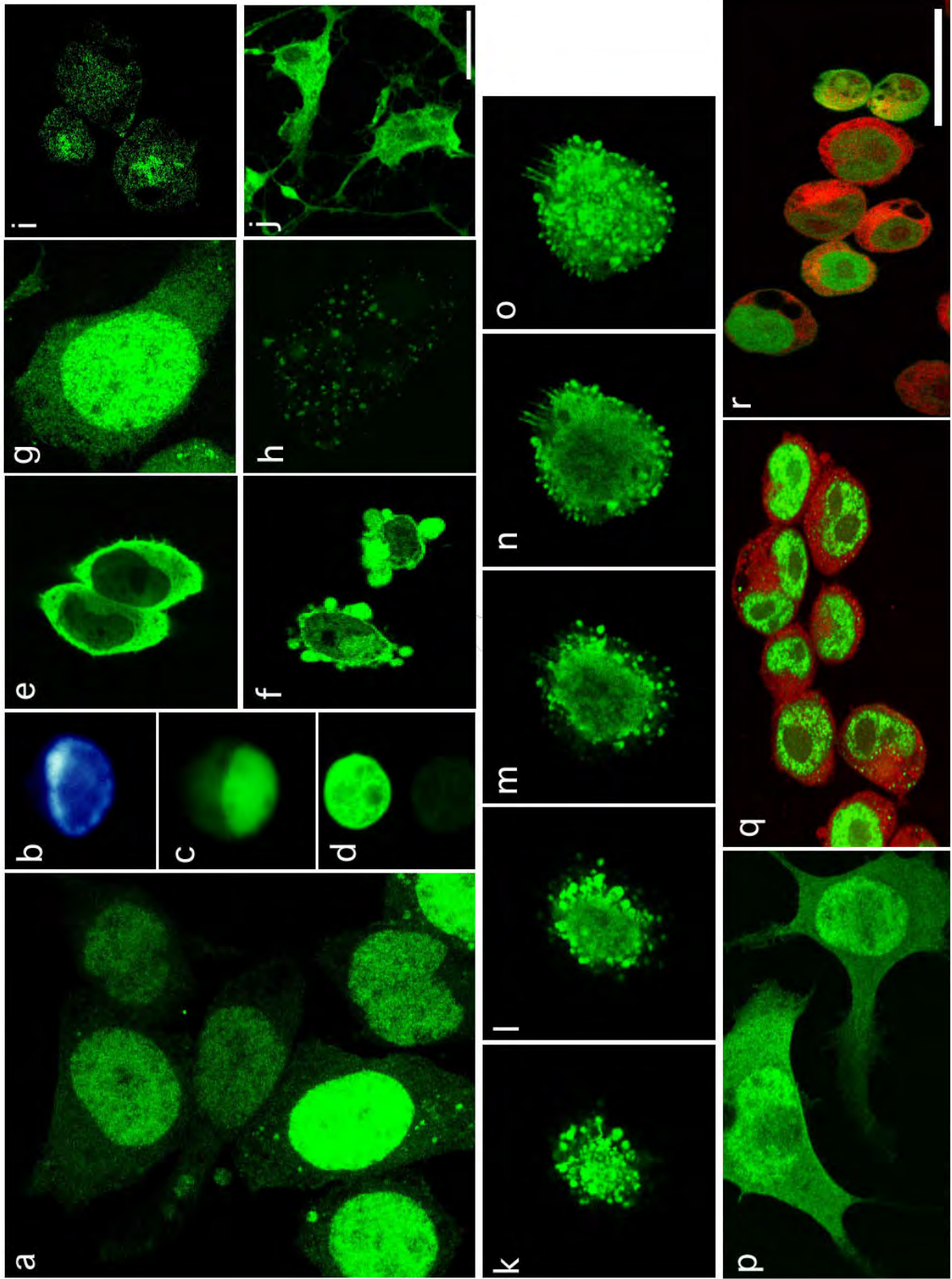
**Picture 2**

<u>Induction of Apoptosis</u>

In contrast to untransfected cells, most of the GAPDH-GFP transfected cells change their morphology after 6 h of incubation with 200 nM staurosporine. Many cells contain only a small cytoplasmic area and have very long axons which form together a network-like structure *(picture 2j)*. These non-apoptotic cells express high levels of GAPDH (about 50% more per cell than control cells) at same the intensity in nucleus and cytoplasm. The apoptotic cells (20%) *(figure 6b)* are shrivelled up, have fragmented nuclei and are much smaller than non-apoptotic cells *(picture 2d)*. They express GAPDH at very high levels in the nucleus, over 3 times over baseline. After 24 h exposure to staurosporine more than one third of the neuroblastoma cells have fragmented nuclei *(table 1)*.

High GAPDH expression is found all over after 6 h exposure to MG132. The number of hedgehog shaped cells, all showing an unfragmented nucleus, increased nearly twofold compared to untransfected cells *(picture 2k-2o)*. The remaining 15% cells were apoptotic *(figure 6c)*. After 24 h of treatment, except for the higher percentage of apoptotic cells, the observations were similar as for untransfected cells under similar conditions *(table 1)*.

<u>Co-transfections of GAPDH-GFP with other proteins</u>

We wanted to test whether any of the other four proteins (enolase, Ulip, Hsc70, and aldolase) known to form a complex together with GAPDH influences GAPDH-GFP expression if it is co-transfected. In these co-transfection experiments one protein was coupled to GFP and the other one to BFP.

Co-transfection of GAPDH-GFP and enolase-BFP together did not change the pattern of GAPDH expression in unstressed cells. After oxidative stress (100 μM $H_2O_2$ or 300 μM FeCN) the percentage of cells forming intracellular GAPDH-speckles or concentrating GAPDH-GFP at the plasma membrane was about doubled compared to cells expressing GAPDH-GFP only.

Similar effects were also seen with Ulip. While in absence of oxidative stress no significant difference was observed, 30% of the cells stressed with FeCN or $H_2O_2$ showed either intracellular GAPDH-speckles or very brightly stained plasma membranes. In addition, in cells exposed to FeCN, 40% of GAPDH was displayed in the nucleus (against less than 10% in cells only carrying the GAPDH plasmid). Since cells

transfected with Ulip-GFP alone show considerable translocation of Ulip into the nucleus after oxidative stress (results shown later), we suggest that Ulip somehow interacts with GAPDH.

We observed that concomitant overexpression of GAPDH with either aldolase or Hsc70, both of which are expressed predominantly in the cytoplasm, increased cytoplasmic GAPDH expression in unstressed and stressed cells. Prior to oxidative stress 55%, and after exposure to 100 μM $H_2O_2$ for 3 h, 40% of GAPDH was expressed in the cytoplasm of these cells. I.e., overexpression of Hsc70 and aldolase partially prevents nuclear translocation of GAPDH.

## 4.4.1.3 Stable cell line overexpressing GAPDH-GFP (NB41[GAPDH-GFP])

Controls

In a bulk population of cells stably overexpressing GAPDH-GFP, 5% NB41A3 show nuclear fragmentation due to high GAPDH-GFP expression *(table 1)*. Most non-apoptotic cells (80%) express 2-4 fold more GAPDH-GFP in the nucleus than in the cytoplasm *(picture 2p, figure 5c)*. Cells forming GAPDH-positive speckles or blebs were not found.

Induction of oxidative stress

Cells stressed with 100 μM $H_2O_2$ for 3 h showed slightly increased nuclear expression *(picture 2q)*. Nevertheless, the nucleoli are devoid of GAPDH-GFP. FeCN incubation showed more effects *(figure 5c)*: the proportion of cells expressing mostly cytoplasmic GAPDH-GFP increased from 15% to 40%, yet over 50% had still a higher nuclear expression *(picture 2r)*. The amount of apoptotic cells after oxidative stress was very small (5-10%) and not higher than in unstressed cells and cells forming GAPDH-GFP "speckles" were rarely found.

Induction of apoptosis

The effects of staurosporine and MG132 on NB41[GAPDH-GFP] were very similar to those ones observed in transiently transfected NB41A3, resulting in increased GAPDH-GFP expression all over the cell and hedgehog-like cell shape. The overexpressed GAPDH-GFP leads to over 30% apoptotic cells after 24 h of MG132 or staurosporine exposure, twice more than in untransfected cells *(figure 6b, 6c, table 1)*.

# 4.4.2 <u>R6 and R6$^{Bcl-2}$</u>

## 4.4.2.1 <u>Untransfected cells</u>

<u>Controls</u>

To test whether the expression of GAPDH protein described above is specific for neuronal cells or whether similar localisation and differential translocation can be also observed in non-neuronal cells, embryonic R6 fibroblasts were used. In addition a R6 cell line permanently overexpressing Bcl-2 (R6$^{Bcl-2}$) was used to investigate the influence of Bcl-2 during apoptosis and oxidative stress. In contrast to what is observed in NB41A3 cells, the endogenous GAPDH is expressed along cytoskeletal fibres in the cytoplasm, especially in the perinuclear area of untransfected R6 cells *(picture 3b, 3d)* and R6$^{Bcl-2}$ cells *(picture 3e)*. 80% of total GAPDH was expressed in cytoplasm, although in about 30 % of the cells GAPDH expression level in the cytoplasm and in the nucleus was about equal *(figure 8a)*. No signs of apoptosis were observed in untransfected fibroblasts before treatment with apoptotic agents *(picture 3a, table 1)*.

➡

**Picture 3: Subcellular localisation of endogenous GAPDH in untransfected R6 and R6$^{Bcl-2}$ fibroblast cells**
Cytoplasmic localisation of GAPDH in unstressed **(a-d)** R6 or **(e)** R6$^{Bcl-2}$ cells.
**(d)** Overlay of **a-c**. The three upper untransfected cells (red) show similar GAPDH expression like the two lower transfected cells (yellow=green+red). The nuclei (blue) are not fragmented. **(f-i)** Nuclear translocation of endogenous GAPDH in **(f)** R6 and **(h)** R6$^{Bcl-2}$ cells, and accumulation of GAPDH in speckles in **(g)** R6 and **(i)** R6$^{Bcl-2}$ cells after exposure to 100 μM H$_2$O$_2$ for 3 h**.** **(j)** 60% of R6 cells with intact nuclei still have cytoplasmic expression of endogenous GAPDH after exposure to 1.5 μM MG132 for 6 h, whereas **(p, q)** 10% are apoptotic. **(k,l,m,n,o,r)** Translocation of GAPDH after exposure to 200 nM staurosporine. **(m-o)** Unchanged cytoplasmic localisation of GAPDH after 2 h. **(o)** Overlay of **m & n**. **(k, l)** Increasing amount of nuclear expression after 6 h. **(r)** Apoptotic cells after 24 h.
**(a,d,j,k,p)** Visualisation of DNA by Hoechst blue staining. Detection of GAPDH by **(b,d,e,f,h,i,j,l,m,o,q,r)** TR or **(g)** FITC staining of anti-GAPDH Ab. **(c,d,n,o)** Visualisation of transfected GAPDH by GFP tag. Scale bar is 50 μM.
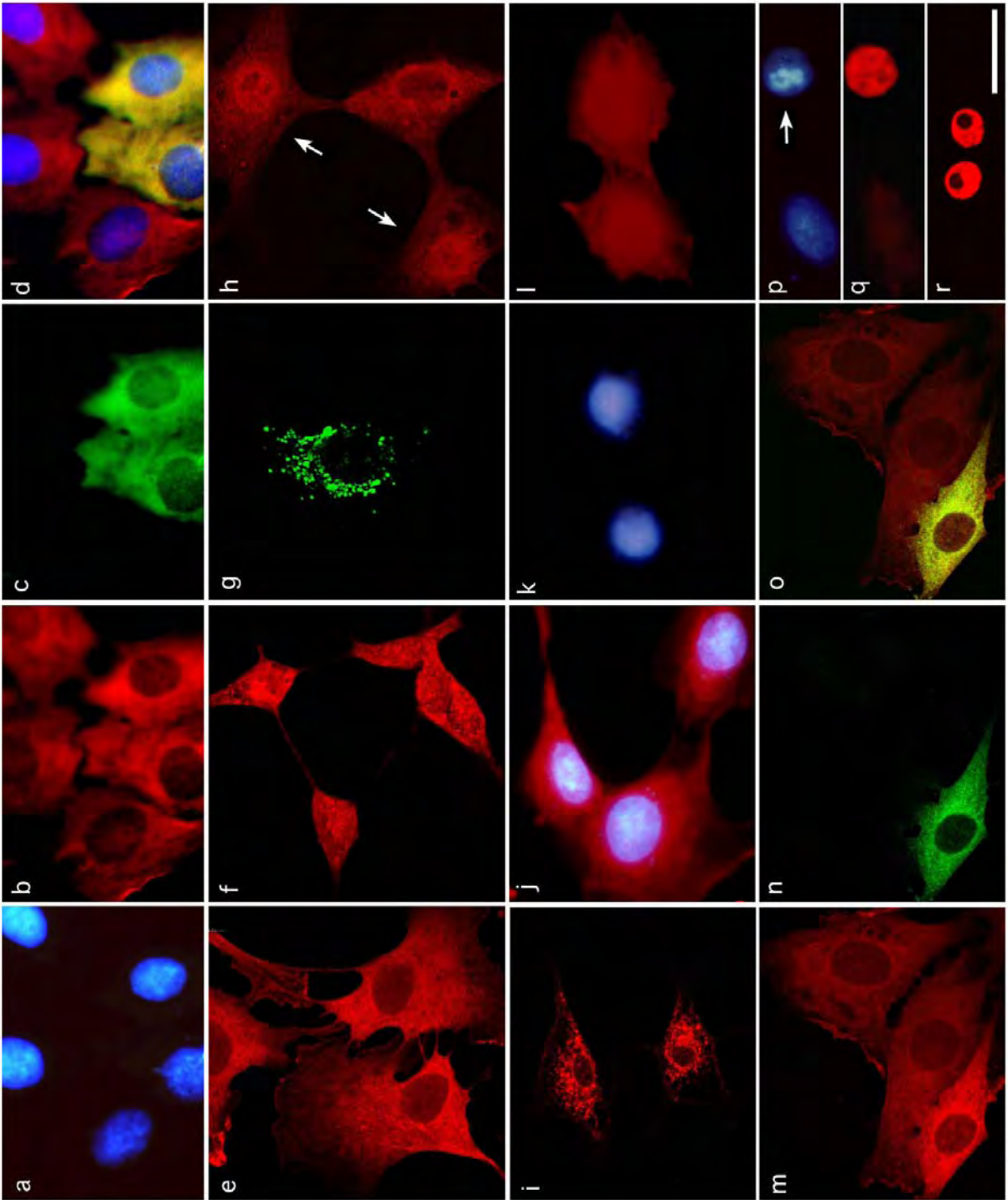
**Picture 3**
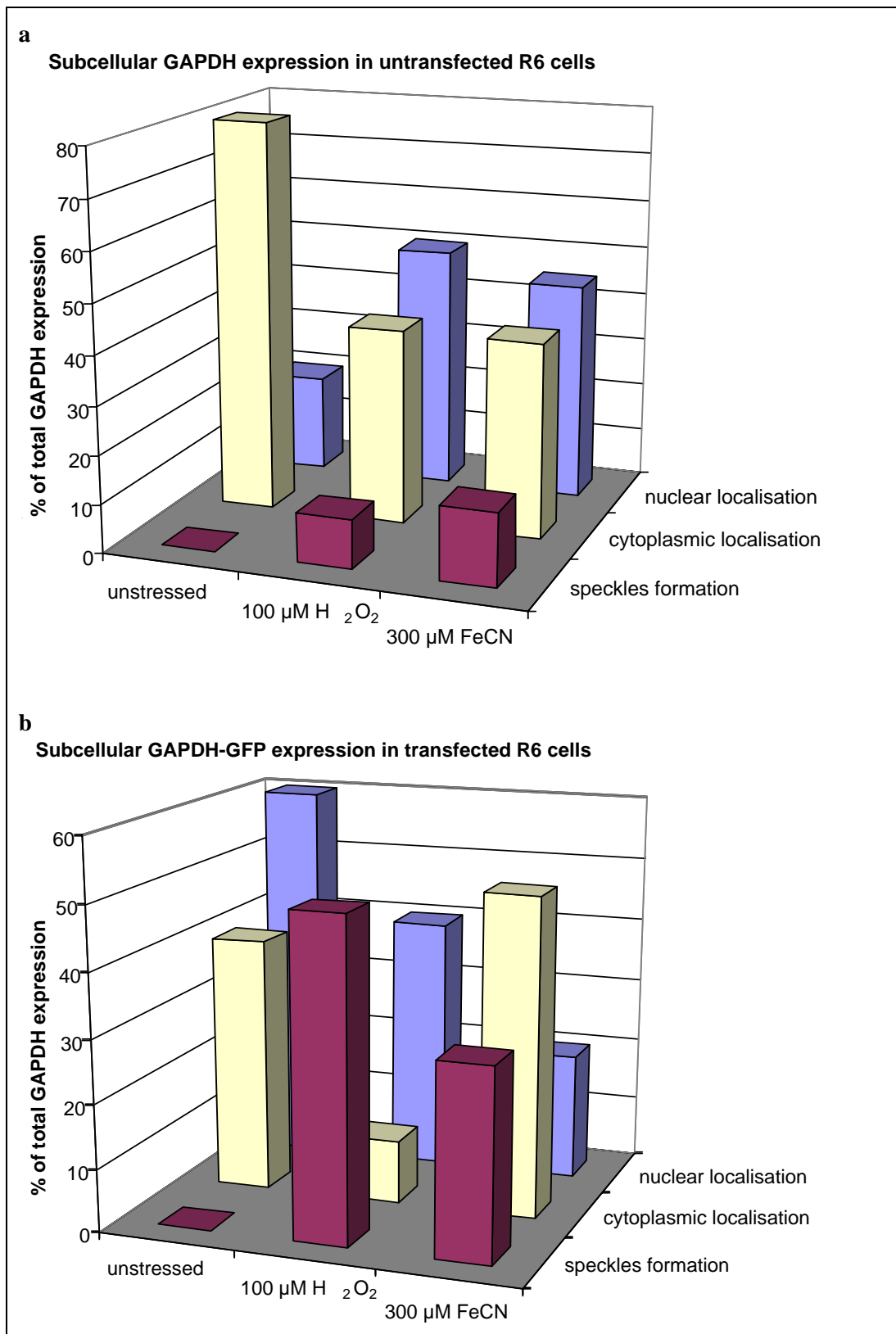
**Figure 8: Subcellular localisation of GAPDH after oxidative stress in R6 cells**. **(a)** Untransfected and **(b)** transiently transfected cells were analysed under unstressed conditions or after 6 h of oxidative stress with either 100 μM $H_2O_2$ or 300 μM FeCN. The percentage of total GAPDH (or of GAPDH-GFP for transfected cells) in the nucleus, in the cytoplasm or in speckles is indicated. Standard deviation is smaller than 5 % in all tested conditions.
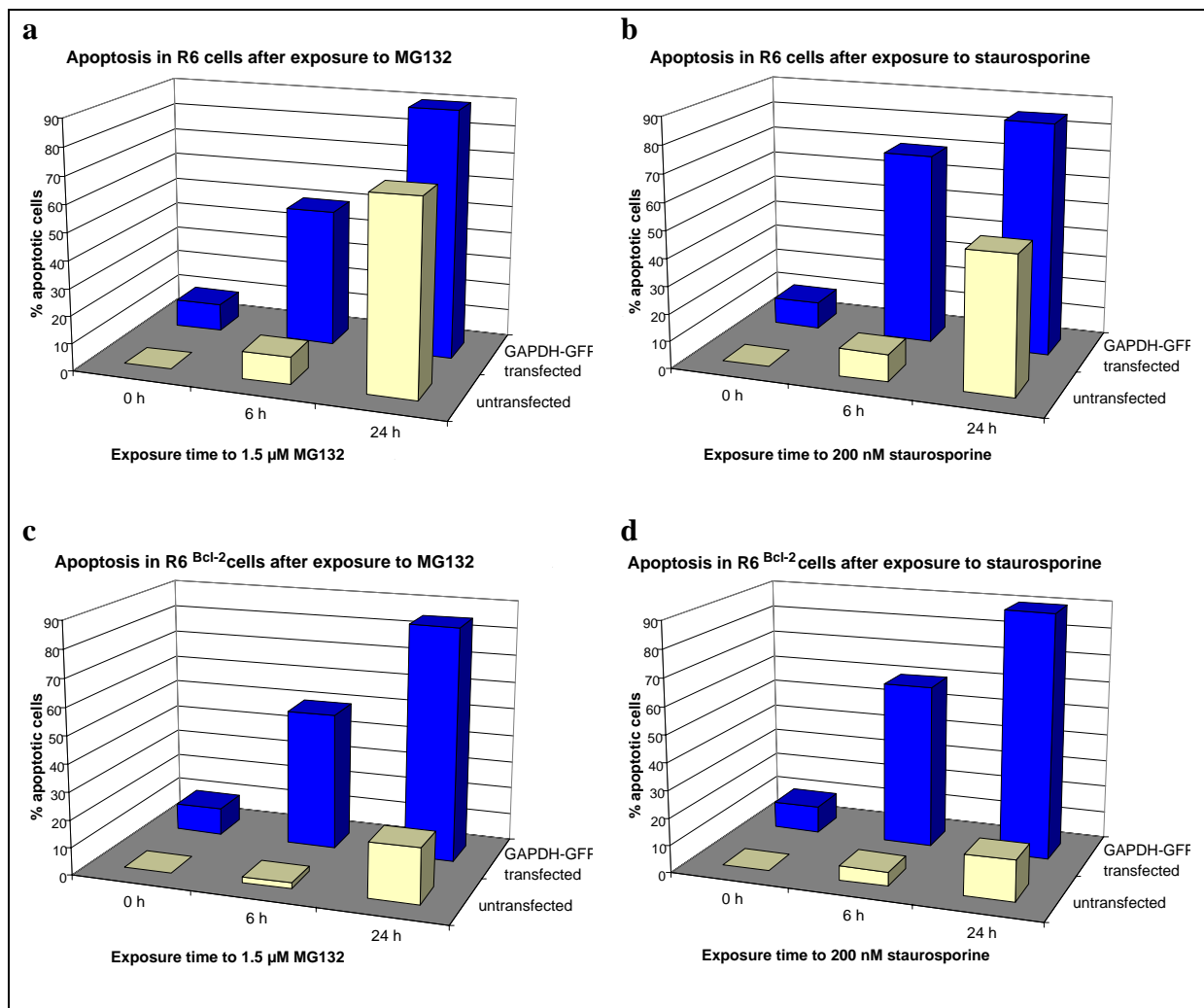
**Figure 9: Apoptosis in R6 and R6<sup>Bcl-2</sup> cells**. (**a, b**) R6 and (**c, d**) R6<sup>Bcl-2</sup> cells were exposed to (**a, c**) MG132 (1.5 μM) or (**b, d**) staurosporine (200nM). The percentage of cells showing nuclear fragmentation or chromatin condensation in cells expressing endogenous GAPDH or transfected GAPDH-GFP is indicated after 0, 6 and 24 h of exposure time.

Induction of oxidative stress

After oxidative stress for 6h with 100 μM $H_2O_2$ or 300 μM FeCN translocation of GAPDH from the cytoplasm to the nucleus was observed in 40%-50% of R6 cells *(figure 8a)*. R6 cells did not show a uniform distribution of GAPDH, neither in the nucleus nor in the cytoplasm *(picture 3f, figure 5d)*, but higher concentrations of GAPDH were found around the nucleolus. In addition, GAPDH spots accumulated at the cell membrane after oxidative stress resembling the "speckled" pattern described in NB41A3 cells *(picture 3g)*. Stable overexpression of Bcl-2 in $R6^{Bcl-2}$ cells does not change the percentage of nuclear translocation *(picture 3h)* nor the formation of GAPDH positive speckles *(picture 3i)* in response to oxidative stress induced by $H_2O_2$ or FeCN.

Induction of apoptosis

R6 cells were examined after 6 h of exposure to MG132. 60% cells display unchanged perinuclear distribution of GAPDH, similar to controls *(picture 3j)*, whereas 30% express GAPDH predominantly in the nucleus. In both cases cells have no visible signs of apoptosis. The 10% remaining cells display nuclear fragmentation *(picture 3p, 3q, figure 9a, table 1)* and the expression of GAPDH is about 2-3 times higher. Under similar experimental conditions $R6^{Bcl-2}$ cells display only 2% apoptotic cells, all showing very high expression of endogenous GAPDH *(figure 9c, table 1)*, and 10% of those also showed nuclear translocation of GAPDH but no nuclear fragmentation.

After 24 h of incubation with MG132 only one third of the R6 cells show the usual perinuclear GAPDH ring around the nucleus without changes in their immunohistochemical pattern, whereas most of the other R6 cells are apoptotic and accumulate very high amounts of GAPDH. Interestingly, in a number of apoptotic cells GAPDH has already fainted away completely *(similar to picture 1j, 1k)*. Under similar conditions $R6^{Bcl-2}$ cells show apoptotic features only in 20% cells *(figure 9c)*. Together these observations are consistent with the fact that Bcl-2 protects cells from apoptosis.

In experiments where apoptosis was induced by the protein kinase inhibitor staurosporine (200 nM and 750 nM) we obtained similar results as for MG132-induced apoptosis *(figure 9b)*. Half the untransfected R6 cells exposed to 200 nM staurosporine for 24 h were apoptotic. The GAPDH pattern changes during staurosporine induced apoptosis as follows: initially, endogenous GAPDH is mainly concentrated at the perinuclear area and along the cytoskeleton *(picture 3m, 3o)*. About 6 h after addition of the apoptotic

agent, the cells start to accumulate GAPDH in the nucleus *(picture 3l)*. Most of the cells do not show apoptotic features such as nuclear fragmentation*(picture 3k)*. But a few hours later small shrivelled up, round apoptotic cells expressing GAPDH at very high levels (about 2-3 times more intense than in not apoptotic cells) can be detected *(picture 3r)*. Another few hours later up to 10% of the apoptotic cells contain no detectable GAPDH any more *(similar to picture 1j, 1k)*.

In R6$^{Bcl-2}$ cells, the protection against staurosporine-induced apoptosis was higher than against MG132 *(table 1, figure 9d)*. After 24 h exposure to staurosporine, GAPDH staining was unchanged in 50% of cells and comparable to controls. 35% of the cells had fewer processes than controls. GAPDH was not expressed predominantly in the perinuclear area, but distributed all over. Only 15% of untransfected R6$^{Bcl-2}$ cells are apoptotic *(figure 9b)* and express 2-3 times higher levels of endogenous GAPDH.

## 4.4.2.2 <u>Transiently transfected cells</u>

<u>Controls</u>

The expression of transiently transfected GAPDH-GFP in R6 fibroblasts and in R6$^{Bcl-2}$ fibroblasts was quite similar. 30% of transiently transfected cells displayed predominantly perinuclear GAPDH expression, similar to untransfected cells *(picture 4a)*. All other cells showed predominantly nuclear GAPDH-GFP expression subsequent to transfection *(picture 4b, figure 8b)*. The percentage of nuclear expression in transfected R6 cells was thus smaller than in transfected NB41A3 neuroblastomas (see above). There was no direct correlation between the expression level of GAPDH-GFP and its localisation. GAPDH-GFP transfected R6 and R6$^{Bcl-2}$ cells were in part apoptotic. In contrast to untransfected cells, after transient transfection with GAPDH-GFP nuclear fragmentation was observed in about 10% of cells *(picture 4c, 4d, table 1)*. These apoptotic cells were shrivelled up and they expressed 2-3 fold higher levels of GAPDH-GFP around the segmented DNA. The rate of apoptotic R6$^{Bcl-2}$ cells transfected with GAPDH-GFP was not different from the one seen in R6 cells *(table 1)*.

<u>Induction of oxidative stress</u>

Exposure of R6 cells to $H_2O_2$ induced drastic changes in GAPDH-GFP localisation already after 3 h. In all cells GAPDH-GFP exerted a punctuated expression pattern. While most R6 fibroblasts accumulated GAPDH-GFP in the nucleus, it is sometimes distributed all over the cell or arranged in speckles, as

described for NB41A3. Cells with very high expression levels of GAPDH-GFP formed GAPDH-GFP positive blebs at the cell surface *(picture 4f)* but had no fragmented nucleoli *(picture 4e)*. Speckles formation was much more frequent than in untransfected R6 cells. In contrast to observations with untransfected fibroblasts, FeCN did not induce nuclear translocation of GAPDH-GFP *(figure 8b)*. Quite the opposite, punctuate GAPDH-GFP expression is observed in many R6 cells predominantly in the perinuclear area of the cytoplasm *(picture 4g)*. However, like with $H_2O_2$, many cells start forming GAPDH-GFP positive speckles at the cell surface. About 15% cells showed nuclear fragmentation.

Changes in GAPDH-GFP localisation were also seen in R6$^{Bcl-2}$ cells. $H_2O_2$ and FeCN both induced GAPDH-GFP expression in the nucleus and in speckles at the plasma membrane *(picture 4h)*. Additionally, many cells with a hedgehog like shape expressing GAPDH-GFP all over the cell were observed. Cells, where GAPDH-GFP was bound to cytoskeletal structures were not found. Interestingly, about 20% of GAPDH-GFP transfected R6$^{Bcl-2}$ cells were apoptotic, i.e. 5% more than in R6 cells.

➔

**Picture 4: Subcellular localisation of GAPDH-GFP in transfected R6 and R6$^{Bcl-2}$ cells**
**(a)** 30 % of GAPDH-GFP transfected, unstressed R6$^{Bcl-2}$ cells (green) show similar perinuclear GAPDH-GFP localisation like endogenous GAPDH detected by TR in untransfected cells (red), while **(b)** 60 % express GAPDH-GFP predominantly in the nucleus and **(c, d)** 10 % are apoptotic. **(e, f)** R6 cell with unfragmented DNA forming GAPDH-GFP positive blebs at the cell surface after exposure to 100 μM $H_2O_2$ for 3 h. **(g, h)** Perinuclear localisation of GAPDH-GFP and formation of cells with GAPDH-GFP positive spikes and speckles at the cell surface after exposure to 300 μM FeCN for 3 h in **(g)** R6 and **(h)** R6$^{Bcl-2}$ cells. **(i, j)** Hedgehog like R6 cells forming speckles and spikes attached two the cell surface shown in two different confocal planes. **(k-p)** Formation of long processes and high expression of GAPDH-GFP in transfected **(k-m)** R6 and **(n-p)** R6$^{Bcl-2}$ cells, but not in untransfected cells after exposure to 200 nM staursprine for 6h. **(k, n)** TR staining by anti-GAPDH, **(l, o)** GAPDH-GFP fluorescence, **(n, p)** overlay of GFP and TR fluorescence.
**(c, e)** Visualisation of DNA by Hoechst blue staining. Scale bar is 50 μM.
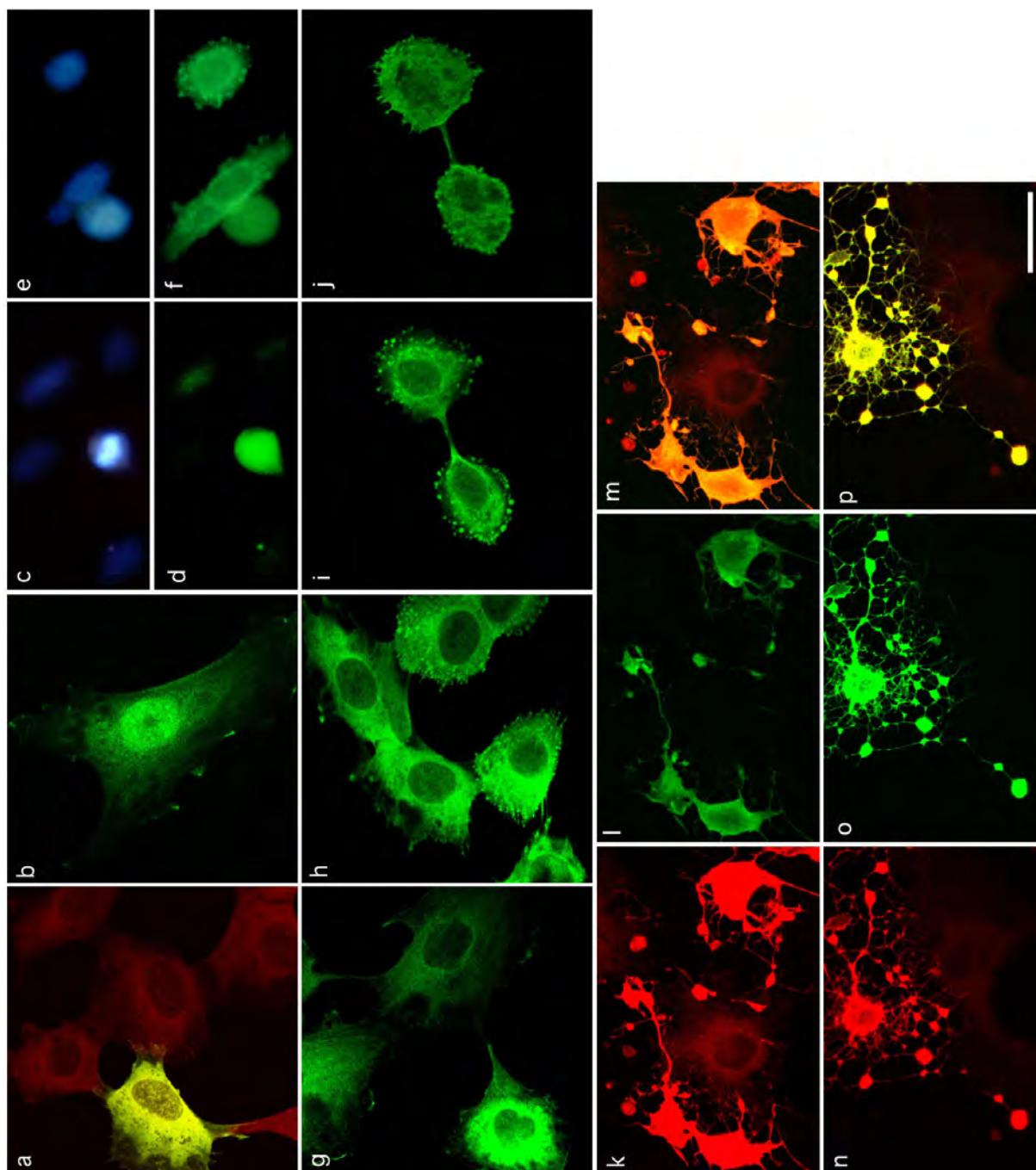
**Picture 4**

<u>Induction of apoptosis</u>

After exposure to MG132 for 6 h or 24 h, 40%, respectively 85% of the GAPDH-GFP transfected R6 cells were apoptotic *(figure 9a)*, indicating that cells overexpressing GAPDH-GFP were more sensitive to MG132 than untransfected cells. The non-apoptotic cells generally expressed nuclear GAPDH-GFP levels close to the baseline. Some cells had a hedgehog like shape and showed a speckled pattern of GAPDH-GFP expression or blebs *(picture 4i, 4j)*. The percentage of apoptotic cells as well as the number of cells forming GAPDH-GFP positive blebs was about the same in R6$^{Bcl-2}$ cells transiently transfected with GAPDH-GFP *(figure 9c)*. Our observations indicate that the sensitivity of GAPDH-GFP transfected cells to apoptosis is dependent on the amount of expressed GAPDH-GFP protein. This observation is supported by the fact that transfected R6$^{Bcl-2}$ cells that expressed GAPDH-GFP at levels close to that of endogenous GAPDH were less sensitive to MG132 induced apoptosis.

GAPDH transfected R6 or R6$^{Bcl-2}$ cells were affected at similar rate by staurosporine *(figure 9b, 9d)*. Several non-apoptotic GAPDH-GFP transfected R6 and R6$^{Bcl-2}$ cells formed a network of interconnected long processes. This network contained junctions where the processes formed enlarged knots *(picture 4k-4p)*. The whole network including the knots and the main cell body expressed twice more GAPDH-GFP compared to controls. Although no nuclear fragmentation was detected, these cells were not always in a good shape and some of them seemed to be dying. After 6 h about 30% and after 24 h only 5-10% of both R6 and R6$^{Bcl-2}$ cells were still normal and showed no signs of cell death *(figure 9b, 9d)*. This confirmed our findings, that Bcl-2 is able to prevent apoptosis in untransfected cells or in transfected cells that express levels of GAPDH protein close to control, but not in transfected cells overexpressing GAPDH at high levels.

# 4.4.3 <u>GAPDH translocation</u>

Overexpression of GAPDH-GFP alone is sufficient to raise the expression of nuclear GAPDH-GFP in NB41A3 cells and in R6 cells.10 % of the cells overexpressing GAPDH-GFP are apoptotic. We established a stable NB41A3$^{GAPDH-GFP}$ cell line constitutively overexpressing GAPDH-GFP that shows the same effects. This is a specific phenomenon and not an effect of transfection because cells transfected with GFP alone or with e.g. aldolase-GFP show neither nuclear translocation nor increased levels of apoptotic cells.

Transfection of GAPDH-GFP into neuronal and non-neuronal cell lines not only induces apoptosis *per se*, but also makes the cells more susceptible to apoptosis induced by different agents *(table 1)*. Cells transiently or permanently overexpressing GAPDH show no difference with respect to staurosporine induced apoptosis *(table 1)*. Compared to untransfected cells, not only the number of cells showing chromatin condensation and nuclear fragmentation, but also the percentage of cells expressing GAPDH-GFP in the nucleus and of cells forming blebs and speckles is increased significantly after 6-24 h exposure to 200 nM staurosporine or to 1.5 µM MG132, respectively. Cells forming speckles do concentrate the vast majority of GAPDH-GFP in the intracellular speckles so that there is practically no diffuse GAPDH-GFP in the cytoplasm or in the nucleus. We were not yet able to better characterise these intracellular speckles, but they were different in cells forming extracellular GAPDH-GFP structures. High resolution CLSM made it possible to identify these as blebs filled with high density of GAPDH-GFP still attached to the cell membrane. These cells express GAPDH-GFP also in the cytoplasm, but none of the cells expressing high amounts of GAPDH-GFP in the nucleus, in intracellular speckles or in blebs showed nuclear fragmentation. This differential translocation of GAPDH observed after apoptosis is intriguing: why do cells that show membrane blebbing, a phenomena that is often observed in context with apoptotic cells, express GAPDH or GAPDH-GFP mainly in the cytoplasm? On the other hand, a typical morphological change is observed in transfected and untransfected cells after exposure to apoptosis inducing drugs, namely the formation of a network of long processes. These cells may thus compensate a weaker adhesion to the culture plate or to the glass coverslip by extending long processes from the cell body.

Transient overexpression of GAPDH-GFP in R6$^{Bcl-2}$ cells showed the same effects as in R6 cells, i.e. apoptosis in 10 % cells even prior to treatment with apoptotic drugs. The percentage of apoptotic cells or the changes in morphology was not different between the two GAPDH-GFP transfected cell lines. Thus, Bcl-2 is able to efficiently decrease nuclear translocation and apoptosis in untransfected cells, but has no effects when GAPDH-GFP is overexpressed, neither in cells at rest nor in cells exposed to apoptotic agents.

Our results demonstrate the role of GAPDH not only in apoptosis, but also in response to oxidative stress and show differential GAPDH translocation in neuronal versus non-neuronal cells. NB41A3 neuroblastoma cells are less sensitive to proapoptotic agents as well as to reagents inducing oxidative stress than R6 fibroblasts. Already 2 h after exposure to either 100 µM $H_2O_2$ or to 300 µM FeCN,

endogenous GAPDH was translocated into the nucleus in untransfected R6 and NB41A3 cells. It must be stressed out that under these conditions no increase in nuclear fragmentation over control cells is observed.

However in contrast to its protective effects during apoptosis, Bcl-2 has no influence in response to oxidative stress induced by either $H_2O_2$ or FeCN, neither on GAPDH translocation nor on the percentage of cells forming GAPDH-positive speckles. This occurs independently of whether cells were transfected with GAPDH-GFP or not and indicates that translocation of GAPDH into the nucleus may be mechanistically different between apoptosis and oxidative stress. While nuclear translocation of endogenous GAPDH in response to apoptosis is influenced by Bcl-2, oxidative stress induces Bcl-2-independent translocation into the nucleus. Also when GAPDH-GFP is overexpressed, its translocation after oxidative stress cannot be blocked by Bcl-2.

Transfection of GAPDH-GFP *per se* without induction of oxidative stress already leads to enhanced levels of GAPDH-GFP in the nucleus. After exposure to $H_2O_2$, the amounts of nuclear GAPDH-GFP increased even more. FeCN different than $H_2O_2$, induced translocation of GAPDH-GFP from the nucleus into the cytoplasm.

Exposure to apoptotic agents induces a four-step translocation of endogenous GAPDH in R6 fibroblasts. First, GAPDH is localised in the perinuclear area of flat, typically fibroblastly shaped cells with clear the cytoskeletal structure. Then it is translocated into the nucleus of the fibroblasts. Although the cytoplasmic structure of the cytoskeleton was not clearly visible, the fibroblasts have not changed their morphology and their nuclei are not fragmented. In a next stage, the typical apoptotic cells which showed cell shrinkage and nuclear fragmentation overexpressed high amounts (3x more than base line levels) of GAPDH around the fragmented nuclei. The cells were rounded up and did not have any processes. In a last step, no GAPDH at all is visible anymore. In NB41A3 cells and in cells overexpressing GAPDH-GFP these steps are similar, but a significant amount of GAPDH is found in the nucleus already before exposure to apoptotic drugs.

The first two steps were also observed in the translocation of GAPDH induced by oxidative stress. However, although nuclear translocation was observed after treatment of cells with reagents inducing oxidative stress, the cells did not undergo subsequent apoptosis.

# 4.5 <u>HSC 70</u>

## 4.5.1 <u>NB41A3</u>

### 4.5.1.1 <u>Untransfected cells</u>

In untransfected NB41A3 cells about 70% of endogenous Hsc70 is expressed in the cytoplasm as shown by means of immunocytochemistry with anti-Hsc70 antibodies *(picture 5a, 5c, figure 10a)*. The ratio of the measured Texas-Red fluorescence between cytoplasm and nucleus is constant in all cells. Nevertheless in many cells the cytoplasmic Hsc70 expression is not uniform.

Oxidative stress by either $H_2O_2$ or FeCN raises the Hsc70 expression in the nucleus *(picture 5d, figure 10a)*. Nuclear Hsc70 is often concentrated around the nucleolus.

After 6 h or 24 h exposure to either staurosporine or MG132 no significant changes in subcellular Hsc70 expression was seen in non-apoptotic cells *(figure 10a)*. In contrast to what is observed with GAPDH, the 20% of NB41A3 cells showing nuclear fragmentation *(figure 10b)* did not accumulate or overexpress endogenous Hsc70 *(picture 5e, 5f)*.

### 4.5.1.2 <u>Transiently transfected cells</u>

<u>Controls</u>

Hsc70-GFP transfected cells contained in the average about twice more GFP fluorescence in the cytoplasm than in the nucleus *(picture 5g, figure 10a)*. This ratio was constant in all cells. Hsc70 was expressed at different intensities in the cytoplasm and displayed a patchy pattern *(picture 5b)*. The nucleolus was devoid of Hsc70-GFP. The expression pattern of Hsc70-GFP was very similar among all unstressed cells and did not depend on the shape of cells. Signs of apoptosis were not detected *(picture 5c, figure 10b)*.

<u>Induction of Oxidative Stress</u>

After treatment with 300 µM FeCN for 4 h, most cells (80%) raised their Hsc70-GFP expression in the nucleus. As a consequence the Hsc70 expression was equal in the
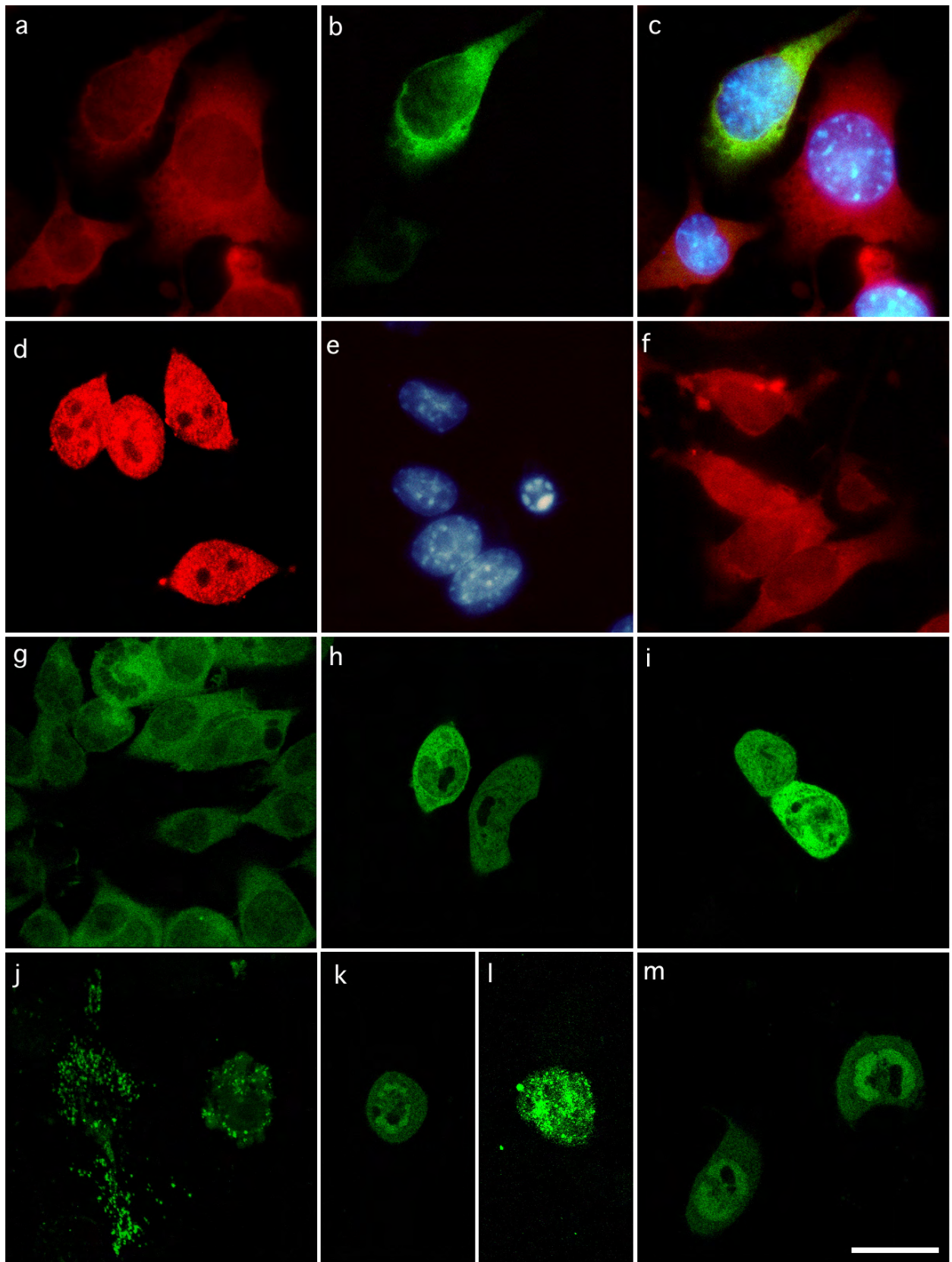
**Picture 5**

nucleus and in the cytoplasm *(picture 5h)* , sometimes even higher in the nucleus *(picture 5i)*. Nuclear Hsc70-GFP fluorescence accumulated in patches around the nucleolus and was weaker in other parts of the nucleus. Within the nucleolus or at the plasma membrane no Hsc70-GFP was expressed. Formation of Hsc70-GFP positive speckled spots was sometimes observed (5% of cells) *(picture 5j)*. The percentage of cells expressing Hsc70-GFP in small speckles increased up to 15% after 6 h in parallel to the exposure time to 300 μM FeCN *(figure 10c)*. In addition, the impact of the effects augmented with increasing concentrations of FeCN. However, staining of nucleolus was not observed, even at high concentration (up to 1000 μM FeCN) or after long exposure time (up to 6h).

Oxidative stress with 100 μM $H_2O_2$ resulted in formation of speckles accumulating Hsc70-GFP in 25% of cells. The remaining cells were mostly of round shape, had short processes and their nuclear Hsc70-GFP expression was increased. In the average slightly more than 50% of Hsc70-GFP was expressed in the nucleus of stressed cells *(picture 5k, figure 10a)*. A correlation between the exposure time to 100 μM $H_2O_2$ and the amount of speckles formation was also observed *(figure 10c)*: Depending upon the incubation time, between 15 and 35% of the cells accumulated Hsc70-GFP fluorescence in speckles. Besides cells expressing Hsc70-GFP only in speckles and not in the nucleus or in the cytoplasm, we found cells in an intermediate state where speckles formation is observed in particular regions of the cell *(5l)*.

Together these results indicate that the formation of Hsc70-GFP positive speckles is directly correlated with the response to oxidative stress. Furthermore, also the amount of nuclear translocation increased in parallel with longer exposure times of cells to $H_2O_2$ or FeCN.

←

**Picture 5: Subcellular localisation of Hsc70 and Hsc70-GFP in NB41A3 cells**
**(a,c,d,f) Endogenous Hsc70 as detected by TR-immunohistochemistry**
**(a-c)** Cytoplasmic localisation in transfected and untransfected control cells. **(c)** Overlay of **a, b** and Hoechst staining. The most upper transfected cell (yellow=green+red) shows similar GAPDH expression like the other untransfected cells (red). The nuclei (blue) are not fragmented. **(d)** Increased expression of endogenous Hsc70 in the nucleus after exposure to 100 μM $H_2O_2$ for 3 h. **(e, f)** Apoptotic cells after exposure to 200 nM staurosporine for 24 h with neither overexpression nor nuclear accumulation of endogenous Hsc70.
**(g-m) Hsc70-GFP transfected cells.**
**(g)** Unstressed NB41A3 cells express Hsc70-GFP mainly in the cytoplasm, whereas **(h-j)** cells exposed to 300 μM FeCN show **(h)** increased nuclear localisation, **(i)** patchy accumulation in the nucleus and **(j)** speckles formation of Hsc70-GfP. **(k)** Nuclear translocation and **(l)** beginning of intracellular speckles formation in cells exposed to 100 μM $H_2O_2$ for 3 h. **(m)** 30% cells also show nuclear translocation 24 h after induction of apoptosis by 200 nM staurosporine.
**(c, e)** Visualisation of DNA by Hoechst blue staining. Scale bar is 50 μM.
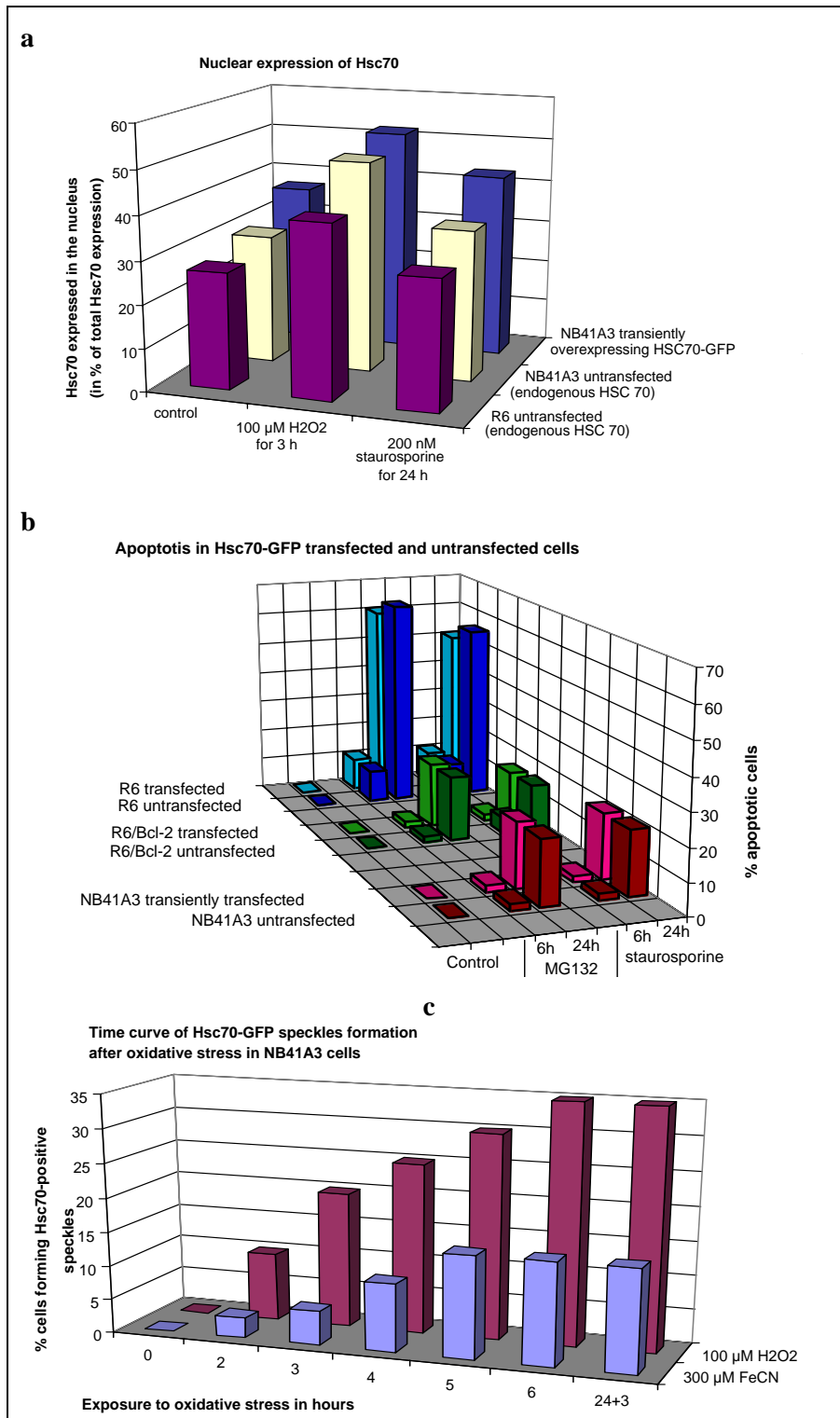
**Figure 10: Analysis of Hsc70 expression and apoptosis in untransfected Hsc70-GFP transfected cells. (a)** Untransfected and transiently transfected cells were analysed under unstressed conditions, after exposure to 100 μM $H_2O_2$ for 3 h or after exposure to 200 nM staurosporine for 24 h. The nuclear expression is indicated as percentage of total GAPDH (or of GAPDH-GFP for transfected cells). Standard deviation is smaller than 5 % in all tested conditions. **(b)** Apoptosis in R6 and R6[Bcl-2] cells after exposure to staurosporine (200nM) or to MG132 (1.5 μM). The percentage of cells showing nuclear fragmentation or chromatin condensation in cells expressing endogenous Hsc70 or transfected Hsc70-GFP is indicated after 0, 6 and 24 h of exposure time. **(c)** Percentage of transfected cells exposed for different time (from 0-6 h) to 100 μM $H_2O_2$ or to 300 μM FeCN forming Hsc70-GFP positive speckles. Additionally, a set of cells (24+3) was first stressed for 6 h, incubated further for 18 h in normal growth medium and then stressed again for 3 h.

79

<u>Induction of Apoptosis</u>

After 6 h exposure to staurosporine or MG132 the majority of the cells had not changed their morphology and expressed Hsc70-GFP at 2 times higher levels in the cytoplasm than in the nucleus. However, in contrast to untransfected cells, after 24 h of incubation nuclear translocation of Hsc70-GFP was observed in 30% of the non-apoptotic cells *(picture 5m)*. Nevertheless, the percentage of apoptotic cells was comparable to untransfected cells, i.e. 2-5% after 6 h, 20% after 24 h exposure to staurosporine or MG132 *(figure 10b)*. In contrast to what is observed in GAPDH-GFP transfected cells, apoptotic cells did not significantly change their morphology and the expression of Hsc70-GFP was identical to the one in non-apoptotic cells.

<u>Co-transfections of Hsc70-GFP with other proteins</u>

When Hsc70-GFP was transfected together with enolase-BFP in neuroblastoma cells, no difference in Hsc70-GFP distribution was observed compared to cells transfected with Hsc70-GFP alone, but after oxidative stress with 100 μM $H_2O_2$, the percentage of cells forming intracellular Hsc70-GFP-speckles augmented to 50%. This effect was not observed after oxidative stress with 300 μM FeCN. Nuclear translocation of Hsc70-GFP was 10% higher under both conditions.

Hsc70-GFP expression is not influenced by GAPDH-BFP co-overexpression in resting cells. But after exposure to 100 μM $H_2O_2$, elevated nuclear Hsc70 localisation was observed, i.e. 40% more in double-transfected cells (85%) than in cells overexpressing Hsc70-GFP alone. Similar effects were also found with 300 μM FeCN.

Aldolase-BFP or Ulip-BFP co-transfected with Hsc70 had no significant influence on Hsc70-GFP expression neither before nor after oxidative stress.

# 4.5.2 R6 and R6<sup>Bcl-2</sup>

## 4.5.2.1 Untransfected cells

In resting R6 fibroblasts endogenous Hsc70 is predominantly in the cytoplasm and bound to the cytoskeleton *(picture 6a)*. Its highest concentration is seen at the perinuclear area and at the plasma membrane. Nuclear Hsc70 levels are lower in R6 cells than in neuroblastoma cells *(figure 10a)*, and identical to most R6<sup>Bcl-2</sup> cells. However, 20% R6<sup>Bcl-2</sup> cells are very flat and show volcanic-like Hsc70 distribution *(picture 6b)*.

3 h after induction of oxidative stress with 100 $\mu$M $H_2O_2$, in spite of some nuclear translocation that is observed, most Hsc70 was still expressed in the perinuclear area of the cytoplasm *(picture 6c)*. However, Hsc70 bound less tightly to cytoskeletal structures than in unstressed cells. In 20% of the cells it was translocated into the nucleus where it was often concentrated in nuclear patches or at the nuclear membrane. R6<sup>Bcl-2</sup> and R6 showed similar localisation of endogenous Hsc70.

➡

**Picture 6: Subcellular localisation of Hsc70 and Hsc70-GFP in R6 and R6<sup>Bcl-2</sup> cells**
**(a-i) Untransfected cells. Endogenous Hsc70 detected by TR-immunohistochemistry.**
Cytoplasmic localisation of Hsc70 in unstressed **(a)** R6 or **(b)** R6<sup>Bcl-2</sup> cells. **(c)** R6 cell after exposure to 100 $\mu$M $H_2O_2$ for 3 h **(d, e)** Cells forming long processes after 6h induction of apoptosis by MG132. The arrow points to the only cell showing chromatin condensation. **(e, f)** Apoptotic R6 and **(i)** R6<sup>Bcl-2</sup> cell after exposure to 1.5 $\mu$M MG132 for 6 h with neither overexpression nor nuclear accumulation of endogenous Hsc70. **(h)** Non-apoptotic R6<sup>Bcl-2</sup> cell with intact nucleus (blue) also after exposure to 1.5 $\mu$M MG132 for 6 h.
**(j-m) Hsc70-GFP transfected cells.**
**(j)** Some unstressed transfected R6 cells still express Hsc70-GFP mainly in the cytoplasm, whereas **(k)** a significant number of transfected R6 cells show increased nuclear localisation of Hsc70-GFP. **(j)** and **(k)** are both overlays showing besides the yellow (=green+red) staining of transfected cells also expression of Hsc70 in untransfected cells as detected by TR-immunohistochemistry; in **(j)** additionally also Hoechst blue staining is shown of intact nuclei. **(l, m)** Nuclear translocation in R6<sup>Bcl-2</sup> cells with intact nucleus (blue) 6 h after induction of apoptosis by 200 nM staurosporine leads to Hsc70-GFP expression in the entire cell.
**(d,f,h,i,j,l)** Visualisation of DNA by Hoechst blue staining. Scale bar is 50 $\mu$M.
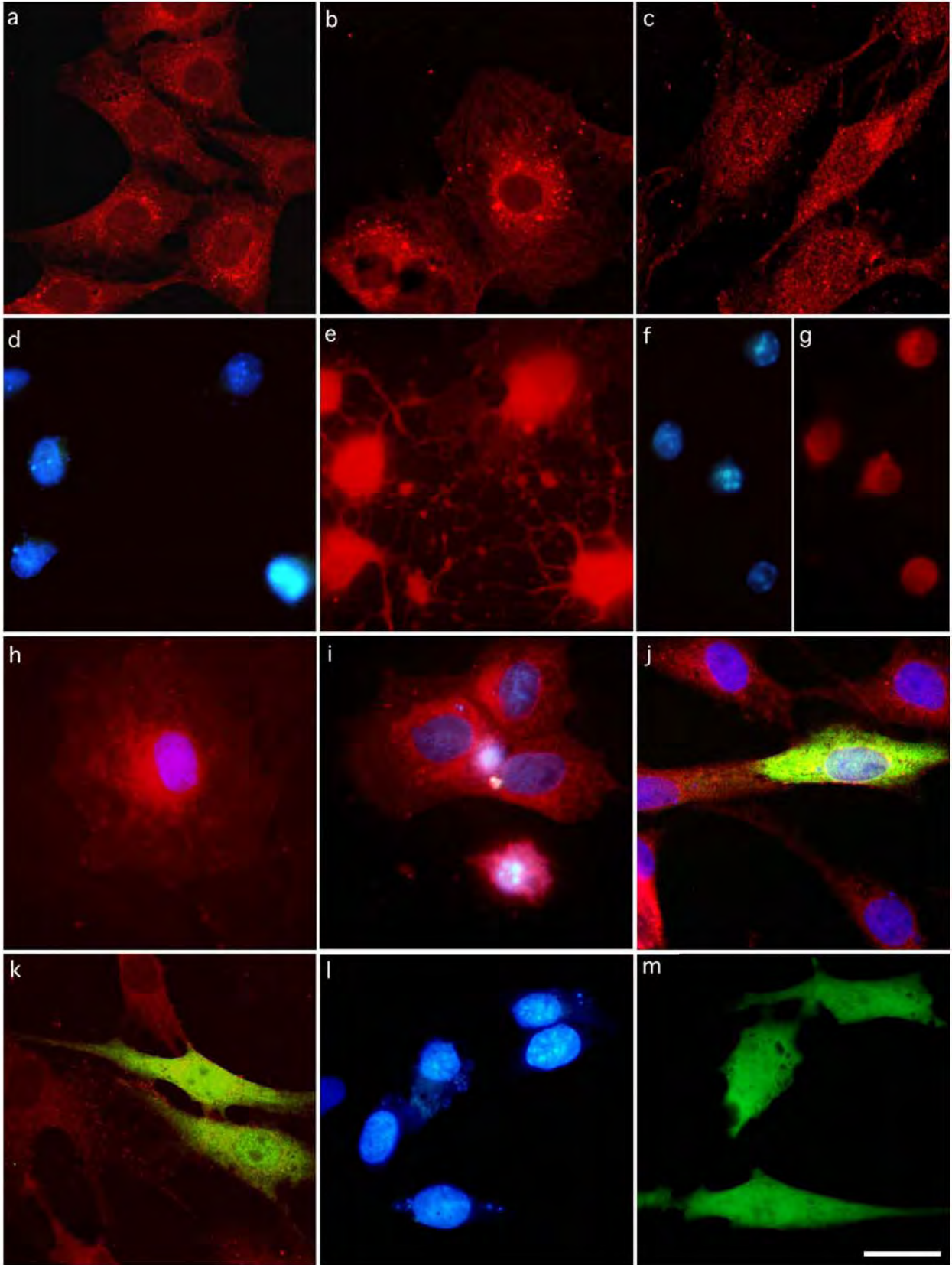
**Picture 6**

Although the response of R6 cells to staurosporine or to MG132 is more pronounced than in NB41A3, most cells do not changed their morphology and express Hsc70 predominantly in the cytoplasm. However many cells typically start to form long processes out of their rounded-up cell body leading to a net-like appearance *(picture 6e)*. Endogenous Hsc70 is expressed in the cytoplasm, including within the processes. Some of these net-like cells (20%) concentrate Hsc70 in specific nuclear regions and are apoptotic *(picture 6d)*. Other apoptotic cells are mostly round and express Hsc70 in the cytoplasm or all over the cell, at levels close to endogenous Hsc70 expression in non-apoptotic control cells *(picture 6f, 6g)*. The overall percentage of cells with fragmented nuclei after exposure to staurosporine or MG132 raises from 10% after 6 h up to 60% after 24 h *(figure 10b)*, comparable to those of GAPDH experiments.

Bcl-2 protects from induction of apoptosis by MG132 or staurosporine *(figure 10b)*. After 6 h exposure to staurosporine, about 95% of the cells did not display nuclear fragmentation. There, two types of Hsc70 expression was observed: either all over the cell (including the nucleus) within a network of cells with long processes expressing Hsc70 or in a perinuclear ring within flat volcano like cells *(picture 6h)*. Nuclear translocation of endogenous Hsc70 was observed in the other cells, with unchanged morphology. After 24 h of staurosporine treatment most cells had small rounded-up cell bodies and formed long processes. In contrast, after incubation with MG132 for 24 h Hsc70 was predominantly in the cytoplasm or in the blebs of the cells, of which the majority did not have any processes at all. The morphology and Hsc70 expression of apoptotic R6$^{Bcl-2}$ cells *(picture 6i)* was similar to what was observed in apoptotic R6 cells.

## 4.5.2.2 **Transiently transfected cells**

Most transfected R6 and R6$^{Bcl-2}$ cells expressed Hsc70-GFP in the perinuclear area of the cytoplasm *(picture 6j)*, similar to untransfected cells. In contrast, in some cells Hsc70-GFP is also localised at high levels in the nucleus *(picture 6k)*. No change in shape or cell viability was observed compared to untransfected cells.

After exposure to MG132 or staurosporine neither nets of long processes branching off from rounded-up cell bodies, nor volcano-like cells were observed. The number of apoptotic cells after 6h and after 24 h exposure was similar to untransfected R6 cells *(figure 10b)*. Hsc70-GFP expression was not increased in these cells and often similar to non-apoptotic cells.

Most Hsc70-GFP transfected R6$^{Bcl-2}$ cells exposed to staurosporine for 6 h had no signs of apoptosis *(figure 10b, picture 6l)* and expressed Hsc70-GFP along intracellular fibres within the entire cell *(picture 6m)*. Also 24 h after staurosporine induction of apoptosis the cell viability of Hsc70-GFP transfected R6$^{Bcl-2}$ cells was about 80%, not significantly altered compared to untransfected R6$^{Bcl-2}$ cells, but significantly higher than in Hsc70-GFP transfected R6 cells *(figure 10b)*. 24 h incubation with either MG132 or staurosporine yielded comparable percentage of nuclear fragmentation, but the number of R6$^{Bcl-2}$ cells with altered shape was much higher with MG132. Most cells were devoid of processes and the cell body had shrunk and was rounded up.

## 4.5.3 <u>Hsc70 translocation</u>

Endogenous Hsc70 is located predominantly in the cytoplasm in both unstressed NB41A3 and unstressed R6 cells. Whereas oxidative stress induces translocation of Hsc70 into the nucleus, apoptosis does not significantly change its expression. In contrast, while cell morphology of oxidatively stressed cells had not significantly changed, many apoptotic cells showed severe effects after treatment with apoptotic agents. As would be expected, the rate of apoptotic cells and of cells forming long processes is comparable to observations with GAPDH. R6$^{Bcl-2}$ cells showed no difference in their Hsc70 expression and in their morphology compared to R6 cells.

In control cells, the subcellular localisation of overexpressed Hsc70-GFP was not different than for endogenous Hsc70 in untransfected cells. Furthermore, none of the cells overexpressing Hsc70-GFP was apoptotic. After induction of oxidative stress by either $H_2O_2$ or FeCN, translocation of Hsc70-GFP into the nucleus was observed in all cell lines, NB41A3, R6 and R6$^{Bcl-2}$. As a consequence, expression levels of Hsc70-GFP in the cytoplasm and in the nucleus were about the same. Like for GAPDH-GFP, speckle formation was observed. However, only very few cells were found which had a shrivelled cell body and formed long processes. In all three cell lines (NB41A3, R6 and R6$^{Bcl-2}$), the percentages of cells showing nuclear fragmentation or chromatin condensation 24 h after exposure to apoptotic agents, was not significantly different in untransfected cells compared to Hsc70-GFP transfected cells. Furthermore, in contrast to GAPDH-GFP overexpressing cells, nuclear translocation of Hsc70-GFP in response to induction of apoptosis was observed. Moreover, apoptotic cells did not express increased levels of either endogenous Hsc70 or overexpressed Hsc70-GFP. Nuclear translocation of endogenous Hsc70 is only observed during oxidative stress and not during apoptosis.

# 4.6 Aldolase c

## 4.6.1 NB41A3

### 4.6.1.1 Untransfected cells

Untransfected NB41A3 cells mainly display cytoplasmic aldolase expression, not as a uniform staining, but rather as accumulation of aldolase-positive dots and patches *(picture 7a)*. Concentration of aldolase-GFP fluorescence in the nucleus was not observed.

After oxidative stress for 3h with 100 μM $H_2O_2$, spots with high aldolase concentration were found both in the cytoplasm and in the nucleus. In 25% of the cells, aldolase level was higher in the nucleus than in the cytoplasm, while 30% of the cells showed extensive expression of aldolase in the somal area at the bases of axons *(picture 7b)*. In the remaining cells, aldolase was expressed in speckles along the plasma membrane or as a speckled circle *(picture 7c)*. The spots were brighter than in unstressed cells.

After exposure to staurosporine or MG132, some concentration and induction of aldolase was seen in apoptotic cells. Half of non apoptotic cells showed a uniform cytoplasmic aldolase expression (TR staining in *picture 7d)*, the other cells displayed long aldolase containing processes but mostly no nuclear fragmentation.

Endogenous aldolase was also examined in GAPDH-GFP overexpressing cells. At rest these cells expressed endogenous aldolase in a patchy pattern pre-dominantly in the cytoplasm and at the plasma membrane, but 15% of cells also expressed similar levels in the nucleus. After oxidative stress these cells exhibit no change on aldolase expression but immunostaining shows a more uniform cytoplasmic distribution.

➔

**Picture 7: Subcellular localisation of aldolase and aldolase-GFP in NB41A3 cells**
**(a-c)** Untransfected cells in which endogenous aldolase detected by FITC-immunohistochemistry is green. **(a)** Punctuate expression in unstressed cells. **(b)** Concentration of aldolase at the bases of axons or **(c)** speckles formation after exposure to 100 μM $H_2O_2$ for 3 h. In **(c)** and the entire cytoplasm was made visible by immunostaining with anti-enolase-γ detected by TR-immunohistochemistry. **(d)** Overlay of non-apoptotic cells 24 h after induction of apoptosis by 200 nM staurosporine, showing besides the red uniform cytoplasmic expression of endogenous aldolase in untransfected cells as detected by TR-immunohistochemistry also yellow (=green+red) staining of transfected cells.
**(e-k)** Transient and **(j, k)** stable overexpression of transfected aldolase-GFP. **(e, j)** Cytoplasmic localisation of aldolase-GFP in unstressed cells. **(f)** Nuclear translocation, **(g)** accumulation in a star patter at the nucleus or **(h, i, k)** intracellular speckles formation after exposure to 100 μM $H_2O_2$ for 3 h. **(h, i)** are two confocal images of single planes of the same cell at different z-axis values. Scale bar is 50 μM.
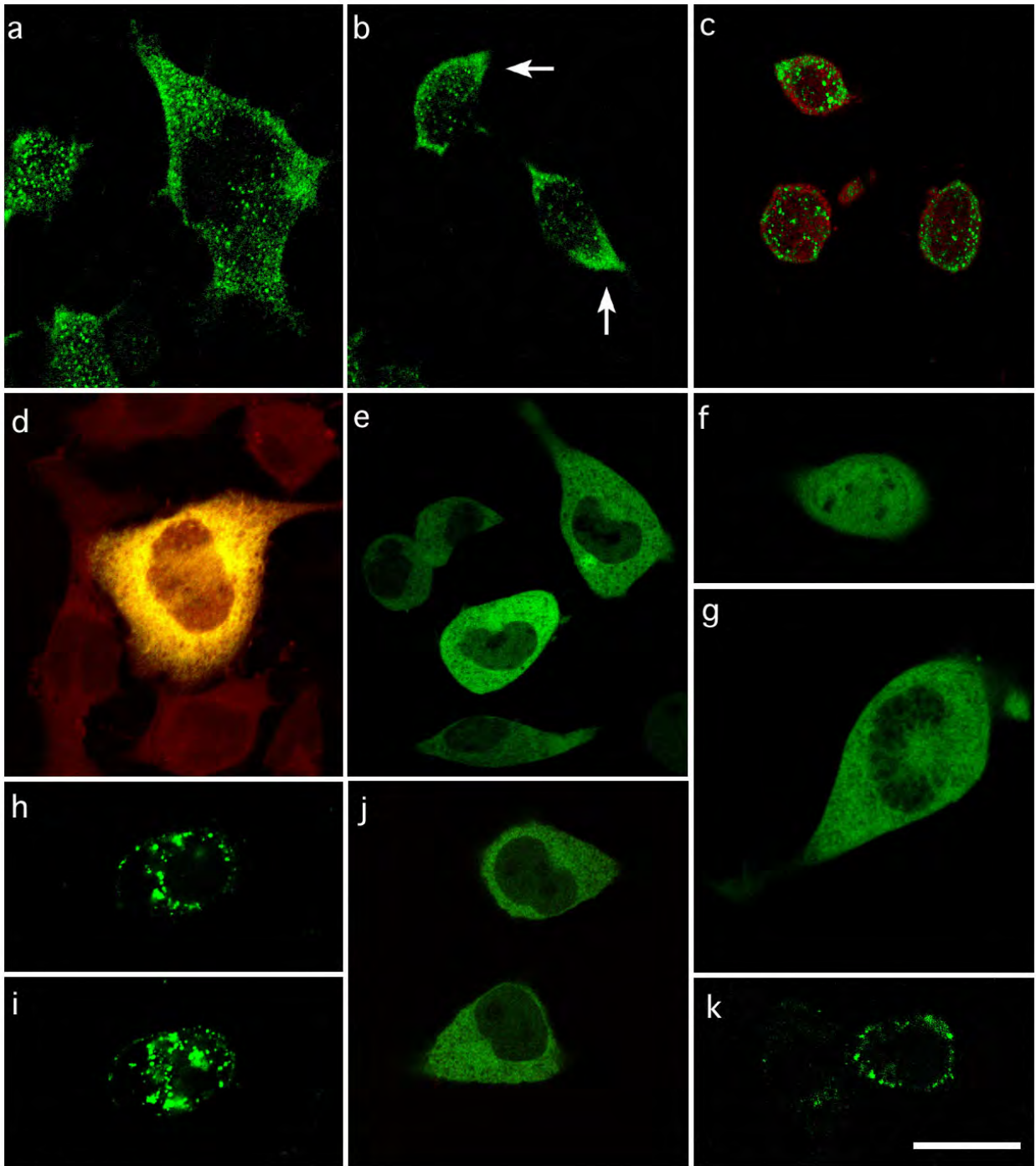
**Picture 7**
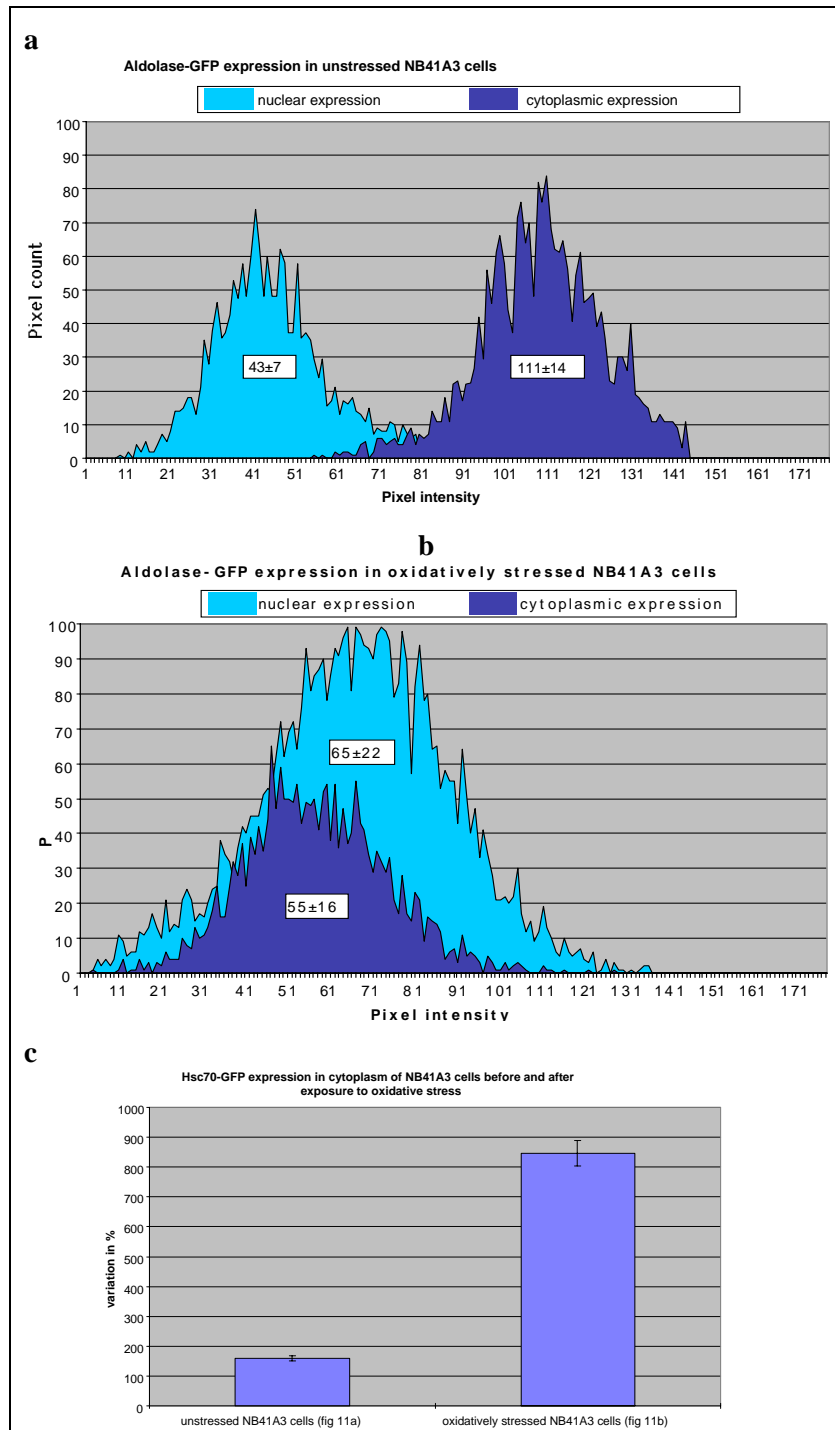
**Figure 11: Intensity and patchiness of aldolase-GFP expression in nucleus and cytoplasm.** Aldolase-GFP expression was analysed with regard to its intensity and to its patchiness in the nucleus and in the cytoplasm of transfected NB41A3 cells. Various histograms of aldolase-GFP were evaluated regarding the mean intensity and the variation (= standard deviation squared) of expression. **(a)** Prior to oxidative stress, aldolase-GFP intensity (= expression level) in the cytoplasm is about 2.5 fold higher than in the nucleus. The cytoplasmic expression curve forms quite a narrow peak and has a relatively small standard deviation (12 %) indicating uniform aldolase-GFP expression. The mean intensity of fluorescence plus/minus standard deviation is indicated for each curve. **(b)** After exposure to 100 μM $H_2O_2$ for 3 h, in some cells (20%) aldolase-GFP expression is higher in the nucleus than in the cytoplasm. The cytoplasmic expression curve forms quite a broad peak with a higher standard deviation (29 %) indicating patchy aldolase-GFP expression. The mean intensity of fluorescence plus/minus standard deviation is indicated for each curve. **(c)** Variation (=patchiness) of cytoplasmic aldolase-GFP expression calculated prior and after oxidative stress from histogram **(a)** and **(b)**.

## 4.6.1.2 <u>Transiently transfected cells</u>

<u>Controls</u>

Unstressed cells were clearly dominated by cytoplasmic expression pattern of aldolase-GFP *(picture 7e)*. Aldolase-GFP expression is about 2.5 fold higher in the cytoplasm than in the nucleus (111 *versus* 43, see *figure 11a)*, whereas the nucleolus appears devoid of aldolase-GFP. In most cells, the intense expression of aldolase-GFP is smooth and regular (indicated by small variation*, figure 11c)*. Chromatin condensation was not found in any cell.

<u>Induction of Oxidative Stress</u>

After oxidative stress with 300 μM FeCN or 100 μM $H_2O_2$ for 4 h nuclear aldolase-GFP expression increased about 50% *(picture 7f)*. Mean expression of aldolase-GFP was lower in the cytoplasm (55) than in the nucleus (65) *(figure 11b)*. The aldolase-GFP expression is patchy in the nucleus as well as in the cytoplasm (indicated in *figure 11b & figure 11c* by high standard deviation and variation), especially in those cells with high nuclear aldolase-GFP expression. Often high aldolase-GFP fluorescence was aggregated in a star like pattern at the nucleus *(picture 7g)*. In 5% of the cells we can observe the formation of speckled circles at the membranes made by spots in which aldolase-GFP is concentrated *(picture 7h, 7i)*.

A correlation between the response to oxidative stress and the concentration of the stressing reagent resp. the exposure time was found. Treatment with either 100 μM FeCN or 30 μM $H_2O_2$ up to for 5 h showed only very weak effects on aldolase-GFP distribution, comparable with the ones obtained after only 2h of oxidative stress with either 300 μM FeCN or 100 μM $H_2O_2$ respectively. The most spectacular changes of aldolase-GFP level in the nucleus and in formation of speckled circles was observed with incubation with 300 μM of FeCN for 5 h. After this treatment aldolase-GFP concentration was sometimes higher in the nucleus than in the cytoplasm. Almost the same response was achieved after 5 h incubation with 100 μM $H_2O_2$, but with 1 mM of FeCN 50% of the cells were dead after 3h.

After apoptosis induction the localisation of aldolase-GFP is not different to the one of endogenous aldolase (GFP staining in *picture 7d)*. As for untransfected NB41A3, only 5%, respectively 20% cells were apoptotic after staurosporine or MG132 exposure for 6 h and 24 h. The majority of other cells showed unchanged morphology and expressed adolase-GFP in the cytoplasm. Only few cells made long processes as we described for untransfected neuroblastomas. So, apparently overexpression of aldolase did not influence apoptosis in NB41A3 cell.

Co-transfections of aldolase-GFP with other proteins

Co-transfection with either GAPDH, enolase, Ulip or Hsc70 did not change the distribution of aldolase-GFP significantly, nor did this distribution be affected after oxidative stress.

## 4.6.1.3 Stable overexpression in aldolase-GFP transfectants

The intensity of aldolase-GFP expression is very variable between different cells, but at least 75% of the aldolase-GFP expression is cytosolic in 98% of the cells under unstressed conditions *(picture 7j)*. The aldolase-GFP protein is expressed in the nucleus at low levels and is absent in the nucleolus.

After oxidative stress aldolase-GFP expression raises in the nucleus. It is still more abundant in the cytosol than in the nucleus in 50% of the cells, but the ratio between the GFP fluorescence in the cytosol and in the nucleus is weaker compared to unstressed cells. In the other 50% of the cells this expression is about the same in the cytosol and in the nucleus or is stronger in the nucleus than in the cytosol. Aldolase-positive speckle formation was observed less frequently than in transiently transfected cells *(picture 7k)*.

In unstressed NB41$^{aldolase-GFP}$ cells endogenous GAPDH is found in about same amounts in the nucleus and in the cytoplasm. After oxidative stress with 100 $\mu$M $H_2O_2$ about 60% of endogenous GAPDH was localised in the nucleus. Thus, cytoplasmic expression of endogenous GAPDH in cells overexpressing aldolase was higher than in untransfected cells.

In NB41$^{aldolase-GFP}$ cells, endogenous Hsc70 shows a different expression than in untransfected controls. In the latter a high cytoplasmic expression of Hsc70 in the cytoplasm and a low nuclear expression is clearly observed, whereas in cells overexpressing aldolase the difference is not significant under rest. After oxidative stress with 100 μM $H_2O_2$ nuclear Hsc70 is concentrated around the nucleolus and its fluorescence is about as strong as in the cytoplasm. Such a rise of endogenous Hsc70 in the nucleus is small, however.


# 4.6.2 R6 AND R6$^{Bcl-2}$

## 4.6.2.1 Untransfected cells

In unstressed R6 and R6$^{Bcl-2}$ cells endogenous aldolase expression was much more uniform than in NB41A3. It was spread all over the cytosol but did not show any fibril structure and was highest in the perinuclear area *(picture 8a)*. At the plasma membrane, it was also sometimes present as bright spots.

After oxidative stress no significant rise of aldolase levels in the nucleus was observed in R6 cells. The expression is still mostly cytoplasmic with highest aldolase-GFP expression in the perinuclear area and at the plasma membrane *(picture 8b)*. Small aldolase-positive spots were seen in the nucleus in 40% of the cells, but concentration of aldolase in intracellular speckles was never observed.

After 6 h incubation with staurosporine or MG132 10% of R6 cells and less than 5% R6$^{Bcl-2}$ cells showed nuclear fragmentation *(picture 8d)*. Aldolase expression was elevated and also some nuclear expression was observed in these cells *(picture 8e)*. A majority of the remaining cells had not changed their morphology nor their aldolase localisation in the perinuclear area of the cytoplasm, but small wrinkled up cells and round cells with neurone-like shape and long processes were also observed *(picture 8c)*. After 24 h of apoptosis induction the percentage of apoptotic cells raised to over 50% for R6 cells and to about 20% for R6$^{Bcl-2}$ cells respectively. The number of cells with unchanged morphology and aldolase distribution was very low. Most cells with unfragmented DNA had no processes and were either rounded up or flat and had a volcano like staining by anti aldolase antibody.
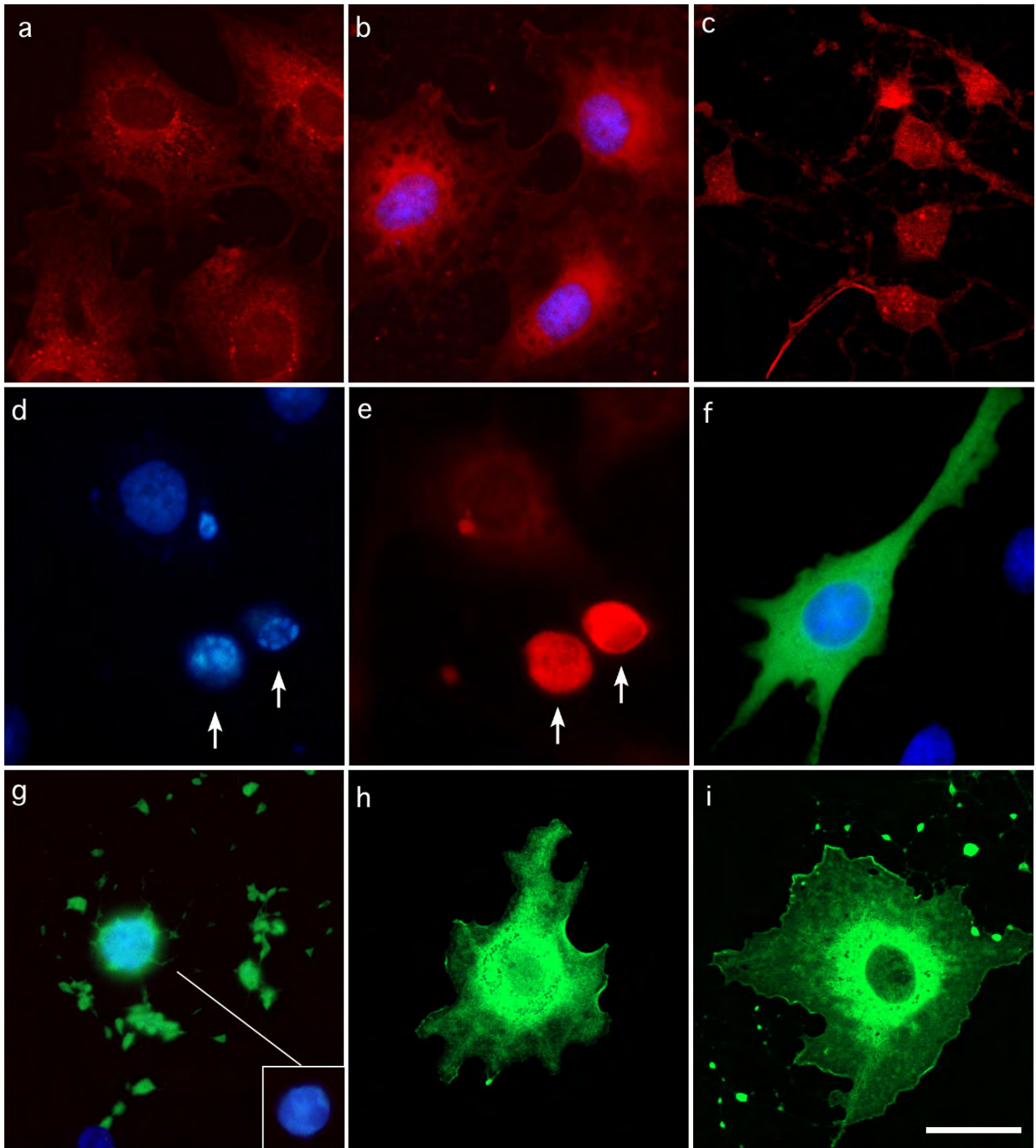
**Picture 8**

## 4.6.2.2 <u>Transiently transfected cells</u>

In unstressed, transiently transfected cells the aldolase-GFP distribution was identical to endogenous aldolase of untransfected cells. The cytoplasmic aldolase-GFP was most intense around the nucleus in the perinuclear area *(picture 8f)*. No apoptosis nor nuclear translocation was observed in R6 or R6$^{Bcl-2}$, even in cells with very high expression levels of aldolase-GFP.

After apoptosis induction by staurosporine or MG132, fibroblasts transiently transfected with aldolase-GFP acted similar to untransfected R6 and R6$^{Bcl-2}$ cells. No correlation between the expression level of aldolase-GFP and changes in morphology or aldolase-GFP localisation was observed. Neither nuclear translocation nor formation of speckles was found, but the percentage of cells with long branched processes *(picture 8g)* or with a volcano-like aldolase distribution *(picture 8h, picture 8i)* was higher than in untransfected cells. The percentage of apoptotic and morphologically changed cells was identical to the one in untransfected cells, i.e. the number of apoptotic R6$^{Bcl-2}$ cells was significantly smaller than in R6 cells 24 h after adding the apoptotic agent.

←

**Picture 8: Subcellular localisation of aldolase and aldolase-GFP in R6 and R6$^{Bcl-2}$ cells**
**(a-e) Untransfected cells. Endogenous aldolase as detected by TR-immunohistochemistry.**
Perinuclear localisation of aldolase in **(a)** unstressed or **(b)** oxidatively stressed (100 μM H$_2$O$_2$ for 3 h) R6 cells. **(c)** R6$^{Bcl-2}$ cells forming long processes and **(d, e)** apoptotic cells after exposure to 1.5 μM MG132 for 24 h. The arrows point to the cells showing chromatin condensation.
**(f-i) aldolase-GFP transfected cells.**
**(f)** Intact nucleus in unstressed R6 cell expressing aldolase-GFP in the cytoplasm. **(g)** R6 cell forming long fine processes to enlarged knots which do not contain any DNA after exposure to 1.5 μM MG132 for 24 h. Volcano like **(h)** R6 or **(i)** R6$^{Bcl-2}$ cells after exposure to 1.5 μM MG132 for 24 h.
**(b,d,f,g)** Visualisation of DNA by Hoechst blue staining. Scale bar is 50 μM.

### 4.6.3 <u>Aldolase and apoptosis</u>

The expression of aldolase was similar the one of Hsc70 under all tested conditions. In resting cells endogenous aldolase and aldolase-GFP were typically located in the cytoplasm, often bound to the cytoskeleton. After oxidative stress we observed nuclear translocation, which was more pronounced in NB41A3 cells than in R6 cells.

The cellular response to apoptosis induced by either MG132 or staurosporine does not seem to be influenced by overexpressed aldolase-GFP. Different than in oxidatively stressed cells, neither in aldolase-GFP transfected nor in untransfected cells was translocation of aldolase to the nucleus observed. The percentage of apoptotic cells and of cells forming long processes was identical to untransfected cells. However, apoptotic cells showed 1-2 fold increased levels of aldolase compared to non-apoptotic cells.

Like in NB41A3, aldolase-GFP transfected and untransfected fibroblasts react similar in their response to induction of apoptosis. Although little nuclear translocation of aldolase is observed and although aldolase concentrates in apoptotic cells, the percentage of apoptotic R6 cells transfected by aldolase-GFP is comparable to untransfected R6 cells. Furthermore, Bcl-2 also protects cells overexpressing aldolase-GFP efficiently from apoptosis, at the same rate as untransfected cells.

# 4.7 <u>Ulip</u>

## 4.7.1 <u>NB41A3</u>

### 4.7.1.1 <u>Untransfected cells</u>

In unstressed cells endogenous Ulip displayed an uniform cytoplasmic expression *(picture 9a)*, without significant concentration in patches *(figure 12a, figure 12c)* . The intensity of Ulip expression found in the nucleus of cells is about 1.5 times less than in the cytoplasm. Intracellular vesicles and the nucleolus are devoid of Ulip..

After oxidative stress, endogenous Ulip is expressed at higher rates in the nucleus than in the cytosol in 60% of the cells *(picture 9b)*. The staining is still very uniform in all the cells.

NB41$^{GAPDH-GFP}$ cells stably overexpressing GAPDH did not influence the localisation of endogenous Ulip, neither in unstressed nor in stressed cells. No increased Ulip-speckles-formation after oxidative stress was detected in NB41$^{GAPDH-GFP}$.

### 4.7.1.2 <u>Transiently transfected cells</u>

<u>Controls</u>

In transiently transfected cells the nucleus contained about 3-4 times less Ulip-GFP than the cytoplasm *(picture 9c, figure 12b, figure 12c)*. More than 95% cells showed high Ulip-GFP expression limited to the cytoplasm. However, in contrast to untransfected cells, the Ulip-GFP pattern was not homogenous within the cytoplasm, but showed a patchy pattern, with Ulip-GFP concentrated in some specific areas, e.g. close to the Golgi apparatus *(picture 9c, figure 12b, figure 12c)*. Ulip-GFP expression was also strong at the plasma membrane. While low levels of Ulip-GFP could also be detected in the nucleus, the nucleolus did not contain any Ulip-GFP.

<u>Induction of Oxidative Stress</u>

After exposure to 300 μM FeCN for 3 h we observed expression of high levels of Ulip-GFP predominantly at the membrane in about 15% cells *(picture 9d)*. In about 10% of cells we detected

formation of intracellular spots which accumulated all the detectable Ulip-GFP fluorescence of the cell. Few cells raised their expression level in specific regions within the nucleus.

Exposure to 100 μM $H_2O_2$ induced nuclear translocation, yet the majority of cells expressed Ulip-GFP predominantly in the cytoplasm. Ulip-GFP was most intense in areas near the nucleus and at the golgi of NB41A3 cells. These cells mostly did not make processes *(picture 9e, 9f)*.

Lower doses, e.g. 100 μM FeCN or 30 μM $H_2O_2$ up to 5 h resulted in very small changes on subcellular localisation of Ulip-GFP, comparable with changes attained after 2h with 300 μM FeCN or 100 μM $H_2O_2$, respectively. Furthermore, the response of Ulip-GFP to oxidative stress is time dependent and the most pronounced changes in Ulip-GFP localisation were found after 6 h exposure to oxidative stress. After exposure to 100 μM $H_2O_2$ for 6h, a high percentage of cells display Ulip-GFP concentrated in small speckles that were arranged in a circle. Altogether, the changes of Ulip-GFP expression in response to oxidative stress correlates with the incubation time and the concentration of stressing agent, but were far not as intense as for GAPDH.

➡

**Picture 9: Subcellular localisation of Ulip and Ulip-GFP in NB41A3 and R6 cells**
Distribution of endogeneous Ulip in untransfected NB41A3, either **(a)** unstressed or **(b)** stressed with 100 μM $H_2O_2$ detected by TR-immunohistochemistry. **(c-f)** Ulip-GFP expression in transiently transfected NB41A3 neuroblastoma cells. Ulip-GFP expression under **(c)** unstressed conditions and after oxidative stress induced by either **(d)** FecN or **(e, f)** $H_2O_2$, detected as GFP fluorescence. **(e, f)** are two confocal images of single planes of the same cells at different z-axis values. Distribution of endogeneous Ulip in untransfected R6 cells, either **(g)** unstressed or **(h)** stressed with 100 μM $H_2O_2$ detected by TR-immunohistochemistry.
Scale bars are 50 μm.
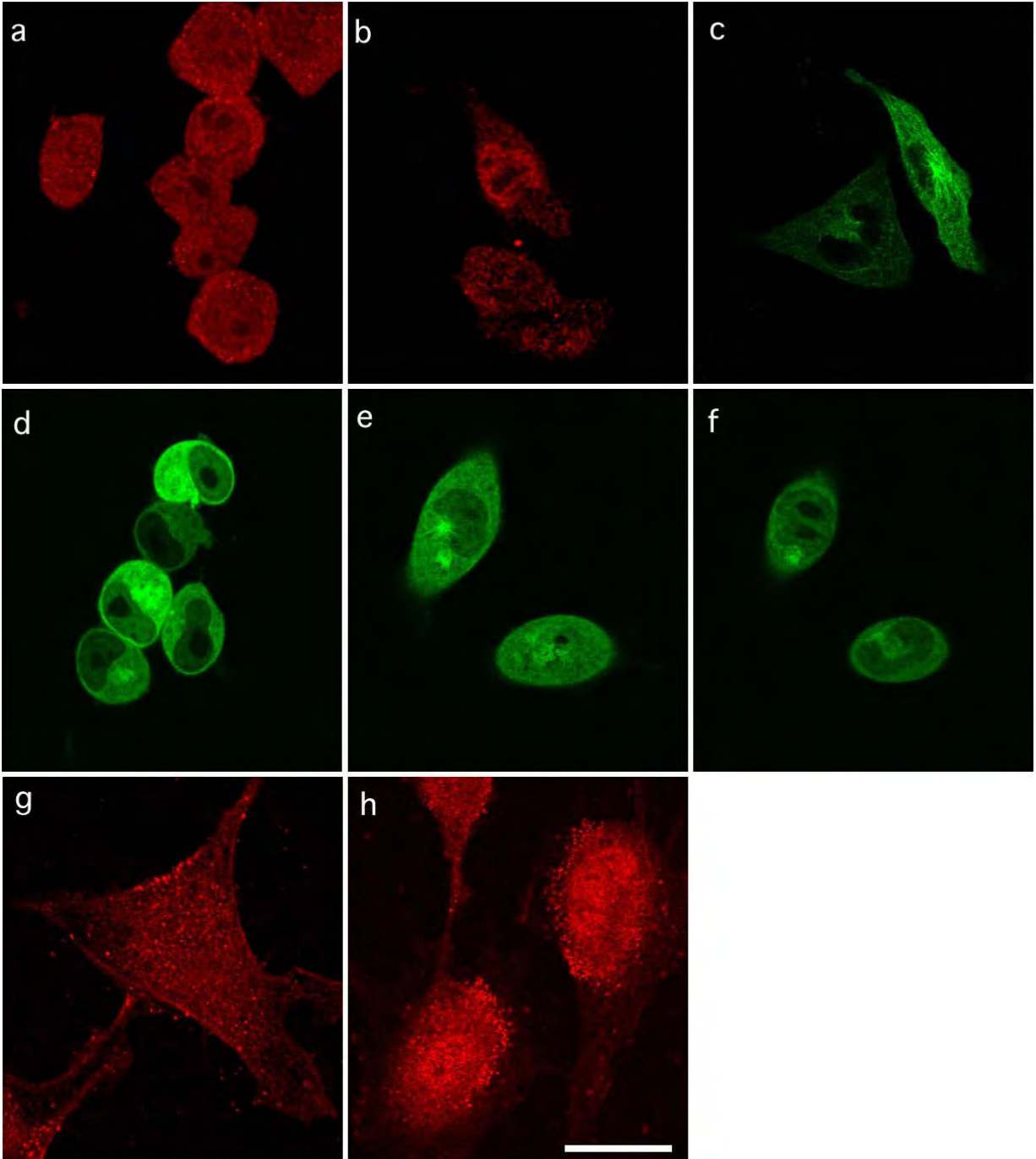
**Picture 9**
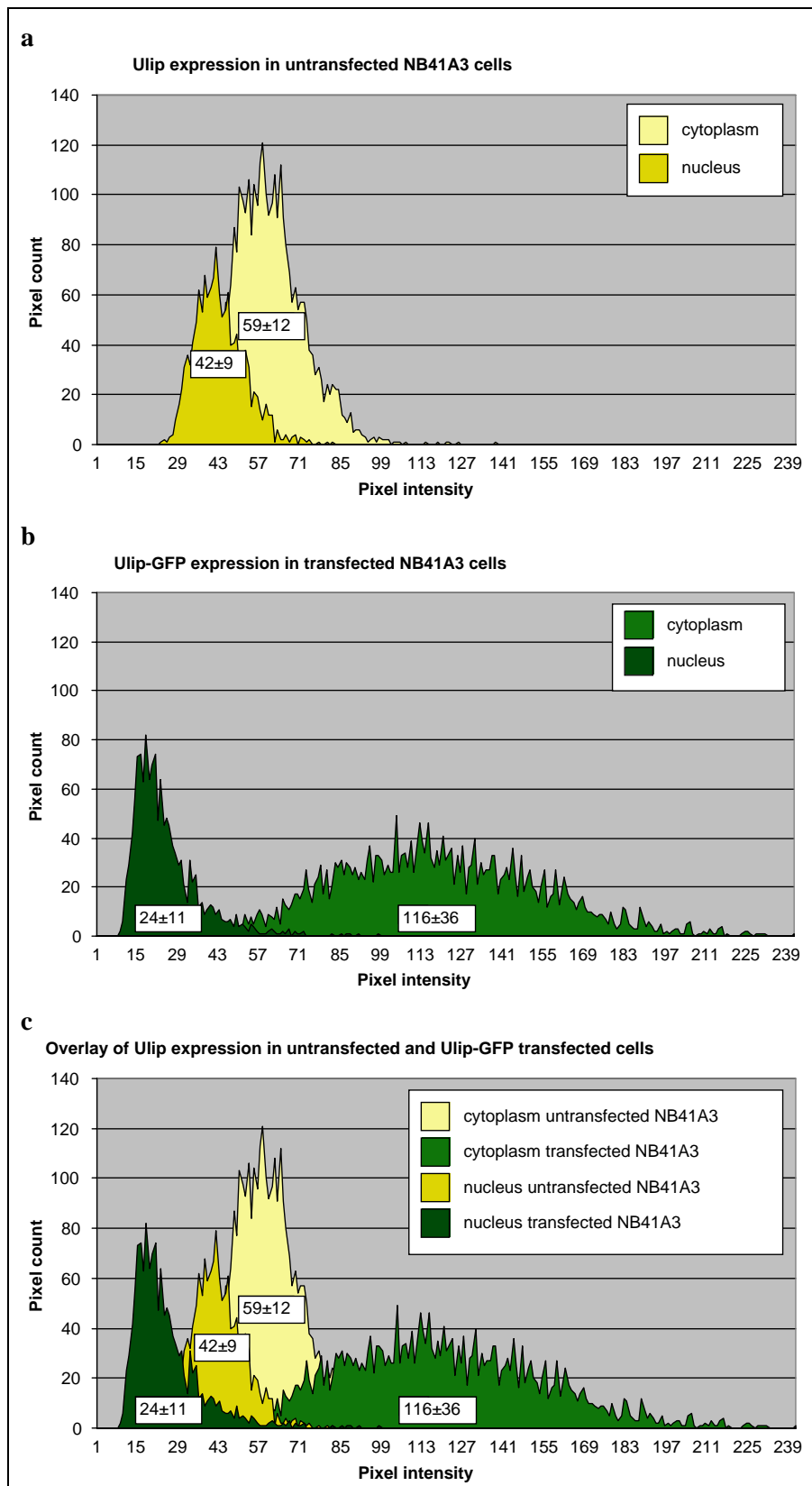
**Figure 12: Intensity and patchiness of Ulip-GFP expression in nucleus and cytoplasm.** Ulip expression was analysed with regard to its intensity and to its uniformity/patchiness in the nucleus and in the cytoplasm of **(a)** untransfected and **(b)** transfected NB41A3 cells. The mean intensity of fluorescence is indicated for each curve with standard deviation. **(c)** Combination of both **(a)** and **(b)** demonstrates that Ulip-GFP transfected cells have a more cytoplasmic and patchier expression than untransfected cells.

97

No influence of overexpressed enolase-BFP on Ulip-GFP was observed in unstressed cells. After extended oxidative stress, however, Ulip-GFP levels in the nucleus raised to a higher extent than in cells transfected with Ulip-GFP alone. In 30% of the enolase-BFP co-transfected cells, Ulip-GFP expression was higher in the nucleus than in the cytosol. In addition, the number of cells concentrating Ulip-GFP either in speckles or at the plasma membrane in response to oxidative stress was about 50% higher in cells co-transfected with enolase-BFP.

The effect of aldolase-BFP on Ulip-GFP was discrete. However, compared to cells transfected with Ulip-GFP alone, before, as well as after oxidative stress, co-transfected cells expressed two fold less nuclear Ulip-GFP.

Both, Hsc70-BFP and GAPDH-BFP influenced Ulip-GFP in the same manner. After stress Ulip-GFP concentrated in spots in the cell about twice more than in cells transfected with Ulip-GFP alone. Hsc70-BFP and GAPDH-BFP were also concentrated in speckles, but no significant colocalisation was seen.

## 4.7.2 R6 AND R6<sup>Bcl-2</sup>

Prior to oxidative stress, endogenous Ulip was expressed along fibres all over the cell, but especially in the cytoplasm and at the plasma membrane *(picture 9g)*. Although mostly fibres were smoothly stained, some intense spots where Ulip was concentrated at the fibres and at the plasma membrane were also observed. The smooth, regular expression of Ulip was slightly weaker in the nucleus than in the cytoplasm.

After oxidative stress the nuclear Ulip expression raised considerably, so that in 80% of the cells Ulip was expressed 2 times more intensively than in the cytoplasm *(picture 9h)*. The Ulip level in the cytoplasm was about the same as before, but the fibril structure could no more be detected. In many cells accumulation of Ulip in small points was found at the plasma membrane and at the nuclear membrane *(picture 9h)*. The accumulation of Ulip at the nuclear membrane may be due to translocation of Ulip from cytosol into the nucleus after stress.

### 4.7.3 <u>Ulip and oxidative stress</u>

In our experiments endogenous Ulip is expressed uniformly in the cytoplasm of untransfected NB41A3 cells. After induction of oxidative stress a significant amount of Ulip translocated into the nucleus. Also in transfected NB41A3 cells Ulip-GFP was localised predominantly in the cytoplasm. Exposure to $H_2O_2$ leads to an increase of nuclear Ulip-GFP expression, whereas exposure to FeCN in addition also raised Ulip-GFP positive speckles formation and concentration of Ulip-GFP at the cell membrane. R6 cells expressed endogenous Ulip along fibres all over the cell at higher levels in the cytoplasm than in the nucleus. However, after oxidative stress most cells expressed Ulip predominantly in the nucleus.

# 4.8 Enolase

## 4.8.1 NB41A3

### 4.8.1.1 Untransfected cells

Untransfected NB41A3 cells mainly display a very diffuse and uniform enolase expression *(picture 10a)*. The cytoplasm including the axons contains about 60% of the expressed enolase and the nucleus contains the remaining 40%, while the nucleolus did not contain any enolase This ratio of 1:1.5 between nuclear and cytoplasmic expression is very constant in all untransfected cells.

The distribution of endogenous enolase did not change significantly after oxidative stress. The majority of cells showed uniform, predominantly cytoplasmic GAPDH expression. In some cells an accumulation of enolase in the Golgi region was observed *(picture 10b)*.

### 4.8.1.2 Transiently transfected cells

In unstressed cells enolase-GFP was predominantly cytoplasmic *(picture 10e)*. Most cells had few processes and overexpressed it at high levels uniformly all over the cytoplasm with some accumulation around the Golgi region and. The level of enolase-GFP fluorescence in the nucleus was around 3-4 times lower than in the cytoplasm and the nucleolus was devoid of enolase-GFP. Some cells with low enolase-GFP fluorescence contained only about 30% more enolase in the cytoplasm than in the nucleus. The difference between cytoplasmic and nuclear enolase expression was more pronounced in transfected than in untransfected cells *(picture 10f, figure 13)*.

After oxidative stress with 300 µM FeCN or 100 µM $H_2O_2$ for 4h, because of nuclear translocation, the uniform enolase expression was only 1-2 times higher in the cytoplasm than in the nucleus *(picture 10c)*. The effects were smaller in cells expressing low levels of enolase-GFP. DNA staining by Hoechst blue shows no nuclear fragmentation in the oxidatively stressed cells. Under these conditions greatest changes in cells highly overexpressing enolase-GFP were observed after 4-5 h. However, the effects of oxidative stress on enolase-GFP localisation were not only time-dependent, but also correlated with the level of total enolase-GFP expression.

**Ratio of cytoplasmic to nuclear enolase expression in correlation to total enolase expression**

(Y-axis: Ratio of cytoplasmic to nuclear enolase expression; X-axis: Total enolase expression per cell (as pixel intensity))
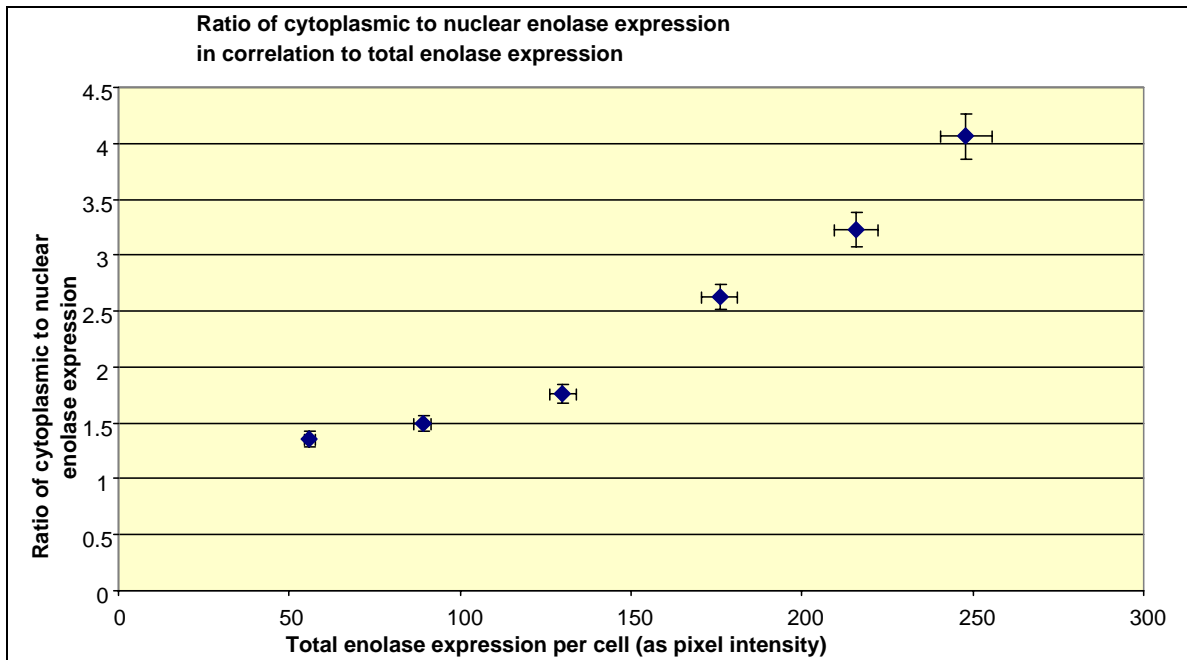
**Figure 13: Relation between total enolase expression and ratio of cytoplasmic to nuclear enolase expression.** The ratio of cytoplasmic to nuclear enolase expression was measured in histograms. They were blotted against the total (nuclear + cytoplasmic) amount of enolase expression. The first point, with a ratio smaller than 1.5 of cytoplasmic to nuclear expression, corresponds to measurements in untransfected cells, whereas the last point corresponds to highly transfected cells that express about 5 times more enolase than untransfected cells. The figure shows that high enolase levels lead to a predominantly cytoplasmic enolase expression.

**Picture 10: Subcellular localisation of enolase and enolase-GFP in NB41A3 and R6 cells**
Distribution of endogeneous enolase in untransfected NB41A3, either **(a)** unstressed or **(b)** stressed with 300 μM FeCN detected by TR-immunohistochemistry. **(d-f)** GAPDH-GFP transfected, unstressed NB41A3 cells (green) show higher difference between cytoplasmic and nuclear enolase expression localisation than endogenous enolase detected by TR in untransfected cells (red). **(f)** Overlay of confocal pictures taken by the red (endogenous enolase) and the green (enolase-GFP) channel . **(c)** GAPDH-GFP transfected NB41A3 cells exposed to 100 μM $H_2O_2$. Distribution of endogeneous Ulip in untransfected R6 cells, either **(g, h)** unstressed or **(i)** stressed with 300 μM FeCN detected by TR-immunohistochemistry. In **(h)** additionally endogenous Hsc70 was made visible (green) by immunostaining with anti-Hsc70 detected by FITC-immunohistochemistry.
Scale bars are 50 μm.
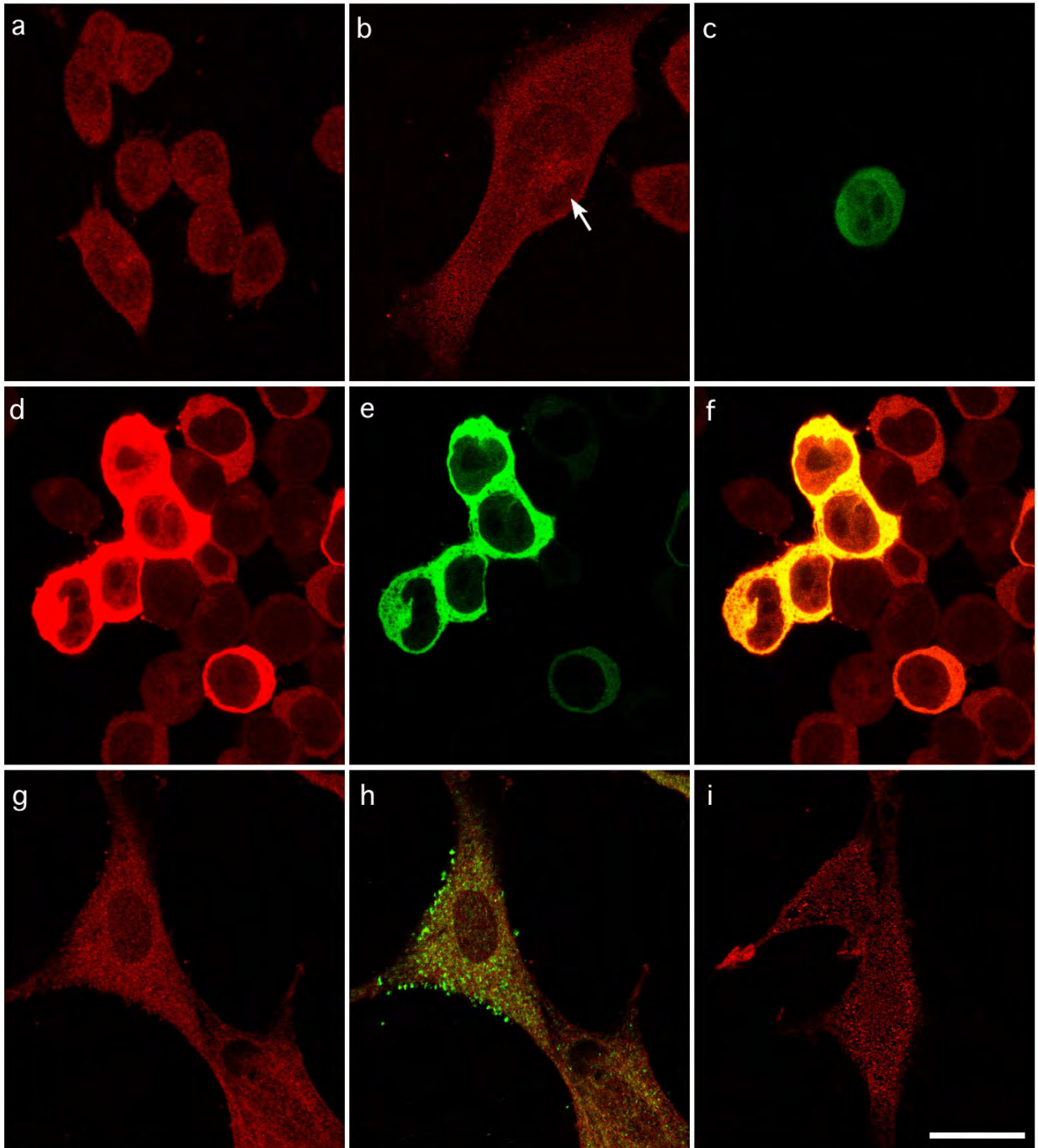
**Picture 10**

Co-transfection with either GAPDH-BFP, aldolase-BFP, Ulip-BFP or Hsc70-BFP did not change the expression of enolase-GFP. The predominantly cytoplasmic localisation of enolase-GFP was not influenced by these proteins, independent of whether the cells were stressed or unstressed.

### 4.8.1.3 Stable overexpression in enolase-GFP transfectants

The intensity of enolase-GFP expression was very variable between different cells. Cells overexpressing enolase at high levels had very high cytoplasmic expression, whereas in cells with weak enolase-GFP fluorescence, the difference between cytoplasmic and nuclear enolase-GFP was smaller. Similar to transiently transfected cells, the ratio of cytoplasmic over nuclear expression correlated with the total level of enolase-GFP expression *(figure 13)*. Endogenous enolase was present at a constant concentration in the nucleus and in the cytoplasm of all cells, while overexpressed enolase-GFP was localised exclusively in the cytoplasm.

NB41A3$^{enolase-GFP}$ cells stably expressing enolase-GFP reacted like transiently transfected cells to agents inducing oxidative stress. Thus, the highest rise of nuclear enolase-GFP was observed in cells overexpressing high levels of enolase-GFP.

## 4.8.2 R6 cells

Unstressed and untransfected R6 cells express enolase along the cytoskeleton, which leads to a fibrillar expression pattern in the cytoplasm *(picture 10g)*. Like in untransfected NB41A3 cells, the amount of enolase in the nucleus is about 30% less than in the cytoplasm. The enolase distribution partly co-localised with the expression of Hsc70 along the fibrils and around the nuclear membrane. However, the enolase pattern is smoother and less spotted than the Hsc70 staining *(picture 10h)*.

After oxidative stress, the nuclear expression of enolase was slightly raised and the fibrillar pattern was less pronounced compared to unstressed cells. We rather observed a diffuse enolase distribution all over the cell *(picture 10i)*.

### 4.8.3 <u>Enolase and oxidative stress</u>

In untreated control cells endogenous enolase as well as transiently or permanently overexpressed enolase-GFP is localised predominantly in the cytoplasm. The expression of enolase is diffuse and uniform. Overexpression of enolase-GFP has no visible effects on cell morphology which also means that overexpression does not induce apoptosis in cells. Of the five enzymes discussed, enolase is the one which shows the least effects following oxidative stress. After exposure to $H_2O_2$ or FeCN the distribution of endogenous enolase in neuroblastomas as well as in fibroblasts is unchanged. However, although in stressed NB41A3 cells enolase-GFP was overexpressed predominantly in the cytoplasm, an increase of nuclear enolase-GFP expression was measured.

# 5 <u>Discussion</u>

## 5.1 <u>GAPDH</u>

### <u>a) GAPDH expression is different in neuroblastoma cells than in fibroblast R6 cells</u>

The most prominent action of GAPDH (EC 1.2.1.12) takes place during glycolysis in the cytoplasm. Also more recent studies investigating the role of GAPDH during apoptosis in COS-7 cells (Tajima et al., 1999), in S49 cells, primary thymocytes (Sawa et al., 1997) in PC12 cells, HEK 293 cells and COS-1 cells (Sawa et al., 1997, Shashidharan et al., 1999), in epithelial cells (Epner et al., 1999) or in cultured cerebellar granule cells (Ishitani et al., 1998, Saunders et al., 1997, Saunders et al., 1999) all showed exclusive or at least highly predominant cytoplasmic expression of GAPDH in control cells in which apoptosis was not induced. Consistent to these studies, our R6 fibroblasts expressed endogenous GAPDH predominantly in the cytoplasm, whereas in control NB41A3 neuroblastoma cells GAPDH was predominantly localised in the nucleus. Thus, the subcellular localisation and expression level of endogenous GAPDH was different in the neuronal and non-neuronal cell lines that were used in this study.

### <u>b) GAPDH expression in the nucleus does not induce apoptosis *per se*</u>

It has been proposed that nuclear localisation alone would be an early indication for apoptotic cells or even responsible for apoptosis (Epner et al., 1999, Ishitani et al., 1998, Saunders et al., 1997, Saunders et al., 1999, Sawa et al., 1997, Shashidharan et al., 1999, Tajima et al., 1999, Tatton, 1999). We show however that control NB41A3 cells, in spite of nuclear GAPDH expression, were not apoptotic *(table 1, figure 6a, figure 6b)*. Nevertheless, the increased levels of nuclear GAPDH measured 24 h after induction of apoptosis by either MG132 or staurosporine in both cell lines, NB41A3 and R6, indicate that there is a correlation between nuclear translocation of GAPDH and programmed cell. But, nuclear localisation of GAPDH alone can not be the only reason for cellular apoptosis.

### c) GAPDH expression in the nucleus is increased after exposure to apoptotic agents

NB41A3 are more resistant to apoptosis: only 20% NB41A3 cells were apoptotic compared to 50% (staurosporine) or 70% (MG132) in R6 fibroblasts. R6[Bcl-2] cells show nuclear fragmentation and chromatin condensation in only 15-20 % of the cells and three times less nuclear translocation. So not only did Bcl-2 protect cells from apoptosis (Allen et al., 1998, Chao and Korsmeyer, 1998), but also efficiently prevented translocation of GAPDH into the nucleus. Bcl-2 mediated inhibition of GAPDH translocation may be a protective mechanism against apoptosis. Most cells with nuclear GAPDH translocation do not have a fragmented nucleus nor show membrane blebbing, so translocation could be an early event in the apoptotic cascade, before the point of no return. Mainly in cells like R6 fibroblasts, where nuclear GAPDH expression is low in rest, higher levels of nuclear GAPDH may be an early marker for apoptosis.

### d) FeCN, but not $H_2O_2$, mediates cytoplasmic translocation of GAPDH-GFP in transfected cells

FeCN, but not $H_2O_2$, mediated cytoplasmic translocation of GAPDH-GFP in transfected cells. This is surprising, because the responses to oxidative stress induced by $H_2O_2$ or FeCN were usually very similar for all other proteins of the PMO complex. However, FeCN is a nitric oxide generator and a potent stimulant for oxidative stress, because NO is directly implicated in cell toxicity as a free radical (Coyle and Puttfarcken, 1993, Hibbs et al., 1987) resulting in the induction of DNA damage (Nguyen et al., 1992, Wink et al., 1991). In contrast to $H_2O_2$, NO is an intracellular messenger and a paracrine extracellular agent (Marletta, 1993, Moncada et al., 1991). Initial studies identified cytoplasmatic guanylate cyclase as NO target, but other studies indicated a role for cGMP-independent pathways by post-translational modification of proteins (Stamler et al., 1992). Specific covalent binding of NAD+ to GAPDH has been demonstrated *in vivo* (Dimmeler and Brune, 1992, Dimmeler and Brune, 1993, Durrieu et al., 1987, Durrieu et al., 1987). GAPDH undergoes two NO-induced post-translational modifications at cys[149](reviewed in (Brune and Lapetina, 1995)), leading first to S-nitrosylation which severely inhibits GAPDH glycolytic activity (Molina y Vedia et al., 1990), and second, to a covalent, NAD+ modification (Brune and Lapetina, 1995, Dimmeler and Brune, 1992, Dimmeler and Brune, 1993, Dimmeler et al., 1992, Molina y Vedia et al., 1990, Zhang and Snyder, 1992). Wu et al. (Wu et al., 1997) isolated a series of glycolytic enzymes including GAPDH in the postsynaptic density (PSD) organelle and demonstrated the close relation between GAPDH and NO synthase. Reversible S-nitrosylation of GAPDH in the cell membrane modulates GAPDH/membrane interactions (Galli et al., 1998). From this and our studies it can

be postulated that in oxidative stress not the function of NO as cellular mediator, but its ability to induce post-translational modifications of GAPDH yields to specific translocation of GAPDH-GFP from the nucleus to the cytoplasm.

**e) GAPDH is differentially translocated after exposure to stress or apoptotic agents**

The recombinant GAPDH-GFP protein was translocated in some cells from the cytoplasm into the nucleus, whereas in some other cells it in intracellular speckles, or in extracellular membrane blebs and spikes. Experimental evidence and GAPDH sequence analysis suggest that the catalytic domain is involved in the regulation of the subcellular localisation of GAPDH. Studies *in vivo* indicate that amino acids within the glyceraldehyde-3-phosphate (G3P) binding site determine GAPDH/membrane interactions, e.g. exposure of GAPDH to pyridoxal phosphate reduced its affinity for membranes (Eby and Kirtley, 1983, Robbins et al., 1995, Ovadi et al., 1973). Sequence analysis suggests that amino acids within the catalytic domain determine the nuclear, cytoplasmic or membrane localisation of GAPDH. Previous studies reveal a series of amino acid motifs which regulate intracellular protein localisation (reviewed in (Dingwall, 1991, Dingwall and Laskey, 1991, Jans, 1994, Yoneda, 1997)). Analysis of the GAPDH sequence reveals several regions which contain such motifs.

However, whether GAPDH would requires such signals is unknown, especially for nuclear translocation, since proteins up to 45 kDa do not require active nuclear transport (reviewed in (Dingwall, 1991, Dingwall and Laskey, 1991, Jans, 1994, Yoneda, 1997)). Previous studies demonstrated the presence of the 37 kDa monomer in mammalian nuclei (Cool and Sirover, 1989). If GAPDH is transported into the nucleus as the 37 kDa monomer, an active nuclear transport would not be required. Alternatively, if GAPDH enters the nucleus as the tetramer (150 kDa), an active transport would be necessary. Studies suggest that apoptosis needs active import of at least some proteins (Yasuhara et al., 1997). From our results we presume that GAPDH itself may serve as a carrier for other proteins during apoptosis.

## f) Intracellular translocation may have various mechanisms

How do cells regulate the differential intracellular translocation of identical 37 kDa GAPDH monomers or 150 kDa GAPDH tetramers? The regulation may be based on structural signals within the GAPDH protein, because the catalytic G3P site contains potential nuclear localisation and export signals. However, as each GAPDH molecule would contain the identical sequences, it is unclear how such signals would enable a mammalian cell to distinguish between individual GAPDH molecules.

A second possibility is the expression of alternative transcripts, as detected in a study in mature testis focusing on differential splicing at intron 1 of the GAPDH gene (Mezquita et al., 1998).

Also post-translational modification results in the formation of singular GAPDH isozymes (Susor et al., 1973, Kester et al., 1977, Lin and Allen, 1986, Soukri et al., 1995, Mazurek et al., 1996, Glaser and Gross, 1995). Ryzlak and Pietruszko reported differential subcellular localisation of GAPDH isozymes in human brain (Ryzlak and Pietruszko, 1988). Post-translational GAPDH modification susceptible to phosphodiesterase treatment suggested a mono-ADP-ribosylation (Soukri et al., 1996).

## g) Subcellular localisation and function of GAPDH change during apoptosis

*In R6 control cells GAPDH exerts predominantly cytoplasmic functions*

In normal R6 fibroblasts, the major function of GAPDH is in glycolysis in the cytosol for energy production. It also enhances bundling of tubulin into microtubules (Kumagai and Sakai, 1983) regulated by ATP (Huitorel and Pantaloni, 1985). GAPDH binds to the C-terminal region of $\alpha$-tubulin (Volker and Knull, 1997). Both dimeric and tetrameric GAPDH bind to microtubules, but bundling is only observed with tetrameric GAPDH (Huitorel and Pantaloni, 1985). GAPDH also catalyses the formation of triad junctions from isolated transverse tubules and terminal cisternae (TC) (Caswell and Corbett, 1985). Binding of GAPDH/TC triad binding inhibits GAPDH dehydrogenase activity. Dissociation of tetrameric GAPDH to the monomeric form is responsible for diminution of dehydrogenase activity (Durrieu et al., 1987, Muronetz et al., 1994) and ATP facilitates tetramer to monomer GAPDH dissociation (Bartholmes and Jaenicke, 1978, Constantinides and Deal, 1969, Oguchi et al., 1973, Stancel and Deal, 1969) which may provide a cellular control mechanism to regulate the functional diversity of GAPDH, its glycolytic activity and cellular requirements for ATP generation. The specificity of GAPDH as a tubulin bundling

protein (Walsh et al., 1989) and its microtubule bundling activity has been well demonstrated (Launay et al., 1989), and glycolytic enzymes which do not bind to microtubules have no effect on bundling (Volker and Knull, 1993, Volker et al., 1995, Somers et al., 1990).

All these studies agree with our observation in control R6 cells that GAPDH is localised predominantly in the cytoplasm where staining of the cytoskeleton can be observed. Concentration of GAPDH in the perinuclear area therefore can be explained by the fact that the cytoskeleton is more dense around the nucleus.

*GAPDH may have other activities after nuclear translocation induced by apoptotic agents*

Translocation of GAPDH into the nucleus is probably important during apoptosis and very relevant in oxidative stress and may be due to a conformational change induced by an apoptotic agent in the NAD+ binding domain. Probably GAPDH exerts another function in the nucleus. Recent investigations suggest an activity as a nuclear RNA transport protein (Singh and Green, 1993). The T stem-loop region may provide a recognition site and its interaction may regulate both GAPDH glycolytic activity and nuclear tRNA binding/export activity. Furthermore a post-transcriptional regulatory cis-element (PRE) is required for the increase in viral transcripts which colocalises with GAPDH into a GAPDH/PRE complex in the nucleus and was immunoprecipitated by anti-GAPDH antibody (Zang et al., 1998). This provides a potential function for GAPDH in the nucleus and indicates the emerging role of GAPDH in viral pathogenesis. Nevertheless, GAPDH-mediated tRNA export in apoptosis is disputed (Sawa et al., 1997).

More relevant to apoptosis and oxidative stress may be the nuclear function of GAPDH as uracil DNA glycosylase (UDG) with DNA repair activity. As cytosine deamination to uracil is a mutagenic event, UDG has a significant function, although the role *in vivo* is unclear at the present time (Arenaz and Sirover, 1983, Vollberg et al., 1987, Vollberg et al., 1989, Meyer-Siegler et al., 1991, McNulty and Toscano, 1995). A recent study  showed that although GAPDH concentration increases in the nucleus of apoptotic cells, the UDG activity which was measured was lower than in control cells (Saunders et al., 1999).

Binding of GAPDH to cellular molecules may thus influence the response to apoptosis or to oxidative stress. Specific binding of GAPDH to the 5'-UTR and the 3'-UTR regions of mRNA have been reported,

e.g. the specific binding to AU sequences in 3'UTR regions of lymphokine mRNA (Nagy and Rigby, 1995). Also GAPDH stimulates the activity of a TNFα ribozyme (Sioud and Jespersen, 1996).

Finally GAPDH also binds specifically to the dinucleoside polyphosphate, $P^1,P^4$-di(adenosine-5') tetraphosphate ($A_{p4}A$) (Vishwanatha and Wei, 1992, Baxi and Vishwanatha, 1995), either to a subunit within the multiprotein DNA pol α complex (Baril et al., 1983) or to cell membranes (Edgecombe et al., 1996). Several reports link diadenine nucleotides to apoptosis (Gasmi et al., 1996, Gasmi et al., 1996). The $Ap_3/Ap_4$ ratio changes during programmed cell death (Vartanian et al., 1997), thus Ap4A and Ap3A may be physiological antagonists in determination of the cellular status: Ap4A induces apoptosis whereas Ap3A is a co-inductor of differentiation (Vartanian et al., 1999).

*Increased expression of GAPDH is observed in apoptotic cells*

In the next stage, the nucleus is fragmented and GAPDH is expressed at very high levels. However, GAPDH is probably not bound to DNA, since it is expressed everywhere except where the fragmented nucleus is detected. These cells have shrunk and are rounded up, which could be related to the loss of tubulin bundling activity of GAPDH in the cytoplasm.

At the final stage, in some cells only the fragmented nucleus can be seen, but no GAPDH. The cell membrane is probably disrupted and GAPDH could have been released.

*Translocation of GAPDH is different in NB41A3 cells and in R6 cells*

In NB41A3 cells the same different stages of apoptosis are observed, except that GAPDH is localised in the nucleus already before exposure to MG132 or to staurosporine. Perhaps neuronal cell lines like NB41A3, need *per se* more nuclear than cytoplasmic functions of GAPDH and therefore express GAPDH predominantly in the nucleus.

## h) There is increasing evidence that GAPDH is involved in apoptosis

Although several studies demonstrate a role of GAPDH in apoptosis, the relevance of these data is not known. Initial studies (Ishitani and Chuang, 1996a, Ishitani, et al., 1996c, Ishitani, et al., 1996b, Ishitani, et al., 1997, Sunaga, et al., 1995) in cerebellar granular cells showed that GAPDH expression was co-ordinated with the induction of apoptosis and reduced by actinomycin D and cycloheximide. Transfection of cerebellar granular cells with antisense, but not sense, GAPDH oligonucleotides inhibited programmed cell death. The generality of GAPDH function in apoptosis was established using a variety of agents to induce apoptosis in various cell types. GAPDH biosynthesis during programmed cell death was observed using cytosine arabinoside (Ishitani and Chuang, 1996a), low K+ (Ishitani et al., 1997), dexamethasone (Sawa et al., 1997), and serum deprivation (Sawa et al., 1997).

Analysis of the subcellular regulation of GAPDH during apoptosis performed by other groups support our findings. It was observed that its participation in apoptosis may involve its specific translocation to the nucleus (Ishitani et al., 1998, Saunders et al., 1997, Saunders et al., 1999, Sawa et al., 1997, Shashidharan et al., 1999). This was established using cell fractionation coupled with immunoblot analysis or immunocytochemistry to detect the presence of nuclear GAPDH as a function of programmed cell death. Interestingly, antisense GAPDH studies demonstrated that its inhibition of apoptosis precluded the appearance of nuclear GAPDH. Further, enzymatic analysis demonstrated the absence of GAPDH glycolytic activity subsequent to the translocation of the GAPDH protein into the nucleus. In accord with this finding, treatment of neuronal NG108-15 cells with koningic acid (which inhibits GAPDH glycolytic activity) resulted in DNA fragmentation and the appearance of apoptotic cells (Nakazawa et al., 1997). However, koningic acid also produces free radicals (Itoh et al., 1980, Tanaka et al., 1998) which can cause programmed cell (Nomura et al., 1996).

Apoptosis in neuronal cells may be delayed by ONO-1603, an anti-dementia drug and a prolyl endopeptidase inhibitor, or by tetrahydroaminoacridine (THA), another anti- dementia drug (Katsube et al., 1999). Both, ONO-1603 and THA, robustly suppressed overexpression of GAPDH mRNA and accumulation of GAPDH protein in a particulate fraction of cultured neurones undergoing age-induced apoptosis.

### i) GAPDH may have several roles in apoptosis

The role of GAPDH in apoptosis may involve one or more of its nuclear, non-glycolytic functions. Its nuclear RNA export function may nevertheless be excluded, since GAPDH tightly binds to nuclear DNA, remaining in the nuclear fraction following treatment either with DNase or 5 M NaCI (Sawa et al., 1997), in accordance with early studies identifying GAPDH as a DNA binding protein (Grosse et al., 1986, Melero et al., 1975, Morgenegg et al., 1986, Perucho et al., 1977, Ronai, 1993, Tsai and Green, 1973). Accordingly, GAPDH may function in apoptosis as an $A_p4A$ binding protein, a glutathione binding protein or as a uracil DNA glycosylase (UDG), although there is no report which links UDG and apoptosis and nuclear accumulation of GAPDH was associated with a progressive decrease in UDG activity (Saunders et al., 1999). Previous investigations link changes in $A_p3A/A_p4A$ levels (Vartanian et al., 1999, Vartanian et al., 1997) as well as glutathione to apoptosis (Boggs et al., 1998, Froissard et al., 1997, Macho et al., 1997, Zhao et al., 1997).

A recent study indicates that the regulation of GAPDH during apoptosis is quite complex (Saunders et al., 1999). Six GAPDH isoforms were detected in the nuclei of AraC- treated cells. Various GAPDH isoforms were differentially regulated and may have distinct apoptotic roles. Pre-treatment of cells with GAPDH antisense oligonucleotide blocked the nuclear translocation of GAPDH isoforms. NAD labelling of nuclear GAPDH induced by FeCN showed a 60% loss of GAPDH labelling after AraC treatment, suggesting that the active site of GAPDH may be covalently modified, denatured, or improperly folded. This modification may be responsible for the fact, that cells exposed to FeCN translocate GAPDH back into the cytoplasm, in contrast to all other agents inducing oxidative stress or apoptosis which lead to a nuclear translocation of GAPDH.

It is interesting to note that only apoptosis, but not necrosis involves overexpression of GAPDH in the nucleus of cells and that GAPDH antisense oligonucleotides preferentially blocked low K+-induced apoptosis rather than necrotic damage (Ishitani et al., 1997).

### j) GAPDH may act as a nuclear carrier during apoptosis

Our results indicate that not the nuclear localisation of GAPDH itself, but rather an event coupled to the import of GAPDH into the nucleus is responsible for the apoptotic action of GAPDH, since under various

different conditions GAPDH is found at high levels in the nucleus without inducing or enhancing apoptosis. Therefore we suggest that GAPDH may function as a molecular chaperon, as supported by earlier studies (Katsube et al., 1999, Sawa et al., 1997).

This may be related to studies on selective binding of GAPDH to gene products of neurodegenerative disease, such as huntingtin of Huntington disease (HD), atrophin of dentatorubropallidoluysian atrophy, ataxin of spinocerebellar ataxia type-1, ataxin-3 of Machado-Joseph disease and androgen receptor of spinobulbar muscular atrophy. It is note worthy that NH2-terminal fragments of huntingtin and ataxin-3 are located to intranuclear inclusions in neurones of affected brain regions (Davies et al., 1997, DiFiglia et al., 1997, Paulson et al., 1997), supporting the notion that GAPDH may serve as a carrier to mediate the translocation of these disease gene products to the nucleus.

Our observations also suggest that GAPDH acts as pro-apoptotic enzyme downstream of Bcl-2. Its nuclear translocation may be a key event during apoptosis in combination with other factors and have a great influence in several neurodegenerative disease.

## k) GAPDH has an important role in cells undergoing oxidative stress

Our results demonstrate that GAPDH does not only have an important role in apoptosis but also in oxidative stress. Studies identified the interaction of GAPDH and glutathione as a result of oxidative stress (Schuppe-Koistinen et al., 1994). *In vitro* analysis probed the interaction of GAPDH and oxidised glutathione using human erythrocyte GAPDH (Lind et al., 1998). Membrane binding sites for glutathione conjugates were examined in inverted erythrocyte membranes (Puder and Soberman, 1997). Association of GAPDH in binding of glutathione to membranes was inhibited by ATP, an indication of GAPDH/glutathione interactions. Recent studies also suggest a role for glutathione in apoptosis (Boggs et al., 1998, Froissard et al., 1997, Macho et al., 1997, Zhao et al., 1997).

A recent report identifies GAPDH as the major target of protein S-thiolation following treatment with hydrogen peroxide in *S. cerevisiae* (Grant et al., 1999). The GAPDH enzyme activity of the two isoenzymes Tdh2 and Tdh3 was decreased following exposure to $H_2O_2$ and restored for Tdh3 (but not for Tdh2) within a 2-h recovery period, indicating that the inhibition of the S-thiolated Tdh3 polypeptide was reversible. The S-thiolated Tdh3 are required for survival during conditions of oxidative stress. In

contrast, the non-thiolated Tdh2 polypeptide was required during exposure to continuous low levels of oxidants, conditions where Tdh3 is inactivated.

Another study examined sub lethal oxidative stress obtained by treating human fibroblasts with 0.5 mM $H_2O_2$ in DMEM plus 5% FCS for times not exceeding 60 min (Mocali et al., 1995). Under these conditions cells remained viable throughout long-term incubation, whereas exposures of the fibroblasts to 0.5 mM $H_2O_2$ for more than 60 min induced a lethal cell injury which was fully expressed 2 days later by leakage of cytosolic components. Early metabolic effects of sub lethal stress included partial decrease of specific activity of GAPDH. We suppose that this is due to the nuclear translocation of GAPDH. Microfilaments of $H_2O_2$-treated cells are morphologically altered due to partial fragmentation of cytoskeleton actin (Mocali et al., 1995). This supports our observations and may be explained by our findings that GAPDH in fibroblasts translocates into the nucleus after oxidative stress and so the tubulin bundling by GAPDH is decreased in the cytoplasm. Moreover, Molcali showed that sub-lethally injured fibroblasts exhibit a reduced adhesive strength to plastic once they were detached and re-seeded into new dishes. This may explain why stressed cells start to form long processes.

Besides nuclear translocation of GAPDH we also observed translocation to other intracellular regions. Non-nuclear translocation was also found in a study that investigated the role of oxygen free radicals in the modulation of GAPDH binding to the erythrocyte membrane (Mallozzi et al., 1995). The reaction of peroxyl radicals with intact red cells induced a time-dependent loss of membrane-bound GAPDH, associated with a concomitant decrease in enzyme activity, which was completely reversible after removal of the oxidative stress. In that way cells can boost or reduce energy production in times of special need such as during a free radical attack.

Increased levels of GAPDH mRNA were also observed in oxidatively stressed cells (Ito et al., 1996, Yan et al., 1999). It was suggested that NAD+ precursors may protect against oxidative stress and DNA damage by up-regulating the stress response genes of GAPDH.

However, the response to oxidative stress is highly dependent on experimental conditions used to induce oxidative stress (Mocali et al., 1995, Castagne and Clarke, 1998, Castagne, et al., 1999). Protective effects of weak, non-lethal oxidative stress may stimulate defence mechanisms, including HSPs, as shown for hyperthermia (Barbe, et al., 1988, Caprioli, et al., 1996).

# 5.2 <u>HSC 70</u>

## a) Overexpression of Hsc70-GFP renders cells more resistant to oxidative stress

As expected, R6[Bcl-2] cells showed no difference in their Hsc70 expression and in their morphology to R6 cells. R6[Bcl-2] cells are less sensitive to MG132 or staurosporine induced apoptosis but not to oxidative stress by $H_2O_2$ or FeCN.

Very few Hsc70-GFP transfected cells exposed to oxidative stress had a shrivelled cell body and formed long processes. This may indicate, that overexpression of Hsc70-GFP helps the cell to trigger cell damages induced by oxidative stress, because the loss of adhesive strength to the growth surface is viewed as marker for stress. The formation of long processes may therefore be a reaction of stressed cells loosing their adherence to the growth surface. However, only few cells form long, oligodendrocyte like processes. Hsc70-GFP does not significantly influence the rate of apoptotic cells.

## b) Translocation of endogenous Hsc70 into the nucleus is more pronounced during oxidative stress than during apoptosis

Our results showed that Bcl-2 protects cells overexpressing Hsc70-GFP at the same rate as in cells expressing endogenous GAPDH. Compared to GAPDH-GFP overexpressing cells, less cells showed nuclear translocation of the Hsc70-GFP in response to induction of apoptosis. Moreover, apoptotic cells did not express increased levels of either endogenous Hsc70 or overexpressed Hsc70-GFP.

Since nuclear translocation of endogenous Hsc70 is only observed during oxidative stress and not during apoptosis, it is tempting to speculate that a) Hsc70 transport to the nucleus is not directly linked to GAPDH translocation and is regulated by another mechanism and b) that the nuclear translocation mechanism for ROS-induced oxidative stress and for MG132 or staurosporine induced apoptosis is not identical.

However, an observation that was made when cells were concomitantly co-transfected with GAPDH-GFP and Hsc70-BFP has to be noted. While the localisation of Hsc70-BFP is not influenced by GAPDH-GFP in unstressed control cells or in cells stressed by FeCN, in cells exposed to $H_2O_2$ significantly higher

rates of nuclear Hsc70-BFP translocation are observed than in cells transfected with Hsc70-BFP or Hsc70-GFP alone.

Translocation of Hsc70 into the nucleus may be related to its function as a molecular chaperone in correct folding of proteins. Oxidative stress may induced damage to some nuclear proteins and Hsc70 may then be imported to the nucleus in order to refold them into a suitable conformation. However, other properties of Hsc70 may be relevant in response to oxidative stress, besides its role in catalysing folding of proteins.

### c) Different molecular mechanisms can be proposed for the nuclear translocation of Hsc70

Interestingly, there is evidence for a mechanism for the nuclear import of Hsc70, since Hsc70 can shuttle between the nucleus and the cytoplasm. Nuclear import of purified Hsc70 was not inhibited by an excess of nuclear localisation signals (NLSs) conjugated with BSA (Lamian et al., 1996). A basic domain (246KRKHKKDISENKRAVRR262) of Hsc70 promotes nuclear import and, therefore, acts as a prototypical basic NLS. However, inactivation of this signal by deleting the first six amino acids had no effect on Hsc70 import, indicating that Hsc70 utilises a novel import signal and enters the nucleus by a different mechanism than that employed by simple and bipartite NLSs. In our studies the GFP tag coupled to Hsc70 may have disturbed nuclear translocation promoted by this signal, partially explaining our observations, that nuclear translocation after oxidative stress is greater for endogenous Hsc70 than for overexpressed Hsc70-GFP. Recently, nuclear translocation of Hsc70, but not of Hsp70, was observed during early S phase of the cell cycle, indicating a role for Hsc70 in the process of S phase entry (Zeise et al., 1998).

In connection with was discussed on GAPDH, recent data indicate that the heat shock response inhibits nuclear translocation of the pro-inflammatory transcription factor NF-κB. Under basal conditions NF-κB is retained in the cytoplasm by the inhibitory protein I-κB. Heat shock increases I-κB mRNA expression by activating the I-κB promoter which leads to inhibition of NF-κB activation (Wong et al., 1999). This supports our observation that GAPDH and Hsc70 may exert opposite roles in the cellular response to stress.

## d) Nuclear translocation of Hsc70 has functional relevance during oxidative stress

Induction of HSPs by oxidative stress contributes to cellular protection and adaptation to stress and is mediated by differential translocation. This is supported by investigations in human monocytes on the expression and subcellular distribution of hsp70 and Hsc70 after heat-shock and inflammation-related stresses leading to generation of reactive oxygen species, such as erythrophagocytosis (E-phi) and the phorbol ester PMA (Mariethoz et al., 1997). All stress factors resulted in an increase in hsp70 expression, but the subcellular distribution pattern was different depending on the type of stress. While heat-shock induced a rapid translocation of hsp70 into the nucleus, no nuclear translocation of hsp70 was observed after PMA or E-phi. Neither of the examined stresses induced membrane expression of hsp70. These observed differences in subcellular distribution pattern were consistent with our findings showing different type of subcellular localisation of Hsc70 depending whether oxidative stress or apoptosis was induced. This differential expression might relate to distinct regulation and specific functions of Hsc70 in apoptosis or oxidative stress.

Another study shows that overexpression of both inducible (hsp70i) and constitutive (hsp70c) forms confers resistance to oxidative challenges generated by ROS, again suggesting an antioxidant role for these proteins (Chong et al., 1998).

## Hsc70 may also have a role in hypoxia and apoptosis

While the phenomenon of heat-shock protection to various types of stresses has been often described, the molecular mechanism underlying this protection remains poorly defined. ROS production is common to apoptosis induced by camptothecin and actinomycin D (agents against which HSPs conferred protection), whereas Fas-mediated apoptosis (against which HSPs showed no protective effect) occurs via a ROS-independent mechanism (Creagh and Cotter, 1999). The selective protection observed against these agents was mimicked by pre-treatment with antioxidant compounds and occurrs downstream of ROS production. Consistent with our results, this study showed no direct correlation between Bcl-2- and HSP70-mediated protection. However, other reports indicate some connections between HSPs and Bcl–2. Investigations on the intracellular responses to metabolic oxidative stress by glucose deprivation show an increase in the level of HSP70 mRNA, which could be suppressed by overexpression of Bcl-2. (Lee and Corry, 1998). The signal transduction pathway in heat shock gene expression under glucose deprivation involved the stress-activated protein kinase.

117

Experiments in hypoxic cells are of special interest since besides Hsc70 expression, also the expression of GAPDH and enolase γ was significantly changed after hypoxia (Graven and Farber, 1995, Graven and Farber, 1998, Graven et al., 1998, Graven et al., 1994). GAPDH and enolase γ are up-regulated in the cytoplasm of hypoxic cells, whereas GAPDH is also up-regulated in the nucleus. GAPDH activity is decreased, suggesting that during hypoxia GAPDH and perhaps enolase exert functions aside from their catalytic function in glycolysis. This is an interesting observation since we isolated a multi-enzyme complex containing among others Hsc70, GAPDH and enolase γ (Bulliard et al., 1997).

Experiments where macrophage cells exposed to hypoxia underwent apoptosis give indications for the role of Hsc70 in apoptosis (Yun et al., 1997). Subpopulations of cells were resistant to hypoxia-induced apoptosis. In contrast to the other cells, in these hypoxia-induced apoptosis-resistant macrophages (HARMs) Hsc70 expression did not decrease, indicating that Hsc70 may play a role in protection against hypoxia-induced apoptosis. After hypoxic treatment, a significant increase in TNFα production in HARM but decrease in other macrophage cells was observed. These results suggest that a selective population of macrophages can adapt to hypoxic conditions by overcoming the apoptotic signal. This selectivity supports our observation that for a given cell population cells do not all react in the same manner in response to oxidative stress.

Altogether, these findings demonstrate, that the differential translocation of Hsc70 observed in our experiments after either induction of oxidative stress or apoptosis, is most probably in direct correlation with one of the specific actions of Hsc70 described above.

# 5.3 <u>Aldolase</u>

## <u>a) Aldolase C is predominantly expressed in the cytoplasm and bound to the cytoskeleton</u>

Distribution of aldolase C in control cells and cells exposed to oxidative stress or apoptosis induction was very similar to the one of Hsc70 discussed above. Endogenous aldolase and overexpressed aldolase-GFP both are predominantly expressed in the cytoplasm of unstressed cells, best visible in the perinuclear area and at the bases of axons. The fibril staining of the cytoskeleton was more distinct in fibroblasts than in neuroblastomas. This observation is confirmed by other studies in which the micro-compartmentation of aldolase and GAPDH was investigated in four different cell types (3T3 cells, SV 40 transformed 3T3 cells, mouse fibroblasts, chick embryo cardiomyocytes) (Minaschek et al., 1992). It was shown that both enzymes exist in a soluble as well as in a structure-bound form. Their findings that the soluble fraction of aldolase and GAPDH is distributed homogeneously throughout the cytoplasm, excluding the nucleus and vesicles and that the permeabilisation-resistant form is associated with the actin cytoskeleton is consistent with our observations. Furthermore they also observed that a considerable amount of both enzymes is located in the perinuclear region and cannot be attributed to a definite structure. Comparing the staining patterns of aldolase and GAPDH in the four different cell types it was found that the distribution of the enzymes corresponds with diverse forms of actin cytoskeletal organisation of these cells. There are also other studies that show interaction of aldolase together with GAPDH with cytomatrix components (Balaban and Goldman, 1990, Mathur et al., 1992, Walsh et al., 1989). Further association of aldolase with GAPDH was also shown in the presence of extracellular stress agents (Maine and Ciejek-Baez, 1991) and in trypanosomes, where aldolase and GAPDH co-purify with unique trypanosomal microtubule-associated protein (p52) (Balaban et al., 1995)

## <u>b) Changes in aldolase C expression are higher during oxidative stress than during apoptosis</u>

Induction of oxidative stress by either FeCN or $H_2O_2$ leads to enhanced nuclear expression of endogenous aldolase in NB41A3 cells. An increase of nuclear aldolase-GFP expression is also observed in transiently or permanently transfected cells, but nevertheless cytoplasmic expression of aldolase-GFP is still higher. This may be due to the fact that NB41A3 cells overexpressing aldolase-GFP have very high expression of aldolase-GFP in the cytoplasm prior to oxidative stress and that only a small amount of this translocates into the nucleus. Therefore the absolute amount expressed in the nucleus after oxidative stress may be the

same as in untransfected cells, but the relative amount is lower. However, both transfected and untransfected cells show formation of aldolase-positive speckles after induction of stress.

R6 and R6[Bcl-2] fibroblasts showed less effects to oxidative stress than NB41A3 cells. No significant translocation of endogenous aldolase to the nucleus was observed. This may be due to the fact that the percentage of cytoskeleton-bound aldolase compared to soluble aldolase is higher in fibroblasts than in neuroblastoma cells, as discussed for other cell lines in the study mentioned above (Minaschek et al., 1992). Therefore less free aldolase is available for translocation into the nucleus after oxidative stress.

Our results demonstrate that aldolase C has no crucial function during apoptosis, but may be involved in oxidative stress. It was reported that oxidation of enzyme-substrate carbanion intermediates by extrinsic oxidants may result in irreversible paracatalytic inactivation of aldolase (Gupta et al., 1993). Aldolase was paracatalytically modified in the presence of fructose 1,6-bisphosphate and hexacyanoferrate(III). That means that ROS cause self-inactivation of aldolase. However, this modification may create a new, unknown function of aldolase. It was shown that mRNA levels of aldolase A is up regulated in proliferating cells and during anoxia (Gautron et al., 1991).

# 5.4 <u>Ulip</u>

## a) Ulip is detected in neuronal and in non-neuronal cell lines

Ulip is described as a neurone-specific intracellular protein implicated in the relay of signals by attracting and repelling molecules which direct neuronal outgrowth. We detected endogenous Ulip in both R6 fibroblasts and NB41A3 neuroblastoma cells. This is an interesting finding, since previous studies stated that Ulip is almost exclusively expressed in the brain and strongly regulated during development. Rat protein TOAD-64 and chick CRMP-62, which correspond to Ulip-2 are used as an early marker in differentiated neurones and have been described to be then down-regulated (Minturn et al., 1995a). Chick-protein CRMP-62 is implicated in the collapsing induced mediation of growth collapse of chick dorsal root ganglion (DRG) neurones (Goshima et al., 1995). This correlates with the findings that Ulip strongly expressed in neurones preferentially localise in the growth cone, and can be readily detected in the pre-synaptic region of the neuromuscular junction (Byk et al., 1996).

## Ulip may have additional functions during apoptosis and oxidative stress

The possible involvement of Ulip in oxidative stress in unknown and therefore the translocation into the nucleus is intriguing. These findings indicate that Ulip may exert additional functions to the ones known in neuritic outgrowth and axonal guidance (Minturn et al., 1995b). It's known that Ulip 1-4, all members of the Ulip family, are expressed as differentially phosphorylated forms and are differentially regulated during development and neuronal differentiation, and that they differ in their tissue specificity (Byk et al., 1998). However, it is not clear whether phosphorylation plays an important role in response to oxidative stress and whether this regulates their nuclear translocation.

A recent study provides evidence linking induction of axon guidance molecules with repulsive cues to the early stages of neuronal apoptosis caused by dopamine (Shirvan et al., 1999). It was shown that mRNA expression of collapsin-1 and of Ulip-2 is induced during neuronal apoptosis and that this induction precedes the time point of commitment of neurones to the death process. It was further indicated that these proteins are not only induced but may have an active role in determining the fate of neurones that are exposed to an oxidative stress-inducing apoptotic trigger. Antibodies directed against a collapsin-derived peptide were capable of conferring protection against the oxidative stress-inducing agent

dopamine. Thus the up-regulation of Ulip-2 during the early stages of dopamine-induced neuronal apoptosis (Shirvan et al., 1999), may be related to the nuclear translocation of Ulip that we observed after three hours of oxidative stress. This may be a major step in the signalling cascade of apoptosis and oxidative stress, in analogy to our observations on GAPDH.

Although caution should be practised when evaluating the relevance of our cellular observations to neurodegenerative disease, it is tempting to speculate that in pathological apoptotic cell death, Ulip together with GAPDH affects the faith of the cell. In support of this view is the recent finding that Ulip2 protein plays a role in the formation of neurofibrillary tangles in Alzheimer's disease (Yoshida et al., 1998).

# 5.5 <u>Enolase γ</u>

## a) Enolase does not show any major translocation after induction of apoptosis or oxidative stress

Enolase and enolase-GFP do not show great changes in their predominantly cytoplasmic expression after induction of oxidative stress. However, although cytoplasmic enolase-GFP was dominant, an increase of nuclear enolase-GFP levels was observed. This may indicate that if enolase is up-regulated and at the same time the cell is stressed, some enolase can translocate into the nucleus.

This can be interesting in context with the hypoxia studies discussed above, showing that enolase together with GAPDH and Hsc70 are up-regulated in hypoxic cells (Graven and Farber, 1998). Both enzymes are so called hypoxia-associated proteins (HAPs), which are distinct from the classical stress proteins induced by heat shock (HSPs) or glucose deprivation. While GAPDH expression during hypoxia is regulated primarily at the level of transcription, the mechanism of enolase mRNA accumulation remains unclear. Enolase is up-regulated by transition metals and desferoxamine and is not inhibited by carbon monoxide. In accordance with our results, subcellular fractionation of hypoxic cells has showed that GAPDH and enolase are up-regulated in the cytoplasmic fraction, whereas only GAPDH is also up-regulated in the nuclear fraction (Graven and Farber, 1998).

Further α-enolase has a close relationship with tau-Crystallin (Wistow et al., 1988). Tau-Crystallin is a major component of the cellular lenses of species throughout vertebrate evolution. Tau-Crystallin is a multi-functional protein and possesses enolase activity, but the activity is greatly reduced, probably because of age-related posttranslational modification. Apparently, in the lens enolase is not recruited for its catalytic activity but for some distinct structural property. This shows that tau-Crystallin/α-enolase is a multi-functional protein.

Like tau-Crystallin, enolase is up-regulated and exerts an important role in differentiation (Deloulme et al., 1996). It was demonstrated that enolase γ is expressed in oligodendroglial cells only at a certain stage of differentiation. The level of γ, but not α, mRNA increased when precursor cells differentiated into oligodendrocytes. So, γ-enolase gene expression is associated with the differentiation of the oligodendrocytes and is repressed in mature cells.

# 5.6 <u>Conclusion: Co-operation of the proteins associated to the PMO complex</u>

**<u>a) All PMO proteins except GAPDH are localised in the cytoplasm of transfected and untransfected control cells</u>**

Since GAPDH, Hsc70, enolase, aldolase and Ulip were previously immuno-precipitated together in a PMO complex (Bulliard et al., 1997), it made sense to investigate whether a functional co-operation between these proteins occurs. Under unstressed conditions, in R6 and $R6^{Bcl-2}$ fibroblasts, and – except for GAPDH - also in NB41A3 neuroblastomas, all endogenous proteins were expressed predominantly in the cytoplasm. However, their cytoplasmic patterns were quite different and there was no clear colocalisation between the proteins. This can be explained if one considers that not all of GAPDH, Hsc70, aldolase C, enolase γ and Ulip is associated with the PMO complex, and that the remaining proteins have also alternate roles with no relation to the PMO complex. Furthermore it is possible that the PMO proteins form a tight complex only in the plasma membrane and disperse when they leave it.

In unstressed cells overexpressing the PMO proteins, the subcellular localisation did not change, except for GAPDH. Overexpression of GAPDH *per se* induced nuclear translocation. All other overexpressed proteins remained in the cytoplasm of transfected control cells.

**<u>b) When overexpressed, all proteins display increased nuclear expression after oxidative stress</u>**

After exposure to $H_2O_2$ nuclear translocation of the endogenous protein is observed for GAPDH, Hsc70, Ulip and aldolase, but not for enolase. This translocation was most pronounced in GAPDH and Hsc70. Furthermore nuclear translocation of endogenous aldolase and Hsc70 was much less significant in non-neuronal R6 cells compared to NB41A3 cells. Aggregation of proteins into speckles was observed in untransfected cells after oxidative stress with endogenous GAPDH, aldolase and Hsc70.

When the proteins are overexpressed, all five components of the PMO complex have increased expression levels in the nucleus after oxidative stress induced by $H_2O_2$. Nuclear translocation is highest in GAPDH-GFP and Hsc70-GFP transfected cells and least in enolase-GFP transfected cells. Except enolase-GFP all transfected proteins show formation of speckles filled with the respective protein (in 5-10% of oxidatively stressed cells).

These observations suggest that co-operation of the proteins may not be operative in resting cells, but is induced after oxidative stress.

**c) Pronounced nuclear translocation is only observed with GAPDH, whereas all tested proteins showed expression in speckles and in long processes**

After induction of apoptosis, the effects of GAPDH, Hsc70 and aldolase is quite different. The response of GAPDH is dramatic, showing nuclear translocation leading to apoptotic cells, whereas differential translocation of Hsc70 is less pronounced and aldolase is relatively unchanged.

Therefore, in contrast to oxidative stress, induction of apoptosis does not reveal a common action of the proteins. This may indicate that the complex falls apart during apoptosis, liberating the individual proteins.

**d) GAPDH-GFP expression is influenced by the overexpression of other proteins**

In respect to its important function during apoptosis it is interesting to note that GAPDH-GFP expression is affected by expression of any of the co-transfected PMO proteins. Co-expression with enolase-BFP or Ulip-BFP enhanced formation of speckles where GAPDH-GFP accumulated after oxidative stress. This increase of speckles formation after oxidative stress was also observed for Hsc70-GFP when co-transfected with enolase-BFP and for Ulip-GFP when co-transfected with either enolase-BFP, Hsc70-BFP or GAPDH-BFP.

We cannot exclude that this phenomenon is an unspecific aggregation of highly overexpressed proteins, but some of our observations indicate that this is not the case. First, we never observed this formation of speckles in unstressed cells, but only in stressed cells. Second, GFP alone and also enolase-GFP or enolase-BFP, under all tested conditions never showed formation of speckles. Furthermore, co-overexpression of BFP with any PMO protein did not influence expression or speckles formation of the PMO protein.

## e) GAPDH and Hsc70 seem to have an antagonistic interaction

Nuclear localisation of GAPDH-GFP was also affected in co-transfections. Ulip-BFP decreased cytoplasmic translocation of GAPDH-GFP after exposure to FeCN. Since Ulip-BFP itself normally increases nuclear expression after oxidative stress induced by FeCN, an interaction with GAPDH-GFP retaining it partially in the nucleus can be hypothesised.

Furthermore, overexpression of aldolase and of Hsc70 both lead to an increased expression of GAPDH-GFP in the cytoplasm, both before and after oxidative stress. Nuclear translocation of Hsc70 is increased after oxidative stress when it is overexpressed together with GAPDH. This observation could indicate that overexpressed GAPDH is normally translocated into the nucleus after exposure to $H_2O_2$, but that this effect can be counteracted by Hsc70, which also shows increased nuclear translocation after oxidative stress in double transfectants. Thus, Hsc70 may protect cells by partially preventing nuclear translocation of GAPDH.

This antagonistic interaction between Hsc70 and GAPDH is especially interesting, because both of them are considered to play important roles in cell viability. The effects of other components of the PMO complex overexpressed in stable cell lines on endogenous GAPDH and Hsc70 are also very interesting, mainly in the case of cells permanently transfected by aldolase-GFP. While GAPDH showed less nuclear localisation than control cells and was partially retained in the cytoplasm, nuclear translocation of Hsc70 after oxidative stress was slightly increased.

Although we do not yet know how the proteins associated to the PMO complex exactly co-operate with each other, our results indicate that co-operation and interaction between these proteins changes after oxidative stress, and probably somehow regulate the antagonistic roles of GAPDH and Hsc70.

# 6 <u>References</u>

1. Abate, C., L. Patel, F. J. d. Rauscher, and T. Curran. 1990. Redox regulation of fos and jun DNA-binding activity *in vitro*.
 *Science*. 249:1157-61.

2. Adams, J. M., and S. Cory. 1998. The Bcl-2 protein family: arbiters of cell survival.
 *Science*. 281:1322-6.

3. Adcock, I. M., C. R. Brown, O. Kwon, and P. J. Barnes. 1994. Oxidative stress induces NF kappa B DNA binding and inducible NOS mRNA in human epithelial cells.
 *Biochem Biophys Res Commun*. 199:1518-24.

4. Ahn, A. H., S. Dziennis, R. Hawkes, and K. Herrup. 1994. The cloning of zebrin II reveals its identity with aldolase C.
 *Development*. 120:2081-90.

5. Albin, R. L., and D. A. Tagle. 1995. Genetics and molecular biology of Huntington's disease.
 *Trends Neurosci*. 18:11-4.

6. Allen, J. B., M. W. Walberg, M. C. Edwards, and S. J. Elledge. 1995. Finding prospective partners in the library: the two-hybrid system and phage display find a match.
 *Trends Biochem Sci*. 20:511-6.

7. Allen, R. T., M. W. Cluck, and D. K. Agrawal. 1998. Mechanisms controlling cellular suicide: role of Bcl-2 and caspases.
 *Cell Mol Life Sci*. 54:427-45.

8. Allen, R. W., K. A. Trach, and J. A. Hoch. 1987. Identification of the 37-kDa protein displaying a variable interaction with the erythroid cell membrane as glyceraldehyde-3-phosphate dehydrogenase.
 *J Biol Chem*. 262:649-53.

9. Allsopp, T. E., S. Kiselev, S. Wyatt, and A. M. Davies. 1995. Role of Bcl-2 in the brain-derived neurotrophic factor survival response.
 *Eur J Neurosci*. 7:1266-72.

10. Allsopp, T. E., S. Wyatt, H. F. Paterson, and A. M. Davies. 1993. The proto-oncogene bcl-2 can selectively rescue neurotrophic factor-dependent neurons from apoptosis.
 *Cell*. 73:295-307.

11. Ambrose, C. M., M. P. Duyao, G. Barnes, G. P. Bates, C. S. Lin, J. Srinidhi, S. Baxendale, H. Hummerich, H. Lehrach, and M. Altherr. 1994. Structure and expression of the Huntington's disease gene: evidence against simple inactivation due to an expanded CAG repeat.
 *Somat Cell Mol Genet*. 20:27-38.

12. Ames, B. N., M. K. Shigenaga, and T. M. Hagen. 1993. Oxidants, antioxidants, and the degenerative diseases of aging.
 *Proc Natl Acad Sci U S A*. 90:7915-22.

13. Ames, B. N., M. K. Shigenaga, and T. M. Hagen. 1995. Mitochondrial decay in aging.
 *Biochim Biophys Acta*. 1271:165-70.

14. Ankarcrona, M., J. M. Dypbukt, S. Orrenius, and P. Nicotera. 1996. Calcineurin and mitochondrial function in glutamate-induced neuronal cell death.
 *FEBS Lett*. 394:321-4.

15. Antoine, J. C., L. Absi, J. Honnorat, J. M. Boulesteix, T. de Brouker, C. Vial, M. Butler, P. De Camilli, and D. Michel. 1999. Antiamphiphysin antibodies are associated with various paraneoplastic neurological syndromes and tumors.
 *Arch Neurol*. 56:172-7.

16. Arai, Y., S. Kajihara, J. Masuda, S. Ohishi, K. Zen, J. Ogata, and T. Mukai. 1994. Position-independent, high-level, and correct regional expression of the rat aldolase C gene in the central nervous system of transgenic mice.
*Eur J Biochem*. 221:253-60.

17. Arenaz, P., and M. A. Sirover. 1983. Isolation and characterization of monoclonal antibodies directed against the DNA repair enzyme uracil DNA glycosylase from human placenta.
*Proc Natl Acad Sci U S A*. 80:5822-6.

18. Arnold, H., and D. Pette. 1970. Binding of aldolase and triosephosphate dehydrogenase to F-actin and modification of catalytic properties of aldolase.
*Eur J Biochem*. 15:360-6.

19. Ashkenazi, A., and V. M. Dixit. 1998. Death receptors: signaling and modulation.
*Science*. 281:1305-8.

20. Ashmarina, L. I., S. E. Louzenko, S. E. Severin, Jr., V. I. Muronetz, and N. K. Nagradova. 1988. Phosphorylation of D-glyceraldehyde-3-phosphate dehydrogenase by Ca2+/calmodulin-dependent protein kinase II.
*FEBS Lett*. 231:413-6.

21. Augusti-Tocco, G., and G. Sato. 1969. Establishment of functional clonal lines of neurons from mouse neuroblastoma.
*Proc Natl Acad Sci U S A*. 64:311-5.

22. Baeuerle, P. A. 1991. The inducible transcription activator NF-kappa B: regulation by distinct protein subunits.
*Biochim Biophys Acta*. 1072:63-80.

23. Baeuerle, P. A., and D. Baltimore. 1988. I kappa B: a specific inhibitor of the NF-kappa B transcription factor.
*Science*. 242:540-6.

24. Baeuerle, P. A., and D. Baltimore. 1996. NF-kappa B: ten years after.
*Cell*. 87:13-20.

25. Baichwal, V. R., and P. A. Baeuerle. 1997. Activate NF-kappa B or die?
*Curr Biol*. 7:R94-6.

26. Bajetta, E., L. Ferrari, A. Martinetti, L. Celio, G. Procopio, S. Artale, N. Zilembo, M. Di Bartolomeo, E. Seregni, and E. Bombardieri. 1999. Chromogranin A, neuron specific enolase, carcinoembryonic antigen, and hydroxyindole acetic acid evaluation in patients with neuroendocrine tumors.
*Cancer*. 86:858-65.

27. Bakhshi, A., J. P. Jensen, P. Goldman, J. J. Wright, O. W. McBride, A. L. Epstein, and S. J. Korsmeyer. 1985. Cloning the chromosomal breakpoint of t(14;18) human lymphomas: clustering around JH on chromosome 14 and near a transcriptional unit on 18.
*Cell*. 41:899-906.

28. Balaban, N., and R. Goldman. 1990. The association of glycosomal enzymes and microtubules: a physiological phenomenon or an experimental artifact?
*Exp Cell Res*. 191:219-26.

29. Balaban, N., H. K. Waithaka, A. R. Njogu, and R. Goldman. 1995. Intracellular antigens (microtubule-associated protein copurified with glycosomal enzymes)--possible vaccines against trypanosomiasis.
*J Infect Dis*. 172:845-50.

30. Barbe, M. F., M. Tytell, D. J. Gower, and W. J. Welch. 1988. Hyperthermia protects against light damage in the rat retina.
*Science*. 241:1817-20.

31. Baril, E., P. Bonin, D. Burstein, K. Mara, and P. Zamecnik. 1983. Resolution of the diadenosine 5',5'''-P1,P4-tetraphosphate binding subunit from a multiprotein form of HeLa cell DNA polymerase alpha.
*Proc Natl Acad Sci U S A*. 80:4931-5.

32. Barr, R., B. A. Branstetter, A. Rajnicek, F. L. Crane, and H. Low. 1991. Chloroquine-sensitive transplasmalemma electron transport in Tetrahymena pyriformis: a hypothesis for control of parasite protozoa through transmembrane redox.
*Biochim Biophys Acta*. 1058:261-8.

33. Barr, R., M. Floreani, J. Weiss, and F. L. Crane. 1988. The effect of platelet activating factor on electron transport of spinach chloroplasts.
*Biochem Biophys Res Commun*. 155:576-82.

34. Barraclough, R., and R. J. Ellis. 1980. Protein synthesis in chloroplasts. IX. Assembly of newly-synthesized large subunits into ribulose bisphosphate carboxylase in isolated intact pea chloroplasts.
*Biochim Biophys Acta*. 608:19-31.

35. Bartel, P., C. T. Chien, R. Sternglanz, and S. Fields. 1993. Elimination of false positives that arise in using the two-hybrid system.
*Biotechniques*. 14:920-4.

36. Bartholmes, P., and R. Jaenicke. 1978. Reassociation and reactivation of yeast glyceraldehyde-3-phosphate dehydrogenase after dissociation in the presence of ATP.
*Eur J Biochem*. 87:563-7.

37. Batistatou, A., D. E. Merry, S. J. Korsmeyer, and L. A. Greene. 1993. Bcl-2 affects survival but not neuronal differentiation of PC12 cells.
*J Neurosci*. 13:4422-8.

38. Baxi, M. D., and J. K. Vishwanatha. 1995. Uracil DNA-glycosylase/glyceraldehyde-3-phosphate dehydrogenase is an Ap4A binding protein.
*Biochemistry*. 34:9700-7.

39. Beckman, J. S., and J. P. Crow. 1993. Pathological implications of nitric oxide, superoxide and peroxynitrite formation.
*Biochem Soc Trans*. 21:330-4.

40. Beckmann, R. P., L. E. Mizzen, and W. J. Welch. 1990. Interaction of Hsp 70 with newly synthesized proteins: implications for protein folding and assembly.
*Science*. 248:850-4.

41. Beg, A. A., T. S. Finco, P. V. Nantermet, and A. S. Baldwin, Jr. 1993. Tumor necrosis factor and interleukin-1 lead to phosphorylation and loss of I kappa B alpha: a mechanism for NF-kappa B activation.
*Mol Cell Biol*. 13:3301-10.

42. Bellmann, K., M. Jaattela, D. Wissing, V. Burkart, and H. Kolb. 1996. Heat shock protein hsp70 overexpression confers resistance against nitric oxide.
*FEBS Lett*. 391:185-8.

43. Benzi, G., and A. Moretti. 1995. Are reactive oxygen species involved in Alzheimer's disease?
*Neurobiol Aging*. 16:661-74.

44. Bertrand, R., E. Solary, P. O'Connor, K. W. Kohn, and Y. Pommier. 1994. Induction of a common pathway of apoptosis by staurosporine.
*Exp Cell Res*. 211:314-21.

45. Bimston, D., J. Song, D. Winchester, S. Takayama, J. C. Reed, and R. I. Morimoto. 1998. BAG-1, a negative regulator of Hsp70 chaperone activity, uncouples nucleotide hydrolysis from substrate release.
*Embo J*. 17:6871-8.

46. Boggs, S. E., T. S. McCormick, and E. G. Lapetina. 1998. Glutathione levels determine apoptosis in macrophages.
*Biochem Biophys Res Commun*. 247:229-33.

47. Boise, L. H., M. Gonzalez-Garcia, C. E. Postema, L. Ding, T. Lindsten, L. A. Turka, X. Mao, G. Nunez, and C. B. Thompson. 1993. bcl-x, a bcl-2-related gene that functions as a dominant regulator of apoptotic cell death.
*Cell*. 74:597-608.

48. Borner, C. 1996. Diminished cell proliferation associated with the death-protective activity of Bcl-2.
*J Biol Chem*. 271:12695-8.

49. Brent, R., and M. Ptashne. 1985. A bacterial repressor protein or a yeast transcriptional terminator can block upstream activation of a yeast gene.
*Nature*. 314:198.

50. Brent, R., and M. Ptashne. 1985. A eukaryotic transcriptional activator bearing the DNA specificity of a prokaryotic repressor.
*Cell*. 43:729-36.

51. Brightman, A. O., J. Wang, R. K. Miu, I. L. Sun, R. Barr, F. L. Crane, and D. J. Morre. 1992. A growth factor- and hormone-stimulated NADH oxidase from rat liver plasma membrane.
*Biochim Biophys Acta*. 1105:109-17.

52. Brune, B., and E. G. Lapetina. 1995. Glyceraldehyde-3-phosphate dehydrogenase: a target for nitric oxide signaling.
*Adv Pharmacol*. 34:351-60.

53. Brune, B., and E. G. Lapetina. 1995. Protein thiol modification of glyceraldehyde-3-phosphate dehydrogenase as a target for nitric oxide signaling.
*Genet Eng (N Y)*. 17:149-64.

54. Brune, B., and E. G. Lapetina. 1996. Nitric oxide-induced covalent modification of glycolytic enzyme glyceraldehyde-3-phosphate dehydrogenase.
*Methods Enzymol*. 269:400-7.

55. Bulliard, C., R. Zurbriggen, J. Tornare, M. Faty, Z. Dastoor, and J. L. Dreyer. 1997. Purification of a dichlorophenol-indophenol oxidoreductase from rat and bovine synaptic membranes: tight complex association of a glyceraldehyde-3-phosphate dehydrogenase isoform, TOAD64, enolase-gamma and aldolase C.
*Biochem J*. 324:555-63.

56. Buono, P., L. de Conciliis, E. Olivetta, P. Izzo, and F. Salvatore. 1993. Cis-acting elements in the promoter region of the human aldolase C gene.
*FEBS Lett*. 328:243-9.

57. Burke, J. R., J. J. Enghild, M. E. Martin, Y. S. Jou, R. M. Myers, A. D. Roses, J. M. Vance, and W. J. Strittmatter. 1996. Huntingtin and DRPLA proteins selectively interact with the enzyme GAPDH.
*Nat Med*. 2:347-50.

58. Buttner, T., B. Lack, M. Jager, W. Wunsche, W. Kuhn, T. Muller, H. Przuntek, and T. Postert. 1999. Serum levels of neuron-specific enolase and S-100 protein after single tonic-clonic seizures.
*J Neurol*. 246:459-61.

59. Byk, T., T. Dobransky, C. Cifuentes-Diaz, and A. Sobel. 1996. Identification and molecular characterization of Unc-33-like phosphoprotein (Ulip), a putative mammalian homolog of the axonal guidance-associated unc-33 gene product.
*J Neurosci*. 16:688-701.

60. Byk, T., S. Ozon, and A. Sobel. 1998. The Ulip family phosphoproteins--common and specific properties.
*Eur J Biochem*. 254:14-24.

61. Cannon, S., P. Wang, and H. Roy. 1986. Inhibition of ribulose bisphosphate carboxylase assembly by antibody to a binding protein.
*J Cell Biol*. 103:1327-35.

62. Caprioli, J., S. Kitano, and J. E. Morgan. 1996. Hyperthermia and hypoxia increase tolerance of retinal ganglion cells to anoxia and excitotoxicity.
*Invest Ophthalmol Vis Sci*. 37:2376-81.

63. Castagne, V., and P. G. Clarke. 1998. Cooperation between glutathione depletion and protein synthesis inhibition against naturally occurring neuronal death.
*Neuroscience*. 86:895-902.

64. Castagne, V., M. Gautschi, K. Lefevre, A. Posada, and P. G. Clarke. 1999. Relationships between neuronal death and the cellular redox status. Focus on the developing nervous system [In Process Citation].
*Prog Neurobiol*. 59:397-423.

65. Caswell, A. H., and A. M. Corbett. 1985. Interaction of glyceraldehyde-3-phosphate dehydrogenase with isolated microsomal subfractions of skeletal muscle.
*J Biol Chem*. 260:6892-8.

66. Cerutti, P. A. 1985. Prooxidant states and tumor promotion.
*Science*. 227:375-81.

67. Chao, D. T., and S. J. Korsmeyer. 1998. Bcl-2 family: regulators of cell death.
*Annu Rev Immunol*. 16:395-419.

68. Checler, F. 1995. Processing of the beta-amyloid precursor protein and its regulation in Alzheimer's disease.
*J Neurochem*. 65:1431-44.

69. Chirico, W. J., M. G. Waters, and G. Blobel. 1988. 70K heat shock related proteins stimulate protein translocation into microsomes.
 *Nature*. 332:805-10.

70. Chittenden, T., E. A. Harrington, R. O'Connor, C. Flemington, R. J. Lutz, G. I. Evan, and B. C. Guild. 1995. Induction of apoptosis by the Bcl-2 homologue Bak.
 *Nature*. 374:733-6.

71. Chong, K. Y., C. C. Lai, S. Lille, C. Chang, and C. Y. Su. 1998. Stable overexpression of the constitutive form of heat shock protein 70 confers oxidative protection.
 *J Mol Cell Cardiol*. 30:599-608.

72. Cohen, G. M. 1997. Caspases: the executioners of apoptosis.
 *Biochem J*. 326:1-16.

73. Constantinides, S. M., and W. C. Deal, Jr. 1969. Reversible dissociation of tetrameric rabbit muscle glyceraldehyde-3-phosphate dehydrogenase into dimers or monomers by adenosine triphosphate.
 *J Biol Chem*. 244:5695-702.

74. Cool, B. L., and M. A. Sirover. 1989. Immunocytochemical localization of the base excision repair enzyme uracil DNA glycosylase in quiescent and proliferating normal human cells.
 *Cancer Res*. 49:3029-36.

75. Cooper, A. J., K. F. Sheu, J. R. Burke, W. J. Strittmatter, and J. P. Blass. 1998. Glyceraldehyde-3-phosphate dehydrogenase abnormality in metabolically stressed Huntington disease fibroblasts.
 *Dev Neurosci*. 20:462-8.

76. Cooper, A. J. L., K. R. Sheu, J. R. Burke, O. Onodera, W. J. Strittmatter, A. D. Roses, and J. P. Blass. 1997. Transglutaminase-catalyzed inactivation of glyceraldehyde-3-phosphate dehydrogenase and alpha-ketoglutarate dehydrogenase complex by polyglutamine domains of pathological length.
 *Proceedings Of The National Academy Of Sciences Of The United States Of America*. 94:12604-9.

77. Coppo, A., A. Manzi, J. F. Pulitzer, and H. Takahashi. 1973. Abortive bacteriophage T4 head assembly in mutants of Escherichia coli.
 *J Mol Biol*. 76:61-87.

78. Correale, J., A. L. Rabinowicz, C. N. Heck, T. D. Smith, W. J. Loskota, and C. M. DeGiorgio. 1998. Status epilepticus increases CSF levels of neuron-specific enolase and alters the blood-brain barrier.
 *Neurology*. 50:1388-91.

79. Coyle, J. T., and P. Puttfarcken. 1993. Oxidative stress, glutamate, and neurodegenerative disorders.
 *Science*. 262:689-95.

80. Crane, F. L. 1989b. Comments on the discovery of coenzyme Q: a commentary on 'Isolation of a Quinone from Beef Heart Mitochondria'.
 *Biochim Biophys Acta*. 1000:358-61.

81. Crane, F. L., Y. Hatefi, R. L. Lester, and C. Widmer. 1989a. Isolation of a quinone from beef heart mitochondria. 1957.
 *Biochim Biophys Acta*. 1000:362-3.

82. Crane, F. L., and P. Navas. 1997. The diversity of coenzyme Q function.
 *Mol Aspects Med*. 18 Suppl:S1-6.

83. Crane, F. L., I. L. Sun, R. Barr, and H. Low. 1991. Electron and proton transport across the plasma membrane.
 *J Bioenerg Biomembr*. 23:773-803.

84. Crane, F. L., I. L. Sun, R. A. Crowe, F. J. Alcain, and H. Low. 1994. Coenzyme Q10, plasma membrane oxidase and growth control.
 *Mol Aspects Med*. 15 Suppl:s1-11.

85. Creagh, E. M., and T. G. Cotter. 1999. Selective protection by hsp 70 against cytotoxic drug-, but not Fas- induced T-cell apoptosis.
 *Immunology*. 97:36-44.

86. Cudkowicz, M., and N. W. Kowall. 1990. Degeneration of pyramidal projection neurons in Huntington's disease cortex.
 *Ann Neurol*. 27:200-4.

87. Davidoff, A. N., and B. V. Mendelow. 1993. C-myc expression is down-regulated in mafosfamide-treated HL-60 cells undergoing apoptosis.
*Anticancer Res.* 13:1167-70.

88. Davies, S. W., M. Turmaine, B. A. Cozens, M. DiFiglia, A. H. Sharp, C. A. Ross, E. Scherzinger, E. E. Wanker, L. Mangiarini, and G. P. Bates. 1997. Formation of neuronal intranuclear inclusions underlies the neurological dysfunction in mice transgenic for the HD mutation.
*Cell.* 90:537-48.

89. De, B. P., S. Gupta, H. Zhao, J. A. Drazba, and A. K. Banerjee. 1996. Specific interaction *in vitro* and *in vivo* of glyceraldehyde-3-phosphate dehydrogenase and LA protein with cis-acting RNAs of human parainfluenza virus type 3.
*J Biol Chem.* 271:24728-35.

90. de la Monte, S. M., J. P. Vonsattel, and E. P. Richardson, Jr. 1988. Morphometric demonstration of atrophic changes in the cerebral cortex, white matter, and neostriatum in Huntington's disease.
*J Neuropathol Exp Neurol.* 47:516-25.

91. de la Rosa, E. J., E. Vega-Nunez, A. V. Morales, J. Serna, E. Rubio, and F. de Pablo. 1998. Modulation of the chaperone heat shock cognate 70 by embryonic (pro)insulin correlates with prevention of apoptosis.
*Proc Natl Acad Sci U S A.* 95:9950-5.

92. DeGiorgio, C. M., C. N. Heck, A. L. Rabinowicz, P. S. Gott, T. Smith, and J. Correale. 1999. Serum neuron-specific enolase in the major subtypes of status epilepticus.
*Neurology.* 52:746-9.

93. Deloulme, J. C., M. Lucas, C. Gaber, P. Bouillon, A. Keller, F. Eclancher, and M. Sensenbrenner. 1996. Expression of the neuron-specific enolase gene by rat oligodendroglial cells during their differentiation.
*J Neurochem.* 66:936-45.

94. Demple, B., and C. F. Amabile-Cuevas. 1991. Redox redux: the control of oxidative stress responses.
*Cell.* 67:837-9.

95. Desai, C., G. Garriga, S. L. McIntire, and H. R. Horvitz. 1988. A genetic pathway for the development of the Caenorhabditis elegans HSN motor neurons.
*Nature.* 336:638-46.

96. Deshaies, R. J., B. D. Koch, M. Werner-Washburne, E. A. Craig, and R. Schekman. 1988. A subfamily of stress proteins facilitates translocation of secretory and mitochondrial precursor polypeptides.
*Nature.* 332:800-5.

97. DiFiglia, M., E. Sapp, K. O. Chase, S. W. Davies, G. P. Bates, J. P. Vonsattel, and N. Aronin. 1997. Aggregation of huntingtin in neuronal intranuclear inclusions and dystrophic neurites in brain.
*Science.* 277:1990-3.

98. Dimmeler, S., and B. Brune. 1992. Characterization of a nitric-oxide-catalysed ADP-ribosylation of glyceraldehyde-3-phosphate dehydrogenase.
*Eur J Biochem.* 210:305-10.

99. Dimmeler, S., and B. Brune. 1993. Nitric oxide preferentially stimulates auto-ADP-ribosylation of glyceraldehyde-3-phosphate dehydrogenase compared to alcohol or lactate dehydrogenase.
*FEBS Lett.* 315:21-4.

100. Dimmeler, S., F. Lottspeich, and B. Brune. 1992. Nitric oxide causes ADP-ribosylation and inhibition of glyceraldehyde-3-phosphate dehydrogenase.
*J Biol Chem.* 267:16771-4.

101. Dingwall, C. 1991. Transport across the nuclear envelope: enigmas and explanations.
*Bioessays.* 13:213-8.

102. Dingwall, C., and R. A. Laskey. 1991. Nuclear targeting sequences--a consensus?
*Trends Biochem Sci.* 16:478-81.

103. Dreyer, J. L. 1990. Plasma membrane dehydrogenases in rat brain synaptic membranes. Multiplicity and subunit composition.
*J Bioenerg Biomembr.* 22:619-33.

104. Duclos-Vallee, J. C., F. Capel, H. Mabit, and M. A. Petit. 1998. Phosphorylation of the hepatitis B virus core protein by glyceraldehyde- 3-phosphate dehydrogenase protein kinase activity.
*J Gen Virol.* 79:1665-70.

105. Dugan, L. L., S. L. Sensi, L. M. Canzoniero, S. D. Handran, S. M. Rothman, T. S. Lin, M. P. Goldberg, and D. W. Choi. 1995. Mitochondrial production of reactive oxygen species in cortical neurons following exposure to N-methyl-D-aspartate.
*J Neurosci*. 15:6377-88.

106. Durrieu, C., F. Bernier-Valentin, and B. Rousset. 1987. Binding of glyceraldehyde-3-phosphate dehydrogenase to microtubules.
*Mol Cell Biochem*. 74:55-65.

107. Durrieu, C., F. Bernier-Valentin, and B. Rousset. 1987. Microtubules bind glyceraldehyde-3-phosphate dehydrogenase and modulate its enzyme activity and quaternary structure.
*Arch Biochem Biophys*. 252:32-40.

108. Duyao, M., C. Ambrose, R. Myers, A. Novelletto, F. Persichetti, M. Frontali, S. Folstein, C. Ross, M. Franz, and M. Abbott. 1993. Trinucleotide repeat length instability and age of onset in Huntington's disease.
*Nat Genet*. 4:387-92.

109. Eby, D., and M. E. Kirtley. 1983. Role of lysine residues in the binding of glyceraldehyde-3-phosphate dehydrogenase to human erythrocyte membranes.
*Biochem Biophys Res Commun*. 116:423-7.

110. Edgecombe, M., A. G. McLennan, and M. J. Fisher. 1996. Characterization of the binding of diadenosine 5',5'''-P1,P4-tetraphosphate (Ap4A) to rat liver cell membranes.
*Biochem J*. 314:687-93.

111. Ellis, J. 1987. Proteins as molecular chaperones.
*Nature*. 328:378-9.

112. Engel, M., M. Seifert, B. Theisinger, U. Seyfert, and C. Welter. 1998. Glyceraldehyde-3-phosphate dehydrogenase and Nm23-H1/nucleoside diphosphate kinase A. Two old enzymes combine for the novel Nm23 protein phosphotransferase function.
*J Biol Chem*. 273:20058-65.

113. Epner, D. E., and D. S. Coffey. 1996. There are multiple forms of glyceraldehyde-3-phosphate dehydrogenase in prostate cancer cells and normal prostate tissue.
*Prostate*. 28:372-8.

114. Epner, D. E., A. W. Partin, J. A. Schalken, J. T. Isaacs, and D. S. Coffey. 1993. Association of glyceraldehyde-3-phosphate dehydrogenase expression with cell motility and metastatic potential of rat prostatic adenocarcinoma.
*Cancer Res*. 53:1995-7.

115. Epner, D. E., A. Sawa, and J. T. Isaacs. 1999. Glyceraldehyde-3-phosphate dehydrogenase expression during apoptosis and proliferation of rat ventral prostate.
*Biol Reprod*. 61:687-91.

116. Ercolani, L., D. Brown, A. Stuart-Tilley, and S. L. Alper. 1992. Colocalization of GAPDH and band 3 (AE1) proteins in rat erythrocytes and kidney intercalated cell membranes.
*Am J Physiol*. 262:F892-6.

117. Estevez, A. G., R. Radi, L. Barbeito, J. T. Shin, J. A. Thompson, and J. S. Beckman. 1995. Peroxynitrite-induced cytotoxicity in PC12 cells: evidence for an apoptotic mechanism differentially modulated by neurotrophic factors.
*J Neurochem*. 65:1543-50.

118. Evers, S., D. W. Droste, P. Ludemann, and C. Oberwittler. 1998. Early elevation of cerebrospinal fluid neuron-specific enolase in Creutzfeldt-Jakob disease.
*J Neurol*. 245:52-3.

119. Farrow, S. N., J. H. White, I. Martinou, T. Raven, K. T. Pun, C. J. Grinham, J. C. Martinou, and R. Brown. 1995. Cloning of a bcl-2 homologue by interaction with adenovirus E1B 19K.
*Nature*. 374:731-3.

120. Fields, S., and R. Sternglanz. 1994. The two-hybrid system: an assay for protein-protein interactions.
*Trends Genet*. 10:286-92.

121. Flynn, G. C., J. Pohl, M. T. Flocco, and J. E. Rothman. 1991. Peptide-binding specificity of the molecular chaperone BiP.
*Nature*. 353:726-30.

122. Froissard, P., H. Monrocq, and D. Duval. 1997. Role of glutathione metabolism in the glutamate-induced programmed cell death of neuronal-like PC12 cells.
*Eur J Pharmacol*. 326:93-9.

123. Frydman, J., and J. Hohfeld. 1997. Chaperones get in touch: the Hip-Hop connection.
*Trends Biochem Sci*. 22:87-92.

124. Gaetano, C., T. Matsuo, and C. J. Thiele. 1997. Identification and characterization of a retinoic acid-regulated human homologue of the unc-33-like phosphoprotein gene (hUlip) from neuroblastoma cells.
*J Biol Chem*. 272:12195-201.

125. Galli, F., S. Rovidati, L. Ghibelli, and F. Canestrari. 1998. S-nitrosylation of glyceraldehyde-3-phosphate dehydrogenase decreases the enzyme affinity to the erythrocyte membrane.
*Nitric Oxide*. 2:17-27.

126. Garcia, I., I. Martinou, Y. Tsujimoto, and J. C. Martinou. 1992. Prevention of programmed cell death of sympathetic neurons by the bcl-2 proto-oncogene.
*Science*. 258:302-4.

127. Gasmi, L., A. G. McLennan, and S. W. Edwards. 1996. The diadenosine polyphosphates Ap3A and Ap4A and adenosine triphosphate interact with granulocyte-macrophage colony-stimulating factor to delay neutrophil apoptosis: implications for neutrophil: platelet interactions during inflammation.
*Blood*. 87:3442-9.

128. Gasmi, L., A. G. McLennan, and S. W. Edwards. 1996. Neutrophil apoptosis is delayed by the diadenosine polyphosphates, Ap5A and Ap6A: synergism with granulocyte-macrophage colony-stimulating factor.
*Br J Haematol*. 95:637-9.

129. Gautron, S., P. Maire, V. Hakim, and A. Kahn. 1991. Regulation of the multiple promoters of the human aldolase A gene: response of its two ubiquitous promoters to agents promoting cell proliferation.
*Nucleic Acids Res*. 19:767-74.

130. Gebhardt, B. R., J. Ries, W. F. Caspary, H. Boehles, and J. Stein. 1999. Superoxide: a major factor for stress protein induction in reoxygenation injury in the intestinal cell line Caco-2.
*Digestion*. 60:238-45.

131. Georgopoulos, C. P., R. W. Hendrix, S. R. Casjens, and A. D. Kaiser. 1973. Host participation in bacteriophage lambda head assembly.
*J Mol Biol*. 76:45-60.

132. Geschwind, D. H., G. M. Kelly, H. Fryer, H. Feeser-Bhatt, and S. Hockfield. 1996. Identification and characterization of novel developmentally regulated proteins in rat spinal cord.
*Brain Res Dev Brain Res*. 97:62-75.

133. Gething, M. J., and J. Sambrook. 1992. Protein folding in the cell.
*Nature*. 355:33-45.

134. Glaser, P. E., and R. W. Gross. 1995. Rapid plasmenylethanolamine-selective fusion of membrane bilayers catalyzed by an isoform of glyceraldehyde-3-phosphate dehydrogenase: discrimination between glycolytic and fusogenic roles of individual isoforms.
*Biochemistry*. 34:12193-203.

135. Goloubinoff, P., A. A. Gatenby, and G. H. Lorimer. 1989. GroE heat-shock proteins promote assembly of foreign prokaryotic ribulose bisphosphate carboxylase oligomers in Escherichia coli.
*Nature*. 337:44-7.

136. Goshima, Y., F. Nakamura, P. Strittmatter, and S. M. Strittmatter. 1995. Collapsin-induced growth cone collapse mediated by an intracellular protein related to UNC-33.
*Nature*. 376:509-14.

137. Grant, C. M., K. A. Quinn, and I. W. Dawes. 1999. Differential protein S-thiolation of glyceraldehyde-3-phosphate dehydrogenase isoenzymes influences sensitivity to oxidative stress.
*Mol Cell Biol*. 19:2650-6.

138. Graveland, G. A., R. S. Williams, and M. DiFiglia. 1985. Evidence for degenerative and regenerative changes in neostriatal spiny neurons in Huntington's disease.
*Science*. 227:770-3.

139. Graven, K. K., and H. W. Farber. 1995. Hypoxia-associated proteins.
*New Horiz*. 3:208-18.

140. Graven, K. K., and H. W. Farber. 1998. Endothelial cell hypoxic stress proteins.
*J Lab Clin Med*. 132:456-63.

141. Graven, K. K., R. J. McDonald, and H. W. Farber. 1998. Hypoxic regulation of endothelial glyceraldehyde-3-phosphate dehydrogenase.
*Am J Physiol*. 274:C347-55.

142. Graven, K. K., R. F. Troxler, H. Kornfeld, M. V. Panchenko, and H. W. Farber. 1994. Regulation of endothelial cell glyceraldehyde-3-phosphate dehydrogenase expression by hypoxia.
*J Biol Chem*. 269:24446-53.

143. Green, D. R. 1998. Apoptotic pathways: the roads to ruin.
*Cell*. 94:695-8.

144. Green, D. R., and J. C. Reed. 1998. Mitochondria and apoptosis.
*Science*. 281:1309-12.

145. Greenlund, L. J., S. J. Korsmeyer, and E. M. Johnson, Jr. 1995. Role of Bcl-2 in the survival and function of developing and mature sympathetic neurons.
*Neuron*. 15:649-61.

146. Gregori, C., F. Ginot, J. F. Decaux, A. Weber, T. Berbar, A. Kahn, and A. L. Pichard. 1991. Expression of the rat aldolase B gene: a liver-specific proximal promoter and an intronic activator.
*Biochem Biophys Res Commun*. 176:722-9.

147. Gross, A., J. M. McDonnell, and S. J. Korsmeyer. 1999. Bcl-2 family members and the mitochondria in apoptosis.
*Genes Dev*. 13:1899-911.

148. Grosse, F., H. P. Nasheuer, S. Scholtissek, and U. Schomburg. 1986. Lactate dehydrogenase and glyceraldehyde-phosphate dehydrogenase are single-stranded DNA-binding proteins that affect the DNA-polymerase- alpha-primase complex.
*Eur J Biochem*. 160:459-67.

149. Group, H. D. 1993. A novel gene containing a trinucleotide repeat that is expanded and unstable on Huntington's disease chromosomes. The Huntington's Disease Collaborative Research Group.
*Cell*. 72:971-83.

150. Guerrini, L., F. Blasi, and S. Denis-Donini. 1995. Synaptic activation of NF-kappa B by glutamate in cerebellar granule neurons *in vitro*.
*Proc Natl Acad Sci U S A*. 92:9077-81.

151. Gupta, S., R. Hollenstein, S. Kochhar, and P. Christen. 1993. Paracatalytic self-inactivation of fructose-1,6-bisphosphate aldolase. Structure of the crosslink formed at the active site.
*Eur J Biochem*. 214:515-9.

152. Gusella, J. F., and M. E. MacDonald. 1996. Trinucleotide instability: a repeating theme in human inherited disorders.
*Annu Rev Med*. 47:201-9.

153. Haas, I. G., and M. Wabl. 1983. Immunoglobulin heavy chain binding protein.
*Nature*. 306:387-9.

154. Hamajima, N., K. Matsuda, S. Sakata, N. Tamaki, M. Sasaki, and M. Nonaka. 1996. A novel gene family defined by human dihydropyrimidinase and three related proteins with differential tissue distribution.
*Gene*. 180:157-63.

155. Hamm-Kunzelmann, B., D. Schafer, C. Weigert, and K. Brand. 1997. Redox-regulated expression of glycolytic enzymes in resting and proliferating rat thymocytes.
*FEBS Lett*. 403:87-90.

156. Han, X., S. Ramanadham, J. Turk, and R. W. Gross. 1998. Reconstitution of membrane fusion between pancreatic islet secretory granules and plasma membranes: catalysis by a protein constituent recognized by monoclonal antibodies directed against glyceraldehyde-3-phosphate dehydrogenase.
*Biochim Biophys Acta*. 1414:95-107.

157. Hartl, F. U. 1996. Molecular chaperones in cellular protein folding.
*Nature*. 381:571-9.

158. Hawkes, R., S. Blyth, V. Chockkan, D. Tano, Z. Ji, and C. Mascher. 1993. Structural and molecular compartmentation in the cerebellum.
*Can J Neurol Sci*. 20 Suppl 3:S29-35.

159. Hawkes, R., and C. Gravel. 1991. The modular cerebellum.
*Prog Neurobiol*. 36:309-27.

160. Hawkes, R., and K. Herrup. 1995. Aldolase C/zebrin II and the regionalization of the cerebellum.
*J Mol Neurosci*. 6:147-58.

161. Hayashi, K., M. Motoi, S. Nose, Y. Horie, T. Akagi, K. Ogawa, K. Taguchi, K. Mizobuchi, and A. Nishimoto. 1987. An immunohistochemical study on the distribution of glial fibrillary acidic protein, S-100 protein, neuron-specific enolase, and neurofilament in medulloblastomas.
*Acta Pathol Jpn*. 37:85-96.

162. Heiskanen, K. M., M. B. Bhat, H. W. Wang, J. Ma, and A. L. Nieminen. 1999. Mitochondrial depolarization accompanies cytochrome c release during apoptosis in PC6 cells.
*J Biol Chem*. 274:5654-8.

163. Hemmingsen, S. M., C. Woolford, S. M. van der Vies, K. Tilly, D. T. Dennis, C. P. Georgopoulos, R. W. Hendrix, and R. J. Ellis. 1988. Homologous plant and bacterial proteins chaperone oligomeric protein assembly.
*Nature*. 333:330-4.

164. Hendrick, J. P., and F. U. Hartl. 1993. Molecular chaperone functions of heat-shock proteins.
*Annu Rev Biochem*. 62:349-84.

165. Hengartner, M. O., and H. R. Horvitz. 1994. C. elegans cell survival gene ced-9 encodes a functional homolog of the mammalian proto-oncogene bcl-2.
*Cell*. 76:665-76.

166. Herrup, K., and B. Kuemerle. 1997. The compartmentalization of the cerebellum.
*Annu Rev Neurosci*. 20:61-90.

167. Hessler, R. J., R. A. Blackwood, T. G. Brock, J. W. Francis, D. M. Harsh, and J. E. Smolen. 1998. Identification of glyceraldehyde-3-phosphate dehydrogenase as a $Ca^{2+}$- dependent fusogen in human neutrophil cytosol.
*J Leukoc Biol*. 63:331-6.

168. Hibbs, J. B., Jr., R. R. Taintor, and Z. Vavrin. 1987. Macrophage cytotoxicity: role for L-arginine deiminase and imino nitrogen oxidation to nitrite.
*Science*. 235:473-6.

169. Hightower, L. E. 1980. Cultured animal cells exposed to amino acid analogues or puromycin rapidly synthesize several polypeptides.
*J Cell Physiol*. 102:407-27.

170. Hofmann, K. 1999. The modular nature of apoptotic signaling proteins.
*Cell Mol Life Sci*. 55:1113-28.

171. Hohfeld, J. 1998. Regulation of the heat shock conjugate Hsc70 in the mammalian cell: the characterization of the anti-apoptotic protein BAG-1 provides novel insights.
*Biol Chem*. 379:269-74.

172. Hohfeld, J., and S. Jentsch. 1997. GrpE-like regulation of the hsc70 chaperone by the anti-apoptotic protein BAG-1.
*Embo J*. 16:6209-16.

173. Hohfeld, J., Y. Minami, and F. U. Hartl. 1995. Hip, a novel cochaperone involved in the eukaryotic Hsc70/Hsp40 reaction cycle.
*Cell*. 83:589-98.

174. Hope, I. A., and K. Struhl. 1986. Functional dissection of a eukaryotic transcriptional activator protein, GCN4 of yeast.
*Cell*. 46:885-94.

175. Hughes, P. E., T. Alexi, and S. S. Schreiber. 1997. A role for the tumour suppressor gene p53 in regulating neuronal apoptosis.
*Neuroreport*. 8:v-xii.

176. Huitorel, P., and D. Pantaloni. 1985. Bundling of microtubules by glyceraldehyde-3-phosphate dehydrogenase and its modulation by ATP.
*Eur J Biochem*. 150:265-9.

177. Ishitani, R., and D. M. Chuang. 1996a. Glyceraldehyde-3-phosphate dehydrogenase antisense oligodeoxynucleotides protect against cytosine arabinonucleoside-induced apoptosis in cultured cerebellar neurons.
*Proc Natl Acad Sci U S A*. 93:9937-41.

178. Ishitani, R., M. Kimura, K. Sunaga, N. Katsube, M. Tanaka, and D. M. Chuang. 1996c. An antisense oligodeoxynucleotide to glyceraldehyde-3-phosphate dehydrogenase blocks age-induced apoptosis of mature cerebrocortical neurons in culture.
*J Pharmacol Exp Ther*. 278:447-54.

179. Ishitani, R., K. Sunaga, A. Hirano, P. Saunders, N. Katsube, and D. M. Chuang. 1996b. Evidence that glyceraldehyde-3-phosphate dehydrogenase is involved in age-induced apoptosis in mature cerebellar neurons in culture.
*J Neurochem*. 66:928-35.

180. Ishitani, R., K. Sunaga, M. Tanaka, H. Aishita, and D. M. Chuang. 1997. Overexpression of glyceraldehyde-3-phosphate dehydrogenase is involved in low $K^+$-induced apoptosis but not necrosis of cultured cerebellar granule cells.
*Mol Pharmacol*. 51:542-50.

181. Ishitani, R., M. Tanaka, K. Sunaga, N. Katsube, and D. M. Chuang. 1998. Nuclear localization of overexpressed glyceraldehyde-3-phosphate dehydrogenase in cultured cerebellar neurons undergoing apoptosis.
*Mol Pharmacol*. 53:701-7.

182. Ito, Y., P. J. Pagano, K. Tornheim, P. Brecher, and R. A. Cohen. 1996. Oxidative stress increases glyceraldehyde-3-phosphate dehydrogenase mRNA levels in isolated rabbit aorta.
*Am J Physiol*. 270:H81-7.

183. Itoh, Y., S. Takahashi, T. Haneishi, and M. Arai. 1980. Structure of heptelidic acid, a new sesquiterpene antibiotic from fungi.
*J Antibiot (Tokyo)*. 33:525-6.

184. Izzo, P., P. Costanzo, A. Lupo, E. Rippa, G. Paolella, and F. Salvatore. 1988. Human aldolase A gene. Structural organization and tissue-specific expression by multiple promoters and alternate mRNA processing.
*Eur J Biochem*. 174:569-78.

185. Jans, D. A. 1994. Nuclear signaling pathways for polypeptide ligands and their membrane receptors?
*Faseb J*. 8:841-7.

186. Joh, K., Y. Arai, T. Mukai, and K. Hori. 1986. Expression of three mRNA species from a single rat aldolase A gene, differing in their 5' non-coding regions.
*J Mol Biol*. 190:401-10.

187. Kaltschmidt, B., M. Uherek, B. Volk, P. A. Baeuerle, and C. Kaltschmidt. 1997. Transcription factor NF-kappaB is activated in primary neurons by amyloid beta peptides and in neurons surrounding early plaques from patients with Alzheimer disease.
*Proc Natl Acad Sci U S A*. 94:2642-7.

188. Kaltschmidt, B., M. Uherek, H. Wellmann, B. Volk, and C. Kaltschmidt. 1999. Inhibition of NF-kappaB potentiates amyloid beta-mediated neuronal apoptosis.
*Proc Natl Acad Sci U S A*. 96:9409-14.

189. Kaltschmidt, C., B. Kaltschmidt, and P. A. Baeuerle. 1993. Brain synapses contain inducible forms of the transcription factor NF- kappa B.
*Mech Dev*. 43:135-47.

190. Kaltschmidt, C., B. Kaltschmidt, and P. A. Baeuerle. 1995. Stimulation of ionotropic glutamate receptors activates transcription factor NF-kappa B in primary neurons.
*Proc Natl Acad Sci U S A*. 92:9618-22.

191. Kaltschmidt, C., B. Kaltschmidt, H. Neumann, H. Wekerle, and P. A. Baeuerle. 1994. Constitutive NF-kappa B activity in neurons.
*Mol Cell Biol*. 14:3981-92.

192. Kamata, T., I. O. Daar, M. Subleski, T. Copeland, H. F. Kung, and R. H. Xu. 1998. Xenopus CRMP-2 is an early response gene to neural induction.
 *Brain Res Mol Brain Res*. 57:201-10.

193. Kamata, T., M. Subleski, Y. Hara, N. Yuhki, H. Kung, N. G. Copeland, N. A. Jenkins, T. Yoshimura, W. Modi, and T. D. Copeland. 1998. Isolation and characterization of a bovine neural specific protein (CRMP-2) cDNA homologous to unc-33, a C. elegans gene implicated in axonal outgrowth and guidance.
 *Brain Res Mol Brain Res*. 54:219-36.

194. Kaneda, M., K. Takeuchi, K. Inoue, and M. Umeda. 1997. Localization of the phosphatidylserine-binding site of glyceraldehyde-3-phosphate dehydrogenase responsible for membrane fusion.
 *J Biochem (Tokyo)*. 122:1233-40.

195. Kao, A. W., Y. Noda, J. H. Johnson, J. E. Pessin, and A. R. Saltiel. 1999. Aldolase mediates the association of F-actin with the insulin- responsive glucose transporter GLUT4.
 *J Biol Chem*. 274:17742-7.

196. Karpel, R. L., and A. C. Burchard. 1981. A basic isozyme of yeast glyceraldehyde-3-phosphate dehydrogenase with nucleic acid helix-destabilizing activity.
 *Biochim Biophys Acta*. 654:256-67.

197. Katsube, N., K. Sunaga, H. Aishita, D. M. Chuang, and R. Ishitani. 1999. ONO-1603, a potential antidementia drug, delays age-induced apoptosis and suppresses overexpression of glyceraldehyde-3-phosphate dehydrogenase in cultured central nervous system neurons.
 *J Pharmacol Exp Ther*. 288:6-13.

198. Kawamoto, R. M., and A. H. Caswell. 1986. Autophosphorylation of glyceraldehydephosphate dehydrogenase and phosphorylation of protein from skeletal muscle microsomes.
 *Biochemistry*. 25:657-61.

199. Keegan, L., G. Gill, and M. Ptashne. 1986. Separation of DNA binding from the transcription-activating function of a eukaryotic regulatory protein.
 *Science*. 231:699-704.

200. Kester, M. V., T. L. Phillips, and R. W. Gracy. 1977. Changes in glycolytic enzyme levels and isozyme expression in human lymphocytes during blast transformation.
 *Arch Biochem Biophys*. 183:700-9.

201. Kiefer, M. C., M. J. Brauer, V. C. Powers, J. J. Wu, S. R. Umansky, L. D. Tomei, and P. J. Barr. 1995. Modulation of apoptosis by the widely distributed Bcl-2 homologue Bak.
 *Nature*. 374:736-9.

202. Kim, Y. M., M. E. de Vera, S. C. Watkins, and T. R. Billiar. 1997. Nitric oxide protects cultured rat hepatocytes from tumor necrosis factor-alpha-induced apoptosis by inducing heat shock protein 70 expression.
 *J Biol Chem*. 272:1402-11.

203. Kish, S. J., I. Lopes-Cendes, M. Guttman, Y. Furukawa, M. Pandolfo, G. A. Rouleau, B. M. Ross, M. Nance, L. Schut, L. Ang, and L. DiStefano. 1998. Brain glyceraldehyde-3-phosphate dehydrogenase activity in human trinucleotide repeat disorders.
 *Archives Of Neurology*. 55:1299-304.

204. Kishi, T., D. M. Morre, and D. J. Morre. 1999. The plasma membrane NADH oxidase of HeLa cells has hydroquinone oxidase activity.
 *Biochim Biophys Acta*. 1412:66-77.

205. Kivela, T. 1986. Neuron-specific enolase in retinoblastoma. An immunohistochemical study.
 *Acta Ophthalmol (Copenh)*. 64:19-25.

206. Kliman, H. J., and T. L. Steck. 1980. Association of glyceraldehyde-3-phosphate dehydrogenase with the human red cell membrane. A kinetic analysis.
 *J Biol Chem*. 255:6314-21.

207. Koshy, B., T. Matilla, E. N. Burright, D. E. Merry, K. H. Fischbeck, H. T. Orr, and H. Y. Zoghbi. 1996. Spinocerebellar ataxia type-1 and spinobulbar muscular atrophy gene products interact with glyceraldehyde-3-phosphate dehydrogenase.
 *Hum Mol Genet*. 5:1311-8.

208. Kroemer, G., N. Zamzami, and S. A. Susin. 1997. Mitochondrial control of apoptosis.
 *Immunol Today*. 18:44-51.

209. Kropp, S., I. Zerr, W. J. Schulz-Schaeffer, C. Riedemann, M. Bodemer, C. Laske, H. A. Kretzschmar, and S. Poser. 1999. Increase of neuron-specific enolase in patients with Creutzfeldt-Jakob disease. *Neurosci Lett*. 261:124-6.

210. Kumagai, H., and H. Sakai. 1983. A porcine brain protein (35 K protein) which bundles microtubules and its identification as glyceraldehyde 3-phosphate dehydrogenase. *J Biochem (Tokyo)*. 93:1259-69.

211. Lamian, V., G. M. Small, and C. M. Feldherr. 1996. Evidence for the existence of a novel mechanism for the nuclear import of Hsc70. *Exp Cell Res*. 228:84-91.

212. Langer, T., C. Lu, H. Echols, J. Flanagan, M. K. Hayer, and F. U. Hartl. 1992. Successive action of DnaK, DnaJ and GroEL along the pathway of chaperone-mediated protein folding. *Nature*. 356:683-9.

213. Laskey, R. A., B. M. Honda, A. D. Mills, and J. T. Finch. 1978. Nucleosomes are assembled by an acidic protein which binds histones and transfers them to DNA. *Nature*. 275:416-20.

214. Launay, J. F., A. Jellali, and M. T. Vanier. 1989. Glyceraldehyde-3-phosphate dehydrogenase is a microtubule binding protein in a human colon tumor cell line. *Biochim Biophys Acta*. 996:103-9.

215. Lebo, R. V., D. R. Tolan, B. D. Bruce, M. C. Cheung, and Y. W. Kan. 1985. Spot-blot analysis of sorted chromosomes assigns a fructose intolerance disease locus to chromosome 9. *Cytometry*. 6:478-83.

216. Lee, K. A., and M. A. Sirover. 1989. Physical association of base excision repair enzymes with parental and replicating DNA in BHK-21 cells. *Cancer Res*. 49:3037-44.

217. Lee, Y. J., and P. M. Corry. 1998. Metabolic oxidative stress-induced HSP70 gene expression is mediated through SAPK pathway. Role of Bcl-2 and c-Jun NH2-terminal kinase. *J Biol Chem*. 273:29857-63.

218. Li, A., W. S. Lane, L. V. Johnson, G. J. Chader, and J. Tombran-Tink. 1995. Neuron-specific enolase: a neuronal survival factor in the retinal extracellular matrix? *J Neurosci*. 15:385-93.

219. Li, H., H. Zhu, C. J. Xu, and J. Yuan. 1998. Cleavage of BID by caspase 8 mediates the mitochondrial damage in the Fas pathway of apoptosis. *Cell*. 94:491-501.

220. Li, W., R. K. Herman, and J. E. Shaw. 1992. Analysis of the Caenorhabditis elegans axonal guidance and outgrowth gene unc-33. *Genetics*. 132:675-89.

221. Lin, K. I., S. H. Lee, R. Narayanan, J. M. Baraban, J. M. Hardwick, and R. R. Ratan. 1995. Thiol agents and Bcl-2 identify an alphavirus-induced apoptotic pathway that requires activation of the transcription factor NF-kappa B. *J Cell Biol*. 131:1149-61.

222. Lin, T., and R. W. Allen. 1986. Isolation and characterization of a 37,000-dalton protein associated with the erythrocyte membrane. *J Biol Chem*. 261:4594-9.

223. Lind, C., R. Gerdes, I. Schuppe-Koistinen, and I. A. Cotgreave. 1998. Studies on the mechanism of oxidative modification of human glyceraldehyde-3-phosphate dehydrogenase by glutathione: catalysis by glutaredoxin. *Biochem Biophys Res Commun*. 247:481-6.

224. Loo, D. T., A. Copani, C. J. Pike, E. R. Whittemore, A. J. Walencewicz, and C. W. Cotman. 1993. Apoptosis is induced by beta-amyloid in cultured central nervous system neurons. *Proc Natl Acad Sci U S A*. 90:7951-5.

225. Luban, J., and S. P. Goff. 1995. The yeast two-hybrid system for studying protein-protein interactions. *Curr Opin Biotechnol*. 6:59-64.

226. Luo, X., I. Budihardjo, H. Zou, C. Slaughter, and X. Wang. 1998. Bid, a Bcl2 interacting protein, mediates cytochrome c release from mitochondria in response to activation of cell surface death receptors.
*Cell*. 94:481-90.

227. Ma, J., and M. Ptashne. 1987. The carboxy-terminal 30 amino acids of GAL4 are recognized by GAL80.
*Cell*. 50:137-42.

228. Ma, J., and M. Ptashne. 1987. Deletion analysis of GAL4 defines two transcriptional activating segments.
*Cell*. 48:847-53.

229. Ma, J., and M. Ptashne. 1987. A new class of yeast transcriptional activators.
*Cell*. 51:113-9.

230. Ma, J., and M. Ptashne. 1988. Converting a eukaryotic transcriptional inhibitor into an activator.
*Cell*. 55:443-6.

231. Macho, A., T. Hirsch, I. Marzo, P. Marchetti, B. Dallaporta, S. A. Susin, N. Zamzami, and G. Kroemer. 1997. Glutathione depletion is an early and calcium elevation is a late event of thymocyte apoptosis.
*J Immunol*. 158:4612-9.

232. Maine, A. B., and E. Ciejek-Baez. 1991. Distinct developmental regulatory mechanisms for two members of the aldolase gene family.
*Dev Genet*. 12:431-6.

233. Maire, P., S. Gautron, V. Hakim, C. Gregori, F. Mennecier, and A. Kahn. 1987. Characterization of three optional promoters in the 5' region of the human aldolase A gene.
*J Mol Biol*. 197:425-38.

234. Makeh, I., M. Thomas, J. P. Hardelin, P. Briand, A. Kahn, and H. Skala. 1994. Analysis of a brain-specific isozyme. Expression and chromatin structure of the rat aldolase C gene and transgenes.
*J Biol Chem*. 269:4194-200.

235. Mallozzi, C., A. M. Di Stasi, and M. Minetti. 1995. Free radicals induce reversible membrane-cytoplasm translocation of glyceraldehyde-3-phosphate dehydrogenase in human erythrocytes.
*Arch Biochem Biophys*. 321:345-52.

236. Mangiarini, L., K. Sathasivam, M. Seller, B. Cozens, A. Harper, C. Hetherington, M. Lawton, Y. Trottier, H. Lehrach, S. W. Davies, and G. P. Bates. 1996. Exon 1 of the HD gene with an expanded CAG repeat is sufficient to cause a progressive neurological phenotype in transgenic mice.
*Cell*. 87:493-506.

237. Marangos, P. J., and D. E. Schmechel. 1987. Neuron specific enolase, a clinically useful marker for neurons and neuroendocrine cells.
*Annu Rev Neurosci*. 10:269-95.

238. Marchetti, P., T. Hirsch, N. Zamzami, M. Castedo, D. Decaudin, S. A. Susin, B. Masse, and G. Kroemer. 1996. Mitochondrial permeability transition triggers lymphocyte apoptosis.
*J Immunol*. 157:4830-6.

239. Mariethoz, E., M. R. Jacquier-Sarlin, G. Multhoff, A. M. Healy, F. Tacchini-Cottier, and B. S. Polla. 1997. Heat shock and proinflammatory stressors induce differential localization of heat shock proteins in human monocytes.
*Inflammation*. 21:629-42.

240. Marletta, M. A. 1993. Nitric oxide synthase structure and mechanism.
*J Biol Chem*. 268:12231-4.

241. Martinou, J. C., M. Dubois-Dauphin, J. K. Staple, I. Rodriguez, H. Frankowski, M. Missotten, P. Albertini, D. Talabot, S. Catsicas, and C. Pietra. 1994. Overexpression of Bcl-2 in transgenic mice protects neurons from naturally occurring cell death and experimental ischemia.
*Neuron*. 13:1017-30.

242. Marzo, I., C. Brenner, N. Zamzami, J. M. Jurgensmeier, S. A. Susin, H. L. Vieira, M. C. Prevost, Z. Xie, S. Matsuyama, J. C. Reed, and G. Kroemer. 1998. Bax and adenine nucleotide translocator cooperate in the mitochondrial control of apoptosis.
*Science*. 281:2027-31.

243. Mathur, R. L., M. C. Reddy, S. Yee, R. Imbesi, B. Groth-Vasselli, and P. N. Farnsworth. 1992. Investigation of lens glycolytic enzymes: species distribution and interaction with supramolecular order.
*Exp Eye Res*. 54:253-60.

244. Matthews, R. T., R. J. Ferrante, B. G. Jenkins, S. E. Browne, K. Goetz, S. Berger, I. Y. Chen, and M. F. Beal. 1997. Iodoacetate produces striatal excitotoxic lesions.
 *J Neurochem*. 69:285-9.

245. Mattson, M. P. 1996. Calcium and Free Radicals: Mediators of neurotrophic factor and excitatory transmitter-regulated developmental plasticity and cell death.
 *Perspect Dev Neurobiol*. 3:79-91.

246. May, J. M. 1999. Is ascorbic acid an antioxidant for the plasma membrane?
 *Faseb J*. 13:995-1006.

247. Mazurek, S., F. Hugo, K. Failing, and E. Eigenbrodt. 1996. Studies on associations of glycolytic and glutaminolytic enzymes in MCF- 7 cells: role of P36.
 *J Cell Physiol*. 167:238-50.

248. McCarty, J. S., A. Buchberger, J. Reinstein, and B. Bukau. 1995. The role of ATP in the functional cycle of the DnaK chaperone system.
 *J Mol Biol*. 249:126-37.

249. McDonald, L. J., and J. Moss. 1993. Stimulation by nitric oxide of an NAD linkage to glyceraldehyde-3- phosphate dehydrogenase.
 *Proc Natl Acad Sci U S A*. 90:6238-41.

250. McDonald, L. J., and J. Moss. 1994. Nitric oxide and NAD-dependent protein modification.
 *Mol Cell Biochem*. 138:201-6.

251. McDonnell, T. J., N. Deane, F. M. Platt, G. Nunez, U. Jaeger, J. P. McKearn, and S. J. Korsmeyer. 1989. bcl-2-immunoglobulin transgenic mice demonstrate extended B cell survival and follicular lymphoproliferation.
 *Cell*. 57:79-88.

252. McDonnell, T. J., G. Nunez, F. M. Platt, D. Hockenberry, L. London, J. P. McKearn, and S. J. Korsmeyer. 1990. Deregulated Bcl-2-immunoglobulin transgene expands a resting but responsive immunoglobulin M and D-expressing B-cell population.
 *Mol Cell Biol*. 10:1901-7.

253. McIntire, S. L., G. Garriga, J. White, D. Jacobson, and H. R. Horvitz. 1992. Genes necessary for directed axonal elongation or fasciculation in C. elegans.
 *Neuron*. 8:307-22.

254. McMullin, T. W., and R. L. Hallberg. 1988. A highly evolutionarily conserved mitochondrial protein is structurally related to the protein encoded by the Escherichia coli groEL gene.
 *Mol Cell Biol*. 8:371-80.

255. McNabb, D. S., and L. Guarente. 1996. Genetic and biochemical probes for protein-protein interactions.
 *Curr Opin Biotechnol*. 7:554-9.

256. McNulty, S. E., and W. A. Toscano, Jr. 1995. Transcriptional regulation of glyceraldehyde-3-phosphate dehydrogenase by 2,3,7,8-tetrachlorodibenzo-p-dioxin.
 *Biochem Biophys Res Commun*. 212:165-71.

257. Medina, M. A., A. del Castillo-Olivares, and I. Nunez de Castro. 1997. Multifunctional plasma membrane redox systems.
 *Bioessays*. 19:977-84.

258. Mejean, C., F. Pons, Y. Benyamin, and C. Roustan. 1989. Antigenic probes locate binding sites for the glycolytic enzymes glyceraldehyde-3-phosphate dehydrogenase, aldolase and phosphofructokinase on the actin monomer in microfilaments.
 *Biochem J*. 264:671-7.

259. Melero, J. A., M. L. Salas, and J. Salas. 1975. Deoxyribonucleic acid-binding proteins in virus-transformed cell lines.
 *J Biol Chem*. 250:3683-9.

260. Mendelsohn, A. R., and R. Brent. 1994. Applications of interaction traps/two-hybrid systems to biotechnology research.
 *Curr Opin Biotechnol*. 5:482-6.

261. Meyer, M., R. Schreck, and P. A. Baeuerle. 1993. H2O2 and antioxidants have opposite effects on activation of NF-kappa B and AP-1 in intact cells: AP-1 as secondary antioxidant-responsive factor.
 *Embo J*. 12:2005-15.

262. Meyer-Siegler, K., D. J. Mauro, G. Seal, J. Wurzer, J. K. deRiel, and M. A. Sirover. 1991. A human nuclear uracil DNA glycosylase is the 37-kDa subunit of glyceraldehyde-3-phosphate dehydrogenase.
*Proc Natl Acad Sci U S A*. 88:8460-4.

263. Mezquita, J., M. Pau, and C. Mezquita. 1998. Several novel transcripts of glyceraldehyde-3-phosphate dehydrogenase expressed in adult chicken testis.
*J Cell Biochem*. 71:127-39.

264. Michaelidis, T. M., M. Sendtner, J. D. Cooper, M. S. Airaksinen, B. Holtmann, M. Meyer, and H. Thoenen. 1996. Inactivation of bcl-2 results in progressive degeneration of motoneurons, sympathetic and sensory neurons during early postnatal development.
*Neuron*. 17:75-89.

265. Minaschek, G., U. Groschel-Stewart, S. Blum, and J. Bereiter-Hahn. 1992. Microcompartmentation of glycolytic enzymes in cultured cells.
*Eur J Cell Biol*. 58:418-28.

266. Minturn, J. E., H. J. Fryer, D. H. Geschwind, and S. Hockfield. 1995b. TOAD-64, a gene expressed early in neuronal differentiation in the rat, is related to unc-33, a C. elegans gene involved in axon outgrowth.
*J Neurosci*. 15:6757-66.

267. Minturn, J. E., D. H. Geschwind, H. J. Fryer, and S. Hockfield. 1995a. Early postmitotic neurons transiently express TOAD-64, a neural specific protein.
*J Comp Neurol*. 355:369-79.

268. Mocali, A., R. Caldini, M. Chevanne, and F. Paoletti. 1995. Induction, effects, and quantification of sublethal oxidative stress by hydrogen peroxide on cultured human fibroblasts.
*Exp Cell Res*. 216:388-95.

269. Molina y Vedia, L., C. A. Ohmstede, and E. G. Lapetina. 1990. Properties of the exchange rate of guanine nucleotides to the novel rap- 2B protein.
*Biochem Biophys Res Commun*. 171:319-24.

270. Molnar, M. L., K. Stefansson, L. S. Marton, R. S. Tripathi, and G. K. Molnar. 1984. Immunohistochemistry of retinoblastomas in humans.
*Am J Ophthalmol*. 97:301-7.

271. Moncada, S., R. M. Palmer, and E. A. Higgs. 1991. Nitric oxide: physiology, pathophysiology, and pharmacology.
*Pharmacol Rev*. 43:109-42.

272. Morgenegg, G., G. C. Winkler, U. Hubscher, C. W. Heizmann, J. Mous, and C. C. Kuenzle. 1986. Glyceraldehyde-3-phosphate dehydrogenase is a nonhistone protein and a possible activator of transcription in neurons.
*J Neurochem*. 47:54-62.

273. Morton, D. J., F. M. Clarke, and C. J. Masters. 1977. An electron microscope study of the interaction between fructose diphosphate aldolase and actin-containing filaments.
*J Cell Biol*. 74:1016-23.

274. Mukai, T., K. Joh, Y. Arai, H. Yatsuki, and K. Hori. 1986. Tissue-specific expression of rat aldolase A mRNAs. Three molecular species differing only in the 5'-terminal sequences.
*J Biol Chem*. 261:3347-54.

275. Mukai, T., H. Yatsuki, S. Masuko, Y. Arai, K. Joh, and K. Hori. 1991. The structure of the brain-specific rat aldolase C gene and its regional expression.
*Biochem Biophys Res Commun*. 174:1035-42.

276. Muronetz, V. I., Z. X. Wang, T. J. Keith, H. R. Knull, and D. K. Srivastava. 1994. Binding constants and stoichiometries of glyceraldehyde 3-phosphate dehydrogenase-tubulin complexes.
*Arch Biochem Biophys*. 313:253-60.

277. Myers, R. H., J. P. Vonsattel, P. A. Paskevich, D. K. Kiely, T. J. Stevens, L. A. Cupples, E. P. Richardson, Jr., and E. D. Bird. 1991. Decreased neuronal and increased oligodendroglial densities in Huntington's disease caudate nucleus.
*J Neuropathol Exp Neurol*. 50:729-42.

278. Nagy, E., and W. F. Rigby. 1995. Glyceraldehyde-3-phosphate dehydrogenase selectively binds AU-rich RNA in the NAD(+)-binding region (Rossmann fold).
 *J Biol Chem*. 270:2755-63.

279. Nakamura, S., I. Tatuno, Y. Noguchi, M. Kitagawa, L. D. Kohn, Y. Saito, and A. Hirai. 1999. 73-kDa heat shock cognate protein interacts directly with P27Kip1, a cyclin-dependent kinase inhibitor, during G1/S transition.
 *Biochem Biophys Res Commun*. 257:340-3.

280. Nakayama, K., K. Nakayama, I. Negishi, K. Kuida, H. Sawa, and D. Y. Loh. 1994. Targeted disruption of Bcl-2 alpha beta in mice: occurrence of gray hair, polycystic kidney disease, and lymphocytopenia.
 *Proc Natl Acad Sci U S A*. 91:3700-4.

281. Nakayama, K., K. Nakayama, I. Negishi, K. Kuida, Y. Shinkai, M. C. Louie, L. E. Fields, P. J. Lucas, V. Stewart, and F. W. Alt. 1993. Disappearance of the lymphoid system in Bcl-2 homozygous mutant chimeric mice.
 *Science*. 261:1584-8.

282. Nakazawa, M., T. Uehara, and Y. Nomura. 1997. Koningic acid (a potent glyceraldehyde-3-phosphate dehydrogenase inhibitor)-induced fragmentation and condensation of DNA in NG108-15 cells.
 *J Neurochem*. 68:2493-9.

283. Nasir, J., Y. P. Goldberg, and M. R. Hayden. 1996. Huntington disease: new insights into the relationship between CAG expansion and disease.
 *Hum Mol Genet*. 5 Spec No:1431-5.

284. Nelson, S. K., G. H. Wong, and J. M. McCord. 1995. Leukemia inhibitory factor and tumor necrosis factor induce manganese superoxide dismutase and protect rabbit hearts from reperfusion injury.
 *J Mol Cell Cardiol*. 27:223-9.

285. Nguyen, T., D. Brunson, C. L. Crespi, B. W. Penman, J. S. Wishnok, and S. R. Tannenbaum. 1992. DNA damage and mutation in human cells exposed to nitric oxide *in vitro*.
 *Proc Natl Acad Sci U S A*. 89:3030-4.

286. Nomura, Y., T. Uehara, and M. Nakazawa. 1996. Neuronal apoptosis by glial NO: involvement of inhibition of glyceraldehyde-3-phosphate dehydrogenase.
 *Hum Cell*. 9:205-14.

287. O'Reilly, G., and F. Clarke. 1993. Identification of an actin binding region in aldolase.
 *FEBS Lett*. 321:69-72.

288. Oguchi, M., E. Gerth, B. Fitzgerald, and J. H. Park. 1973. Regulation of glyceraldehyde 3-phosphate dehydrogenase by phosphocreatine and adenosine triphosphate. IV. Factors affecting *in vivo* control of enzymatic activity.
 *J Biol Chem*. 248:5571-6.

289. Oh, Y. J., B. C. Swarzenski, and K. L. O'Malley. 1996. Overexpression of Bcl-2 in a murine dopaminergic neuronal cell line leads to neurite outgrowth.
 *Neurosci Lett*. 202:161-4.

290. Oltvai, Z. N., C. L. Milliman, and S. J. Korsmeyer. 1993. Bcl-2 heterodimerizes *in vivo* with a conserved homolog, Bax, that accelerates programmed cell death.
 *Cell*. 74:609-19.

291. Oppenheim, R. W. 1991. Cell death during development of the nervous system.
 *Annu Rev Neurosci*. 14:453-501.

292. Ostermann, J., A. L. Horwich, W. Neupert, and F. U. Hartl. 1989. Protein folding in mitochondria requires complex formation with hsp60 and ATP hydrolysis.
 *Nature*. 341:125-30.

293. Ovadi, M. Nuridsany, and T. Keleti. 1973. SH groups masked by subunit interaction in glyceraldehyde-3-phosphate dehydrogenase.
 *Biochim Biophys Acta*. 302:191-9.

294. Paulson, H. L., M. K. Perez, Y. Trottier, J. Q. Trojanowski, S. H. Subramony, S. S. Das, P. Vig, J. L. Mandel, K. H. Fischbeck, and R. N. Pittman. 1997. Intranuclear inclusions of expanded polyglutamine protein in spinocerebellar ataxia type 3.
 *Neuron*. 19:333-44.

295. Pelham, H. R. 1986. Speculations on the functions of the major heat shock and glucose-regulated proteins.

*Cell*. 46:959-61.

296. Perucho, M., J. Salas, and M. L. Salas. 1977. Identification of the mammalian DNA-binding protein P8 as glyceraldehyde-3-phosphate dehydrogenase.
*Eur J Biochem*. 81:557-62.

297. Piantadosi, C. A., and J. Zhang. 1996. Mitochondrial generation of reactive oxygen species after brain ischemia in the rat.
*Stroke*. 27:327-31; discussion 332.

298. Pinon, L. G., G. Middleton, and A. M. Davies. 1997. Bcl-2 is required for cranial sensory neuron survival at defined stages of embryonic development.
*Development*. 124:4173-8.

299. Pittman, R. N., J. C. Mills, A. J. DiBenedetto, W. P. Hynicka, and S. Wang. 1994. Neuronal cell death: searching for the smoking gun.
*Curr Opin Neurobiol*. 4:87-94.

300. Popovici, T., Y. Berwald-Netter, M. Vibert, A. Kahn, and H. Skala. 1990. Localization of aldolase C mRNA in brain cells.
*FEBS Lett*. 268:189-93.

301. Pourzand, C., G. Rossier, O. Reelfs, C. Borner, and R. M. Tyrrell. 1997. Overxpression of Bcl-2 inhibits UVA-mediated immediate apoptosiinrat 6 fibroblasts: evidence for the involvement of Bcl-2 as an antioxidant.
*Cancer Res*. 57:1405-11.

302. Puder, M., and R. J. Soberman. 1997. Glutathione conjugates recognize the Rossmann fold of glyceraldehyde-3-phosphate dehydrogenase.
*Journal Of Biological Chemistry*. 272:10936-40.

303. Quach, T. T., Y. Rong, M. F. Belin, A. M. Duchemin, H. Akaoka, S. Ding, M. Baudry, P. E. Kolattukudy, and J. Honnorat. 1997. Molecular cloning of a new unc-33-like cDNA from rat brain and its relation to paraneoplastic neurological syndromes.
*Brain Res Mol Brain Res*. 46:329-32.

304. Raff, M. 1998. Cell suicide for beginners.
*Nature*. 396:119-22.

305. Raff, M. C., B. A. Barres, J. F. Burne, H. S. Coles, Y. Ishizaki, and M. D. Jacobson. 1993. Programmed cell death and the control of cell survival: lessons from the nervous system.
*Science*. 262:695-700.

306. Rauchova, H., Z. Drahota, and G. Lenaz. 1995. Function of coenzyme Q in the cell: some biochemical and physiological properties.
*Physiol Res*. 44:209-16.

307. Reed, J. C. 1997. Bcl-2 family proteins and the hormonal control of cell life and death in normalcy and neoplasia.
*Vitam Horm*. 53:99-138.

308. Reed, J. C. 1997. Double identity for proteins of the Bcl-2 family.
*Nature*. 387:773-6.

309. Reed, J. C. 1998. Bcl-2 family proteins.
*Oncogene*. 17:3225-36.

310. Reed, J. C., J. M. Jurgensmeier, and S. Matsuyama. 1998. Bcl-2 family proteins and mitochondria.
*Biochim Biophys Acta*. 1366:127-37.

311. Reiss, N., J. Hermon, A. Oplatka, and Z. Naor. 1996. Interaction of purified protein kinase C with key proteins of energy metabolism and cellular motility.
*Biochem Mol Biol Int*. 38:711-9.

312. Reiss, N., H. Kanety, and J. Schlessinger. 1986. Five enzymes of the glycolytic pathway serve as substrates for purified epidermal-growth-factor-receptor kinase.
*Biochem J*. 239:691-7.

313. Reiss, N., A. Oplatka, J. Hermon, and Z. Naor. 1996. Phosphatidylserine directs differential phosphorylation of actin and glyceraldehyde-3-phosphate dehydrogenase by protein kinase C: possible implications for regulation of actin polymerization.
*Biochem Mol Biol Int*. 40:1191-200.

314. Reiss, N. A., and R. J. Schwartz. 1987. High performance purification of glycolytic enzymes and creatine kinase from chicken breast muscle and preparation of their specific immunological probes.
*Prep Biochem*. 17:157-72.

315. Ripple, M. O., and G. Wilding. 1995. Alteration of glyceraldehyde-3-phosphate dehydrogenase activity and messenger RNA content by androgen in human prostate carcinoma cells.
*Cancer Res*. 55:4234-6.

316. Robbins, A. R., R. D. Ward, and C. Oliver. 1995. A mutation in glyceraldehyde-3-phosphate dehydrogenase alters endocytosis in CHO cells.
*J Cell Biol*. 130:1093-104.

317. Ronai, Z. 1993. Glycolytic enzymes as DNA binding proteins.
*Int J Biochem*. 25:1073-6.

318. Rosse, T., R. Olivier, L. Monney, M. Rager, S. Conus, I. Fellay, B. Jansen, and C. Borner. 1998. Bcl-2 prolongs cell survival after Bax-induced release of cytochrome c.
*Nature*. 391:496-9.

319. Rothman, J. E. 1989. Polypeptide chain binding proteins: catalysts of protein folding and related processes in cells.
*Cell*. 59:591-601.

320. Royds, J. A., J. W. Ironside, S. O. Warnaar, C. B. Taylor, and W. R. Timperley. 1987. Monoclonal antibody to aldolase C: a selective marker for Purkinje cells in the human cerebellum.
*Neuropathol Appl Neurobiol*. 13:11-21.

321. Ryzlak, M. T., and R. Pietruszko. 1988. Heterogeneity of glyceraldehyde-3-phosphate dehydrogenase from human brain.
*Biochim Biophys Acta*. 954:309-24.

322. Sabourin, J. C., A. S. Kern, C. Gregori, A. Porteu, C. Cywiner, F. P. Chatelet, A. Kahn, and A. L. Pichard. 1996. An intronic enhancer essential for tissue-specific expression of the aldolase B transgenes.
*J Biol Chem*. 271:3469-73.

323. Sakimura, K., E. Kushiya, M. Obinata, S. Odani, and Y. Takahashi. 1985. Molecular cloning and the nucleotide sequence of cDNA for neuron- specific enolase messenger RNA of rat brain.
*Proc Natl Acad Sci U S A*. 82:7453-7.

324. Salminen, M., S. Lopez, P. Maire, A. Kahn, and D. Daegelen. 1996. Fast-muscle-specific DNA-protein interactions occurring *in vivo* at the human aldolase A M promoter are necessary for correct promoter activity in transgenic mice.
*Mol Cell Biol*. 16:76-85.

325. Salminen, M., P. Maire, J. P. Concordet, C. Moch, A. Porteu, A. Kahn, and D. Daegelen. 1994. Fast-muscle-specific expression of human aldolase A transgenes.
*Mol Cell Biol*. 14:6797-808.

326. Salvesen, G. S., and V. M. Dixit. 1997. Caspases: intracellular signaling by proteolysis.
*Cell*. 91:443-6.

327. Saunders, P. A., E. Chalecka-Franaszek, and D. M. Chuang. 1997. Subcellular distribution of glyceraldehyde-3-phosphate dehydrogenase in cerebellar granule cells undergoing cytosine arabinoside-induced apoptosis.
*J Neurochem*. 69:1820-8.

328. Saunders, P. A., R. W. Chen, and D. M. Chuang. 1999. Nuclear translocation of glyceraldehyde-3-phosphate dehydrogenase isoforms during neuronal apoptosis.
*J Neurochem*. 72:925-32.

329. Sawa, A., A. A. Khan, L. D. Hester, and S. H. Snyder. 1997. Glyceraldehyde-3-phosphate dehydrogenase: nuclear translocation participates in neuronal and nonneuronal cell death.
*Proc Natl Acad Sci U S A*. 94:11669-74.

330. Schafer, D., B. Hamm-Kunzelmann, and K. Brand. 1997. Glucose regulates the promoter activity of aldolase A and pyruvate kinase M2 via dephosphorylation of Sp1.
*FEBS Lett*. 417:325-8.

331. Schafer, D., B. Hamm-Kunzelmann, U. Hermfisse, and K. Brand. 1996. Differences in DNA-binding efficiency of Sp1 to aldolase and pyruvate kinase promoter correlate with altered redox states in resting and proliferating rat thymocytes.
*FEBS Lett*. 391:35-8.

332. Schapira, F., M. D. Reuber, and A. Hatzfeld. 1970. Resurgence of two fetal-types of aldolases (A and C) in some fast-growing hepatomas.
*Biochem Biophys Res Commun*. 40:321-7.

333. Schmechel, D. E., M. W. Brightman, and P. J. Marangos. 1980. Neurons switch from non-neuronal enolase to neuron-specific enolase during differentiation.
*Brain Res*. 190:195-214.

334. Schreck, R., B. Meier, D. N. Mannel, W. Droge, and P. A. Baeuerle. 1992. Dithiocarbamates as potent inhibitors of nuclear factor kappa B activation in intact cells.
*J Exp Med*. 175:1181-94.

335. Schreck, R., P. Rieber, and P. A. Baeuerle. 1991. Reactive oxygen intermediates as apparently widely used messengers in the activation of the NF-kappa B transcription factor and HIV-1.
*Embo J*. 10:2247-58.

336. Schrenzel, J., L. Serrander, B. Banfi, O. Nusse, R. Fouyouzi, D. P. Lew, N. Demaurex, and K. H. Krause. 1998. Electron currents generated by the human phagocyte NADPH oxidase.
*Nature*. 392:734-7.

337. Schultz, D. E., C. C. Hardin, and S. M. Lemon. 1996. Specific interaction of glyceraldehyde 3-phosphate dehydrogenase with the 5'-nontranslated RNA of hepatitis A virus.
*J Biol Chem*. 271:14134-42.

338. Schulze, H., A. Schuler, D. Stuber, H. Dobeli, H. Langen, and G. Huber. 1993. Rat brain glyceraldehyde-3-phosphate dehydrogenase interacts with the recombinant cytoplasmic domain of Alzheimer's beta-amyloid precursor protein.
*J Neurochem*. 60:1915-22.

339. Schulze-Osthoff, K., A. C. Bakker, B. Vanhaesebroeck, R. Beyaert, W. A. Jacob, and W. Fiers. 1992. Cytotoxic activity of tumor necrosis factor is mediated by early damage of mitochondrial functions. Evidence for the involvement of mitochondrial radical generation.
*J Biol Chem*. 267:5317-23.

340. Schulze-Osthoff, K., R. Beyaert, V. Vandevoorde, G. Haegeman, and W. Fiers. 1993. Depletion of the mitochondrial electron transport abrogates the cytotoxic and gene-inductive effects of TNF.
*Embo J*. 12:3095-104.

341. Schuppe-Koistinen, I., P. Moldeus, T. Bergman, and I. A. Cotgreave. 1994. S-thiolation of human endothelial cell glyceraldehyde-3-phosphate dehydrogenase after hydrogen peroxide treatment.
*Eur J Biochem*. 221:1033-7.

342. Selkoe, D. J. 1994. Cell biology of the amyloid beta-protein precursor and the mechanism of Alzheimer's disease.
*Annu Rev Cell Biol*. 10:373-403.

343. Sergienko, E. A., A. I. Kharitonenkov, T. V. Bulargina, V. V. Muronetz, and N. K. Nagradova. 1992. D-glyceraldehyde-3-phosphate dehydrogenase purified from rabbit muscle contains phosphotyrosine.
*FEBS Lett*. 304:21-3.

344. Sharief, F. S., J. L. Mohler, Y. Sharief, and S. S. Li. 1994. Expression of human prostatic acid phosphatase and prostate specific antigen genes in neoplastic and benign tissues.
*Biochem Mol Biol Int*. 33:567-74.

345. Shashidharan, P., R. M. Chalmers-Redman, G. W. Carlile, V. Rodic, N. Gurvich, T. Yuen, W. G. Tatton, and S. C. Sealfon. 1999. Nuclear translocation of GAPDH-GFP fusion protein during apoptosis.
*Neuroreport*. 10:1149-53.

346. Shigenaga, M. K., T. M. Hagen, and B. N. Ames. 1994. Oxidative damage and mitochondrial decay in aging.
*Proc Natl Acad Sci U S A*. 91:10771-8.

347. Shimizu, S., Y. Eguchi, W. Kamiike, Y. Akao, H. Kosaka, J. Hasegawa, H. Matsuda, and Y. Tsujimoto. 1996. Involvement of ICE family proteases in apoptosis induced by reoxygenation of hypoxic hepatocytes.
*Am J Physiol*. 271:G949-58.

348. Shimizu, S., M. Narita, and Y. Tsujimoto. 1999. Bcl-2 family proteins regulate the release of apoptogenic cytochrome c by the mitochondrial channel VDAC.
*Nature*. 399:483-7.

349. Shirvan, A., I. Ziv, G. Fleminger, R. Shina, Z. He, I. Brudo, E. Melamed, and A. Barzilai. 1999. Semaphorins as mediators of neuronal apoptosis.
*J Neurochem*. 73:961-71.

350. Singh, R., and M. R. Green. 1993. Sequence-specific binding of transfer RNA by glyceraldehyde-3-phosphate dehydrogenase.
*Science*. 259:365-8.

351. Sioud, M., and L. Jespersen. 1996. Enhancement of hammerhead ribozyme catalysis by glyceraldehyde-3- phosphate dehydrogenase.
*J Mol Biol*. 257:775-89.

352. Slater, A. F., C. S. Nobel, and S. Orrenius. 1995b. The role of intracellular oxidants in apoptosis.
*Biochim Biophys Acta*. 1271:59-62.

353. Slater, A. F., C. Stefan, I. Nobel, D. J. van den Dobbelsteen, and S. Orrenius. 1995a. Signalling mechanisms and oxidative stress in apoptosis.
*Toxicol Lett*. 82-83:149-53.

354. Somers, M., Y. Engelborghs, and J. Baert. 1990. Analysis of the binding of glyceraldehyde-3-phosphate dehydrogenase to microtubules, the mechanism of bundle formation and the linkage effect.
*Eur J Biochem*. 193:437-44.

355. Soukri, A., N. Hafid, F. Valverde, M. S. Elkebbaj, and A. Serrano. 1996. Evidence for a posttranslational covalent modification of liver glyceraldehyde-3-phosphate dehydrogenase in hibernating jerboa (Jaculus orientalis).
*Biochim Biophys Acta*. 1292:177-87.

356. Soukri, A., F. Valverde, N. Hafid, M. S. Elkebbaj, and A. Serrano. 1995. Characterization of muscle glyceraldehyde-3-phosphate dehydrogenase isoforms from euthermic and induced hibernating Jaculus orientalis.
*Biochim Biophys Acta*. 1243:161-8.

357. Stadtman, E. R. 1992. Protein oxidation and aging.
*Science*. 257:1220-4.

358. Stamler, J. S., D. I. Simon, J. A. Osborne, M. E. Mullins, O. Jaraki, T. Michel, D. J. Singel, and J. Loscalzo. 1992. S-nitrosylation of proteins with nitric oxide: synthesis and characterization of biologically active compounds.
*Proc Natl Acad Sci U S A*. 89:444-8.

359. Stancel, G. M., and W. C. Deal, Jr. 1969. Reversible dissociation of yeast glyceraldehyde 3-phosphate dehydrogenase by adenosine triphosphate.
*Biochemistry*. 8:4005-11.

360. Stewart, M., D. J. Morton, and F. M. Clarke. 1980. Interaction of aldolase with actin-containing filaments. Structural studies.
*Biochem J*. 186:99-104.

361. Stine, O. C., N. Pleasant, M. L. Franz, M. H. Abbott, S. E. Folstein, and C. A. Ross. 1993. Correlation between the onset age of Huntington's disease and length of the trinucleotide repeat in IT-15.
*Hum Mol Genet*. 2:1547-9.

362. Stuart, J. K., D. G. Myszka, L. Joss, R. S. Mitchell, S. M. McDonald, Z. Xie, S. Takayama, J. C. Reed, and K. R. Ely. 1998. Characterization of interactions between the anti-apoptotic protein BAG- 1 and Hsc70 molecular chaperones.
*J Biol Chem*. 273:22506-14.

363. Sulter, G., J. W. Elting, and J. De Keyser. 1998. Increased serum neuron specific enolase concentrations in patients with hyperglycemic cortical ischemic stroke.
*Neurosci Lett*. 253:71-3.

364. Sunaga, K., H. Takahashi, D. M. Chuang, and R. Ishitani. 1995. Glyceraldehyde-3-phosphate dehydrogenase is over-expressed during apoptotic death of neuronal cultures and is recognized by a monoclonal antibody against amyloid plaques from Alzheimer's brain.
*Neurosci Lett*. 200:133-6.

365. Susin, S. A., H. K. Lorenzo, N. Zamzami, I. Marzo, B. E. Snow, G. M. Brothers, J. Mangion, E. Jacotot, P. Costantini, M. Loeffler, N. Larochette, D. R. Goodlett, R. Aebersold, D. P. Siderovski, J. M. Penninger, and G. Kroemer. 1999. Molecular characterization of mitochondrial apoptosis-inducing factor.
 *Nature*. 397:441-6.

366. Susin, S. A., N. Zamzami, and G. Kroemer. 1998. Mitochondria as regulators of apoptosis: doubt no more.
 *Biochim Biophys Acta*. 1366:151-65.

367. Susor, W. A., M. Kochman, and W. J. Rutter. 1973. Structure determinations of FDP aldolase and the fine resolution of some glycolytic enzymes by isoelectric focusing.
 *Ann N Y Acad Sci*. 209:328-44.

368. Szabo, C. 1996. DNA strand breakage and activation of poly-ADP ribosyltransferase: a cytotoxic pathway triggered by peroxynitrite.
 *Free Radic Biol Med*. 21:855-69.

369. Szturmowicz, M., J. Burakowski, W. Tomkowski, A. Sakowicz, and S. Filipecki. 1998. Neuron-specific enolase in non-neoplastic lung diseases, a marker of hypoxemia?
 *Int J Biol Markers*. 13:150-3.

370. Tabrizi, S. J., M. W. Cleeter, J. Xuereb, J. W. Taanman, J. M. Cooper, and A. H. Schapira. 1999. Biochemical abnormalities and excitotoxicity in Huntington's disease brain.
 *Ann Neurol*. 45:25-32.

371. Tajima, H., K. Tsuchiya, M. Yamada, K. Kondo, N. Katsube, and R. Ishitani. 1999. Over-expression of GAPDH induces apoptosis in COS-7 cells transfected with cloned GAPDH cDNAs.
 *Neuroreport*. 10:2029-33.

372. Takayama, S., D. N. Bimston, S. Matsuzawa, B. C. Freeman, C. Aime-Sempe, Z. Xie, R. I. Morimoto, and J. C. Reed. 1997. BAG-1 modulates the chaperone activity of Hsp70/Hsc70.
 *Embo J*. 16:4887-96.

373. Takayama, S., S. Krajewski, M. Krajewska, S. Kitada, J. M. Zapata, K. Kochel, D. Knee, D. Scudiero, G. Tudor, G. J. Miller, T. Miyashita, M. Yamada, and J. C. Reed. 1998. Expression and location of Hsp70/Hsc-binding anti-apoptotic protein BAG- 1 and its variants in normal tissues and tumor cell lines.
 *Cancer Res*. 58:3116-31.

374. Takayama, S., Z. Xie, and J. C. Reed. 1999. An evolutionarily conserved family of Hsp70/Hsc70 molecular chaperone regulators.
 *J Biol Chem*. 274:781-6.

375. Takei, N., J. Kondo, K. Nagaike, K. Ohsawa, K. Kato, and S. Kohsaka. 1991. Neuronal survival factor from bovine brain is identical to neuron- specific enolase.
 *J Neurochem*. 57:1178-84.

376. Tanaka, Y., F. Fang, C. H. Zhang, X. W. Zhang, and S. Omura. 1998. Heme-dependent radical generation from antimalarial fungal metabolites, radicicol and heptelidic acid.
 *J Antibiot (Tokyo)*. 51:451-3.

377. Tatton, W. G. 1999. Apoptotic mechanisms in neurodegeneration: possible relevance to glaucoma.
 *Eur J Ophthalmol*. 9 Suppl 1:S22-9.

378. Thomas, M., H. Skala, A. Kahn, and F. P. Tuy. 1995. Functional dissection of the brain-specific rat aldolase C gene promoter in transgenic mice. Essential role of two GC-rich boxes and an HNF3 binding site.
 *J Biol Chem*. 270:20316-21.

379. Thompson, C. B. 1995. Apoptosis in the pathogenesis and treatment of disease.
 *Science*. 267:1456-62.

380. Thompson, R. J., P. A. Kynoch, and V. J. Willson. 1982. Cellular localization of aldolase C subunits in human brain.
 *Brain Res*. 232:489-93.

381. Thornberry, N. A., and Y. Lazebnik. 1998. Caspases: enemies within.
 *Science*. 281:1312-6.

382. Thulasiraman, V., Z. Xu, S. Uma, Y. Gu, J. J. Chen, and R. L. Matts. 1998. Evidence that Hsc70 negatively modulates the activation of the heme- regulated eIF-2alpha kinase in rabbit reticulocyte lysate.
 *Eur J Biochem*. 255:552-62.

383. Tolan, D. R., J. Niclas, B. D. Bruce, and R. V. Lebo. 1987. Evolutionary implications of the human aldolase-A, -B, -C, and - pseudogene chromosome locations.
*Am J Hum Genet*. 41:907-24.

384. Toledano, M. B., and W. J. Leonard. 1991. Modulation of transcription factor NF-kappa B binding activity by oxidation-reduction *in vitro*.
*Proc Natl Acad Sci U S A*. 88:4328-32.

385. Tomassini, J., R. Roychoudhury, R. Wu, and R. J. Roberts. 1978. Recognition sequence of restriction endonuclease KpnI from Klebsiella pneumoniae.
*Nucleic Acids Res*. 5:4055-64.

386. Torres, R., and M. H. Polymeropoulos. 1998. Genomic organization and localization of the human CRMP-1 gene.
*DNA Res*. 5:393-5.

387. Tsai, I. H., S. N. Murthy, and T. L. Steck. 1982. Effect of red cell membrane binding on the catalytic activity of glyceraldehyde-3-phosphate dehydrogenase.
*J Biol Chem*. 257:1438-42.

388. Tsai, R. L., and H. Green. 1973. Studies on a mammalian cell protein (P8) with affinity for DNA *in vitro*.
*J Mol Biol*. 73:307-16.

389. Tsutsumi, K., K. Ito, and K. Ishikawa. 1989. Developmental appearance of transcription factors that regulate liver- specific expression of the aldolase B gene.
*Mol Cell Biol*. 9:4923-31.

390. Turner, C. P., S. S. Panter, and F. R. Sharp. 1999. Anti-oxidants prevent focal rat brain injury as assessed by induction of heat shock proteins (HSP70, HO-1/HSP32, HSP47) following subarachnoid injections of lysed blood.
*Brain Res Mol Brain Res*. 65:87-102.

391. Uma, S., V. Thulasiraman, and R. L. Matts. 1999. Dual role for Hsc70 in the biogenesis and regulation of the heme-regulated kinase of the alpha subunit of eukaryotic translation initiation factor 2.
*Mol Cell Biol*. 19:5861-71.

392. Umeki, S. 1994. Activation factors of neutrophil NADPH oxidase complex.
*Life Sci*. 55:1-13.

393. Van Antwerp, D. J., S. J. Martin, T. Kafri, D. R. Green, and I. M. Verma. 1996. Suppression of TNF-alpha-induced apoptosis by NF-kappaB.
*Science*. 274:787-9.

394. Vander Heiden, M. G., N. S. Chandel, E. K. Williamson, P. T. Schumacker, and C. B. Thompson. 1997. Bcl-xL regulates the membrane potential and volume homeostasis of mitochondria.
*Cell*. 91:627-37.

395. Vartanian, A., I. Alexandrov, I. Prudowski, A. McLennan, and L. Kisselev. 1999. Ap4A induces apoptosis in human cultured cells.
*FEBS Lett*. 456:175-80.

396. Vartanian, A., I. Prudovsky, H. Suzuki, I. Dal Pra, and L. Kisselev. 1997. Opposite effects of cell differentiation and apoptosis on Ap3A/Ap4A ratio in human cell cultures.
*FEBS Lett*. 415:160-2.

397. Vaux, D. L. 1997. CED-4--the third horseman of apoptosis.
*Cell*. 90:389-90.

398. Vaux, D. L., and S. J. Korsmeyer. 1999. Cell death in development.
*Cell*. 96:245-54.

399. Veis, D. J., C. M. Sorenson, J. R. Shutter, and S. J. Korsmeyer. 1993. Bcl-2-deficient mice demonstrate fulminant lymphoid apoptosis, polycystic kidneys, and hypopigmented hair.
*Cell*. 75:229-40.

400. Vibert, M., J. Henry, A. Kahn, and H. Skala. 1989. The brain-specific gene for rat aldolase C possesses an unusual housekeeping-type promoter.
*Eur J Biochem*. 181:33-9.

401. Vishwanatha, J. K., and Z. Wei. 1992. Diadenosine tetraphosphate binding protein from human HeLa cells: purification and characterization.
*Biochemistry*. 31:1631-5.

402. Volker, K. W., and H. Knull. 1997. A glycolytic enzyme binding domain on tubulin.
*Arch Biochem Biophys*. 338:237-43.

403. Volker, K. W., and H. R. Knull. 1993. Glycolytic enzyme-tubulin interactions: role of tubulin carboxy terminals.
*J Mol Recognit*. 6:167-77.

404. Volker, K. W., C. A. Reinitz, and H. R. Knull. 1995. Glycolytic enzymes and assembly of microtubule networks.
*Comp Biochem Physiol B Biochem Mol Biol*. 112:503-14.

405. Vollberg, T. M., B. L. Cool, and M. A. Sirover. 1987. Biosynthesis of the human base excision repair enzyme uracil-DNA glycosylase.
*Cancer Res*. 47:123-8.

406. Vollberg, T. M., K. M. Siegler, B. L. Cool, and M. A. Sirover. 1989. Isolation and characterization of the human uracil DNA glycosylase gene.
*Proc Natl Acad Sci U S A*. 86:8693-7.

407. Wachsmuth, E. D., M. Thoner, and G. Pfleiderer. 1975. The cellular distribution of aldolase isozymes in rat kidney and brain determined in tissue sections by the immuno-histochemical method.
*Histochemistry*. 45:143-61.

408. Wadia, J. S., R. M. E. Chalmers-Redman, W. J. H. Ju, G. W. Carlile, J. L. Phillips, A. D. Fraser, and W. G. Tatton. 1998. Mitochondrial membrane potential and nuclear changes in apoptosis caused by serum and nerve growth factor withdrawal: time course and modification by (-)-deprenyl.
*J Neurosci*. 18:932-47.

409. Walsh, J. L., T. J. Keith, and H. R. Knull. 1989. Glycolytic enzyme interactions with tubulin and microtubules.
*Biochim Biophys Acta*. 999:64-70.

410. Walsh, T. P., D. J. Winzor, F. M. Clarke, C. J. Masters, and D. J. Morton. 1980. Binding of aldolase to actin-containing filaments. Evidence of interaction with the regulatory proteins of skeletal muscle.
*Biochem J*. 186:89-98.

411. Wang, J., A. J. Morris, D. R. Tolan, and L. Pagliaro. 1996. The molecular nature of the F-actin binding activity of aldolase revealed with site-directed mutants.
*J Biol Chem*. 271:6861-5.

412. Wang, L. H., and S. M. Strittmatter. 1996. A family of rat CRMP genes is differentially expressed in the nervous system.
*J Neurosci*. 16:6197-207.

413. Wang, L. H., and S. M. Strittmatter. 1997. Brain CRMP forms heterotetramers similar to liver dihydropyrimidinase.
*J Neurochem*. 69:2261-9.

414. Weber, A., J. Marie, D. Cottreau, M. P. Simon, C. Besmond, J. C. Dreyfus, and A. Kahn. 1984. Dietary control of aldolase B and L-type pyruvate kinase mRNAs in rat. Study of translational activity and hybridization with cloned cDNA probes.
*J Biol Chem*. 259:1798-802.

415. Weisiger, R. A., and I. Fridovich. 1973. Mitochondrial superoxide simutase. Site of synthesis and intramitochondrial localization.
*J Biol Chem*. 248:4793-6.

416. Westin, G., T. Gerster, M. M. Muller, G. Schaffner, and W. Schaffner. 1987. OVEC, a versatile system to study transcription in mammalian cells and cell-free extracts.
*Nucleic Acids Res*. 15:6787-98.

417. Wilson, J. X. 1997. Antioxidant defense of the brain: a role for astrocytes.
*Can J Physiol Pharmacol*. 75:1149-63.

418. Wink, D. A., K. S. Kasprzak, C. M. Maragos, R. K. Elespuru, M. Misra, T. M. Dunams, T. A. Cebula, W. H. Koch, A. W. Andrews, and J. S. Allen. 1991. DNA deaminating ability and genotoxicity of nitric oxide and its progenitors.
*Science*. 254:1001-3.

419. Wistow, G. J., T. Lietman, L. A. Williams, S. O. Stapel, W. W. de Jong, J. Horwitz, and J. Piatigorsky. 1988. Tau-crystallin/alpha-enolase: one gene encodes both an enzyme and a lens structural protein.
*J Cell Biol*. 107:2729-36.

420. Wolf, B. B., and D. R. Green. 1999. Suicidal tendencies: apoptotic cell death by caspase family proteinases.
*J Biol Chem*. 274:20049-52.

421. Wong, G. H., and D. V. Goeddel. 1988. Induction of manganous superoxide dismutase by tumor necrosis factor: possible protective mechanism.
*Science*. 242:941-4.

422. Wong, H. R., M. A. Ryan, I. Y. Menendez, and J. R. Wisp. 1999. Heat shock activates the I-kappaBalpha promoter and increases I- kappaBalpha mRNA expression.
*Cell Stress Chaperones*. 4:1-7.

423. Wu, H., and G. Lozano. 1994. NF-kappa B activation of p53. A potential mechanism for suppressing cell growth in response to stress.
*J Biol Chem*. 269:20067-74.

424. Wu, K., C. Aoki, A. Elste, A. A. Rogalski-Wilk, and P. Siekevitz. 1997. The synthesis of ATP by glycolytic enzymes in the postsynaptic density and the effect of endogenously generated nitric oxide.
*Proc Natl Acad Sci U S A*. 94:13273-8.

425. Yan, Q., M. Briehl, C. L. Crowley, C. M. Payne, H. Bernstein, and C. Bernstein. 1999. The NAD+ precursors, nicotinic acid and nicotinamide upregulate glyceraldehyde-3-phosphate dehydrogenase and glucose-6-phosphate dehydrogenase mRNA in jurkat cells.
*Biochem Biophys Res Commun*. 255:133-6.

426. Yang, E., J. Zha, J. Jockel, L. H. Boise, C. B. Thompson, and S. J. Korsmeyer. 1995. Bad, a heterodimeric partner for Bcl-XL and Bcl-2, displaces Bax and promotes cell death.
*Cell*. 80:285-91.

427. Yasuhara, N., Y. Eguchi, T. Tachibana, N. Imamoto, Y. Yoneda, and Y. Tsujimoto. 1997. Essential role of active nuclear transport in apoptosis.
*Genes Cells*. 2:55-64.

428. Yoneda, Y. 1997. How proteins are transported from cytoplasm to the nucleus.
*J Biochem (Tokyo)*. 121:811-7.

429. Yong, Y., and J. L. Dreyer. 1995. Developmental changes in the localization of the transplasma membrane NADH-dehydrogenases in the rat brain.
*Brain Res Dev Brain Res*. 89:253-63.

430. Yong, Y., and J. L. Dreyer. 1995. Distribution of six transplasma membrane NADH-dehydrogenases in rat brain tissue.
*Brain Res Dev Brain Res*. 89:235-52.

431. Yoshida, H., A. Watanabe, and Y. Ihara. 1998. Collapsin response mediator protein-2 is associated with neurofibrillary tangles in Alzheimer's disease.
*J Biol Chem*. 273:9761-8.

432. Yun, J. K., T. S. McCormick, C. Villabona, R. R. Judware, M. B. Espinosa, and E. G. Lapetina. 1997. Inflammatory mediators are perpetuated in macrophages resistant to apoptosis induced by hypoxia.
*Proc Natl Acad Sci U S A*. 94:13903-8.

433. Zamzami, N., P. Marchetti, M. Castedo, T. Hirsch, S. A. Susin, B. Masse, and G. Kroemer. 1996b. Inhibitors of permeability transition interfere with the disruption of the mitochondrial transmembrane potential during apoptosis.
*FEBS Lett*. 384:53-7.

434. Zamzami, N., I. Marzo, S. A. Susin, C. Brenner, N. Larochette, P. Marchetti, J. Reed, R. Kofler, and G. Kroemer. 1998. The thiol crosslinking agent diamide overcomes the apoptosis-inhibitory effect of Bcl-2 by enforcing mitochondrial permeability transition.
*Oncogene*. 16:1055-63.

435. Zamzami, N., S. A. Susin, P. Marchetti, T. Hirsch, I. Gomez-Monterrey, M. Castedo, and G. Kroemer. 1996a. Mitochondrial control of nuclear apoptosis.
*J Exp Med*. 183:1533-44.

436. Zang, W. Q., A. M. Fieno, R. A. Grant, and T. S. Yen. 1998. Identification of glyceraldehyde-3-phosphate dehydrogenase as a cellular protein that binds to the hepatitis B virus posttranscriptional regulatory element.
*Virology*. 248:46-52.

437. Zeise, E., N. Kuhl, J. Kunz, and L. Rensing. 1998. Nuclear translocation of stress protein Hsc70 during S phase in rat C6 glioma cells.
*Cell Stress Chaperones*. 3:94-9.

438. Zhang, J., and S. H. Snyder. 1992. Nitric oxide stimulates auto-ADP-ribosylation of glyceraldehyde-3- phosphate dehydrogenase.
*Proc Natl Acad Sci U S A*. 89:9382-5.

439. Zhang, K. Z., J. A. Westberg, E. Holtta, and L. C. Andersson. 1996. BCL2 regulates neural differentiation.
*Proc Natl Acad Sci U S A*. 93:4504-8.

440. Zhao, Z., C. E. Francis, G. Welch, J. Loscalzo, and K. Ravid. 1997. Reduced glutathione prevents nitric oxide-induced apoptosis in vascular smooth muscle cells.
*Biochim Biophys Acta*. 1359:143-52.

441. Zhivotovsky, B., S. Orrenius, O. T. Brustugun, and S. O. Doskeland. 1998. Injected cytochrome c induces apoptosis.
*Nature*. 391:449-50.

442. Zimmermann, R., M. Sagstetter, M. J. Lewis, and H. R. Pelham. 1988. Seventy-kilodalton heat shock proteins and an additional component from reticulocyte lysate stimulate import of M13 procoat protein into microsomes.
*Embo J*. 7:2875-80.

443. Zoratti, M., and I. Szabo. 1995. The mitochondrial permeability transition.
*Biochim Biophys Acta*. 1241:139-76.

444. Zurbriggen, R., and J. L. Dreyer. 1994. An NADH-diaphorase is located at the cell plasma membrane in a mouse neuroblastoma cell line NB41A3.
*Biochim Biophys Acta*. 1183:513-20.

445. Zurbriggen, R., and J. L. Dreyer. 1996. The plasma membrane NADH-diaphorase is active during selective phases of the cell cycle in mouse neuroblastoma cell line NB41A3. Its relation to cell growth and differentiation.
*Biochim Biophys Acta*. 1312:215-22.

# 7 **APPENDIX**

## 7.1 Additional studies

### 7.1.1 S1-Nuclease mapping assay

To get a first indication whether the proteins in the PMO complex are induced after stress, the induction of the components of the PMO complex was investigated by S1-nuclease protection assay. The agents used to stress synchronised NB41A3 cells were DCIP (up to 400 µM) and $H_2O_2$ (up to 200 µM). We observed a concentration dependent increase of Ulip in stressed NB41A3 cells (see figure 7b of the attached article (Bulliard et al., 1997)). The induction reached its peak at 100 µM DCIP or 100 µM $H_2O_2$ respectively, where mRNA levels were at about 150 %, before they decreased at higher concentrations. This induction was significant and was able to re-produced by several different probes used to detect the same mRNA. For Ulip four DNA probes that were different in size (114, 203, 250 and 395 nt), were used.

### 7.1.2 Two-hybrid system

#### 7.1.2.1 Method and principle of the two-hybrid assay

We used the MATCHMAKER two-hybrid systems from CLONTECH to test our five previously cloned proteins for interaction. The MATCHMAKER Two-Hybrid System is a complete GAL4-based two-hybrid system that provids a transcriptional assay for detecting specific protein-protein interactions in yeast. For general reviews on yeast two-hybrid systems, see (Allen, et al., 1995, Bartel, et al., 1993, Fields and Sternglanz, 1994, Luban and Goff, 1995, McNabb and Guarente, 1996, Mendelsohn and Brent, 1994).

The yeast two-hybrid assay is based on the fact that many eukaryotic trans-acting transcription factors are composed of physically separable, functionally independent domains. Such regulators often contain a DNA-binding domain (DNA-BD) that binds to a specific enhancer-like sequence, which in yeast is referred to as an upstream activation site (UAS). One or more activation domains (AD) direct the RNA

polymerase II complex to transcribe the gene downstream of the UAS (Hope and Struhl, 1986, Keegan, et al., 1986, Ma and Ptashne, 1987, Ma and Ptashne, 1987, Ma and Ptashne, 1987). Both the DNA-BD and the AD are required to activate a gene and normally, as in the case of the native yeast GAL4 protein, the two domains are part of the same protein. If physically separated by recombinant DNA technology and expressed in the same host cell, the DNA-BD and AD peptides do not directly interact with each other and thus cannot activate the responsive genes (Brent and Ptashne, 1985, Brent and Ptashne, 1985, Ma and Ptashne, 1988). However, if the DNA-BD and AD can be brought into close physical proximity in the promoter region, the transcriptional activation function will be restored. In principle, any AD can be paired with any DNA-BD to activate transcription,with the DNA-BD providing the promoter specificity (Brent and Ptashne, 1985, Brent and Ptashne, 1985).

In the two-hybrid systems we used, the DNA-BD and the AD are both derived from the yeast GAL4 protein (a.a. 1–147 and 768–881, respectively). Two different cloning vectors are used to generate fusions of these domains to genes encoding proteins that potentially interact with each other. The recombinant hybrid proteins are co-expressed in yeast and are targeted to the yeast nucleus. An interaction between a first protein (fused to the DNA-BD) and a second library-encoded protein (fused to the AD) creates a novel transcriptional activator with binding affinity for a GAL4-responsive UAS. This factor then activates reporter genes having upstream GAL4- responsive elements in their promoter and this makes the protein-protein interaction phenotypically detectable. If the two hybrid proteins do not interact with each other, the reporter genes will not be transcibed.

Our GAL4 two-hybrid saccharomyces cerevisiae Y187 host strain contains the lacZ reporter. We utilised a lacZ reporter gene under the control of a GAL4-responsive UAS. The b-galactosidase encoded by the lacZ reporter was detected by using the Colony Lift β-galactosidase Filter assay. For detailed protocols see product protocol "MATCHMAKER Two-Hybrid System 2" (PT1030-1) and "Yeast Protocols Handbook" (PT3024-1) from CLONTECH (Paolo Alto, CA, USA).

## 7.1.2.2 <u>Results</u>

<u>Control experiments</u>

The phenotype of our Y187 yeast strain was verified successfully. Y187 cells did not grow on SD/-Trp, SD/-Leu, SD/-His and YPD/+cycloheximide plates, whereas positive colonies were detected on SD/-Ura and YPD plates.

To test the functionality of our system and to avoid false positives we performed some control transformations with the following plasmids:

| Plasmid name | Purpose | Description |
|---|---|---|
| pAS2-1 | 8.4-kb cloning vector | used to generate fusions of the bait protein with the GAL4 DNA-BD. |
| pACT2 | 8.1-kb cloning vector | used to generate fusions of a known protein with the GAL4 AD. |
| pVA3-1 | 9.4-kb positive control plasmid used with pTD1-1 | encodes a DNA-BD/murine p53 fusion protein in pAS2-1. |
| pTD1-1 | 9.9-kb positive control plasmid used with pVA3-1 | encodes an AD/SV40 large T-antigen fusion protein in pACT2. |
| pCL1 | 15.3-kb positive control plasmid | encodes the full-length, wild-type GAL4 protein. |
| pLAM5'-1 | 9.1-kb false-positive detection plasmid | encodes a DNA-BD/human lamin C fusion protein in pAS2-1. |

The results of the control transformations performed with these plasmids are listed below:

| Plasmid 1 (DNA-BD) | Plasmid 2 (AD) | SD Selection Medium | Colony growth | LacZ ex-pression |
|---|---|---|---|---|
| - | pCL1 | -Leu | yes | yes |
| pAS2-1 | - | -Trp | yes | no |
| - | pACT2 | -Leu | yes | no |
| pAS2-1 | pACT2 | -Leu, -Trp | yes | no |
| pVA3-1 | - | -Trp | yes | no |
| pVA3-1 | pACT2 | -Leu, -Trp | yes | no |
| - | pTD1-1 | -Leu | yes | no |
| pAS2-1 | pTD1-1 | -Leu, -Trp | yes | no |
| pVA3-1 | pTD1-1 | -Leu, -Trp | yes | yes |
| pLAM5'-1 | - | -Trp | yes | no |
| pLAM5'-1 | pTD1-1 | -Leu, -Trp | yes | no |

The results of these transformations demonstrate that besides transformation of pCL1 which encodes the full-length, wild-type GAL4 protein, also double-transformation of pVA3-1 and pTD1-1 (which are DNA-BD and AD fusion plasmids, respectively, containing Murine p53 and SV40 large T-antigen which are known to interact in a yeast two-hybrid assay) provide positive results for the -galactosidase assay. In contrast, pLam5'-1 which encodes a fusion of the DNA-BD with human lamin C (which has been reported not to form complexes nor to interact with most other proteins and therefore provides a control for a fortuitous interaction) did not interact with AD/T-antigen control (pTD1-1). In all other transformations we also obtained the expected results, confirming the relevance of our two-hybrid system.

We then constructed fusion genes using standard techniques. The genes coding for GAPDH, Hsc70, enolase γ, aldolase C, Ulip 2 and Ulip 3 were each fused separately to the DNA-BD in the pAS2-1 vector and to the AD in the pACT2 vector. These constructs are referred to as DNA-BD/protein X and AD/protein Y, respectively. The orientation and reading frame of each fusion was maintained so that hybrid proteins were able to be expressed.

We first verified that the hybrid constructs alone did not activate the reporter genes. The DNA-BD/protein X and AD/protein Y constructs were transformed independently into strain Y187 and were

tested for activation of the lacZ reporter gene. None of the transformant colonies turned blue, thus autonomous activation could be excluded.

Two-hybrid system assay between proteins of the PMO complex

To assay the proteins for interaction two types of hybrid plasmids (DNA-BD/protein X and AD/protein Y were co-transformed into Y187. We tested all possible combinations between the proteins. The co-transformation mixtures were plated on SD/–Leu/–Trp to select for colonies containing both hybrid plasmids. The 4-day-old transformant colonies were assayed for activation of the lacZ reporter gene using the β-galactosidase colony-lift filter. Colonies were about 1-5 mm in diameter when they were transferred to the filter. The results of the two-hybrid experiment were compared with the positive and negative controls performed in parallel. While positive control transformant colonies with pVA3-1 and pTD1-1 (see above) turned blue within about 1-2 h, all other transformants did not show any significant β–galactosidase activity even after 24 h.

Different possibilities can be considered as reason for this surprising result. First, the fused GAL4 domains may occlude the site of interaction. Second, the hybrid proteins may fold improperly or the hybrid protein cannot be localised to the yeast nucleus. However, the probability that one of this is the case is quite small, since we cannot find interaction between any of our PMO complex proteins. Therefore it was more accurate to propose that either all our proteins needed another unknown, additional protein to interact with each other, or that the hybrid proteins may not be stably expressed in the host cell at all.

To test whether the last hypothesis is true, we tried to verify whether the fusion proteins are expressed in yeast. The DNA-BD/protein X and AD/protein Y constructs were transformed separately into Y187. Western blots using soluble protein extracts were prepared from the transformants and probed with PMO protein specific and GAL4 domain-specific antibodies (Abs), such as the GAL4 DNA-BD and AD mAbs. Quite interestingly we observed multiple bands for each band indicating that the transformed proteins rather then being stably expressed, they were degraded in the yeast cells. We therefore suppose that degradation of our proteins in yeast cells is the reason why we were not able to detect interaction between proteins of the PMO complex by the two-hybrid system.

# 7.2 **Detailed protocols**

## 7.2.1 Stock Solutions

Buffers and solutions that we routinely used in molecular biology

**Water:**

It is recommended to keep using the same bottles for ddH2O, to avoid contamination with detergents. Preparation of "H2O certified storage bottles" is done as follows: Rinse bottle several times with ddH2O. Fill 1/3 of the volume and autoclave. Empty the autoclaved water, fill with fresh ddH2O and autoclave again. Keep using the same bottle (rinse before refilling and autoclaving only with ddH2O).

**Acids and bases (do not autoclave!!):**

| | | |
|---|---|---|
| NaOH (40 g/mol) | 10M | Dissolve 80 g of solid NaOH in 200 ml ddH$_2$0 |
| | 2M | Dissolve 16 g of solid NaOH in 200 ml ddH$_2$0 |
| HCl (36.5 g/mol) | 1M | Dilute 15 ml conc. HCl (11.6M) in 160 ml ddH$_2$0 |
| TCA | 100% | To a bottle containing 500 g of Trichloroacetic |

acid, add 227 ml of H$_2$O. The resulting solution will contain 100% (w/v) TCA.

**Salt solutions**

| | | |
|---|---|---|
| NaCl (58.44 g/mol) | 5M | Dissolve 146.1 g of NaCl in 400 ml ddH$_2$O. |
| | | Adjust the volume to 500 ml. Autoclave. |
| | 3M | Dissolve 35 g of NaCl in 160 ml ddH$_2$O. |
| | | Adjust the volume to 200 ml. Autoclave. |
| KCl (74.56 g/mol) | 1M | Dissolve 37.3 g KCl in 400 ml ddH$_2$O. |
| | | Adjust the volume to 500 ml. Autoclave. |
| NaOAc pH=7.0 | 3M | Dissolve 98.45 g of Natrium acetate anhydrous in |
| (anhidrous.82.04 g/mol) | | 300 ml ddH$_2$O. Adjust the pH with acetic acid |

glacial. Adjust the volume to 400 ml, aliquote in 2 bottle of 200 ml each and autoclave

| | | |
|---|---|---|
| MgCl$_2$ | 1M | Dissolve 40.66 g of MgCl$_2$·6H$_2$O in 160 ml (·6H$_2$0 203.31 |
| g/mol) | | ddH$_2$O. Adjust the volume to 200 ml. Autoclave |

**Buffers**

Tris.Cl pH=9, 8.5, 8.3, 8.0, 7.5

| | | |
|---|---|---|
| (121.1 g/mol) | 1M | Dissolve 60.55 g Tris base in 400 ml ddH$_2$O. |
| | | Adjust the pH with conc. HCl and ajust the volume to 500 ml. Autoclave. Prepare only 100 ml if shorter time work planned. |

Hepes pH=7.5      1M      Dissolve 23.83 g of Hepes in 80 g ddH$_2$O.

(238.31 g/mol)      Adjust the pH with 10 M NaOH. Adjust the
volume to 100 ml. Filter sterilize.

## Chelators

EDTA pH=8.0      0.5M      "Dissolve" 93.1 g of Na$_2$EDTA·2H$_2$O in 400 ml

(Na$_2$ salt, ·2H$_2$O 186,1 g/mol)  ddH$_2$O.
Adjust the pH with 10M NaOH.
Adjust  the voume to 500 ml. Autoclave.
Prepare 200 ml if shorter time planned.

## Pre-Mixed buffer solutions

Make them in sterile containers (e.g autoclaved bottles or sterile plastic tubes) and with sterile
components. In general it is not recommended to autoclave these mixes if they are made with pre-autovclaved reagents..

| | | | |
|---|---|---|---|
| 10x TE | 100 mM Tris pH=7.5 | for 200 ml: | 20 ml 1 M |
| | 10 mM EDTA pH=8.0 | | 4 ml 0.5 M |
| | | | |
| 10x TNE | 3 M NaCl | for 200 ml: | 120 ml 5 M |
| | 200 mM Tris pH=7.5 | | 40 ml 1 M |
| | 100 mM EDTA | | 40 ml 0.5 M |
| | | | |
| *10x TAE | 400 mM Tris-acetate | for 10 l | 484 g Tris base |
| | | | 114.2 ml glacial acetic acid |
| | 10 mM EDTA | | 37.2 g Na$_2$EDTA·2H$_2$O |
| *10x LOE | 0.36 M Tris | for 10 l | 436 g Tris base |
| | 2.65 M NaH$_2$PO$_4$ | | 414 g NaH$_2$PO$_4$·2H$_2$O |
| | 10 mM EDTA | | 37.2 g Na$_2$EDTA·2H$_2$O |
| *5x TBE | 445 mM Tris | for 10 l | 540 g Tris base |
| | 445 mM boric acid | | 275 g boric acid |
| | 5 mM EDTA | | 18.6 g Na$_2$EDTA·2H$_2$O |

* electrophoresis buffers are kept in centralised, 10 L stocks

## Organic solvents

H2O saturated Phenol: Melt phenol in its original container, supplemented with H$_2$O (400 ml) and a few
milligram of the radical scavenger 8-hydroxyquinoline at 50°C. Transfer into a brown glass bottle.
This stock solution can be stored at 4°C for several months. Watch out, phenol is extremely
aggressive, thus avoid mouth pipetting, aerosols etc. Keep adsorbing paper at hand. In case of spill
on skin: wash first abundantly with water, then with soap. Generous rubbing with a fine cloth wetted
with olive oil is the best cure to restore normal skin in minor phenol burns.

Na/Tris saturated phenol working solution:
to 200 ml of stock solution add:      20 ml ddH$_2$O

<div align="right">10 ml 1M Tris 8.0

10 ml 5M NaCl</div>

Mix well, can be stored for one month at room temperature in a dark bottle.
1 Volume of this  working solution can be mixed with 1 vol. chloroform to obtain
Phenol/Chloroform 1:1 solution (Exclusion of 10% water)

Chloroform. Make an aliquot of 100-200 ml preferably in a brown bottle.

100% ethanol. Store this working solution in a 100 or 200 ml bottle, well labelled. You can also fill a squirt plastic bottle (please rinse two or three times with clean alcohol before. Brown bottles should be preferred. When you use for rinsing pellets, be sure you do not go back with a pipette that has touched any of the samples or that may be sprayed by aerosols. DNA keeps for several years in EtOH!!!.

80% ethanol. You prepare it by adding 20%  ddH2O. Preferably in brown bottle. It is not necessary to have a cold ethanol stock as suggested in many protocols.

75% Ethanol. This is mostly used as a disinfectant in cell cultures. A good lab should have one or two squirt bottles of this in a conventional place. Do not squirt directly onto surface: rather do wet a paper with the alcohol and rub it on the surface.

## Detergents

SDS                     20%                     Dissolve 40 g of SDS in 150 ml ddH$_2$O + 10 ml

1M Tris pH=8.0. Adjust the volume to 200 ml.

Can be autoclaved (max 20 min)

Titon X-100             10%                     Dissolve 20 g Triton X-100 in 160 ml ddH$_2$O
Adjust the volume to 200 ml.

Can be autoclaved.


## Miscellaneous

DTT (154.5 g/mol)       1 M                     Dissolve 1.55 g of DTT in 10 ml ddH$_2$O.

Dispense into 1 ml aliquots and store at -20°C.
NEVER AUTOCLAVE DTT!

BSA                     10 mg/ml                Dissolve 100 mg BSA (fraction V) in 10 ml
ddH$_2$O. Add 10 μl 1M DTT.

Dispense into 1 ml aliquots and store at -20°C.

Ethidium bromide        10 mg/ml                Dissolve 1 g EtBr in 100 ml ddH$_2$O. Mix well.

Wrap the bottle in aluminium foil and store in a                dark place. **Do not make your own if one**

**bottle already exists in the same room!**


ATP                     100 mM                  Dissolve 30 mg of ATP disodium salt in 800 μl
(2NaCl  551.2 g/mol)                            ddH$_2$O. Adjust the pH to 7.0 with 0.1M NaOH.

(Ph Paper). Adjust the volume to 1 ml.
Dispense into small  aliquots and store at -20°C .


## Solutions for PAGE

40 % Acrylamide/ N,N'-Methylenbisacrylamide (19:1) stock solution (AA/MBAA), deionised:

1) 380 g Acrylamide
   20 g N,N'-Methylenebisacrylamide
2) fill up to almost 1 litre with distilled $H_2O$, mix until completely dissolved, then set        volume
   to 1 litre.
3) add a big spoon of Amberlite MB-1 to remove ions, stir the solution 30 min.
4) filtrate solution (paper filter), store in a dark bottle at 4 ˚C (for some months).

20 % Acrylamide,1xTBE, 8 M Urea solution:

1) In a GLASS beaker, add:
   240.2 g Urea
   250 ml 40 % AA/MBAA (19:1) stock solution
   50 ml 10xTBE stock solution
2) add distilled $H_2O$ to reach 450 ml, help dissolve the urea by heating (max 60 ˚C; on
   magnetic strirrer heater))
3) adjust to 500 ml with $H_2O$

1xTBE, 8 M Urea solution:

1) Add in a GLASS beaker:
   240.2 g Urea
   50 ml 10xTBE stock solution
2) add distilled $H_2O$ to reach 450 ml, dissolve the urea by heating ($\leq 60$ ˚C)
3) Adjust to 500 ml with $H_2O$

30 % Acrylamide/ N,N'-Methylene-bisacrylamide (29:1) stock solution:

1) 290 g Acrylamide
   10 g N,N'-Methylenebisacrylamide
2) fill up with $H_2O$ to aprox. 950 ml, dissolve completely, then fill up to 1 litre
3) deionise with a spoon Amberlite MB-1 stirring during half an hour
4) filtrate solution (paper filter), store in a dark bottle at 4 ˚C (for some months).

**Polymerisation is done by adding 1/1000 vol TEMED and 1/100 Vol 10% APS**

**Loading buffer**

Blue Juice (agarose or PAA native gels):

80 % glycerol (v/v)
20 % 0.5 M EDTA pH 8.0
Bromophenoleblue, Xylenecyanol FF
Used for standard horizontal agarose electrophoresis or native PAA EE.

Blue Juice with SDS:

80 % glycerol (v/v)
20 % 0.5 M EDTA pH 8.0
0.1 % SDS

Bromophenoleblue, Xylenecyanol FF
Used for SCOPs, RNA gels, to disrupt DNA protein complexes (RNAase tests!)


Formamide gel loading buffer 1:

10 ml deionised formamide
200 µl 0.5 M EDTA pH 8.0
Bromophenoleblue, Xylenecyanol FF
Used for sequencing, S1-mapping etc.


Formamide gel loading buffer 2 :

10 ml formamide
50 µl 10 x TBE
Bromophenoleblue, Xylenecyanol FF
Used for sequencing, S1-mapping etc.


Sample loading buffer for Northern Blot:

50 % deionised formamide
1 mM EDTA pH 8.0
Bromophenoleblue, Xylenecyanol FF
Used for Northern Blot (see related protocol)


Sample loading buffer for alkaline gels:

500 µl glycerol
400 µl $H_2O$
15 µl  10 N NaOH
Bromophenoleblue, Xylenecyanol FF (become purple-red because of high pH)
Used for alkaline agarose gel electrophoresis

# 7.2.2 Assays

## 7.2.2.1 Vesicle Preperation

**Cell harvesting:**

- Remove the medium of cells that have reached 80 % confluence

- Rinse the cells with 10 ml of PBS

- Incubate the cells for about 2 min at 20°C in 5 ml of 0.25 % Trypsin and 0.1 % EDTA

- Remove the Trypsin/EDTA containing the cells and collect in a sterile tube containing 5 ml of growth media

- Centrifuge the cells for 10 min at 500 g

- Discard the supernatant and resolve the cells carefully in 10 ml PBS

- Centrifuge the cells for 10 min at 500 g

- Remove PBS and add homogenisation buffer

**Homogenisation:**

Solution A:     10.9% Saccharose (fresh!)
(at 4° C !)     1 mM EDTA
          0.3 mM PMSF
          0.1 μg/ml Aprotinin (= 25 U/ml)
          0.7 μg/ml Pepstatin

The cells are homogenised at 20% (weight/volume) in Solution A by 5 strokes for 5 s with a Polytron

   1200 at full speed. After each stroke the homogenate is cooled for 50 s on ice.

**Preparation of synaptic vesicles**

Material :       Biofuge 17 RS Ultracentrifuge Sorval OTD 65 B, rotor T 865

Solutions:         A:     10.9% Saccharose (always fresh!)
   (at 4° C !)     1 mM EDTA
          0.3 mM PMSF
          0.1 mg/ml Aprotinin (= 25 U/ml)
          0.7 μg/ml Pepstatin

To prepare 2 ml of A:    70 μl  Pepstatin      (= 1.4 μg)
                    10 μl  Aprotinin    (= 0.2 μg)
                    20 μl  PMSF 30 mM
                    20 μl  EDTA 100 mM
                    218 mg        Saccharose
            *Always prepare a fresh solution !*

          B:     30 mM PMSF in EtOH, dilute 1:100 in water just before
   use

To prepare Solution B (5 ml):   26 mg   PMSF
                 *Dissolve in* 5 ml EtOH $\Rightarrow$ *30 mM PMSF*

          C:     Tris/malate 10 mM pH 6.5

To Prepare C (100 ml):  116 mg Maleate (Maleinsäure)
                     121 mg Tris
                     200  μl  NaOH 4 N
    *Fill up to 100 ml with H₂O, check if pH= 6.5*        $\Rightarrow$ *10 mM Tris/ maleic acid (=10x)*

          D:     $MgCl_2 . 6 H_2O$ 100 mM

To prepare D (50 ml):   1.017 g $MgCl_2 \cdot 6H_2O$ $\Rightarrow$ *100 mM*

100 mM EDTA (1 l):   29.225 g         EDTA

**All procedures are performed at 4°C**

- Centrifuge the cell-homogenate for 10 min at 1000g (precool to 4°C)

- Centrifuge the supernatant for 13 min at 25000 g

- Wash the pellet with solution A *(Vortex)* and re centrifuge for 13 min at 25000 g (15000 rpm)

- Homogenise the pellet with 10 strokes in a glass homogenisator in 800 μl of solution B

- Neutralise with 40 μl of solution C after 30 sec *(This osmotic shock must be performed as fast as possible to ensure that the big vesicles are broken up and that their organelles and cytoplasm is evacuated without lysing the mitochondria)*

- Centrifuge the extract for 25 min at 20000 g (13000 rpm)

- Add so much of solution D to the supernatant that you obtain a final concentration of 1 mM $Mg^{2+}$

- Centrifuge for 45 min at 55000 g (21000 or 22000 rpm)

- The supernatant *(can be stored at -80°C)* is centrifuged for 4h at 140000 g (34000 rpm)

- Take up the vesicles in 10 μl of solution A

- Store the extracts in liquid nitrogen


## 7.2.2.2 <u>Cytoplasmic RNA Harvesting (if not Amplicon Kit is used)</u>


The aim of this protocol is the purification of cytoplasmic RNA from transfected or non transfected cells grown in culture. A yield between 50 and 300 μg from a confluent 10 cm Petri dish is expected (it depends on cell type). This protocol works fine for most established cell lines.

<u>Protocol:</u>

1) Rinse cells 2 times with 5 ml PBS (1x); add 2 ml Trypsin /EDTA (1x); incubate 10 minutes at room temperature.

2) Collect cells with ice cold PBS and pool them in a 50 ml Falcon tube with 5 ml of medium, centrifuge for 5 min at 1000 g. Wash pellet once with 10 ml ice-cold PBS and re-centrifuge. <u>From now on, work on ice.</u>

3) Aspirate the supernatant. <u>Rapidly</u> suspend pellets in 500 μl IsoHi**∗** by pipetting up and down 3-4 times. Transfer pelleted cells in a sterile Eppendorf. Incubate at least 5 min (no more than 7-8 min). Therefore, split your samples in convenient series (max 12 dishes per series)

   **∗**"IsoHi" lysis buffer:      140 mM NaCl
       1.5 mM $MgCl_2$
       10 mM Tris.HCl pH 8.6
       0.5 % Nonidet P-40
       0.015% (w/v) Macaloid

4) Spin 5 minutes at 13000 rpm, 4 °C. Next step to be conducted swiftly, have all prepared!!!

5) Transfer the supernatants to fresh ED tubes containing 500 μl Phenol and 25 μl 10x TNE; mix well immediately.(The mix can be stored at -20°C before further processing.) Spin 10 min at 13 000 rpm at 4°C. After extraction with 1x Phenol transfer upper phase of supernatant to a fresh tube.

6) Add 500 μl 1x Phenol/Chloroform1:1 and mix well. Spin 5 min at 13 000 rpm at 4°C. After extraction transfer upper phase of supernatant to a fresh tube.

7) Add 500 μl 1x Chloroform (or put already before in fresh tube) and mix well. Spin 3 min at 13 000 rpm at 4°C. After extraction transfer upper phase of supernatant to a fresh tube. This last supernatant can be stored for several weeks at -20°C.

You can work at RT, provided you do it rapidly.

OPTIONS:

A) At stage 6, RNA can be directly used for S1 nuclease mapping, It is recommended to verify concentrations by loading 4 µl RNA (about 1/100 of the prep) on a fresh 0.8% agarose minigel for semi-quantitation (SDS should be included in the loading buffer and in the electrophoresis buffer for best results).

B) If more precise quantification is required, then proceed further to steps 8-10

8) Precipitate by adding 1000 µl ethanol 100%. Mix. Let 30 minutes at -20$^{O}$C, spin 15 minutes at 4 $^{O}$C, 13000 rpm.

9) Remove the supernatant, rinse with first ice cold ethanol (100% / 80%) and dry tube for 5 min in a vacuumed desiccator (or let dry the inverted tube on a cleenex).

10) Resuspend in 100 µl 1x TE (or smaller volumes if necessary). Measure OD. Label tubes. Store at -20$^{O}$C for short term (less than one week), or at -80$^{O}$C for long term (more than a week)

Measure the OD at 260 by diluting **1:100** in 1x TE (400 µl; OD value multiplied by 4 gives µg/µl

## 7.2.2.3 <u>Preparation of Agarose Gels</u>

**<u>Material:</u>**

a)   A glass plate with sharp edges, measuring 6 cm x 8 cm
   b)  1 mm thick Teflon combs. The theets width is 3 mm for analytical gels and ca. 1 cm for preparative gels. Distance between theets is 1 mm for the analytical and 2 mm for the preparative. The teeth depth is 5 mm for both types
   c)  Agarose: there are two fundamental types: Type II is suited for analytical gels (about 1 Fr/gram). Type VII (usually called "low melting") is suitable for preparative gels (better purified).
   d)  Ethidium bromide: 10 mg/ml solution (see StockSol)
   e)  Buffer: Two types of buffers are currently used: LOE (Loeninger) buffer and TAE buffer. LOE buffer is not suitable for preparative gels because the phosphate it contains may cause precipitation in the preparative steps or during ligation.
       10x LOE: for 10 litres:   436. g Tris base
       414. g NaH$_2$PO$_4$ ·2 H$_2$O
       37.2g Na$_2$EDTA·2 H$_2$O

       10xTAE: for 10 litres:       484 g Tris base
         114.2 ml glacial acetic acid
         37.2 g Na$_2$EDTA·2H$_2$O

       LOE buffer should be used at a end concentration of 0.6x

**<u>Protocol:</u>**
   1) Dissolve 0.8 to 2 g of agarose in 100 ml of 1x TAE containing 0.5 µg/ml EtBr (100 µl EtBr stock in 2 litres; preparative gels) or in 0.6x LOE containing 1 µg/ml (200 µl EtBr stock in 2 litres; analytic gels). The gel concentration depends on the length of the bands you want to visualize. See Appendix)
       Analytic gel (2%, 100 ml):       2 g    Agarose (Mol. biol. grade)
                                         10 µl   Ethidium bromide (10 mg/ml)
                                         99 ml   0.6 LOE

2) Boil the mixture in the oven until the agarose is completely dissolved. Sometimes it is necessary to boil two or three times (don't overboil, the solution spills out!).

3) Let the agarose cool down. This can be speeded by putting the erlenmeyer under running water (keep shaking). desired temperature: 50-55 degrees (Criterion: Erlenmeyer can be touched by hands without serious burning). Meanwhile, adjust plates and combs such that comb is parallel to plate border (distance ca. 5 mm, distance from glass, ca 0.1 mm). You can use the combs in both orientation depending on the number of samples and on the separation you desire. In wide orientation it gives 20-22 slots, in narrow orientation, 16 slots.

4) When the gel has reached the desired temperature (see 3), pour 16 ml (=1/3 cm$^3$ per cm$^2$) of gel on the plates with a 20 ml pipette.

5) Let cool the gel to room temperature, then remove the comb. The gel can be stored in the refrigerator for several days in a box humidified at 100%.

LOADING THE GEL

6) Mix 5 µl of PCR product with 1 µl of "blue juice" and load it on the gel

7) Load 4 µl of 100 bp ladder marker on gel, too.

8) Run gel at 100 V for 20 min, until lower blue line has reached the two third of the gel.

**Appendix:**
% Type II Agarose gel and resolution of linear DNA:

0.8 %   700-11000 bp              2%   50-2000 bp


# 7.2.2.4 **Preparation of 5' labelled S1-oligonucleotide probe:**

The aim of this protocol is to prepare a 5' end-labelled oligonucleotide for S1 mapping. A specific radioactivity of ca 2 x 10$^6$ cpm/pmol is expected.

**Protocol:**

1)                          Prepare or use ready made 10 x T4 Polynucleotide Kinase Buffer:
                             10 x T4 Polynucleotide Kinase Buffer:           500 mM Tris.HCl pH 7.6
(Maniatis/Boehringer recipe)  100 mM MgCl$_2$
                             50 mM DTT
                             1 mM Spermidine HCl
                             1 mM EDTA

                             Pipet in an ED-tube:          1 µl 10xPNK Buffer + 1 µl H$_2$O
                             1 µl S1 Oligo (1 pmol/µl)
                             3 µl [γ-$^{32}$P]-ATP (20 to 30 µCi)(3000 Ci/mMol, 10 mCi/ml; Amerham)
                             3 µl H$_2$O

Start the reaction adding 2 µl T4 Polynucleotide Kinase (1 U/µl)(New England Biolabs). This mixture can be scaled up to larger amounts if required.
                             Incubate at RT 30 min to 1 h. Meanwhile prepare heating block at 100 ˚C and assembly gel.

2)                          Preparative PAGE: Normally 8 % PAA/Urea (8M) gel is OK. For other probes use the appropriate gel percentage. Use comb with wide slots (2 cm). Prerun 30 min at 25 W.

3)                          Add 40 µl of formamide gel loading buffer to the reaction tube, mix, quickspin, denature 3 minutes at 100 ˚C in the heating block, the chill on ice. Alternatively, the

reaction can be first extracted with Phenol, precipitated and then load on freshly rinsed slot.

4) Run the gel at 25 W . Stop the electrophoresis if possible before the free $[^{32}P]$-γATP comes out from the gel into the lower buffer tank (in our case BPB dye has migrated ca 50 % of the gel length.

5) Remove the ear-notched glass plate, cover gel with a Saran wrap (fix well behind the glass plate), put a tape onto the wrap beside and below the gel (for the easier positioning of the X-Ray film with magic marker) and expose a X-Ray film during 2-5 min in the dark room. Develop the film, carve out a window on the signal corresponding to kinased oligo and position the film onto the gel with heel of the pen marks.

6) Excise gel slice with a scalpel blade, if necessary, crush the gel slice by centrifuging through a bottom-pierced ED tube placed inside an intact tube. Add 500 µl 1xTNE/0.2 % SDS count total cpms, and incubate at 50 ˚C  30 min - 1 h.

7) Chill on ice 5 min , spin at 4 ˚C 10 min, transfer carefully supernatant to a fresh tube (if kept in the cold, the SDS will precipitate and form a thin interphase between crushed gel and supernatant). Check eluted counts and compare with residual on crushed PAA. If necessary, repeat extraction from the crushed gel with a second aliquot of 1xTNE/0.2 % SDS.

8) Pool elution aliquots; 1 x Phenol CHCl$_3$, 1 x CHCl$_3$

9) Measure counts of an aliquot with ß-Counter (Cerenkov). Probe should have ca 2 Mio cpm/pmol. Yield of gel elution is around 70%
Store at -20 ˚C.

# 7.2.2.5 S1 MAPPING

The aim of this protocol is the quantification of the amount of specific mRNAs classes in RNAs extracted from transfected cultured cells. The mRNA of interest is hybridised to an end-labelled single stranded DNA probe (S1 probe, see "S1 probe" protocol) and non hybridised regions are digested with S1 nuclease. Digestion products are run on a PAA gel. The resultant autoradiogram is analysed by densitrometric scanning. Reference: (Westin et al., 1987)

**Protocol:**

1) Mix in an ED tube:
20-40 µg RNA
50 kcpm-300 kcpm S1 probe (depending on specific activity)
in a total volume ranging between 100 and 300 µl of 1x TNE.(Add 1x TNE where necessary).
Briefly check uniformity of counts with Geiger counter

2) Add 3 volumes ethanol. Mix well by inverting tubes. Incubate 15-30 minutes at -20$^O$C, spin at least 15 minutes at 4$^O$C, 13 krpm. Remove the supernatant, rinse the pellet with ethanol, dry the tube inverted on a cleenex.

3) Add 16 µl Formamide (Fluka), mix well (it takes several minutes of work).

Prepare 5x Hybridisation buffer:

200mM PIPES pH 6.4
2M NaCl
25mM EDTA pH 8

Add 4 µl of 5x Hybridisation buffer, mix, spin to collect liquid.

4) Denature 5 minutes at 100 $^O$C, transfer tubes to a 30$^O$C bath and incubate at least 4 hours. During this incubation it is recommended to prepare the gel for the analysis and two series of labelled tubes

5) Prepare 10x S1 digest buffer:

2.5M NaCl

0,3 M NaOAc pH 4.6

10 mM $ZnSO_4$

For S1 digestion, prepare the following cocktail (For **n** samples, mix on ice):

-270 μl x (**n+1**) ice-cold water

-30 μl x (**n+1**) S1 digest buffer

-3 μg x(**n+1**) calf thymus DNA (sonicated, average size ca 400 bp; freshly    denatured 5 min at 100 ˚C), mix well

-150 units x (**n+1**) S1 nuclease (Sigma)

Mix very well the components (beware of enzyme-glycerol sedimenting at bottom!)

6) Add 300 μl of the digest cocktail to each sample, mix well by pipetting up and down. Put immediately on ice.

7) Warm samples shortly at $37^O$C for 10-20 seconds, centrifuge briefly to collect liquid.

8) Incubate 1 hour at RT.

9) Transfer the reaction into ED tubes containing 300 μl PC+ 15 μl TNE; vortex briefly, centrifuge 5 minutes at 13 krpm, RT. IMPORTANT: do not add PC to S1 digestion tubes!

10) Transfer the supernatants into new tubes, add 900 μl ethanol, measure the counts (Cerenkov input cpm).

11) Incubate at least 15 minutes on ice or at -$20^O$C. Centrifuge 20 minutes at 13 krpm, $4^O$C. Discard the supernatant. Rinse 1x with ethanol, dry on a cleenex.

12) Add 5 or 10 μl of Formamide loading buffer (vol depends on gel size and shape), count Cerenkov the S1-resistant cpm. Centrifuge briefly, boil 5 minutes and load on the denaturing gel. For β-globin S1 probe use 8% or 10% PAA 19:1 with 8M Urea.

13) Count residual radioactivity in emptied tubes.

### Remarks

-Point 4: For probes different from β-globin the temperature may vary (up to 65 $^O$C)

-Point 9: a certain amount of the ss DNA probe sticks to plastic and is only partially digested by S1. If PC is added to reaction tubes then adsorbed material is released and gives a high background of partially digested signals.

## 7.2.2.6 Klenow DNA polymerase treatment:

**Aim:**              fill up 5'-overhangs to create blunt ends

**Buffer:**           10 mM Tris.HCl pH 7.5, 5 mM $MgCl_2$, 7.5 mM DTT

Klenow is also active in the standard NEB or in L, H and M salt buffers

**Conditions:**       DNA at ca 50 μg/ml in Klenow buffer or restriction buffer;

dNTPs: each 200 μM (from 10 or 5 mM stock)

use 1 U of enzyme per μg DNA

**Reaction time:**    30 min at 25 ˚C.

Stop reaction adding $^1/_{10}$ vol of 10xTNE (if necessary raise volume in order to allow the following extraction steps but always adjust the end concentrations to 10 mM EDTA, 300 mM NaCl using 10xTNE)

Extract 1xPh, 1xPh / CHCl$_3$, 1xCHCl$_3$, precipitate with 3 vol. of EtOH

## 7.2.2.7 <u>T4 DNA polymerase treatment:</u>

**Aim:**          removal of 3'-overhangs to create blunt ends
             fill -in of 5'-overhangs

**Buffer:**       10 mM Tris.HCl pH 7.9, 10 mM MgCl$_2$, 50 mM NaCl, 1 mM DTT
             supplement with 50 µg/ ml acetylated BSA
             T4 DNA polymerase is also active in the standard restriction-buffers.

**Conditions:**   DNA at ca 50 µg/ml in T4 DNA pol- buffer or NEB-buffer;
             dNTPs: each 200 µM (from 10 or 5 mM stock)
             use 1 U of enzyme per µg DNA

**Reaction time:**     30 min at 16 ˚C.

Stop reaction adding $^1/_{10}$ vol of 10xTNE (if necessary raise volume in order to allow the following extraction steps but always adjust the end concentrations to 10 mM EDTA, 300 mM NaCl using 10xTNE). Alternatively, heat inactivate 10 min. at 75 ˚C.

Extract 1xPh, 1xPh / CHCl$_3$, 1xCHCl$_3$, precipitate with 3 vol. of EtOH

## 7.2.2.8 <u>Dilution of T4 Ligase</u>

**<u>Method:</u>**

Prepare 10x Ligase Storage Buffer Salts:

> 100 mM Tris.HCl pH 7.5
> 500 mM KCl
> 10 mM DTT
> 1 mM EDTA
>
> filter 0.2 µm,
> store at ≤ 4 ˚C / -20 ˚C

Prepare a 1x Storage Buffer with 50 % glycerol content and 100 µg/ml BSA ( can also be frozen) from the solutions above and use it to dilute T4 DNA Ligase
Make some aliquots of this diluted ligase and store at -20 ˚C.

## 7.2.2.9 Ligation in Low Melting Agarose

This is a method for the *in agarose* ligation of DNA fragments separated on preparative "low melting" agarose (type V, e.g. FMC SeaPlaque) gels without further purification steps. The procedure is based on the fact that this kind of agarose can be melted at 65 ˚C and stays in the liquid state at 37 ˚C.

**Protocol:**

1) Separate the DNA restriction fragments on a "low melting" agarose gel Low melting agarose (type V, FMC Bioproducts SeaPlaque , Cat.Nr. 50102) of convenient percentage with 1xTAE buffer and 0.5 µg/ml ethidium bromide[1] in the preparative gel and in the running buffer.
Load ca 1 µg of total DNA per lane for a plasmid of 3 kb like an empty cloning vector (Bluescript) or proportionally more DNA for bigger plasmids.

2) Take a picture of the gel [2], mark the relevant DNA bands with a pen. Cut out the interesting bands with a clean scalpel blade with the aid of a UV hand lamp or on the UV transilluminator (don't expose too long to UV light!) and transfer them into sterile ED tubes [3]. Keep on ice or freeze if not used at that time point.

3) Meanwhile set one heating block on 65 ˚C and the other on 37 ˚C. Put a ED tube with 500 µl of ddH$_2$O in the block at 65 ˚C.

   Prepare enough ED tubes as required for the ligation and all necessary pos. and neg. controls [4].

   Prepare Ligation buffers (can be made as stock solutions):

   | 10 x A | 10 x B |
   |---|---|
   | 10 mM ATP | 500 mM Tris.HCl pH 7.5 |
   | 100 mM DTT | 100 mM MgCl2 |
   | | 2 mg/ml BSA (Fraction V) |

   Pipet into each tubes 7.5 µl 10xA, 7.5 µl 10xB and 25 µl ddH$_2$O (should be made poolwise!). We assume that 5 µl of each needed DNA fragment in form of melted agarose and 1-2 µl of T4 DNA Ligase will be added into the tube later. If the amount of DNA in the excised bands is not exactly known, other volumes have to be pipetted based on the estimation made with the fluorescence intensity. It is very useful to have a detailed table [5] for the ligation components and their required amounts. Generally the total volume of the ligation is about 50 µl.[6] Keep on ice until needed. However, there can be some flexibility in the final volume, depending on how many fragments will be present in a particular tube [5].

4) Melt the excised DNA bands in the heating block at 65 ˚C (for higher percentage gels (e.g. 2%) some degrees more are needed to completely melt the agarose), mix well with vortexer, quick spin and keep in the heating block.[7]
Put the tubes with the prepipetted buffers and ddH$_2$O in the heating block at 37 ˚C.

   Prewarm each pipette tip in the water-containing ED tube at 65 ˚C aspirating up and down, pipet DNA fragments where required (following the mentioned **table**) into the tubes at 37 ˚C. The melted agarose will remain liquid until kept at this temperature.

5) While keeping the tubes at 37 ˚C, add 1-2 µl of ligase at 0.2 U/µl or 1 µl of ligase at 1 U/µl T4 DNA Ligase (Pharmacia 27-0870-04, appropriately diluted to 0.2 or 1.0 Weiss U/ µl.), depending on

complexity of the ligation [8] (keep the enzyme in a cooling block (-20˚C)!
Mix well, quick spin, incubate at 4 ˚C, 16°C or RT for few hours to overnight, depending on complexity of the ligation [8].

6) For transformation of bacteria: melt ligation again at 65 ˚C before pipetting 10 µl to an aliquot of CaCl$_2$ competent bacteria on ice (see protocol BacTransfo).


## Remarks

**1**   this is half the amount of ethidium bromide normally used in analytical gels. TAE should be used as running buffer instead of LOE to avoid the presence of phosphate in the ligation reaction. The running buffer in the electrophoresis tank should be used only once due to the reduced buffer capacity of TAE and to avoid contamination.

**2**   A picture of the gel is essential in the case where the digested DNAs were not loaded in equimolar amount on the preparative gel. The relative amounts of the fragments to be ligated can be estimated proportionally to the intensity of the bands on the gel picture (provided that the picture is not overexposed).

**3**   the approximate volume of an excised band is 100 µl. Otherwise the volume can be adjusted with ddH$_2$O comparing with a second ED tube containing 100 µl of H$_2$O.

**4**   One essential control is for example the DNA-fragment encoding the antibiotic resistance gene alone (with or without enzymatic treatment with calf intestinal phosphatase (CIP)), but other combinations of fragments are sometimes useful to determine the reason of the presence of background in the ligation. This, however, is mostly depending on the adopted cloning strategy.

**5    Example:**



558  BamH I

HinD III

AmpR

D

Mun I

A

C

*pEXAMPLE*

B
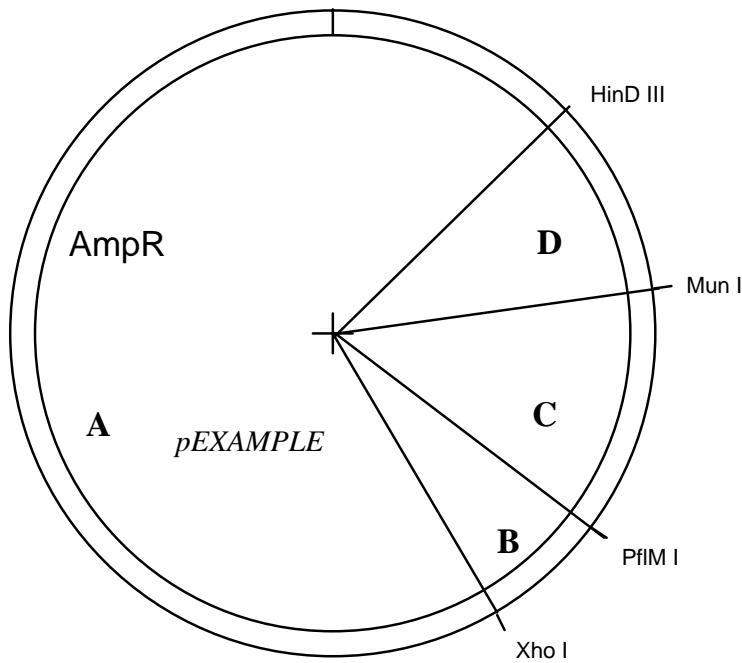
PflM I

Xho I

| A | Plasmid 1 | XhoI-HindIII | 2584 bp |
| B | Plasmid 2 | XhoI-PflMI | 642 bp |
| C | Plasmid 3 | PflMI-MunI | 1312 bp |
| D | Plasmid 4 | MunI-HindIII | 978 bp |

A+B+C+D = pEXAMPLE

| Nr | Fragment | | | | 10xA 10xB | H2O | Product Name | Nr of colonies |
|---|---|---|---|---|---|---|---|---|
| | A | B | C | D | | | | |
| 1 | 5 µl | 8 µl | 5 µl | 10 µl | 5 µl 5 µl | 12 µl | pEXAMPLE | 226 |
| 2 | 5 µl | | | | 5 µl 5 µl | 35 µl | neg. control 1 | 54 |
| 3 | 5 µl | 8 µl | 5 µl | | 5 µl 5 µl | 25 µl | neg. control 2 | 96 |

**6**    The important parameters in a ligation are:

**the equimolarity of each DNA fragment**
**a concentration < 0.5 fmol/µl of each fragment**

Assuming the presence of 1µg of a fragment of 3 kb (e.g. corresponding to 0.5 pmol of linearised

cloning vector) in an excised band of 100 µl volume, the contribution of 5 µl of melted agarose of this fragment into 50 µl end ligation volume leads to a final concentration of 0.5 fmol/µl, so much as required; higher concentrations lead to the formation of multimers, too low concentrations preferentially lead to intramolecular reaction (e.g. vector closing himself).

**7**    The melted agarose can be stored at -20 ˚C and eventually used again. However, not more than once again, due to the high mutagenesis risk heating in presence of ethidium bromide.

**8**    **General rules:**

| | |
|---|---|
| Ligations with overhangs(oh): | 16 ˚C (better hybridisation) |
| | 0.4 U ligase/ tube enough |
| | 3-4 hours enough |
| Ligations with only blunt ends: | RT (actually irrelevant for "hybridisation"). |
| | 0.4 - 1 U ligase/tube |
| | overnight |
| Ligations with mixed ends: ligate first, then blunts). | Temperature gradient on melting ice in beaker at       RT (oh |
| | 0.4- 1 U ligase/tube |
| | Overnight |

High number of fragments (>5) to be ligated also require some more ligase than normally (1 U/tube).

## 7.2.2.10 <u>Cloning with oligonucleotides</u>

1)    Dissolve oligonucleotides (0.01 or 0.04 µmol synthesis scale) in 200 µl of TE or more.

2)    Measure concentration of this stock dissolving 10 µl oligonucleotide into 490 µl TE according to this formula:

**for oligos below 40 NT: 1OD~30µg/ml (dilute 1/30 or multiple thereof)**
**for oligos above 50 NT: 1OD~40 µg/ml (dilute 1:25 or multiple thereof)**

OD has only a sense if the oligo is reasonably pure. In case of doubts purify oligos by gel electrophoresis (see **OligoPurif**)

3)    Mix 100 pmol of each oligonucleotide (sense + antisense) in a total volume of 40 µl of TE. Heat shortly at 100 ˚C and letting cool down to 37 ˚C. (if oligos are insufficiently concentrated, volume can be scaled up to 80 µl

4)    Add 10 µl of 5xligase buffer (A+B 1:1; see **DNALigation**), keep on ice; add 50 µl 1x ligase buffer

This solution ($C_0$)has a concentration of 1 pmol/µl.

5)    Generally the molarity in ligations is kept 0.5 fmol/µl ( this means 25 fmol of a fragment in a 50 µl-reaction):

Make dilutions in 1 x Ligation Buffer ( **1xLiB**)of the annealed oligos in order to obtain the 10-fold, 3-fold, 1-fold, 0.3-fold molar amount of oligos in the ligations and keep them on ice.

| e.g.: | 10 µl $C_0$ + 190 µl **1xLB** $\rightarrow$ | 50 fmol /µl ($C_1$) |
|---|---|---|
| | 30 µl $C_1$ + 70 µl **1xLB** $\rightarrow$ | 15 fmol /µl ($C_2$) |
| | 10 µl $C_1$ + 90 µl **1xLB** $\rightarrow$ | 5 fmol /µl ($C_3$) |
| | 10 µl $C_2$ + 90 µl **1xLB** $\rightarrow$ | 1.5 fmol /µl ($C_4$) |

6)    Use 5 µl of solution $C_1$-$C_4$ for 4 different ligations to titrate the best result.

### 7.2.2.11 <u>Bacterial agar dishes</u>

**Protocol:**

1)  Dissolve 25 g LB-Broth Base (Gibco 12780-052, 500g) per each litre of distilled $H_2O$.

2)  Add 13 g (in general 1.25 %) of agar bacteriological (Gibco 30391-023, 500 g) per litre of LB-medium.

3)  Autoclave.

4)  Let cool down to ca 50 ˚C, then add 1 ml (2 ml if dishes shall be kept longer than 3 weeks) of ampicilline stock solution\* for each litre of LB/agar-solution. Mix well.

    \*Ampicilline stock solution at 50 mg/ml in $H_2O$ (Ampicilline from Sigma, A0166, 100 g or Boehringer 835269, 50 g ). This is a 1000x solution. Store at -20 ˚C

5)  Distribute about 20 ml of this solution into each bacteria dish.

6)  Let solidify and partly dry (at least 2 hrs to avoid humidity condensation problems), then store in plastic bags at 4 ˚C.


-Ampicillin: add 1 ml stock solution (1000x) for each litre of LB/agar
    => agar dish supplemented with 50 µg/ml (100 µg/ml) ampicillin

-X-Gal and IPTG can be plated out on solidified Amp/Tet dishes (40 µl of each stock solution\*\* for each dish) or also added to the liquefied LB/agar at 50 ˚C. Add 40 µl of each stock for 3 ml of top agar.

    \*\*IPTG stock solution, 20 mg/ml in $H_2O$ (Bachem Q-1280); X-Gal stock solution, 20 mg/ml in N,N'-DMF (Biofinex B80C)


### 7.2.2.12 <u>Transformation of bacteria</u>

**Protocol:**

1)  Prepare for each DNA to be transfected into the bacteria a ED-tube on ice. Prepare an additional ED-tube for the transformation positive control.

2)  Resuspend well the competent bacteria using a micropipette, distribute 100 µl ($\approx 10^8$ bacteria) in the precooled, appropriately labelled ED-tubes, keep tubes on ice.

3)  Add 25 µl ligation mix (liquefy if low-melting agar!) to the bacteria, mix well with the pipette (<u>never use vortexer</u>).

4)  Incubate on ice 5 min.
    Meanwhile distribute the bacterial dishes open on the desk to allow them to dry (this is necessary to evaporate condensation water that accumulates during storage at 4 ˚C ).
    Also put a L-Broth culture flask into the 46 ˚C water bath to prewarm it.

5)  First temperature shock:  a) put the tubes 3 min into the 37 ˚C water bath
                                 b) let stand ca 5 min on ice

6)  Second temperature shock:   Pipet ca 1 ml of prewarmed L-Broth to the bacteria tubes using a glass pipette. (The 50 ˚C warm L-Broth should be allowed to cool down in the pipette to ca 40 ˚C otherwise the bacteria will die). Close tube and mix well (invert , <u>don't vortex</u>).

7) Incubate ca 5 min. in the 37 ˚C water bath (mix occasionally). During this time bacteria will recover and start synthesising resistance genes, there should be no more than one duplication.

8) Prepare Pasteur pipettes for bacteria plating: Melt the end of the Pasteur pipettes on the Bunsenburner flame to close the hole, then melt the pipette in order to create a plating tool like depicted in the following illustration.
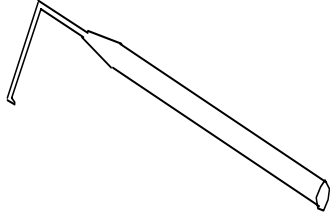


9) Spin down the bacteria in a ED-centrifuge for about 20 seconds, aspirate all supernatant but ca 100 µl (Sterile Pasteur)

10) Resuspend the bacteria well (up and down with Pasteur), plate 50 µl onto an appropriate agar plate and store the other 50 µl at -20°C

11) Put the dishes <u>turned upside down</u> into a 37 ˚C incubator and incubate overnight.

12) Colonies shall be clearly visible after 14-16 hr. If the density of colonies cannot be anticipated, it is recommended to plate the transformed bacteria at different densities.

## 7.2.2.13 <u>SCOP-Assay</u>

The aim of this protocol is to quickly analyse the size of plasmid DNA from a large number of transformed bacterial colonies or streaks (SCOP= <u>S</u>ingle <u>CO</u>lony <u>P</u>rep).

**<u>Protocol:</u>**

1) Fill 15 µl LETR in labelled Eppendorf tubes, put on ice.

2)  Prepare LETR, 15 µl pro colony to analize:

> Lysozyme 2 mg/ml
> EDTA pH 8 100 mM
> Tris pH 8 50 mM
> RNaseA (DNase free) 20 mg/ml in $H_2O$ stock 0.1 mg/ml

> Dissolve first lysozyme in $H_2O$ and then add the rest in the order shown. Can be stored at -20°C for several months. Avoid repeated Thawing.

> Gently aspirate entire colony or 0.5 cm length of a streak with 20 µl pipette and resuspend in the LETR. Incubate 20-30 min. at RT . REMARK: Be sure you labeled your streak, or if you use a colony then save a streak of it with the yellow tip onto a fresh plate prior to resuspending in LETR.

3) Add one drop of phenol to each tube, mix, centrifuge about 1 min.

4) Take 3-5 µl supernatant and load onto gel together with comparative markers (plasmid DNA diluted to ca. 5 ng/µl).

5) Run gel, take picture, compare with marker plasmids.

## 7.2.2.14 <u>Minipreparation of DNA (if not performed by Spincolumn -Kits)</u>

The aim of this protocol is to purifiy plasmid DNA from transformed small bacterial cultures.

**Protocol:**

**A] Growth**

1) Inoculate with one bacterial colony or streak 5 ml LB medium supplemented with 10μl ampicillin (50 mg/ml in $H_2O$ = 50x-100x solution)

2) Grow the culture at 37°C in the shaker for 18-24 h (up to 36 h).

**B] Lysis & extraction**

1) Centrifuge the bacteria for 15 min at 5000 rpm..

2) Resuspend the pellet in 500 µl of ice cold LETR.

LETR, 500µl pro 5 ml culture:
    Lysozyme        2 mg/ml
    EDTA pH 8       100 mM
    Tris pH 8       50 mM
    DNase-free RNaseA (20 mg/ml) 0.1 mg/ml
Dissolve first lysozyme in $H_2O$ and then add the rest in the order shown. Can be stored at -20°C for several months. Do not thaw repeatedly.

Mix well. Transfer into Eppendorf tube, Incubate 20-30 min at RT.

3) Add 25 µl 10 % triton X-100, mix gently. Incubate for further 5 min. at RT (optional).

4) Centrifuge 10-15 min. in Eppendorf centrifuge (13 kRPM)

5) Remove the pellet with the P20 pipette loaded with a yellow tip.

6) Extract 1x phenol (centrifuge 15 min), 1x phenol:chloroform 1:1 (centrifuge 10 min), 1x chloroform (centrifuge 5 min) (500 µl each, transfer acqueous onto fresh tube each time)

7) Adjust the volume to 500 µl with water, add 50 µl 3M NaCl and 300 µl isopropanol. Incubate 10 min at RT.

8) Centrifuge 10 min. in Eppendorf centrifuge at RT (13 kRPM).

9) Discard supernatant, wash pellet 1x 80% EtOH and 1x 100% EtOH. Let dry .

10) Resuspend the DNA in 50-100 µl 1x TE.

**C] If sequencing is foreseen**

1) Dilute to 300 µl. Add to your DNA 1 volume of 13% $PEG_{6000}$/1.6M NaCl. Incubate 1 h on ice

2) Centrifuge 15-20 min in Eppendorf centrifuge at 4°C (13kRPM)

3) Discard the supernatant and rinse the pellet with 80% EtOH. Spin another 5 min.

4) Discard the alcohol; let dry the pellet and resuspend it in 30-50 µl 1x TE.

# 7.2.2.15 Plasmid Preparation (if not performed with Midipreps of Qiagen)

The aim of this protocol is to purifiy plasmid DNA from transformed bacterial cultures. The amount of DNA recovered should be ~ 500-1000ug/100 ml culture (for a pUC-like plasmid). DNA can be further purified by CsCl (see **WhiteCes**).

**Protocol:**

## A] Growth

1) Inoculate with one big bacterial colony or streak 100 ml LB medium supplemented with 200 ml ampicillin (50 mg/ml in $H_2O$ = 50x-100x solution).

2) Grow the culture at 37°C in the shaker for 18-24 h (better 36-48 h). **Optional:** let stand the grown culture at 4°C for 24-72 h. (improves yield by a factor of 2).

## B] Lysis

1) Centrifuge bacteria in a 100 ml tube at 3000-4000 RPM for 15-20 min. at 4°C (Hermle). (**Optional**: The pellet can be stored at -20°C )

2) Prepare LETR, 6-7 ml pro 100 ml culture:
   | | |
   |---|---|
   | Lysozyme | 2 mg/ml |
   | EDTA pH 8 | 100 mM |
   | Tris pH 8 | 50 mM |
   | DNase free RNaseA (20 mg/ml) | 0.1 mg/ml |

   Dissolve first lysozyme in $H_2O$ and then add the rest in the order shown. Can be stored at -20°C for several months

   Resuspend the pellet in 6-7 ml of ice cold LETR (if frozen pellet is used, do not allow to thaw prior to LETR addition). Mix well. Transfer into an Oak Ridge tube. Incubate ~ 30 min at RT (suspension should get slightly viscous).

3) Add 100 µl 10 % triton X-100, mix (2-3 strong strokes, rotate). Should get very viscous. Incubate for further 10-30 min.

4) Centrifuge at 10000-15000 RPM for 30-40 min at 4°C in SS-34 rotor (or Hermle) Transfer the clear supernatant to a fresh corex tube or another suitable tube for organicextractions

## C] Purification

All manipulations at room temperature!

1) Extract 1x1 vol. phenol. If you don't foresee a caesium chloride purification then extract also 1x1 vol. phenol/chloroform and 1x1 vol. chloroform (You can use 15 ml polypropilene Falcon tubes or corex tubes sealed with *Parafilm M* (phenol) or with *Dura Seal* (phenol:chloroform & chloroform).

2) Adjust the volume to 7 ml. Add 0.7 ml 3M NaCl (3M NaOAc can also be used), add 4.2 ml isopropanol. Mix well, incubate ~10 min at RT and spin at 10000 RPM for 15-20 min in HB-4 rotors (not more than 9000 RPM if you use snap cap tubes!).

3) Discard the supernatant and rinse the pellet carefully with 80% ethanol and with 100% ethanol. Put the tube inverted on a Kleenex until the DNA pellet is dry (you can carefully help drying with a tiny jet of compressed air or N2).

4) Resuspend the pellet in        a) 0.5-1 ml TE if you don't foresee CsCl or
                                    b) 1.1 ml TE if you plan a CsCl purification.
                                    (-> WhiteCes)

## 7.2.2.16 <u>CsCl Plasmid Purification: White Caesium (6 ml)</u>

The aim of this protocol is to obtain highly purified plasmid DNA from a 100-200 ml culture preparation.

### <u>Equipment:</u>

6 ml Kontron polycarbonate tubes with crimper system, 12 ml disposable polystyrene or polypropylene tubes, 15 ml corex tubes .

Kontron Centrikon T-1190 ultracentrifuge with Sorvall T-865 rotor and teflon adapters (with caps), (Alternatively, Sorwall ultracentrifuge with same rotor); Selecta angular centrifuge, Sorvall centrifuge with HB-4 rotor at RT.

2 ml syringes loaded with 18 gauge needles (pink), long wave UV transilluminator or hand-held lamp, Quartz cuvettes and spectrophotometer, scale.

### <u>Protocol:</u>

1) Mix in a 12 ml PP tube: 4.35 ml CsCl stock, 1.00 ml DNA, 5 μl of diluted EtBr. Transfer into a 6 ml Kontron tube (fill the remaining volume with isoionic CsCl solution obtained by mixing 1 ml TE with 4.35 ml CsCl stock). Check weight on the scale. Seal the tubes with the crimper.

CsCl stock Solution: dissolve 200 g CsCl in 120 ml of 20 mM Tris pH 8 / 5 mM EDTA
          Final vol. should be ~172 ml; refractive index between 1.4135 and 1.4142

2) Ultracentrifuge at 45000 RPM for 20-24 h at 22°C in T-865 rotor. Use the option "Slow". Remove tubes carefully. Inspect on top of Long wave UV or hand-held lamp (360 nm, protect eyes in either cases, avoid prolonged illumination of DNA+EtBr.)

3) Punch the top of the tube with a syringe and aspirate the fluorescent band (monitor work with the UV hand-led lamp or on the transilluminator) by puncturing under the band with the syringe. Aspirated volume should be ~1 ml or less. Transfer into a 12 ml polystirene tube.

4) Extract 2x2 vol. isoamyl alcohol saturated with $H_2O$ (=isopentyl alcohol; =3-methyl-1-butanol).(Watch out! Organic phase this time is **above**!). (Vortex well and spin 2-3 min). Monitor extraction by inspecting under UV, and repeat as often as necessary. Transfer the acqueous phase into a 15 ml corex or into a snap cap tube

5) Add $H_2O$ to 6 ml, add 6 ml isopropanol, mix and incubate up to 30 min at RT. Centrifuge at 11000 RPM (9000 RPM if snap-cap plastic Falcon tube) for 20 min at RT in HB-4 rotor.

6) Discard the supernatant and rinse the walls and pellet carefully but throughly with 80% ethanol and (now be x-careful, since pelllet usually detaches) with 100% ethanol. Put the tube inverted or side-side on a cleenex until the DNA pellet is dry.

7) Resuspend in 400 µl TE. Transfer into an Eppendorf tube, add 40 µl 3M NaCl, fill the tube with ethanol and mix. A white clump of DNA should appear. Incubate a few minutes at RT.

8) Spin 5 min (or even less, depending on the amount of DNA). Discard supernatant and wash the DNA pellet once with 80% ethanol and once with 100% ethanol. Put the tube inverted on a Kleenex until the DNA pellet is dry.

9) Resuspend the DNA in 400-500 µl TE (be patient) and calculate the concentration by measuring the OD260 (typically you dilute 10 µl of the stock DNA in TE to 400 µl. The $OD_{260}$ value x2 gives your stock DNA concentration in µg/µl). Use quartz cuvette!

## 7.2.2.17 <u>Lipofection (using DOTMA)</u>

This protocol is to transfect 10 cm diameter cell culture dishes[1] by the reagent DOTMA (PNAS USA 84:7413-7417 (1987)), which can be easily synthesised by an organic chemist.

**MATERIALS:**

    15 ml or 6 ml Falcon Snap Cap tubes (and no other kind of plastics)
    Optimem PSG (Gibco BRL)
    DOTMA Solution (1 mg/ml, diluted from stock 10 mg/ml) in ddH20 or Lipofectin™,
    LipofectAMIN™, LipofectACE™ or other lipofection reagents from commercial suppliers (Gibco BRL, Boehringer)

**PROTOCOL:**

All solutions must be at room temperature in the sterile hood.

    1)Prepare a serie of 15 ml snap cap tubes containing the DNA (5-20 µg in up to 100 µl)
    2)Prepare a second serie of 15 ml snap cap tubes containing 80 µl DOTMA (1 mg/ml).
    (40 µl for Lipofectin from Gibco BRL (1 mg/ml))
    3)      Add 2 ml of Optimem to all tubes, mix heavily by finger flicking, let stand at least 10 min.
    4)Meanwhile rinse the cells once with TBS.
    5)Combine the tubes containing DNA and DOTMA by pouring from one tube to the other, mix heavily by finger flicking, let stand for at least 10 min.
    6)Meanwhile rinse the culture dishes once with TBS, then aspirate completely and pour the DNA-DOTMA-Optimem mix onto the cells while gently moving the dish.
    7)      Incubate 3-4 hours at 37 ˚C / 5 % $CO_2$.
    8)Aspirate lipofection medium, rinse dishes with TBS, add medium appropriately complemented for the particular cell line used.
    9)    Incubate 36-48 hrs at 37 ˚C / 5 % $CO_2$, then proceed as required for your particular experiment (harvest, fix, stain etc.)

    Remarks

    1        For 5 cm diameter dishes use half of the volumes.
    2Recommended cell density:      for RNA mapping:30-40 % confluent
    for protein expression: 70-80 % confluent

Calcium and Phosphate Mixes for DNA Transfection in cell cultures

The aim of this protocol is to describe a DNA-calcium phosphate co-precipitation method to transfect eukaryotic adherent cells.

**Protocol:**

A) 4x Ca-Mix (500 ml)      0.5 M $CaCl_2$  [$CaCl_2 \cdot 2H_2O$: Mr: 147.02]

                             0.05 M Hepes pH=7.05

fill a 500 ml bottle with 500 ml $ddH_2O$. Put a mark on it to recognise the volume.

Discard 50-100 ml of the water.

Dissolve 36.76 g of $CaCl_2 \cdot 2H_2O$ in the bottle and autoclave.

Add 25 ml 1 M Hepes pH=7.05 [c]. Adjust the volume with autoclaved $ddH_2O$.

Store at 4°C

B) 2x P-Mix (1 liter)0.75 mM $Na_2HPO_4$

                      0.75 mM $NaH_2PO$

                      0.05 M Hepes pH=7.0

                      0.28 M NaCl

Fill a 1000 ml bottle with 1000 ml $ddH_2O$. Put a mark on it to recognise the volume.

Discard ca. 200 ml of water and autoclave.

Add:                2.5 ml 400x Phophate solution (0.3 M $Na_2HPO_4$, 0.3 M $NaH_2PO_4$)

               100 ml 2.8 M NaCl NaCl solution (=10x)

                50 ml 1 M Hepes pH=7.05

Adjust the volume with autoclaved $ddH_2O$

Store at 4°C.

D) **Test the solutions!**

Test the solutions with Ca and Pi aliquots at <u>room temperature</u>. Transfect  10 cm diameter cell culture (NB41A3) or dishes with 10 ml CO2 equilibrated medium.

Prepare several samples with 20 µg of CsCl purified plasmid DNA ( e.g. OVEC) and 5 µg carrier DNA. Dilute the DNAs with TE to 50 µl.

standard test: to three samples: Add $H_2O$ to 250 µl, add 250 4x Ca-Mix (RT!).

Wait 5 min. Add 500 µl of 2x P-Mix (RT!) and pour onto cells after 5, 10 and 20 minutes incubation. Observe the precipitates (take about 30-40 min to be at bottom). A value between 1 and 10 (see below) is acceptable, much larger or much finer precipitates will give erratic transfections.

**Scale of precipitate is:** <u>10</u> if diameter of crystals is equivalent to diameter of average nucleoli; values such as <u>5, 2, 1 and <1</u> are indicative of smaller precipitates; value of <u>20, 50 or 100</u> indicate proportionately larger crystals.

The 2x P-Mix is conceived in such a way that it should give rather fine crystals (scale 1-10) in 10 min incubation. If they are too large even at 5 min incubation then start from scratch or inform a more experienced colleague. If the precipitate is <1, then add 1/4000 to 1/2000 vol of 400x phosphate solution to an aliquot. Test again until satisfactory. Then supplement rest of solution with equivalent amounts of 400x Pi. Test again and store if ok.

# References Appendix

Allen, J. B., M. W. Walberg, M. C. Edwards, and S. J. Elledge. 1995. Finding prospective partners in the library: the two-hybrid system and phage display find a match.
*Trends Biochem Sci*. 20:511-6.


Bartel, P., C. T. Chien, R. Sternglanz, and S. Fields. 1993. Elimination of false positives that arise in using the two-hybrid system.
*Biotechniques*. 14:920-4.

Brent, R., and M. Ptashne. 1985. A bacterial repressor protein or a yeast transcriptional terminator can block upstream activation of a yeast gene.
*Nature*. 314:198.

Brent, R., and M. Ptashne. 1985. A eukaryotic transcriptional activator bearing the DNA specificity of a prokaryotic repressor.
*Cell*. 43:729-36.

Bulliard, C., R. Zurbriggen, J. Tornare, M. Faty, Z. Dastoor, and J. L. Dreyer. 1997. Purification of a dichlorophenol-indophenol oxidoreductase from rat and bovine synaptic membranes: tight complex association of a glyceraldehyde-3-phosphate dehydrogenase isoform, TOAD64, enolase-gamma and aldolase C.
*Biochem J*. 324:555-63.

Fields, S., and R. Sternglanz. 1994. The two-hybrid system: an assay for protein-protein interactions.
*Trends Genet*. 10:286-92.

Hope, I. A., and K. Struhl. 1986. Functional dissection of a eukaryotic transcriptional activator protein, GCN4 of yeast.
*Cell*. 46:885-94.

Keegan, L., G. Gill, and M. Ptashne. 1986. Separation of DNA binding from the transcription-activating function of a eukaryotic regulatory protein.
*Science*. 231:699-704.

Luban, J., and S. P. Goff. 1995. The yeast two-hybrid system for studying protein-protein interactions.
*Curr Opin Biotechnol*. 6:59-64.

Ma, J., and M. Ptashne. 1987. The carboxy-terminal 30 amino acids of GAL4 are recognized by GAL80.
*Cell*. 50:137-42.

Ma, J., and M. Ptashne. 1987. Deletion analysis of GAL4 defines two transcriptional activating segments.
*Cell*. 48:847-53.

Ma, J., and M. Ptashne. 1987. A new class of yeast transcriptional activators.
*Cell*. 51:113-9.

Ma, J., and M. Ptashne. 1988. Converting a eukaryotic transcriptional inhibitor into an activator.
*Cell*. 55:443-6.

McNabb, D. S., and L. Guarente. 1996. Genetic and biochemical probes for protein-protein interactions.
*Curr Opin Biotechnol*. 7:554-9.

Mendelsohn, A. R., and R. Brent. 1994. Applications of interaction traps/two-hybrid systems to biotechnology research.
*Curr Opin Biotechnol*. 5:482-6.

# Curriculum vitae

**Personal Data**

Name:                          Zubin DASTOOR

Academic grade:                PhD Student

Date & Place of Birth:         14 Mai 1971 in Basel,  Switzerland

Nationality:                   Swiss

Marital Status:        Single

Children:                      None

Language Knowledge:            German (native), English, French

Permanent Address:             Im Niederholzboden 42, 4125 Riehen, Switzerland

Current Address:               Route du Centre 20, 1723 Marly, Switzerland
                               (++41) 26 436 28 23

University Address:            Institute of Biochemistry
                               University of Fribourg
                               Rue du Musée 5, 1700 Fribourg, Switzerland

                               E-mail: Zubin.Dastoor@unifr.ch

**Education**

Okt. 1995-present:             PhD Thesis in biochemistry at the University of
                               Fribourg under supervision of Prof. J.-L. Dreyer

1994-1995:                     Diploma thesis in pharmacology at the Biocenter
                               (Basel) under supervision of Prof. U.A. Meyer

Nov. 1990-March 1995:          Studies of "Biologie II" at the University of Basel,
                               Degree in Biologie II (cell biology, biochemistry,
                               molecular genetics and biophysical chemistry)

Apr. 1987-June 1990            Upper secondary education at Gymnasium
                               Bäumlihof, Basel (Typ C: specialisation in sciences)

**Positions**

1995-1999             Teaching assistant at the Institute for Biochemistry for medical
                      and biochemistry students

| | |
|---|---|
| 1991-1996 | Substitute teacher in chemistry, biology, mathematics, physics, French and sports at various high schools in Basel |
| 1991 | Trainee in a CNS research project at CIBA (now called Novartis), Pharmaceutical division, Basel |

## Scientific meetings and courses

| | |
|---|---|
| Oct. 1999 | Annual meeting of NFP37 "Somatic gene therapy", Fribourg |
| Sept. 1999 | Symposium "Recombinant Adeno99", Fribourg |
| April 1998 | International Conference "Plasma Membrane Redox Systems and their role in Biological stress and Disease", Antwerp (Belgium), Poster presentation |
| June 1998 | SKMB Workshop on "Transfection", Basel |
| March 1998 | USGEB Annual meeting, Lausannne, poster presentation |
| Sept. 1997 | III$^e$ cycle practical course in "Bioinformatics: Introduction to sequence analysis", Lausanne |
| Sept. 1997 | Meeting on "Biological Defence Mechanisms" organised by III$^e$ cycle Romand, Villars-s/Ollon |
| March 1997 | USGEB Annual meeting, Geneva |
| Sept. 1996 | Meeting on "Viruses as tools in research & therapy" organised by III$^e$ cycle Romand, Villars-s/Ollon |
| Sept. 1996 | III$^e$ cycle course in "Biology of nematode parasites", Lausanne |

## Publications

Bulliard, C., R. Zurbriggen, J. Tornare, M. Faty, Z. Dastoor, and J. L. Dreyer. 1997. Purification of a dichlorophenol-indophenol oxidoreductase from rat and bovine synaptic membranes: tight complex association of a glyceraldehyde-3-phosphate dehydrogenase isoform, TOAD64, enolase-gamma and aldolase C. *Biochem J.* 324:555-63.

Dastoor Z. and J.-L. Dreyer. Induction of apoptosis after nuclear translocation of GAPDH in neuroblastoma NB41A3 cells and in fibroblast R6 cells.  (Submitted).

Dastoor Z. and J.-L. Dreyer. Differential translocation of Hsc70 after induction of apoptosis or oxidative stress. (Manuscript in preparation).

**Memberships**

Swiss Society of Experimental Biology (USGEB)

Swiss Society of Cell Biology, Molecular Biology and Genetics (ZMG)

Freiburger Chemische Gesellschaft (FCG)

Zubin Dastoor
Route du Centre 20
1723 Marly

Aux personnes concernées

Sujet:    Thèse présentée à l'Université de Fribourg (Suisse) pour l'obtention du grade de *Doctor rerum naturalium*

Messieurs,

Par la présente, je certifie que j'ai rédigé ma thèse " Differential translocation of five transplasma membrane oxidoreductase (PMO) complex proteins after induction of apoptosis and oxidative stress" moi-même et sur la base d'un travail personnel sans aide illicite.

Zubin Dastoor

# **Publications**

1. Purification of a dichlorophenol-indophenol oxidoreductase from rat and bovine synaptic membranes: tight complex association of a glyceraldehyde-3-phosphate dehydrogenase isoform, TOAD64, enolase-γ and aldolase C.
Bulliard, C., R. Zurbriggen, J. Tornare, M. Faty, Z. Dastoor, and J. L. Dreyer. 1997. *Biochem J.* 324:555-63.


2. Potential role of nuclear translocation of glyceraldehyde-3-phosphate dehydrogenase in apoptosis and in oxidative stress.
Z. Dastoor and J.L. Dreyer. *J. Cell Biol.*, submitted.


3. Hsc70 undergoes nuclear translocation under oxidative stress but not during apoptosis.
 Z. Dastoor and J.L. Dreyer. *J. Cell Sci.*, manuscript in preperation.